



University of HUDDERSFIELD

University of Huddersfield Repository

Ashton, Gage P.

The Development & Evaluation of Hot-stage Microscopy Direct Analysis in Real-Time Mass Spectrometry

Original Citation

Ashton, Gage P. (2018) The Development & Evaluation of Hot-stage Microscopy Direct Analysis in Real-Time Mass Spectrometry. Doctoral thesis, University of Huddersfield.

This version is available at <http://eprints.hud.ac.uk/id/eprint/34797/>

The University Repository is a digital collection of the research output of the University, available on Open Access. Copyright and Moral Rights for the items on this site are retained by the individual author and/or other copyright owners. Users may access full items free of charge; copies of full text items generally can be reproduced, displayed or performed and given to third parties in any format or medium for personal research or study, educational or not-for-profit purposes without prior permission or charge, provided:

- The authors, title and full bibliographic details is credited in any copy;
- A hyperlink and/or URL is included for the original metadata page; and
- The content is not changed in any way.

For more information, including our policy and submission procedure, please contact the Repository Team at: E.mailbox@hud.ac.uk.

<http://eprints.hud.ac.uk/>

University of
HUDDERSFIELD

The Development & Evaluation of Hot-stage Microscopy
Direct Analysis in Real-Time Mass Spectrometry

Gage Patrick Ashton

Submitted August 2018

Acknowledgments

I would like to dedicate this thesis to my partner Louise. Her continued support and constant belief in me and my work gave me the encouragement to push on that bit harder and reassured me it will all be worth it in the end. I will always be grateful for having you by my side during this time, thank you.

To Dr Lindsay Harding and Dr Gareth Parkes, my supervisors and importantly my friends. I am indebted to them for the help, guidance and the time they have provided to me over the years, without them I truly would not be the researcher that I am today.

To Dr Gary Midgley and Prof. Mark Heron, thank you for your time to talk over my reactions, you helped drive my understanding of the research I was undertaking.

To Prof. Edward Charsley thank you for sharing your extensive knowledge on the topic of thermal analysis, particularly for highlighting key developments of hot-stage microscopy.

Huge thanks for the technical support within our department. They offered constant assistance and encouragement to my project no matter how obscure the request was...

To the master of PowerPoint measurement, Sophie Pownall. Thank you for your commitment to the project and your friendship during the time with our research group.

Finally, thank you to my family and close friends. Between you all you gave me support and the welcomed distractions preventing me from going completely insane whilst writing this thesis.

Abstract

The thesis describes the development and evaluation of a novel instrument combining hot-stage microscopy (HSM) with an ambient ionisation technique known as direct analysis in real-time mass spectrometry (DART-MS).

Hot-stage microscopy DART-MS (HDM) combines two complementary analytical techniques to maximise the information obtained from a single experiment. DART-MS has the ability to quickly analyse materials at atmospheric pressure without sample preparation. HSM provides both a controllable temperature stage (essential for accurate thermal analysis) and gives information on the physical changes in a sample arising from a change in colour or morphology.

HDM comprises of a hot-stage designed and constructed to fit between a DART-100 source (IonSense) and an ion trap mass spectrometer (Bruker). It incorporates a digital microscope situated 90 ° to the DART-MS path and is focused on samples placed in metal or ceramic crucibles on the hot-stage. Experiments typically use samples of a few milligrams in mass and heating rates of 0.1 to 50 °C min⁻¹ standard for many conventional thermal analysis techniques. Software was developed using Visual Studio 2017, (Microsoft) to control the hot-stage, collect micrographs and record optical and colorimetric data in real-time. Software was also developed to extract selected ion intensity data from the MS and combine it with temperature and optical data.

HDM was successfully evaluated with a range of applications. Synthetic organic reactions have been performed *in situ*. Reactants, products and transient intermediates were successfully monitored and profiled as a function of temperature, with correlations between the reaction colour and micrographs being made to mass spectra. Physical properties of common polymers including melting points, cold crystallisations and glass transitions have all been shown optically with relation to their mass spectrum. An optical method to measure and calculate the coefficient of thermal expansion (applied to silicone polymers) is described and shown to be consistent with literature data. HDM has also been applied to the thermal profiling of inks adsorbed on alumina matrices. Studies with mixtures of energetic materials collected from surfaces demonstrate that limits of detection at the nanogram level are readily achievable.

Further developments of both instrumentation and software are also discussed.

Keywords – *Hot-stage microscopy, thermomicroscopy, DART-MS, thermal analysis, ambient ionisation, mass spectrometry, hyphenated techniques.*

Contents

Cover page	1
Acknowledgments.....	2
Abstract.....	3
1.0 Introduction.....	8
1.1 Project Preface	9
1.2 Mass spectrometry	9
1.2.1 Fundamental operation of MS	9
1.2.2 Mass spectrometers	11
1.2.3 Ionisation sources	14
1.2.4 Recent ambient ionisation techniques	17
1.3 DART-MS.....	18
1.4 Applications of DART-MS	21
1.4.1 Forensics	21
1.4.2 Quality control.....	22
1.5 Recent developments DART-MS.....	23
1.6 Thermal analysis	25
1.6.1. Thermogravimetric Analysis (TGA)	27
1.6.2 Differential temperature techniques - DTA and DSC	28
1.6.3 Thermomechanical Analysis (TMA)	30
1.7 Hot-Stage Microscopy	31
1.7.1 Applications of HSM.....	32
1.8 Simultaneous TA & Hyphenated TA techniques	34
1.9 Introduction References	37
2.0 Instrumentation Development	D41
2.1 Introduction.....	42
2.2 Initial evaluation studies using DART-MS	43
2.2.1 Suppression effects	43
2.2.2 DART-MS Temperature profiling.....	47
2.3 Development of HDM	50
2.3.1 HDM Instrument Overview	50
2.3.2 Temperature control - PID algorithm and pulse width modulation	54
2.3.3 HDM – Digital microscopy and image processing	58
2.3.4 HDM – Temperature measurement.....	63
2.3.5 HDM – DART and MS	65

2.3.5.1 MS Inlet heater	66
2.4 Hot-stage designs.....	67
2.4.1 Hot-stage design 1.....	67
2.4.2 Hot-stage design 2.....	69
2.5 Software	71
2.5.1 Experimental header editor	71
2.5.1.1 Sample information (A).....	72
2.5.1.2 Experiment type (B)	72
2.5.1.3 Acquisition trips (C).....	72
2.5.1.4 Developments (D)	72
2.5.1.5 Image capture (E).....	72
2.5.1.6 RGB pixel monitoring (F).....	72
2.5.1.7 Temperature calibration (G)	73
2.5.1.8 Experiment control (H)	73
2.5.1.9 Microscope parameters (I).....	73
2.5.1.10 Control buttons (J)	73
2.5.2 Temperature programme editor	73
2.5.3 Pixel monitoring window	74
2.5.4 Acquisition window.....	75
2.5.5 Data extract.....	76
2.6 Development of an alternative ion source (μ -DART)	77
2.7 Current and Future developments.....	81
2.7.1 DTA hot-stages.....	81
2.7.2 Desorption stage.	83
2.7.3 Induction heating thermal desorption DART-MS	85
2.7.4 Software developments	87
2.7.4.1 SCTA applied to HDM.....	87
2.7.4.2 Incorporation of Arduino microcontrollers	88
2.7.4.3 Automated positioning of the hot-stage.....	91
2.7.4.4 Automated positioning of the μ -DART	92
2.8 Conclusions	94
2.9 Instrumentation Development References	95
3.0 Reaction Profiling.....	96
3.1 Introduction.....	97
3.1.1 Green Chemistry.....	99
3.1.2 Aims	99
3.2 Hydrobenzamide Synthesis.....	100
3.3 Binol Synthesis.....	106

3.4 14-Aryl Xanthene Synthesis	113
3.5 2-Phenylbenzimidazole Synthesis	119
3.6 2,3-Diphenylquinoxaline Synthesis	125
3.7 Tetraphenylpyrazine Synthesis	134
3.8 Benzodiazepine Synthesis.....	142
3.9 Phenylbisbenzimidazole Synthesis	147
3.10 Incomplete Reactions	153
3.10.1 Dibenzylideneacetone	153
3.10.2 Tetraphenylporphyrin	156
3.10.3 Diimide substituted NTCDA.....	159
3.10.4 Dilatin.....	161
3.11 Conclusions.....	163
3.12 Reactions Profiling References	164
4.0 Polymers Studies	166
4.1 Introduction.....	167
4.1.1 Aims	168
4.2 Polymer standards evaluation using HDM	169
4.2.1 Polystyrene (PS)	169
4.2.2 Polyethylene terephthalate (PET)	173
4.2.3 Polyvinyl Alcohol (PVOH).....	177
4.3 HDM and silicone polymers	181
4.3.1 Initial experiment to replicate the work of Gross	182
4.3.2 Isothermal step experiments using the HDM	183
4.3.3 Linear heating and cooling experiments	184
4.3.4 Cyclic isothermal step experiments	185
4.3.5 Cyclic linear heating and cooling experiments	186
4.3.6 Cyclic linear heating and cooling experiments with pre-treated and untreated samples	187
4.3.7 Cyclic linear heating and cooling experiments to a higher maximum temperature ..	188
4.4 Monitoring the thermal expansion of silicone polymers using HDM	190
4.4.1 Initial thermal expansion experiment.....	190
4.4.2 Development of a method to monitor thermal expansion using real-time processing of pixel values.....	192
4.4.3 Measuring expansion and contraction during thermal cycling to 200 °C	193
4.4.4 Measuring expansion and contraction during thermal cycling to 300 °C	195
4.4.5 Monitoring of change in size during a 9 hour isotherm at 200 °C.....	196
4.4.6 Using optical data to calculate the coefficient of thermal expansion	197

4.5 Conclusions and further work	198
4.6 Polymer Studies References	200
5.0 Desorption Studies	202
5.1 Introduction	203
5.1.2 Aims	204
5.2 Dyes	205
5.2.1 Selected ink example	205
5.2.2 Overview of inks	208
5.2.3 Quantitation	211
5.3 Energetic Materials	213
5.3.1 Conventional HDM analysis	215
5.3.2 Limits of detection using conventional HDM analysis	218
5.3.3 Evaluation of swabbing materials	223
5.3.3.1 Cotton medical swab	225
5.3.3.2 Cellulose acetate filter	226
5.3.3.3 Quartz wool	227
5.3.3.4 Fibre glass	228
5.3.3.5 Brass fibres	229
5.3.4 Thermal separation	231
5.3.5 Dopants	234
5.4 Further work	236
5.5 Conclusion	238
5.6 Desorption Studies References	239
6.0 Overall Conclusions	240

1.0 Introduction

1.1 Project Preface

The project described in this thesis combines two analytical instruments from two different disciplines, mass spectrometry (MS) and thermal analysis (TA). A modern ambient ionisation technique known as direct analysis in real-time mass spectrometry (DART-MS) has been integrated with a thermal analysis system called a hot-stage microscope (HSM). To set the context of the project each technique (DART-MS and HSM) is introduced in turn within this chapter. The project findings and results follow in subsequent self-contained chapters.

1.2 Mass spectrometry

1.2.1 Fundamental operation of MS

Mass spectrometry (MS) is concerned with the separation, detection and evaluation of ionised chemical species within the gaseous state. This is achieved through monitoring differences in mass-to-charge ratio (m/z , the mass of an ion divided by the number of charges it possesses) and their relative abundances. MS can be used to determine elemental compositions of analytes (compounds of interest), through assignment of characteristic profiles and using more advanced methods molecular structures may be postulated.¹

Today, mass spectrometers come in an array of very different types but fundamentally rely on the same operational principles, these have been summarised below as a flow diagram in Figure 1.1.

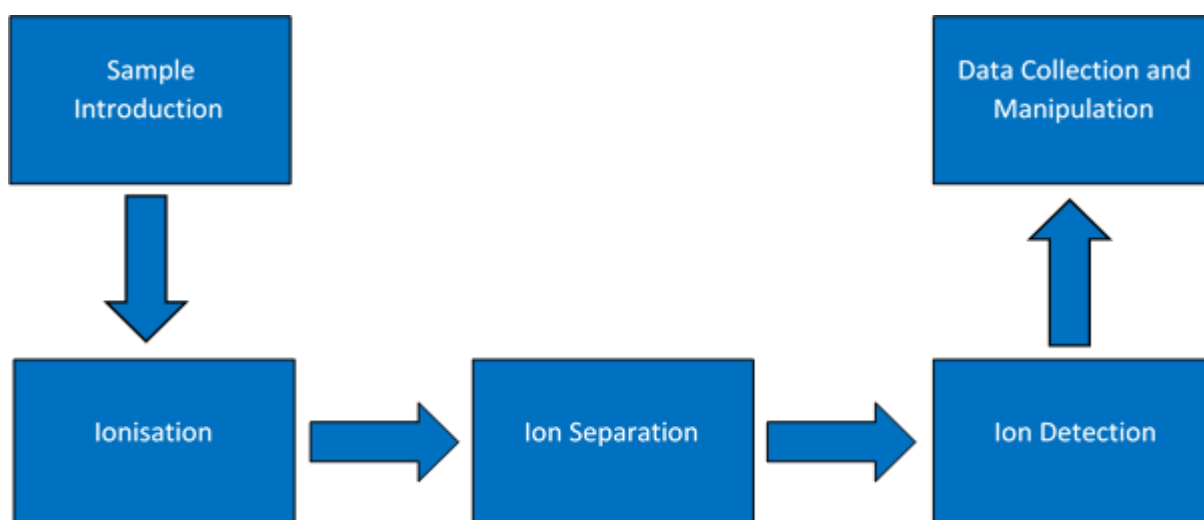


Figure 1.1 Basic flow diagram of the operation of a mass spectrometer.

a) Ionisation.

Analytes must be in the gas phase and carry a charge (be ionised) before reaching the separation step. Typically, ionisation takes place under reduced pressures. Methods such as electron ionisation (EI), achieved through bombardment of neutral analytes with a stream of electrons, are used to induce a charge on a neutral species.² However, developments within mass spectrometry have led to ionisation taking place prior to the spectrometer using a family of techniques known as atmospheric pressure ionisation (API) (see Section 1.2.3).³

b) Separation and focusing.

Ions are separated using a section of a mass spectrometer known as a mass analyser, operating under high vacuum. The high vacuum used within this section assists with the separation of the gaseous ions introduced previously. Non-ionised species (molecules, atoms and radicals) are removed through the high vacuum pumping system with only ionised species being amenable to the focusing and separation provided by electrical and magnetic fields.⁴

Ions are focused towards each section within the mass spectrometer using a series of devices known broadly as ion guides. By changing the electrical and magnetic fields incoming ions with specific m/z ratios can be selected and guided towards the detector.⁵

c) Detection.

A range of MS detectors exists and the choice is determined by several key factors such as response time, sensitivity and accuracy.⁶ Typical MS detectors include Faraday cages and electron multipliers. The output from the detector is then sent to a PC and stored as individual mass spectra for post processing. Real-time data may also be manipulated using more advanced MS techniques introduced later.

The combination of these components results in the ability to analyse samples as functions of their ion abundance *vs* their m/z distribution. An example mass spectrum of air generated by EI-MS is shown in Figure 1.2. It can be seen that the spectrum shows both a qualitative measure of *what* is in air and quantitative measure of *how much* is analysed.

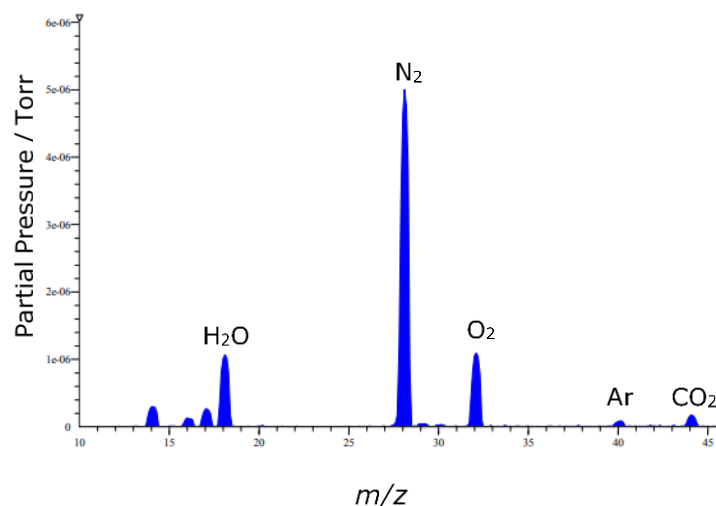


Figure 1.2 An example of the mass spectrum of air generated through EI-MS.

1.2.2 Mass spectrometers

The fundamental work of mass spectrometry began before the turn of the 20th century, with investigations by W. Wein into how 'canal rays' (a beam of positive ions) were affected by the presence of strong electric and magnetic fields.⁷ Sir J.J. Thomson developed the first type of mass spectrometer, the 'parabola mass spectrograph', that could separate ions by parabolic trajectories shown using photographic plate.⁸ The quoted first application paper published using MS was by F.W. Aston (a colleague of Thomson) who proved the existence of isotopes for the non-radioactive element neon in 1920 in the form of a mass spectrograph (accurate mass separation).⁹ Meanwhile, A.J. Dempster had developed the first magnetic sector MS instrument used to determine accurate ion abundances as opposed to the accurate mass measurements performed by Aston.¹⁰ During the late 1920's Dempster proposed the combination of the two types of analyser the *mass spectrograph* developed by Aston and his own *mass spectrometer* forming the first dual focusing mass spectrometer¹¹ and with it the base of modern mass spectrometry.

The introduction of an *in situ* ionisation source was an important addition to early mass spectrometry producing the first electron ionisation mass spectrometers EI-MS. EI gives characteristic 'fingerprints' of analytes, owing to EI being a hard ionisation technique, that is, an ionisation method that usually induces significant, but repeatable, fragmentation of molecules.

The early EI-MS instruments would often produce extra peaks in profiles generated in the absence of a sample. Later, organic chemists realised that these peaks arose from hydrocarbon compounds (presumably within the atmosphere or materials used to construct the spectrometers) and an appreciation for the use of MS for a wider range of

materials was realised.¹ The analysis of hydrocarbons became important prior to the start of World War II, as new analytical methods were required to quickly analyse aviation fuel for high octane content.¹²

The start of World War II propelled MS research. Instruments called 'Calutrons' were developed that could separate fissionable isotopes in a technique known as preparative MS. This was used to enrich plutonium and uranium ores by collection as opposed to detection to form weapons grade material, in the lead up to the first nuclear weapon being deployed. US scientists also invested a significant amount of research effort into synthetic rubber, including characterisation by MS, as the supply of natural rubber from Malaysia was cut when the country fell under Japanese occupation.^{1,12}

Time-of-flight (ToF) technology had been developed earlier and was used to separate gas phase ions¹⁴ but was not coupled to a mass spectrometer until the 1950s.¹⁵⁻¹⁶

ToF-MS works by measuring the time taken for ions to travel between the ion source and the detector (typically over a distance greater than 1 m). Ion separation occurs by all ions having the same initial kinetic energy (after acceleration) and the difference in m/z ratios causes differences in momentum and hence velocity. The ions travel freely within the high vacuum region between source and detector, and the differing velocities result in separation determined proportional to their m/z value.¹⁷

The development of ToF-MS was revolutionary for mass spectrometrists as the operation of the ToF-MS system meant that there was theoretically no upper m/z limit¹ - a factor that became of great importance for the later study of large structures such as biomolecules. The issue with early ToF-MS instruments was poor resolving power¹⁸ and, for this reason, it became less used until the invention of softer ionisation techniques (see Section 1.1.3) such as chemical ionisation (CI) and matrix-assisted laser desorption ionisation (MALDI).¹⁹

ToF-MS was surpassed in general popularity for many years through the introduction of the quadrupole mass analyser (QMA) and ion trap (IT) technology, typically providing cheaper instruments with significant space saving over the larger ToF-MS instruments of the time.

The QMA became a highly selective analyser towards monitoring single ions of interest, which later became an invaluable tool when used in combination with separation techniques such as gas chromatography (GC)²⁰ and liquid chromatography (LC).²¹ The QMA can operate at relatively high pressures (10^{-5} – 10^{-4} Torr) and fast scan rates owing to the fact it uses relatively low voltages during operation, ideal for linking with GC or LC but offering only integer m/z resolution.²² QMA operates by applying out of phase radio frequency (RF) voltages to opposing rods (2 pairs) typically arranged co-axially towards

the ionisation source and detector as shown in Figure 1.3.²³ Ions travel between the four rods (hence the term quadrupole) towards the detector, and only ions of a specific m/z range will be focused and reach the detector determined by the applied voltages to the quadrupole itself.

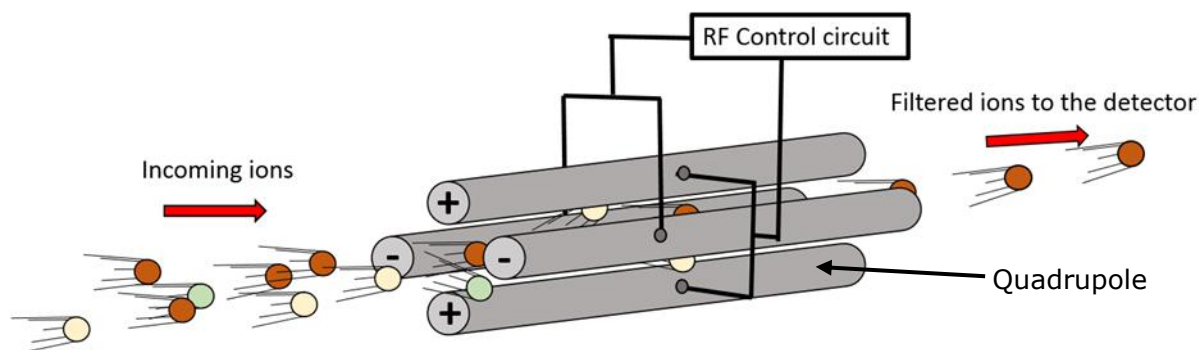


Figure 1.3 Schematic representation of a QMA quadrupole mass analyser, incoming ions are filtered by an alternating RF control circuit to only allow certain ions to the detector. Adapted from²⁴

The use of QMAs remains popular with many analytical scientists purely due to the ease of operation and relatively low costs when compared to other mass analysers.²⁵ Many techniques such as thermogravimetric analysis (TGA) may utilise evolved gas analysis (EGA) in combination with a quadrupole mass spectrometer for the study of simple evolved gases such as H_2O , CO_2 and NH_3 (see Section 1.8).²⁶

The ion trap mass analyser was a development from QMA.²⁷ As its name implies, it traps ions through the application of alternating RF DC voltages on a set of electrodes to form a potential energy well.²⁸ Ion traps are able to 'concentrate' analytes prior to analysis, achieved through trapping the ions before discharging them towards the detector in a sweeping motion across a range of m/z values (achieved by adjusting the potential well).²⁹

Ion trap technology was crucial in the development of tandem MS (MS^n).³⁰ Today, there are a variety of ion trap technologies including Fourier transform ion cyclotron resonance (FTICR),³¹ quadrupole ion trap (QIT)³² and orbitrap.³³ Figure 1.4 shows a QIT schematic.

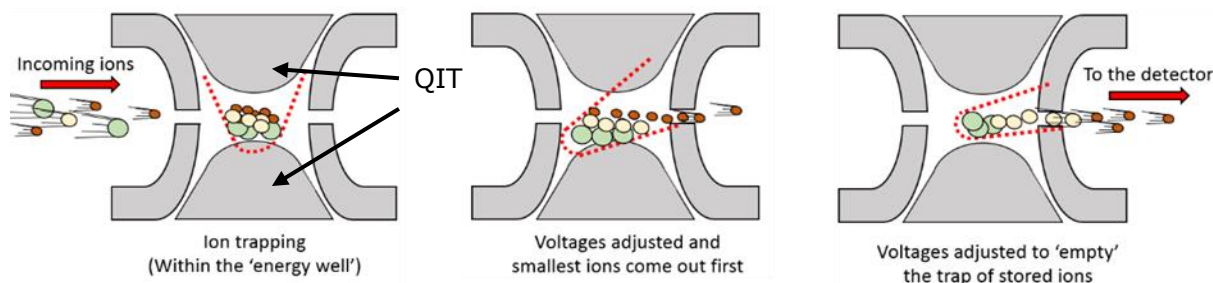


Figure 1.4 Quadrupole Ion trap schematic. Ions are introduced and stored within the potential energy well (illustrated by a red dashed line). The voltages are adjusted (to change the potential well) so that small ions are ejected first and larger last. Adapted from¹

1.2.3 Ionisation sources

The ionisation stage is crucial in mass spectrometry and has undergone many developments. One of the earliest forms was electron ionisation (EI). In EI energetic electrons are ejected (usually from a hot filament) and accelerated by applying a voltage between the filament and the trapping plate (an internal component) to form a continuous helical beam of electrons.³⁴ If the electrons in the beam have sufficient kinetic energy when they hit an analyte molecule then a radical molecular ion is produced. Typically, electrons are accelerated to a standard energy of 70 eV (set as a standard by convention for comparisons with original databases) which is significantly higher than molecular ionisation energies (usually between 7 and 15 eV).³⁵ A schematic of an EI source is shown in Figure 1.5 and fragmentation pathway shown in Schematic 1.1 for nitrobenzene.

Although the radical molecular ion is unstable and undergoes fragmentation in a predictable manner depending on the makeup of the molecule.³⁶ Fragmentation usually occurs at the weakest bond, moving from the radical molecular ion to a fragment cation (MS detectable) and a free radical. It is also possible that a starting radical molecular ion (directly after EI impact) can fragment to another radical molecular ion of lower mass after losing a neutral fragment. This series of fragmentation is what gives EI its characteristic and reproducible fingerprint patterns of analytes.

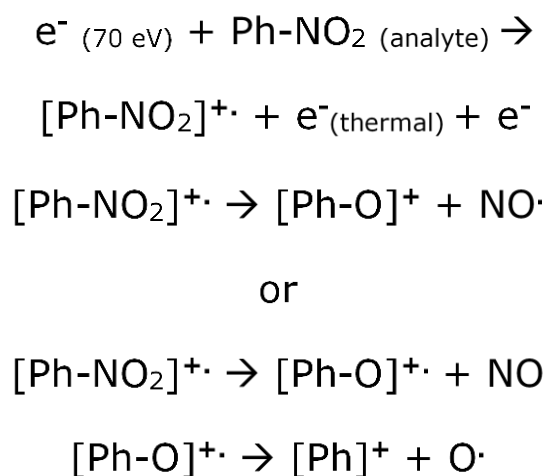
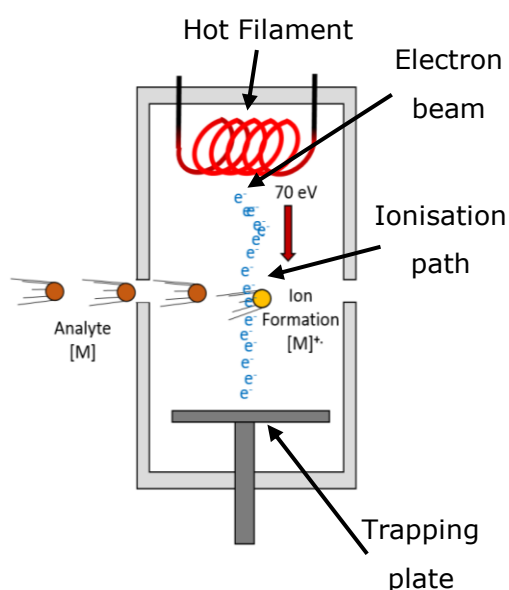


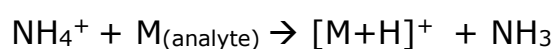
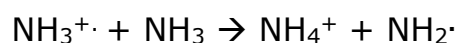
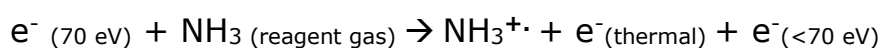
Figure 1.5 Left) Schematic of an EI source adapted from¹ Schematic 1.1 Right) EI mechanism using nitrobenzene as an example.

The predictable fragmentation afforded by EI allowed the development of mass spectral libraries for thousands of compounds, particularly useful for chromatography, and EI remains one of the most common ionisation methods used in GC-MS.³⁷

The primary problem for EI is that it is considered a 'hard ionisation' technique which can cause considerable fragmentation when analysing larger molecules which can lead to

ambiguity in the data interpretation for significantly large molecules such as polymers. In 1966 a 'soft ionisation' technique named chemical ionisation (CI) was developed.³⁸

The CI name was derived through the mechanism in which ionisation occurs. The process requires a reagent gas (such as ammonia or methane) to be introduced into an EI source (one which the analytes do not come in direct contact with but the carrier gas does), forming reagent ions. These ions collide directly with the neutral gas phase analyte and produces a range of simple analyte ions, most commonly molecular ions ($[M]^+$) or adduct ions ($[M+H]^+$) depending on the reagent gas used as shown in Schematic 1.2.³⁹



Or



Schematic 1.2 An example mechanistic route for chemical ionisation using ammonia.

The strength of CI lies with the formation of intact molecular ions as opposed to excessive fragmentation produced with EI. However, CI remains only applicable to compounds that are highly volatile.⁴⁰

Later ionisation developments included desorption ionisation (DI)⁴¹ and fast atom bombardment (FAB).⁴² These techniques led to the development of mass spectrometers capable of detecting ions above 1000 m/z , something which previously wasn't required as the size of the ions generated was small, either from EI fragmentation or through high volatility small molecules in CI.

In 1973 a new technique known as atmospheric pressure ionisation (API), later renamed atmospheric pressure *chemical* ionisation (APCI), was introduced by Horning's group.⁴³ In operation, solutions are introduced into a needle and form a spray of micro-droplets through interaction with a co-axial stream of high pressure gas. Ionisation occurs when the micro-droplets of solvent and sample (now heated) interact with a coronal discharge (a type of high voltage discharge) and the solvent becomes ionised.²²

Mechanistically the process is initially very similar to CI (hence its inclusion in the name) as the high pressure carrier gas is ionised through interaction with an electron. Depending on the carrier gas (commonly nitrogen) the corresponding energetic ion is formed. The ionisation is transferred through to a molecule of water, which in turn forms a cluster of water carrying a charge. Finally, the analyte interacts with the protonated water cluster to become protonated itself prior to the introduction to the mass spectrometer.⁴⁴ The APCI source is shown in Figure 1.6 and the ionisation mechanism is shown in Schematic 1.3.

The benefit of having an atmospheric pressure ionisation source is that the sensitivity was improved significantly due to the increase in ionisation efficiency caused by the source operating at significantly higher pressures leading to more gas phase collisions.¹

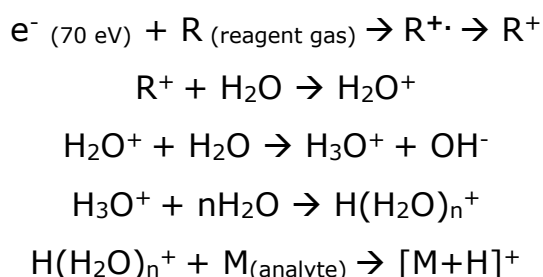
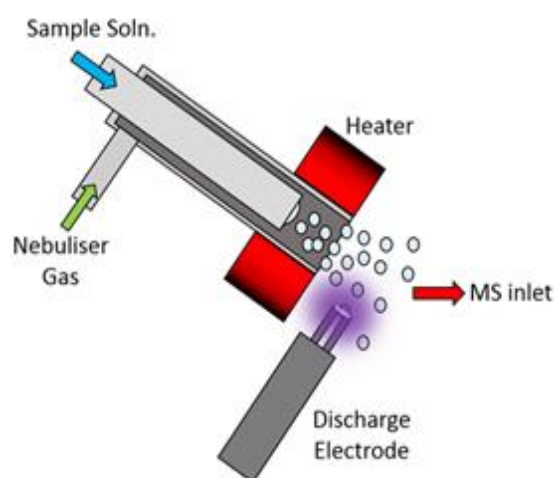


Figure 1.6 Left) the schematic operation of an APCI source adapted from⁴⁵ and Schematic 1.3 Right) an example of an APCI ionisation mechanism route through water cluster formation.

The APCI technique did not gain significant popularity within the MS community until the introduction of electrospray ionisation (ESI) and matrix assisted laser desorption ionisation (MALDI). This was mainly due to the inability of the inlet systems of the mass spectrometers of the time to cope with the significantly higher pressures that APCI operates under. Although, significant work was being undertaken to improve MS inlet technology to cope with these higher pressures.⁴⁶

ESI is very similar to APCI although the ionisation of the solvent takes place within the liquid phase as opposed to within the gas phase. The ionised solvent is forced into droplets, as in APCI, through a high pressure spray before they undergo coulombic explosion forming even finer droplets. Finally the solvent is removed and the charge is transferred to the analyte prior to MS analysis.⁴⁷

MALDI however, operates in a significantly different way from all the previously introduced techniques. In MALDI the analyte is mixed together with a matrix compound (for example dihydroxybenzoic acid) in molar ratios 1:5000 respectively within a suitable solvent. The mixture is then applied to a plate and allowed to dry, a pulsed laser is fired at the plate and the rapid gain in internal energy of the matrix induces a localised explosion of the matrix material forming gas phase analytes.^{1,48} The details of the ionisation mechanism of MALDI are still disputed,⁴⁹ but is still regarded as a soft ionisation technique owing to the formation of a variety of adducts of the analytes' molecular ion such as the protonated and sodiated forms.

APCI, ESI and MALDI set the foundations for a new class of techniques known as 'ambient ionisation' described in the next section.

1.2.4 Recent ambient ionisation techniques

Today a wide range of ambient ionisation techniques are available with variants being constantly reported.⁵⁰ Although the earlier ambient pressure techniques (ESI and APCI) were being used and had been commercialised they still required sample preparation prior to analysis. Two techniques, developed almost simultaneously, desorption electrospray ionisation (DESI)⁵¹ and direct analysis in real-time (DART)⁵² were the first to allow analysis of unprocessed samples in the open atmosphere. In essence, almost any sample could be placed in front of the ionisation source and a mass spectrum could be obtained from the sample's natural state.

At the time of writing there are almost thirty recognised ambient ionisation techniques, the majority of which are fundamentally based on APCI and ESI ionisation. The list of ambient ionisation methods is too extensive to cover in meaningful detail therefore only DESI and DART will be discussed here.

In DESI, samples are introduced in front of the DESI source as opposed to being incorporated into the solvent spray as in the ESI method. An ionised spray is directed towards the sample and analytes are removed through a solid-liquid extraction process. This extraction process is a combination of pneumatic action and localised electrostatic repulsion upon introduction of the sample into the DESI stream. DESI-MS is able to achieve experiments (for solid samples) that weren't previously available to ESI users. DESI was found to be extremely useful for biological applications⁵³ owing to the soft ionisation and a spin off from these original biological investigations was found in DESI imaging.

DESI imaging is possible due to the extremely fine solvent jet that delivers the extraction solvent. By placing the sample onto a motorised stage below the DESI source, pieces of biological sample may be moved across a 2D plane. A scanning type motion can be made and at each location a DESI mass spectrum can be collected. Microscopic images can then be overlaid with mass spectral intensity profiles correlating to ions of interest to show locations of particular analytes within biological media. Figure 1.7 shows a schematic of the operation of DESI and an example of DESI imaging of a flower.

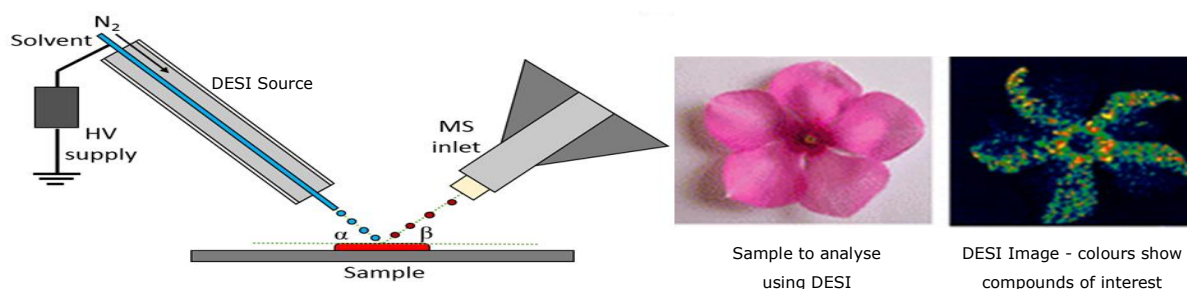


Figure 1.7 Left) Schematic representation of a DESI source in operation adapted from⁵¹ & Right) an example of DESI imaging of a flower highlighting a particular compound of interest.⁵⁴

1.3 DART-MS

Direct analysis in real-time mass spectrometry (DART-MS) was introduced by Cody and co-workers in a 2003 patent (filed),⁵² and was later introduced in an introductory paper in 2005.⁵⁵ DART is a type of APCI technique that requires no sample preparation. The key components of a DART source are shown in Figure 1.8.

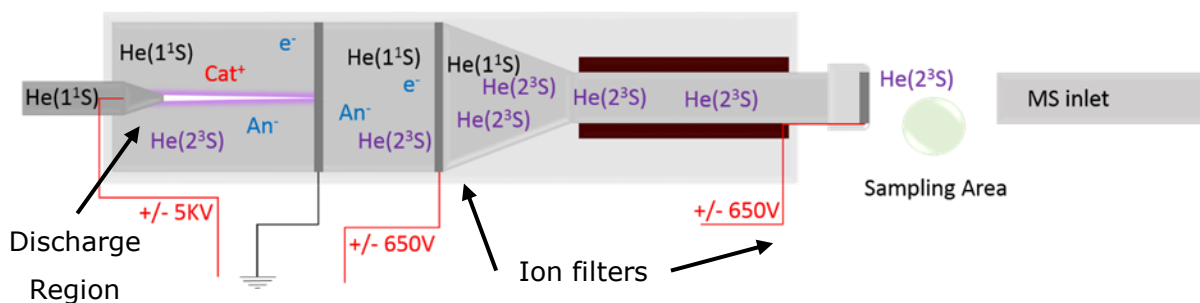


Figure 1.8 A schematic cutaway view of the original DART source operating under helium. Ground state helium (1^1S) is moved to its metastable state (2^3S) inducing sample ionisation. Adapted from⁵⁶

The name DART doesn't describe the mechanism by which the source operates unlike many other techniques. As described by Gross⁵⁷ the actual name that describes the DART source is a 'TDPIIAPCI' thermal desorption Penning ionisation-induced atmospheric pressure chemical ionisation source. The simpler acronym DART describes what the source does: analyse samples directly in real-time.

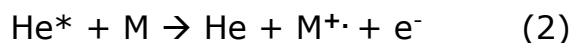
Since DART is an APCI based technique, it requires a carrier gas which is most often helium, nitrogen or argon. The choice of carrier is significant as the energetic species formed during the ionisation carry varying amounts of energy, which is of critical importance to the type of mass spectrum obtained.

The carrier gas is passed through a tube into the first region of the DART source where the gas becomes energised. If a noble gas such as helium or argon is used Penning ionisation occurs. Penning ionisation occurs through interaction of the gases with a glow discharge (a high voltage discharge between two points), the Penning ionisation induces the carrier gas into a metastable state (either vibrational or electronic). Around the discharge area other energetic species are developed radicals, ions (both cationic and anionic) and electrons carried through the gas stream, left hand region of Figure 1.8.

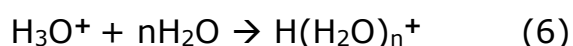
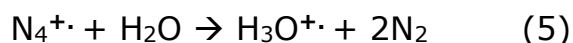
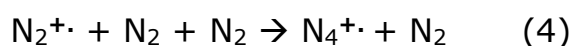
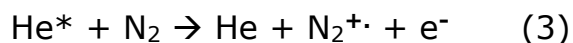
The charged species are filtered out by a series of electrodes as shown in Figure 1.8. These electrodes have a bias charge applied to them so that the ionisation polarity may be selected, this may be either positive or negative.

The DART source also contains a heating element so that a hot gas can be produced to aid the thermal desorption processes often required to analyse samples.

Since helium is almost exclusively used as the ionisation gas the ionisation mechanism will be explained using helium (see Schematic 1.4).



or



Schematic 1.4 Positive ionisation of analytes through interaction with metastable helium

Initially helium is energised into a metastable state (denoted as He*) through Penning ionisation induced by the corona-glow discharge (1).⁵⁸ The reason helium is used is one of its metastable forms (He 2³S) holds a high energy of 19.8 eV, sufficient to ionise most materials⁵⁹ The He* can interact with gas phase species upon reaching the atmosphere, either, naturally abundant gases (such as N₂ or O₂) or with gas phase analytes themselves. If He* reacts directly with a gas phase analyte with a lower ionisation energy than 19.8 eV then the molecular radical ion may be produced (2). Alternatively the He* follows a similar route to standard APCI ionisation where the charge is generated and passed on to form protonated water clusters (3-6).⁶⁰ The water clusters then act as reagent ions (as in APCI) and protonate the analyte (7).⁶¹

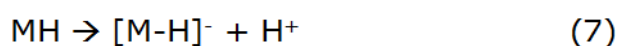
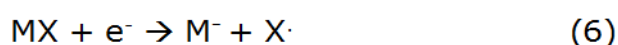
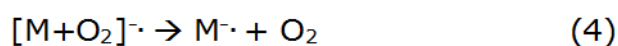
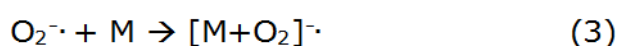
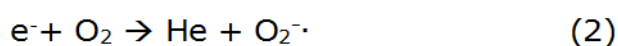
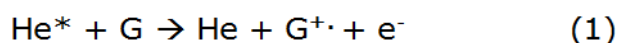
Again, since He* carries a relatively large amount of energy it may generate a range of ions that may induce Penning ionisation directly with gaseous analytes. N₄^{•+}, O₂^{•+} and NO^{•+} have all been shown to form analyte molecular ions [M]^{•+}.⁵⁷

Adducts may also be generated and are commonly observed depending on the atmosphere around the DART source. Typically, ammonium adducts ([M+NH₄]⁺) may be observed along with protonated molecular ions due to the natural ammonia present in the atmosphere (between 0.2 and 22 μg m⁻³ in the UK).⁶² It was found that ammonium adduct formation was significantly more stable than the corresponding protonated molecular ion formation when using selected gases.⁶³

Schematic 1.5 shows the potential analyte ion formation through negative mode interactions operating in DART. The same metastable helium formation is assumed to generate the thermally ejected electrons generating the reagent ions (1). Electron capture

processes occur between atmospheric oxygen and the liberated thermal electrons forming oxygen radicals (2). Molecular ions may be generated as either oxygen adducts (3) or as the molecular radical ion through loss of the recently bound oxygen (4).⁵⁵

Electrons may also react directly with the analyte to form the molecular radical ion through direct electron capture (5), or a molecular ion may be generated through dissociative electron capture (6). Deprotonation can generate a molecular ion (7) with basic interactions or through anionic attachment (8).⁶⁴



Schematic 1.5 Negative ionisation of analytes using negative mode DART.

The DART source relies on thermal desorption of analytes from the surface of the introduced sample. Typically a working temperature range of ambient to 500 °C may be set, with higher boiling point compounds requiring higher temperatures for thermal desorption to occur,⁶⁵ while low temperatures may be used for highly volatile compounds.⁴⁵ Significant differences between the set temperature and the measured temperature of the DART gas have been explored⁶⁶ and are covered in more detail in Chapter 2.

In some cases ionisation can occur without external heating, even for low volatility compounds such as salts. It was proposed that this effect arises from a chemical sputtering process which occurs when charge clusters build up on solid analytes.⁵⁵

Since DART is a thermal based technique increasing temperatures have been shown to lead to an increase in in-source fragmentation, a method in which an analyte has sufficient excess energy (in this case provided thermally) to undergo self-fragmentation. This can be particularly problematic at higher temperatures when relative signal intensities of fragment ions increase leading to undesirable excessive fragmentation, profile misinterpretation and overall loss of signal.⁶⁷

Another important factor directly relating to the temperature is the distance between the sample, DART exit and MS inlet. Manufacturers guidelines recommended that samples should be introduced close to the DART source (within 3 mm) but care must be taken not to contaminate the exit cap of the source. The distance variation created here causes significantly different mass spectral profiles to be obtained⁶⁸ and may impact the DART's ability to be used quantitatively.

Originally, samples were introduced directly into the DART stream using a pair of tweezers but a range of sample introduction methods have now been developed. For qualitative analysis most samples can be introduced directly into the heated gas stream using tweezers or on a glass rod (either a melting point tube or the commercially available DIP-it[®] tip). This approach provides a mass spectrum usually within seconds of sample introduction. For quantitative analysis using DART the use of transmission mode (TM) DART is often employed. TM-DART works by introducing a rail (often motorised) across the path of the DART stream, samples (primarily liquids) are placed onto a metal mesh and placed within the sample rail. The metal mesh is gradually passed in front of the DART source and the ionising stream passes through the mesh and ionises analytes bound to the mesh itself.

Less common techniques include thin layer chromatography (TLC) plate holders, for synthetic reaction monitoring,⁶⁹ and tablet holders for pharmaceutical applications.⁷⁰

1.4 Applications of DART-MS

DART-MS has found applications in a wide variety of fields since its commercial introduction in 2005. Some of the key applications, discoveries and recent advancements are described below.

1.4.1 Forensics

In a recent review by Hall *et al.* the authors note the use of DART as an excellent analytical tool for the forensic scientist.⁷¹

DART-MS was found to be an excellent method for analysis of energetic compounds, such as explosives, having rapid and sensitive screening whilst adding the additional resolution needed for qualitative assignment.⁷² The analysis of energetic materials is covered in further detail in Chapter 5.0.

The risk associated with chemical warfare agents are currently headline news.⁷³ Understandably the detection of these compounds (which are usually volatile and in low concentrations) is of paramount importance. DART-MS has been applied to the

identification of a nerve agent and its derivatives which were successfully detected on a range of surfaces, concrete, foliage and even bird feathers.⁷⁴

In a novel application DART-MS was applied to the analysis of exotic woods. The sale of certain lumbers is internationally prohibited on rare and endangered species of certain trees. Usually, it requires a specialist to identify different species of the same genus and this is usually achieved through morphological studies, a time consuming process. The study monitored volatiles released from lumber samples during DART-MS analysis. Characteristic compounds were noted between species and using a type of statistical analysis known as principle component analysis (PCA) trends were found to correctly identify unknown samples.⁷⁵

The literature contains a large number of forensic and potential forensic applications of DART-MS including seized drug identification,⁷⁶ toxicological studies of metabolites⁷⁷ and determination of document authenticity through studies of papers.⁷⁸ The potential of DART-MS as a screening tool for forensic science has become so apparent that a freely available mass spectral database has been created to quickly help identify unknown substances of forensic interest. Currently, the database holds spectra for over 800 substances of forensics interest.⁷⁹

1.4.2 Quality control

DART-MS has also been found to be particularly useful for routine analysis within the quality control (QC) sector. The attractiveness of the technique is the high throughput that can be obtained using the rapid analysis capability of DART-MS.

A paper by Zhang *et al.* described work on the analysis of illegal compounds added to cosmetics particularly glucocorticoids which serve as anti-inflammatories reducing acne and dermal creasing. Although these compounds have desirable properties, repeated exposure has been associated with adverse skin problems. The authors used a 96 well plate attached to a motorised stage to allow for rapid screening of liquid samples deposited on individual glass slides. This method allowed quantitative detection of glucocorticoids through the addition of an internal standard.⁸⁰

In another study, DART-MS was employed to analyse pharmaceutical products for ethylene glycol and diethylene glycol which are toxic and their level in formulations is strictly regulated. Samples were spiked with both ethylene glycol and diethylene glycol at threshold concentrations to determine if DART was able to analyse the compounds in the matrix of the formulation. The authors demonstrated that DART-MS was excellent at detecting the spiked trace components and the speed of analysis was significantly higher than the traditional method using a GC.⁸¹

The food and drinks sector has found applications for DART-MS to study polymer additives in food packaging. This is of particular importance as certain additives have been shown to migrate into the food through close contact with the encasing plastic. Ackerman *et al.* used DART-MS to identify Irganox, a common stabilising agent, in a HDPE polymer matrix.⁸² The potential benefit of DART-MS is that the additives can be rapidly analysed directly from both the polymer itself and also samples of the packaged food.

In addition, DART-MS has also been used for environmental analysis,⁸³ pharmaceutical studies⁸⁴ and the profiling of synthetic chemistry reactions.⁸⁵

1.5 Recent developments in DART-MS

The introduction of DART-MS has provided a powerful technique for the analytical chemist. However, limitations of the initial system were recognised both by IonSense®, a manufacturer, and the broader DART-MS community.⁸⁶

The first major development for DART came from the introduction of the DART-SVP the DART-100's replacement (see Figure 1.9) in 2009. The DART-SVP uses a fixed flow rate and pressure of carrier gas to help with lab-to-lab reproducibility. Further consideration of the fluid dynamics of the gases exiting the source cap were used in the design of the successor model, the results from the study were based on how the stream of gas moves around introduced glass rods.⁸⁷

Most plasma ionisation techniques use helium, and the majority of the literature reports the use of this gas with DART-MS. However, the expense and possible eventual shortage of helium is of increasing concern.⁸⁸ To tackle this users are starting to evaluate the potential of cheaper and plentiful gases such as nitrogen and argon.⁸⁷

Nitrogen DART has been shown to typically rely on direct Penning ionisation of the analytes themselves since the ionisation energy of nitrogen is insufficient to generate water clusters as in helium DART.⁸⁹ The use of nitrogen metastables appears to generate ammonia adducts (lower ionisation energy required to form ammonium adducts and insufficient energy to generate water clusters), which are more selective to non-polar molecules whilst helium remains more sensitive to the generation of protonated adducts.⁸⁹

IonSense® have introduced a number of ancillary attachments for the DART source, including the HT (high throughput) for large numbers of samples and the infusion module for assisted calibrations.⁹⁰

BioChromato have recently introduced a modification to the DART-MS inlet system known as the 'IonRocket'.⁹¹

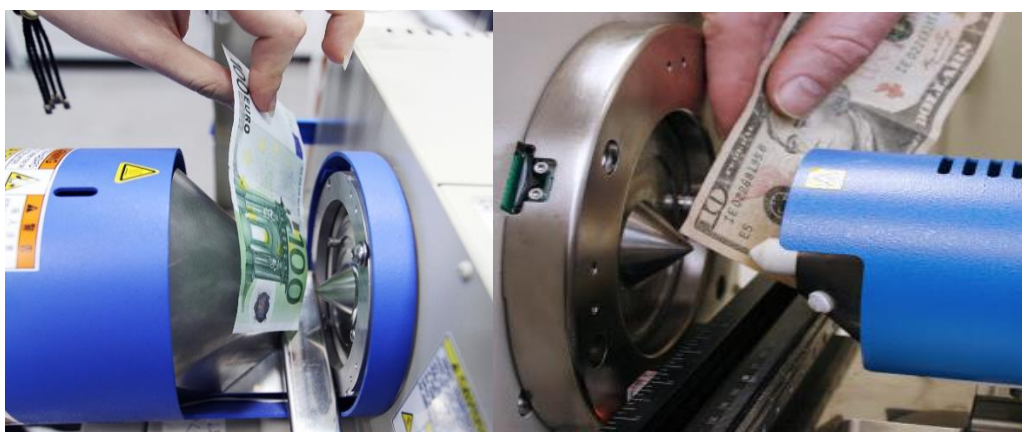


Figure 1.9 Left) The original DART-100 source⁹² and Right) the successor, DART-SVP.⁹³ Both analysing currency for trace compounds of drugs.

The IonRocket attempts to address the limitations of conventional DART associated with how the sample is heated. The unit is installed between the DART and MS interface with samples being placed in a small copper pot which is quoted to heat at a rate of $100\text{ }^{\circ}\text{C min}^{-1}$ between ambient and $600\text{ }^{\circ}\text{C}$. Evolved volatiles are ionised by the flowing DART stream before being pulled into the mass spectrometer.

Bridge *et al.* investigated the analysis of vehicle paint for forensic purposes. They thermally profiled layers of paint using an IonRocket-DART combination and detected analytes not seen using conventional DART-MS or by pyrolysis GC-MS.⁹⁴ H. Abe *et al.* also used the thermal profiling capability of the IonRocket for the rapid screening of drugs directly within complex matrices such as blood and urine noting the ease of sample preparation compared with alternative techniques.⁹⁵

Forbes and co-workers have introduced two techniques for thermally desorbing samples directly into the DART stream. In 2017 the group introduced the JHTD-DART-MS system, the name Joule heating thermal desorption describes the sample preparation step prior to DART ionisation. Samples are rapidly heated through heating of a resistive wire which causes them to thermally desorb. The group reported the additional benefit for the detection of explosive compounds that typically have low vapour pressures through the additional heat energy applied.⁹⁶ Another recent development by the group used an infrared heater to thermally desorb analytes on various swabbing materials, in a technique known as IRTD-DART-MS.⁹⁷

DART-MS continues to show significant growth and development within the field of MS. The rapid nature of the technique has allowed users to report on a variety of materials and an extensive bank of literature knowledge is being created. The hyphenation of ambient techniques as a whole appears to be a promising avenue for MS ensuring analytes remain intact for ease of deconvolution, opening the door of MS for non-mass spectrometrists.

1.6 Thermal analysis

Thermal analysis (TA) is a branch of analytical science concerned with the study and evaluation of the properties of a material with respect to temperature.

The initial IUPAC definition of TA excluded some key experiment types such as isothermal analysis and sample controlled thermal analysis (covered in Section 2.7.4.1).⁹⁸ As such, the definition was modified in 2014 to include these 'forgotten' experimental types, the latest IUPAC recommendation as presented by the ICTAC council is '*Thermal analysis (TA) is the study of the relationship between a sample property and its temperature as the sample is heated or cooled in a controlled manner*'.⁹⁹

In short, how does a material behave when heated or cooled?

In its broadest context TA has been practised for centuries, even if the methods were crude by today's standards. The earliest accounts of the utilisation of TA start with extracting metals from their ores around 8000 BC, the firing of pottery and later making glasses around 3400 BC, leading to the developments of Fahrenheit thermometry (the measurement of temperature) in the 18th century. It was after the development of thermometry and the introduction of the analytical balance that the controlled and quantitative studies of materials under the influence of temperature could be evaluated.¹⁰⁰

Today most thermal analysis techniques are typically categorised by the sample property which is being studied. Table 1.1 includes a list of some of the commonest TA techniques and the properties that are measured. Table 1.2 illustrates some common observable thermal events, the property of the sample measured and the associated TA technique used.

Table 1.1 The most common thermal analysis techniques

Thermal Analysis Technique	Property evaluated
Thermogravimetry (TG) Thermogravimetric Analysis (TGA)	Mass
Differential Thermal Analysis (DTA)	Temperature Difference
Differential Scanning Calorimetry (DSC)	Heat Flow (Enthalpy)
Thermomechanical Analysis (TMA)	Mechanical properties
Dynamic Mechanical Analysis (DMA)	Elastic modulus and dampening
Themomicroscopy (TM)	Optical properties

Table 1.2 A representation of common events observed during thermal analysis.

Thermal Event	Property Measured	TA used to measure the event
Solid → Solid	Phase transition	DTA, DSC, DMA & TM
Solid → Liquid	Melting	DTA, DSC & TM
Solid → Gas Liquid → Gas	Sublimation Evaporation	TGA, DTA, DSC,
Expansion	Size change	TMA, TM
Glass transition Solid(glassy)→Solid(rubbery)	Enthalpy Modulus Volume Change	DSC DMA TM

In accordance with the definition of TA, the sample must be subjected to a controlled temperature programme. This is achieved in a number of ways (see Chapter 2) but in essence the sample is situated in a furnace with heating achieved through applying current to a resistive wire, common in TGA. A thermal analysis experiment may comprise a sequence of heating, cooling and isothermal stages called a temperature programme. Most TA techniques measure the temperature of the sample directly. This is achieved through a variety of means including the measurement of changes in resistance in platinum wire¹⁰¹ or measurement of the voltage produced through thermoelectric generation between two metals of different composition known as the Seebeck effect (achieved by charge carriers migrating due to temperature differences between the materials).¹⁰²

The Seebeck effect is commonly employed in devices known as thermocouples. A range of thermocouples exist and are typically selected for the instrument's application, high temperature, sub-ambient or chemically aggressive environments.

Most TA instruments use samples with masses in the 1 – 20 mg range which are placed in pans or crucibles (typically made from metal or a ceramic) for analysis. The plot of the measured property as a function of temperature is sometimes called a 'thermogram'.

Atmospheric control is often an important factor in many TA experiments and the use of inert (such as helium or nitrogen) or oxidative (air) atmospheres can have a significant impact on the results obtained. In addition to the reactive nature of the atmosphere, differences in thermal conductivity and density can also have an effect.

1.6.1 Thermogravimetric Analysis (TGA)

Thermogravimetric analysis (TGA) measures changes in mass as a function of temperature. As mass is a fundamental property of a material it has wide application and is innately quantitative. TGA is used to measure thermal stability under different atmospheres as well as decomposition and adsorption/desorption processes.¹⁰³ TGA instruments operate over a wide temperature range from sub-ambient (ca. -120 °C) to well over 2000 °C in some commercial models.¹⁰⁴

The key component of TGA (apart from the furnace) is the balance mechanism which needs to be able to detect mass changes down to the microgram level. Figure 1.10 (left) shows a schematic representation of a TGA balance mechanism. A sample is supported on one side of the balance whilst an inert reference counter mass is on the opposite side of the cantilever. The amount of power input to keep the balance level will be proportional to the mass. The sample is situated within a furnace and the temperature is monitored by a nearby thermocouple.

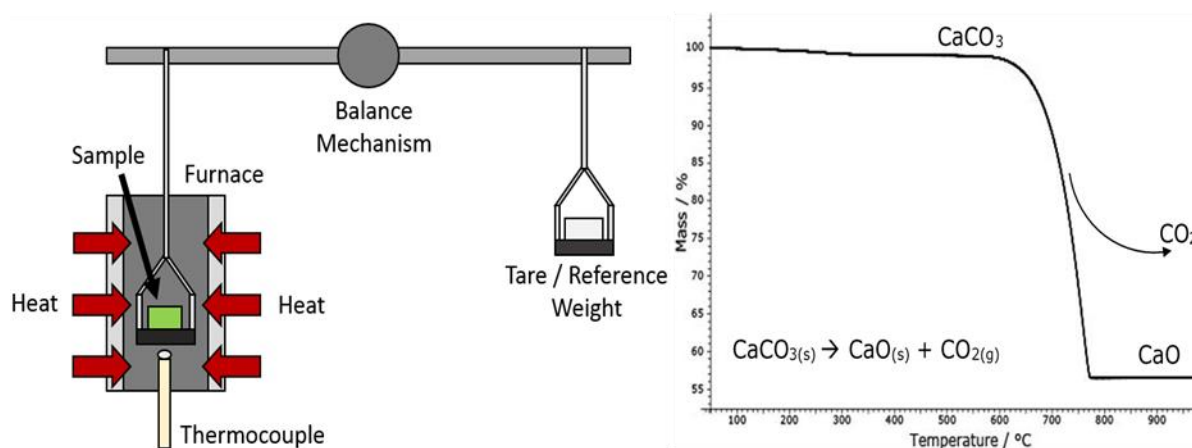


Figure 1.10 Left) A schematic representation of the 'hang down' balance mechanism used in some thermogravimetric analysers. Adapted from¹⁰³ & right) An example of a thermogram produced by TGA monitoring the decomposition of calcium carbonate.

Figure 1.10 (right) is an example of a TGA thermogram for the decomposition of calcium carbonate showing the quantitative nature of the technique. CaCO_3 (RMM 100 g mol^{-1}) decomposes to CaO (RMM 56 g mol^{-1}) with the loss of CO_2 (RMM 44 g mol^{-1}). The process is reflected by the mass loss of 44%.¹⁰⁵

The quantitative feature of TGA can be used to evaluate even quite complex materials which is often exploited within the polymer industry.

Jeske *et al.* showed that TGA could be used to determine the amounts of wood and co-polymer in a wood plastic composite demonstrating a clear use for the technique in manufacturing quality control.¹⁰⁶

1.6.2 Differential temperature techniques - DTA and DSC

Differential thermal analysis (DTA) and differential scanning calorimetry (DSC) are related techniques which utilise the difference in temperature between a sample and an inert reference material caused by enthalpic or heat capacity changes in the sample. As every physical or chemical process involves releasing or absorbing heat energy then DTA and DSC can be considered as universal TA techniques.

Figure 1.11 shows schematics of a DTA and DSC system. In DTA the sample and reference are separated and (nominally) there is no direct heat path between them. In standard (heat-flux) DSC the sample and reference are normally thermally linked through a shared thermally conductive metal plate.

Both techniques utilise a pair of thermocouples arranged in such a way that a differential signal (typically μV) is produced whenever there is a temperature difference between the sample and reference.

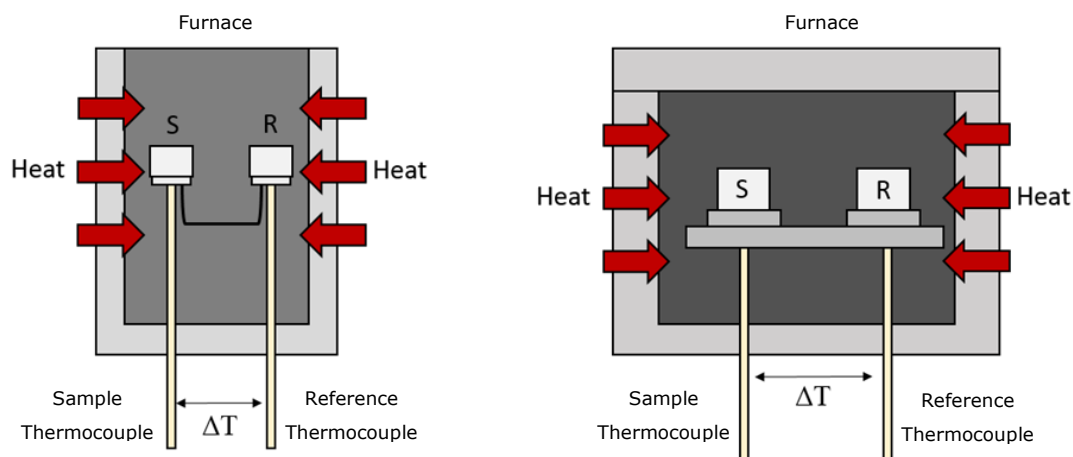


Figure 1.11 Schematic instrumental comparisons of DTA (Left) adapted from¹⁰⁷ and DSC (right) adapted from¹⁰⁸

The presence of a heat path in DSC means that the heat flow between sample and reference can be monitored and converted to a measurement of power after a suitable calibration factor is determined by using melting point standards. It is also considered more sensitive at lower temperatures. DTA on the other hand, is generally more sensitive at higher temperatures and without the requirement for an efficient heat path between sample and reference crucibles constructed from alumina or another refractory material.¹⁰⁹

The thermogram profiles obtained for these differential techniques are functionally identical, although as stated it is the measurement that differs.¹¹⁰ When the sample temperature lags behind the reference temperature the sample is undergoing an endothermic transition such as a melting or dehydration. In contrast when the sample leads the reference temperature the process is exothermic, examples of observable exothermic processes include crystallisations and oxidations.¹¹¹

Figure 1.12 shows an example of a DTA thermogram obtained for polylactic acid.¹¹²

This example serves well to demonstrate some of the key features noted by differential temperature techniques. Initially an endotherm is shown around 60 °C, and this can be attributed to the glass transition (T_g) of the polymer, note the step change in baseline (due to a heat capacity change) and the accompanying endotherm caused by the polymer 'relaxing'. The second event between 90 and 120 °C shows a broad exothermic process known as cold crystallisation, this is a common event that occurs between T_g and the melting point, this process is covered in further detail in the Chapter 4. The final event is the endothermic melting around 140 °C, since the material requires more energy to melt and undergo a solid-liquid phase transition the sample 'lags' behind the reference during the event and gives the melting profile before returning to the baseline when sample and reference show no changes in enthalpy.

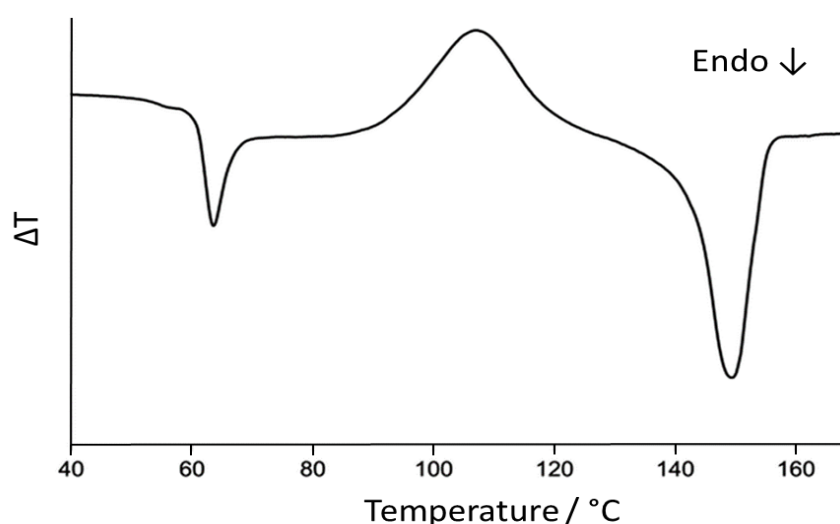


Figure 1.12 A differential temperature trace obtained for polylactic acid. Adapted from.¹¹²

Low temperature phase change materials (PCMs) are increasingly being incorporated into construction materials (such as concrete) as a chemical means of energy storage. During the day the materials will be heated until they undergo an endothermic phase change taking in excess energy. During the night when temperatures fall, the materials exothermically revert to their original phase releasing the stored energy.¹¹³ Ge *et al.* have shown how DSC is an ideal technique to evaluate the effectiveness of different PCMs.¹¹⁴

DTA finds its main uses today as a complimentary technique for TGA or for high temperature work. A simultaneous thermal analyser (STA) combines both a TGA and a DTA (or sometimes DSC) to yield a very powerful technique, resulting in both enthalpic changes and mass losses being monitored simultaneously. Applications of DTA used in a STA system are numerous. Lalia-Kantouri *et al.* have shown how the technique can be used to determine the authenticity of historically significant bricks and the temperatures at which they were likely to have been formed.¹¹⁵

1.6.3 Thermomechanical Analysis (TMA)

Thermomechanical analysis (TMA) is the study of the dimensional changes of a material as a function of temperature and is widely applied to the study of deformations or relaxations of materials that will be subjected to environmental temperature changes.¹⁰³

TMA works by applying stress, usually compressive or tensional, to a material as it is heated. It is ideally suited to studying the softening of a material during a glass transition (T_g) or measuring the extent of expansion of a material during a heating or cooling.

Figure 1.13 shows examples of how these properties are measured, the probe distance changes when the material softens through T_g the probe displacement is continuous for a thermally expansive material.

Ouyang *et al.* applied TMA to the determination of the glass transition temperature (T_g) of synthetic fibres through the change in the coefficient of linear thermal expansion (CTLE) above and below the glass transition temperature.¹¹⁶ The authors used this method to evaluate the properties of the fibrous material as a function of different spinning speeds used in the manufacturing process.

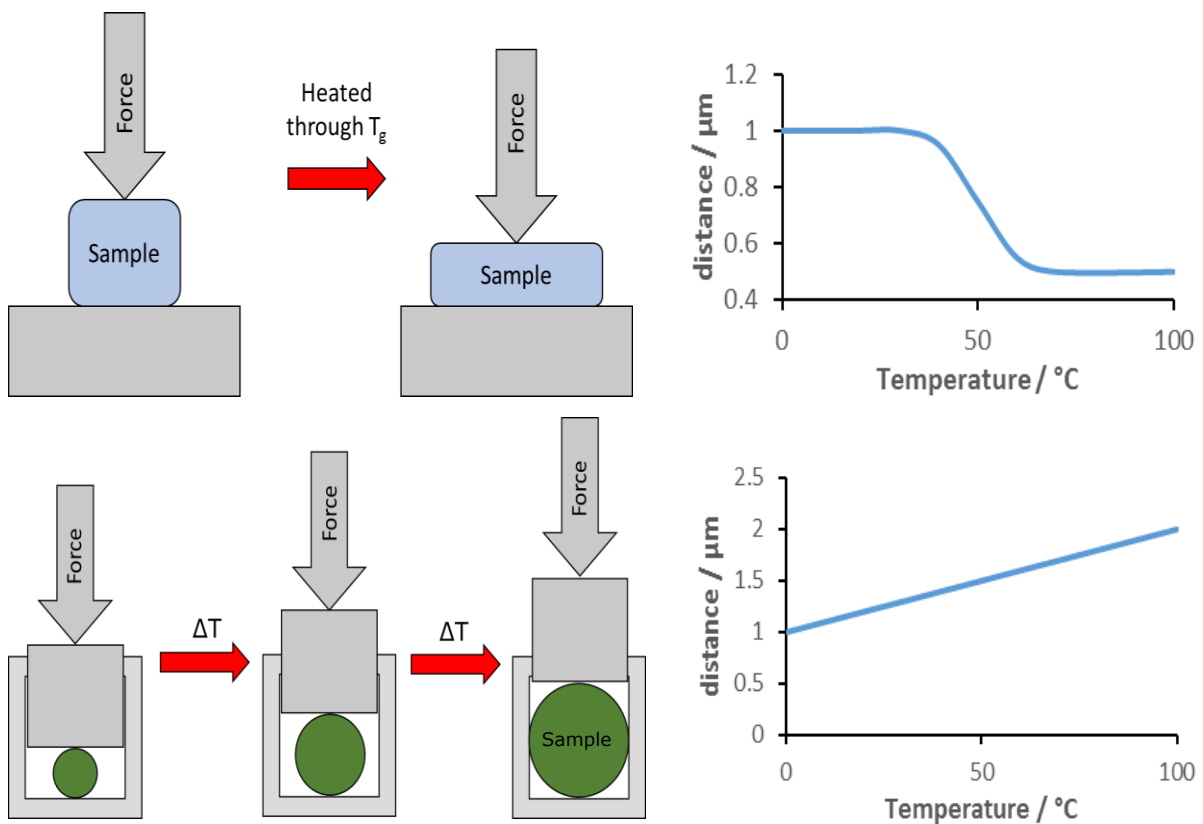


Figure 1.13 Representation of how TMA is applied to monitor dimensional changes in materials.

1.7 Hot-Stage Microscopy

Hot-stage microscopy (HSM) and thermomicroscopy (TM) are terms used interchangeably to describe instrumental techniques for thermoptometry, a process where an optical property is monitored as a function of temperature.

There are many variants of thermoptometry including, thermoluminescence analysis (monitoring light emitted from a material), thermophotometric analysis (monitoring the intensity of reflected light) and thermospectrometric analysis (monitoring the reflected or transmitted wavelengths).¹⁰⁰ However, in contrast to TG and DTA/DSC, HSM is a relatively unused technique and many TA users may not realise the useful information that it can provide.

There are broadly two main types of HSM systems distinguished by how the optics are orientated and the nature of the sample being analysed. Both use a heated stage to transmit heat through to the sample so that optical data may be collected as a function of temperature.

One type of HSM uses a compound microscope (Figure 1.14, left hand image). Typically, this type uses higher magnifications and relies on the sample being transparent as light is transmitted through the sample. It is particularly useful for studying processes such as melting or phase changes in small samples such as single crystals.

The other HSM type utilises a stereoscopic microscope (Figure 1.14, right hand image). This form is a surface imaging technique and is not limited to transparent samples. It is most useful for materials that undergo changes in colour or geometry and is mainly applied to the study of larger samples around 10 mg (more typical of conventional TA).

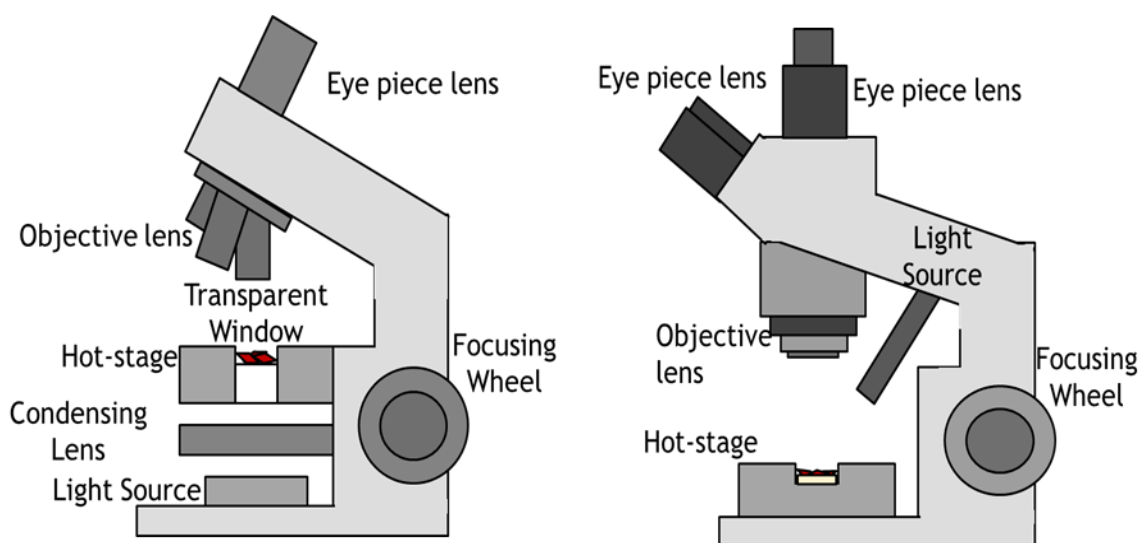


Figure 1.14 A graphical comparison of the two types of hot-stage microscope system. Left) Compound HSM and Right) Stereoscopic HSM.

1.7.1 Applications of HSM

Both compound and stereoscopic hot-stages are available commercially and often come with a range of attachments for analysis in more demanding environments. The atmosphere of most HSM systems can be controlled by covering the sample with a transparent window allowing the effects of oxidative and inert atmospheres to be studied.

In a study by Charsley *et al.* a reductive atmosphere was used to convert lead oxide into its metallic form, since the reduction occurred at a temperature above the melting point of lead (327 °C) the metallic lead was found to coalesce into a single bead of molten metal.¹¹⁷

As well as selective atmosphere control, reduced atmospheres may be generated through the attachment of a vacuum. Thorsen *et al.* applied HSM to high temperature welding studies under vacuum conditions and showed that by adjusting the pressure the temperature at which metallic brazing occurred could be shifted.¹¹⁸

Many HSM systems allow sub-ambient studies through the use of Peltier coolers or liquid nitrogen. Diogo and Ramos have recently demonstrated the identification of two different polymorphic forms of a potential pharmaceutical compound by using a combination of sub-ambient HSM and DSC.¹¹⁹

There are many published articles on the application of compound HSM to the study of cocrystals. Perpétuo *et al.* studied the formation of a cocrystal between ketoprofen and nicotinamide using polarised (light oriented in a single plane) light microscopy (PLTM).¹²⁰ PLTM allows investigation into the birefringence of a material, a type of double refraction causing a colour to appear in crystalline materials although for amorphous materials or crystals in a cubic form this effect is not observed and the material cannot be discerned from background due to low contrast.¹²¹

Compound HSM has also been applied to the study of liquid crystals where phase changes can have low energy, making DSC studies difficult, but have significant optical changes. Meltzer and co-workers have reported this effect through comparative studies between DSC and polarised HSM when investigating a cholesterol-based liquid crystal system.¹²²

HSM has the capability to monitor formation of gases when the sample is liquid or submerged within an oil. Small microbubbles, formed as gaseous products are released can be detected. This can be particularly important for monitoring the degradation of pyrotechnic compositions to show the onset of degradation prior to the ignition temperature. Pyrotechnic compositions will typically show sharp mass losses through TGA, but through HSM earlier stages of decomposition can be seen.¹²³ The method of monitoring gaseous product formation is commonly utilised in HSM by submerging the sample in a liquid (demonstrated in Figure 1.15).¹²⁴

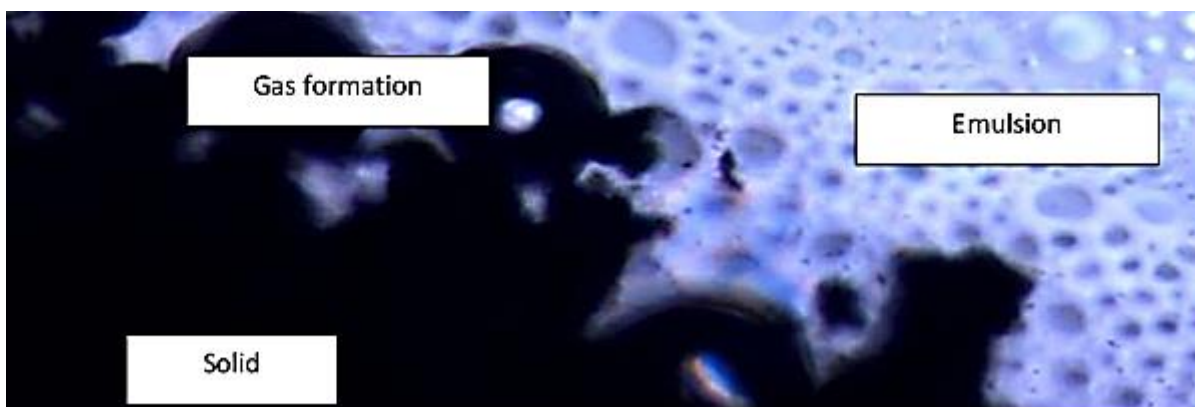


Figure 1.15 An example of HDM monitoring gaseous product release. Adapted from¹²⁴

Thermochromics are a class of compounds which undergo a phase change, often reversible, associated with a colour change making thermochromics ideally suited to HSM analysis. Bourne *et al.* showed the potential of HSM in their study of thermochromism for crystals of an organometallic cobalt complex as shown in Figure 1.16.¹²⁵

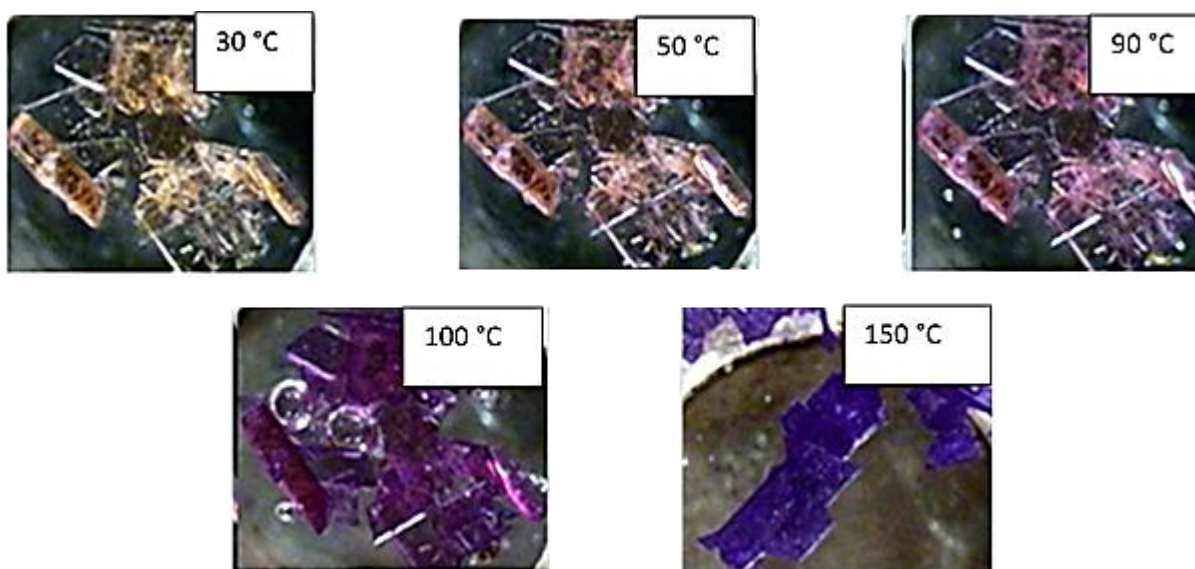


Figure 1.16 An example of a thermochromic material studied using HSM. Adapted from¹²⁵

Another study by Miyake *et al.* used stereoscopic HSM to study the effects of the decomposition of ammonium dinitramide, a solid classified as an energetic material. The decomposition was initiated through the melting of the dinitramide and subsequent reaction with a copper oxide catalyst. Through monitoring the colour, surface effects and correlation with evolved gases techniques the authors were able to evaluate a decomposition pathway.¹²⁶

1.8 Simultaneous TA & Hyphenated TA techniques

The benefits of combining thermal analysis techniques (sometimes termed hyphenated techniques) to increase the information obtained in a single experiment has long been recognised, particularly in cases where samples may be in limited supply such as extraterrestrial samples, historical artefacts or materials that are difficult or expensive to synthesise.¹⁰⁰

The combination of TG-DTA, or TG-DSC, discussed earlier, is the most common hyphenated technique and the term simultaneous thermal analysis (STA) specifically applies to it. Although there are benefits, there can be compromises with hyphenated techniques as the desirable conditions for one technique may conflict with the other so the results may be weaker than both performed individually. However, these difficulties have been partly addressed with the improvements in electronics, computing and modern precision engineering.¹⁰³

Evolved gas analysis (EGA) is a thermal analysis technique where gases released by a sample during heating (either through desorption, decomposition or reaction) are monitored. Typically, techniques such as MS or Fourier transform infrared spectroscopy (FTIR) are used to allow identification of unknown volatiles. Although sometimes used as a separate technique, EGA is most commonly linked with another TA technique such as thermogravimetry. In TG-FTIR, the whole gas flow (carrier, reactant and product gases) passes directly from the TGA to the FTIR for analysis so the concentrations of gaseous analyte remain representative of product evolution.¹²⁷

TG-MS is typically quicker, more sensitive and is significantly less subjective to spectral interpretation than FTIR, but does come with compromises such as higher instrument maintenance and generally higher instrument cost. In addition, reduced flow rates are usually required for better mass spectra generation, meaning that only a small portion of the gas stream is sampled.¹²⁸ There is the additional complexity of ensuring the transfer line between the sample and gas analyser is short and sufficiently heated to ensure that minimal condensation occurs and the lag between vapour formation and detection is minimal.

In both methods (MS or FTIR) of TG-EGA advanced graphics such as 3D plots may be produced to represent how the chemical information (m/z or wavenumber) and intensity change as a function of temperature or time. This is usually combined with an overlay of the TG thermogram. Bakierska and co-workers¹²⁹ used TG-FTIR to investigate the decomposition products generated through the thermal analysis of aerogels synthesised from different polysaccharides (see Figure 1.17).

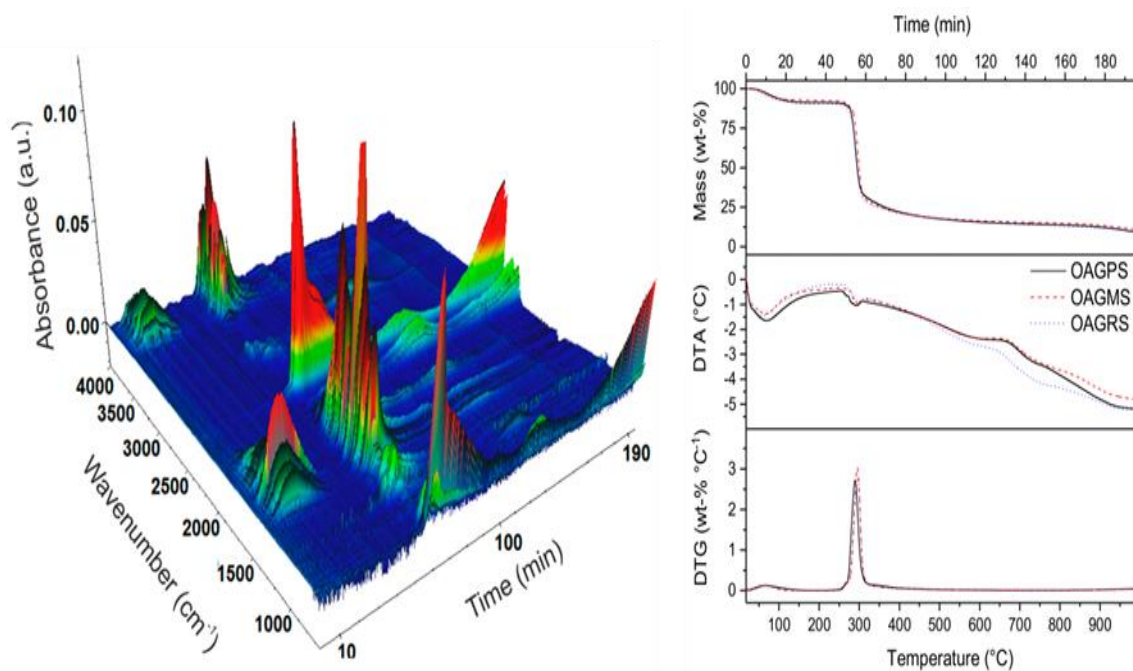


Figure 1.17 An example of data generated through TG-FTIR. Left) FTIR time profile Right) TA data. Adapted from¹²⁹

In early research by Haines and Skinner, a DSC was modified so that a microscope could be focused onto the sample pan. The authors noted that topological changes in the sample could be monitored by the addition of a light sensor to the microscope eyepiece to measure the reflected light intensity (RLI). RLI allowed subtle changes in the sample, not detected by the DSC, to be observed and highlighted the benefit of the combination of the two techniques.¹³⁰

HSM-DSC has seen significant growth recently with the introduction of commercial instrumentation Sorrentino *et al.* noted how crystal growth in polymers is typically studied separately through enthalpic methods (such as DTA or DSC) and through surface analysis (microscopy) and that combining the techniques had obvious benefits.¹³¹

Alimi *et al.* used a DSC600 HSM-DSC (Linkam) to study a property known as thermosalience where a crystal 'jumps' or explodes during thermal cycling as a result of changes in internal mechanical strain (Figure 1.18). The DSC trace shows how a large exotherm accompanies the thermosalience of the crystal during cooling whilst the micrographs provided by the microscope show the crystal fragmentation.¹³²

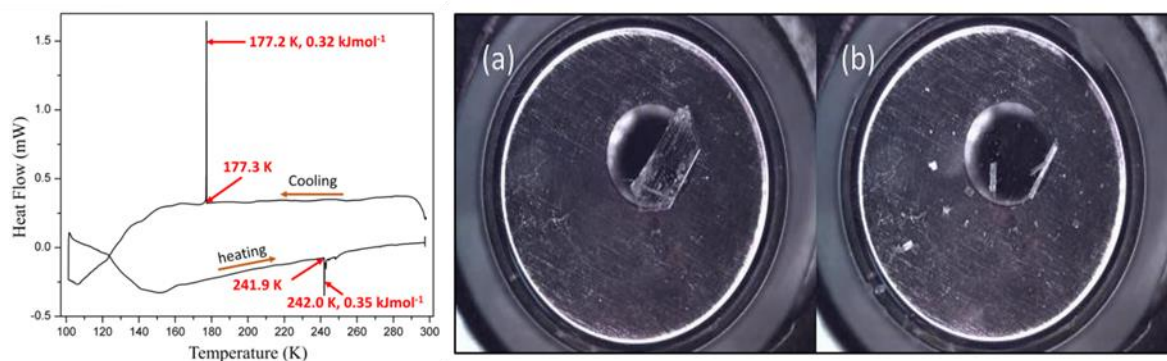


Figure 1.18 Thermosalience demonstrated using HSM-DSC. Left) DSC of the energetic event & Right) micrographs of a single crystal of *p*-aminobenzonitrile exploding during cooling.

The combination of microscopy with TGA has been evaluated by Matzakos and Zygourakis who used a TGA coupled with a video microscope to allow monitoring of samples within the sample pan of a hang down balance mechanism within a furnace. The authors used this arrangement to monitor coal under rapid heating and pyrolysis conditions.¹³³

The literature does appear to be lacking in hyphenated HSM-EGA techniques. As described earlier HSM users readily submerge their samples to monitor the formation of gaseous products, but monitoring these products through more sophisticated techniques appears almost unexplored. The use of microscopy with mass spectrometry is becoming more abundant within the literature even though HSM and EGA is lacking.^{134, 135}

One of a few papers that documents HSM used in combination with a mass spectrometer was reported by Lamprecht *et al.* The technique hyphenation was actually developed from a HSM-TG arrangement. To further characterise the TG profile the vented gas stream from the hot-stage was introduced directly into a quadrupole MS.¹³⁶

The authors used the combination of the three techniques HSM, TG & MS to monitor differences in how lichens (a symbiotic organism between an algae and fungi) deteriorate ancient pigments. This was achieved by monitoring the degradation of calcium oxalate films formed by the different organisms and thermally profiling them.

The technique shows how morphological changes can be linked to mass losses and with the addition of a mass spectrometer the gaseous products could be assigned.

The development and application of an integrated *hot-stage microscope direct analysis in real-time mass spectrometry* system is described within the upcoming chapters combining well established thermal analysis and mass spectrometry methods. This work aims to address the missing 'gap' within the literature through this combination of analytical techniques HSM and DART-MS.

1.9 Introduction References

- ¹ J.T. Watson & O.D. Sparkman, *Introduction to Mass Spectrometry*, 2007, 4th ed., John Wiley & Sons, West Sussex, England
- ² T.D.Märk & G.H. Dunn, *Electron Impact Ionization*, 1985, Springer-Verlag Wien
- ³ D.I. Carrol, I. Dzidic, E.C. Homing and R.N. Stillwell, *Appl. Spectrosc. Rev.* 1981, **17**, 337-352
- ⁴ J.B. Farmer & C.A. McDowell, *Mass Spectrometry*, 1963, McGraw-Hill, NY
- ⁵ S. Guan & A.G. Marshall, *J. Am. Soc. Mass. Spectrom.*, 1996, **7**, 101-106
- ⁶ D.W. Koppenaal, C.J. Barinaga, M.B. Denton, R.P. Sperline, G.M. Hieftje, G.D. Schilling, F.J. Andrade & J.H. Barnes, *Anal. Chem.*, 2005, **77**, 418-427
- ⁷ W. Wien, *Ann. Physik.*, 1898, **65**, 440
- ⁸ J.J. Thomson, *Rays of Positive Electricity and their Application to Chemical Analysis*, 1913, Green and Co. London.
- ⁹ F.W. Aston, *Phil Mag.* 1920, **39**(323), 449-455
- ¹⁰ A.J. Dempster, *Phys. Rev.*, 1918, **11**(4), 316-325
- ¹¹ W. Bartky & A.J. Dempster, *Phys. Rev.*, 1929, **33**, 1019
- ¹² M.A. Grayson, *Measuring Mass: From Positive Rays to Proteins*, 2002, Chemical Heritage Press, Philadelphia.
- ¹³ F.H. Field, *Mass Spectrom. Rev.*, 1994, **13**, 99-101
- ¹⁴ W.R. Smythe and J.H.E. Mattauch, *Phys. Rev.*, 1932, **40**, 429-433
- ¹⁵ W.E. Stephens, *Phys. Rev.* 1946, **69**, 691
- ¹⁶ M.M. Wolff & W.E. Stephens, *Rev. Sci. Instr.*, 1953, **24**, 616-617
- ¹⁷ M. Guilhaus, *J. Mass Spectrom.*, 1995, **30**, 1519-1532
- ¹⁸ D. Ioanoviciu, *Int. J. Mass Spectrom. Ion Proc.*, 1994, **131**, 43-65
- ¹⁹ M. Karas, D. Bachmann, U. Bahr & F. Hillenkamp, *Int. J. Mass Spec. Ion Proc.*, 1987, **78**, 53-68
- ²⁰ K.A. Nier, A.L. Yergey & P.J. Gale, *The Encyclopedia of Mass Spectrometry: Volume 9: Historical Perspectives, Part B: Notable People in Mass Spectrometry*, 2015, Elsevier
- ²¹ R.E. Ardrey, *Liquid Chromatography-Mass Spectrometry : An Introduction*, 2003 Hoboken, John Wiley & Sons, Incorporated.
- ²² C. Dass, *Fundamentals of Contemporary Mass Spectrometry*, 2007, Hoboken, N.J. Wiley-Interscience
- ²³ C.G. Herbert, R.A.W. Johnstone, *Mass Spectrometry Basics*, 2003, London, Boca, Raton, CRC Press
- ²⁴ Paul *et al.* US 2939952 Apparatus For Separating Charged Particles Of Different Specific Charges Jun 1960
- ²⁵ B. Brkić, N. France, A.T. Clare, C.J. Sutcliffe, P.R. Chalker & S. Taylora, *J. AM. Soc. Mass Spectrom.*, 2009, **20**, 1359-1365
- ²⁶ E. Lopez-Capel, G.D. Abbott, K.M. Thomas & D.A.C. Manning, *J. Anal. Appl. Pyrolysis*, 2006, **75**, 82-89
- ²⁷ W. Paul, *Agewandte Chemie- International Edition*, 1990, **29**, 739
- ²⁸ R.E. March, *Int. J. Mass Spectrom.*, 2000, **200**(1-3), 285-312
- ²⁹ L.D. Bowers & D.J. Borts, *Clinical Chemistry*, 1997, **43**(6), 1033-1039
- ³⁰ P.S.H. Wong & R.G. Cooks, *Bioanalytical Systems, Inc.*, 1997, **16**(3)
- ³¹ A.G. Marshall, C.L. Hendrickson & G.S. Jackson, *Mass Spectrom. Rev.* 1998, **17**(1), 1-35
- ³² W. Paul & H. Steinwedel, *Rzeitschrift für Naturforschung A*, 1953, **8**(7), 448-450
- ³³ Q. Hu, R.J. Noll, H. Li, A. Makarov, M. Hardman & R.G. Cooks, *J. Mass Spectrom.*, 2005, **40**(4), 430-43
- ³⁴ J.H. Gross, *Electron Ionization. In: Mass Spectrometry*. 2004, Springer, Berlin, Heidelberg
- ³⁵ J.-P. Schermann, *Spectroscopy and Modeling of Biomolecular Building Blocks*, 2008, 1st ed., Elsevier Science, Netherlands.
- ³⁶ S. Alves, E. Rathahao-paris, J.C. Tabet, *Potential of fourier transform mass spectrometry for high-throughput metabolomics analysis*, 2013, vol. 67, Amsterdam Elsevier Ltd.
- ³⁷ R.A. Hites, *Anal. Chem.*, 2016, **88**, 6955–6961
- ³⁸ M.S.B. Munson and F.H. Field, *J. Am. Chem. Soc.*, 1966, **88**, 2621
- ³⁹ F.H. Field, *Accounts of Chemical Research*, 1968, **1**(2), 42-49
- ⁴⁰ R.J. Cotter, *Anal. Chem.*, 1980, **52**, 1589-1599
- ⁴¹ K.L. Busch, *J. Mass Spectrom.*, 1995, **30**, 233-240
- ⁴² M. Barber, R.S. Bordoli, R.D. Sedgewick, & A.N. Tyler, *Nature*, 1981, **293**, 270-275
- ⁴³ E.C. Horning, M.G. Horning, D.I. Carroll, I. Dzidic, & R.N. Stillwell, *Anal. Chem.*, 1973 **45**(6), 936–943
- ⁴⁴ W.C. Byrdwell, *Lipids*, 2001, **36**(4), 327-346
- ⁴⁵ Y. Dong, *Direct Analysis in Real Time Mass Spectrometry: Principles and Practices of DART-MS*, 2018, 1st ed. DE, Wiley-VCH.

- ⁴⁶ M. Barber, R.S. Bordoli, R.D. Segwick & A.N. Tyler, *J. Chem. Soc. Chem. Commun.*, 1981, **0**, 325-327
- ⁴⁷ P. Kebarle, *J. Mass Spectrom.*, 2000, **35**, 804-817
- ⁴⁸ M. Karas, D. Bachmann & F. Hillenkamp, *Anal. Chem.*, 1985, **57**, 2935-2939
- ⁴⁹ Y.-H. Lai & Y.-S. Wang, *Mass Spectrometry*, 2017, **6**, S0072
- ⁵⁰ M.E. Monge, G.A. Harris, P. Dwivedi, & F.M. Fernandez, *Chem. Rev.*, 2013, **113**, 2269–2308
- ⁵¹ Z. Takas, J.M. Wiseman, B. Gologan & R.G. Cooks, *Science*, 2004, **306**, 471
- ⁵² R.B. Cody & J.A. Laramee, *US Patent*, 6949741, 2005
- ⁵³ L.S. Eberlin, I. Norton, D. Orringer, I.F. Dunn, X.H. Liu, J.L. Ide, A.K. Jarmusch, K.L. Ligon, F.A. Jolesz, A.J. Golby, S. Santagata, N.Y.R. Agar & R.G. Cooks, *Proc. Natl. Acad. Sci. U.S.A.*, 2013, **110**, 1611
- ⁵⁴ R.G. Hemalatha & T. Pradeep, *J. Agric. Food Chem.*, 2013, **61**, 7477–7487
- ⁵⁵ R.B. Cody, J.A. Laramée & H.D. Durst, *Anal. Chem.*, 2005, **77**(8), 2297–2302
- ⁵⁶ Jeol, <https://www.jeol.co.jp/en/products/detail/DART.html> (accessed Aug 2018)
- ⁵⁷ J.H. Gross, *Anal. Bioanal. Chem.*, 2014, **406**, 63-80
- ⁵⁸ F.M. Penning, *Naturwissenschaften*, 1927, **15**, 818
- ⁵⁹ J.T. Shelley, J.S. Wiley, G.C.Y. Chan, G.D. Schilling, S.J. Ray & G.M. Hieftje, *J. Am. Soc. Mass Spectrom.*, 2009, **20**, 837–844
- ⁶⁰ F.J. Andrade, J.T. Shelley, W.C. Wetzell, M.R. Webb, G. Gamez, S.J. Ray & G.M. Hieftje, *Anal. Chem.*, 2008, **80**, 2646-2653
- ⁶¹ L. Song, A.B. Dykstra, H. Yao & J.E. Bartmess, *J. Am. Soc. Mass Spectrom.*, 2009, **20**, 42–50
- ⁶² Y.S. Tang, C.F. Braban, U. Dragosits, A.J. Dore, I. Simmons, N. van Dijk, J. Poskitt, G.D.S. Pereira, P.O. Keenan, C. Conolly, K. Vincent, R.I. Smith, M.R. Heal & M. A. Sutton, *Atmos. Chem. Phys.*, 2018, **18**, 705–733
- ⁶³ N. Sugimura, A. Furuya, T. Yatsu, Y. Igarashi, R. Aoyama, C. Izutani, Y. Yamamoto & T. Shibue, *European Journal of Mass Spectrometry*, 2017, **23**(1), 4-10
- ⁶⁴ C.N. McEwen & B.S. Larsen, *J. Am. Soc. Mass Spectrom.*, 2009, **20**, 1518-1521
- ⁶⁵ S.D. Maleknia, T.M. Vail, R.B. Cody, D.O. Sparkman, T.L. Bell & M.A. Adams, *Rapid Commun. Mass Spectrom.*, 2009, **23**(15), 2241-2246
- ⁶⁶ L.P. Harding, G.M.B. Parkes & J.D. Townend, *Analyst*, 2014, **139**, 4176-4180
- ⁶⁷ M. Curtis, M.A. Minier, P. Chitranshi, O.D. Sparkman, P.R. Jones & L. Xue, *J. Am. Soc. Mass Spectrom.* 2010, **21**, 1371
- ⁶⁸ G.A. Harris, C.E. Falcone & F.M. Fernández, *J. Am. Soc. Mass Spectrom.*, 2012, **23**(1), 153-161
- ⁶⁹ E.S. Chernetsova, A.I. Revelsky & G.E. Morlock, *Rapid Commun. Mass Spectrom.*, 2011, **25**(16), 2275-2282
- ⁷⁰ J.M. Wells, M.J. Roth, A.D. Keil, J.W. Grossenbacher, D.R. Justes, G.E. Patterson & D.J. Barket Jr, *J. Am. Soc. Mass Spectrom.*, 2008, **19**(10), 1419-1424
- ⁷¹ M.J. Pavlovich, B. Musselman & A.B. Hall, *Mass Spectrom. Rev.* 2018, **37**, 171-187
- ⁷² E. Sisco & T.P. Forbes, *Analyst*, 2015, **140**, 2785-2796
- ⁷³ The Guardian <https://www.theguardian.com/uk-news/2018/mar/10/salisbury-poisoning-sergei-skiprial-local-news-international-incident> (accessed Aug 2018)
- ⁷⁴ J.A. Laramee, H. Durst, T.R. Connell & J.M. Nilles, *Am. Lab.*, 2008, **40**(16), 16-20
- ⁷⁵ C. Lancaster & E. Espinoza, *Rapid Commun. Mass Spectrom.*, 2012, **26**, 1147-1156
- ⁷⁶ K.N. Moore, D. Garvin, B.F. Thomas & M. Grabenauer, *J. Forensic Sci.*, 2017, **62**(5), 1151-1158
- ⁷⁷ J. Lapointe, B. Musselman, T. O'Neill, J.R.E. Shepard, *J. Am. Soc. Mass Spectrom.*, 2015, **26**, 159-165
- ⁷⁸ J. Adams, *Int. J. Mass Spectrom.* 2011, **301**(1-3), 109-126
- ⁷⁹ Chemdata.Nist.Gov Mass spectrometry data center, <https://chemdata.nist.gov/dokuwiki/doku.php?id=chemdata:start> (accessed Aug 2018)
- ⁸⁰ J. Zhang, Z. Li, Z. Zhou, Y. Bai & H. Liu, *Rapid Commun. Mass Spectrom.*, 2016, **30**, 133-140.
- ⁸¹ R.L. Self, *J. Pharm. Biomed. Anal.*, 2013, **80**, 155-158
- ⁸² L.K. Ackerman, G.O. Noonan & T.H. Begley, *Food Addit. Contam.*, 2009, **26**(12), 1611-1618
- ⁸³ J. Schurek, L. Vaclavik, H.D. Hooijernik, O. Lacina, J. Poustka, M. Sharman & J. Hajslova, *Anal. Chem.*, 2008, **80**(24), 9567-9575
- ⁸⁴ J. Srbeek, B. Klejdus, M. Douša, J. Břicháč, P. Stasiak, J. Reitmajer & L. Nováková, *Talanta*, 2014, **130**, 518-526
- ⁸⁵ C. Petucci, J. Diffendal, D. Kaufman, B. Mekonnen, G. Terefenko & B. Musselman, *Anal. Chem.*, 2007, **79**(13), 5064-5070
- ⁸⁶ M.C. Bridoux & X. Machuron-Mandard, *Rapid Commun. Mass Spectrom.*, 2013, **27**, 2057–2070
- ⁸⁷ M. Domin & R. Cody, Ambient Ionization Mass Spectrometry, 2014, RSC Publishing
- ⁸⁸ S.R. Bare, M. Lilly, J. Chermak, R. Eggert, W. Halperin, S. Hannahs, S. Hayes, M. Hendrich, A. Hurd, M. Osofsky, C. Tway, *The US Research Community's Liquid Helium Crisis*, 2016, APS, Washington DC

- ⁸⁹ L. Song, W.C. Chuah, X. Lu, E. Remsen & J.E. Bartmess, *J. Am. Soc. Mass. Spectrom.*, 2018, **29**(4), 640-650
- ⁹⁰ Tonsense, <https://www.ionsense.com/About/Mission/en>, (accessed Aug 2018)
- ⁹¹ Biochromato, <https://biochromato.com/ionrocket/> (accessed Aug 2018)
- ⁹² SREC PFUR, <http://ccp.rudn.ru/en/?pagec=936>, (accessed Aug 2018)
- ⁹³ Lab Manager, <http://www.labmanager.com/did-you-know/2015/05/what-s-on-your-dollar-bill-#.W22GYs5KiUk>,
- ⁹⁴ M. Maric, J. Marano, R.B. Cody & C. Bridge, *Anal. Chem.*, 2018, **90**(11), 6877-6884
- ⁹⁵ H. Abe, C. Takei, M. Sakakura, D. Yajima, H. Iwase, *Methods in molecular biology*, 2018, Elsevier B.V., Clifton, N.J.
- ⁹⁶ T.P. Forbes, E. Sisco, M. Staymatesa & G. Gillena, *Analytical Methods*, 2017, **9**, 4988-4996
- ⁹⁷ T.P. Forbes, E. Sisco & M. Staymates, *Anal. Chem.*, 2018, **90**(11), 6419-6425
- ⁹⁸ A. D. McNaught & A. Wilkinson, *IUPAC. Compendium of Chemical Terminology*, 2nd ed. (the "Gold Book"), 1997, Blackwell Scientific Publications, Oxford.
- ⁹⁹ T. Lever, P. Haines, J. Rouquerol, E. Charsley, P.V. Eckeren & D. Burlett, *Pure Appl. Chem.*, 2014, **86**, 545-553
- ¹⁰⁰ M.E. Brown, *Introduction to Thermal Analysis: Techniques and Applications*, 1988, Chapman and Hall, London & N.Y.
- ¹⁰¹ J. P. Evans & S. D. Wood, *Metrologia*, 1971, **7**(3), 108-130,
- ¹⁰² H. Hardianto, G.D. Mey, I. Ciesielska-Wróbel, C. Hertleer & L.V. Langenhove, *Materials*, 2018, **11**, doi:10.3390
- ¹⁰³ S. Gaisford, V. Kett & P. Haines, *Principles of Thermal Analysis and Calorimetry*, 2016 2nd ed., RSC Publishing, UK
- ¹⁰⁴ Setaram, https://www.setaram.com/product_categories/thermal-analysis/thermogravimetry-tga/, (accessed Aug 2018)
- ¹⁰⁵ Perkinelmer, http://www.perkinelmer.co.uk/CMSResources/Images/44-74556GDE_TGABeginnersGuide.pdf, (accessed Aug 2018)
- ¹⁰⁶ H. Jeske, A. Schrip & F. Cornelius, *Thermochimica Acta*, 2012, **543**, 165-171
- ¹⁰⁷ M.E. Brown, *Introduction to Thermal Analysis. Hot Topics in Thermal Analysis and Calorimetry*, 2004 Springer, Dordrecht
- ¹⁰⁸ S.C. Smith, *Materials Measurement Methods*, 2006, Springer
- ¹⁰⁹ A.N. Sembira, J.G. Dunn, *Thermochimica Acta*, 1996, **274**, 113-124
- ¹¹⁰ S.A. Jackson, *Characterization of Materials*, 2012, 2nd ed., John Wiley & Sons, Inc.
- ¹¹¹ P. Gabbott, *Principles and applications of thermal analysis*, 2008, Oxford, Blackwell.
- ¹¹² I. Kelnar, J. Kratochvíl, I. Fortelný, L. Kaprálková, A. Zhigunov, M. Nevorálová, M. Kotrisová & V. Khunová, *RSC Adv.*, 2016, **6**, 30755-30762
- ¹¹³ T.-C. Ling & C.-S. Poon, *Construction and Building Materials*, 2013, **46**, 55-62
- ¹¹⁴ Z. Ge., F. Ye & Y. Ding, *ChemSusChem*, 2014, **7**(5), 1318-1325
- ¹¹⁵ D. N. Papadopoulou, M. Lalia-Kantouri, N. Kantiranis & J. A. Stratis¹, *J. Therm. Anal. Cal.*, 2006, **84**, 39-45.
- ¹¹⁶ F. Luo, T. Ouyang, Y. Fei, *J Mater Sci.*, 2016, **51**, 3408-3414
- ¹¹⁷ E. Charsley, *Unpublished results*
- ¹¹⁸ K.A. Thorsen, H. Fordsmand, & P.L. Praestgaard, *Welding Journal*, 1984, **63**(11), 339s-344s
- ¹¹⁹ H.P. Diogo & J.J.M. Ramos, *Journal of Molecular Structure*, 2014, **1078**, 174-180
- ¹²⁰ G.L. Perpétuo, G.O. Chierice, L.T. Ferreira, T.F.C. Fraga-Silva, J. Venturini, M.S.P. Arruda, G. Bannach & R.A.E. Castrod, *Thermochimica Acta*, 2017, **651**, 1-10
- ¹²¹ S.R. Byrn, G. Zografi & X. Chen, *Solid-State Properties of Pharmaceutical Materials*, 2017, John Wiley & Sons
- ¹²² D.-C. Marinescu, E. Pincu & V. Meltzer, *Journal of Thermal Analysis and Calorimetry*, 2012, **110**(2), 985-990.
- ¹²³ R.R. Mahajan, P.S. Makashir & J.P. Agrawal, *J. Therm. Anal. Cal.*, 2001, **65**, 935-942
- ¹²⁴ A.M. Djerdjiev, P. Priyananda, J.Gore, J.K. Beattie, C. Neto, B.S. Hawkett, *Journal of Environmental Chemical Eng.*, 2006, **6**, 281-288
- ¹²⁵ G. Mehlana, C. Wilkinson, G. Ramon & S.A. Bourne, *Polyhedron*, 2015, **98**, 224-229
- ¹²⁶ H. Matsunaga, Y. Izato, H. Habu & A. Miyake, *J. Therm. Anal. Calorim.*, 2015, **121**, 319-326
- ¹²⁷ J. Zhao, W. Xiuwen, J. Hu, Q. Liu, D. Shen & R. Xiao, *Polymer Degradation and Stability* 2014, **108**, 133-138
- ¹²⁸ C.-W. Tang, C.-B. Wang & S.-H. Chien, *Thermochimica Acta*, 2008, **473**(1-2), 68-73
- ¹²⁹ M. Bakierska, A. Chojnacka, M. Świątosławski, P. Natkański, M. Gajewska, M. Rutkowska & M. Molenda, *Materials*, 2017, **10**, doi:10.3390
- ¹³⁰ P.J. Haines & G.A. Skinner, *Thermochimica Acta*, 1982, **59**, 343-359
- ¹³¹ V. Speranza, A. Sorrentino, F. De Santis & R. Pantani, *The Scientific World Journal*, 2014, Article ID 720157

- ¹³² L.O. Alimi, D.P. van Heerden, P. Lama, V.J. Smith & L.J. Barbour, *Chem Comm.*, 2018, **54**, 6208-6211
- ¹³³ A.N. Matzakos & K. Zygourakis, *Rev. Sci. Instr.*, 1993, **64**, 1541
- ¹³⁴ C.-C. Hsu, N.M. White, M. Hayashi, E.C. Lin, T. Poon, I. Banerjee, J. Chen, S.L. Pfaff, E.R. Macagno & P.C. Dorrestein, *Proc. Natl. Acad. Sci. U.S.A.* 2013, **110**, 14855– 14860
- ¹³⁵ C.-C. Hsu, M.W. Baker, T. Gaasterland, M.J. Meehan, E.R. Macagno & P.C. Dorrestein, *Anal. Chem.* 2017, **89**(16), 8251-8258
- ¹³⁶ I. Lamprecht, A. Reller, R. Riesen & H.G. Wiedemann, *Journal of Thermal Analysis*, 1997, **49**, 1601-1607

2.0 Instrumentation Development

2.1 Introduction

This chapter describes the various stages in the development of the Hot-stage Microscopy Direct Analysis in Real-Time Mass Spectrometry (HDM) instrument and software.

The idea of HDM developed from an earlier project investigating the 'suppression effects' commonly observed within DART-MS where the apparent intensity of an ion may be reduced by the presence of other analytes or the sample introduction matrix itself. The plan for this study involved using optical microscopy to determine if any correlations could be drawn between the ablation processes (the removal of compounds, or layers of compounds) observed during DART analysis and the order of layers applied to surfaces of common DART sample introduction matrices such as DIP-it® tips or wire meshes.

A related preliminary project investigated the relationship between the set temperatures, as applied by the heated DART source, and how the actual temperature of the sampling region varies, through the use of low mass thermocouples.

The result of these initial studies demonstrated that there could be many benefits in a true combination of DART-MS and hot-stage microscopy. At the start of the current project a list of desirable features for the proposed HDM were devised with the aim of constructing a truly integrated instrument:

1. To have a hot-stage that could be accommodated within the geometry of the DART-MS while heating samples under the controlled conditions required for thermal analysis.
2. To be able to accept samples as either liquids or solids in the typical mass range used in conventional thermal analysis (from a few milligrams).
3. To incorporate a simple but effective digital microscope that could be accommodated within the geometry of the DART-MS.
4. To be as simple as possible to facilitate construction and minimise cost.
5. To modify existing software to allow real-time collection of images and other optical information from the sample during an experiment.
6. To modify the existing software to allow the future incorporation of cheaper computing platforms to eliminate the need for expensive temperature programmers.
7. To incorporate an alternative, simpler, ionisation source.

The HDM went through a series of iterations of both hardware and software as improvements in design and functionality were implemented.

2.2 Initial evaluation studies using DART-MS

2.2.1 Suppression effects

This investigation was one of two preliminary studies that led to the development of the HDM system. Its aim was to evaluate the effect of having compounds deposited in layers on a wire mesh (utilised in transmission mode DART-MS (TM-DART)) when analysed using DART-MS. As part of the initial study a simple rig was developed (see Figure 2.1) – that incorporates the use of a digital USB microscope (Supereyes, B008). The microscope provides a series of images to link mass spectra with the extent of ablation or thermal desorption depending on the set temperature of the DART outlet.

The rig consisted of a wooden frame incorporating a mount to hold the USB microscope (away from the DART source) that was adjustable using M8 threaded rods, and a linear rail to allow accurate positioning of the wire mesh sample holder relative to the USB microscope.

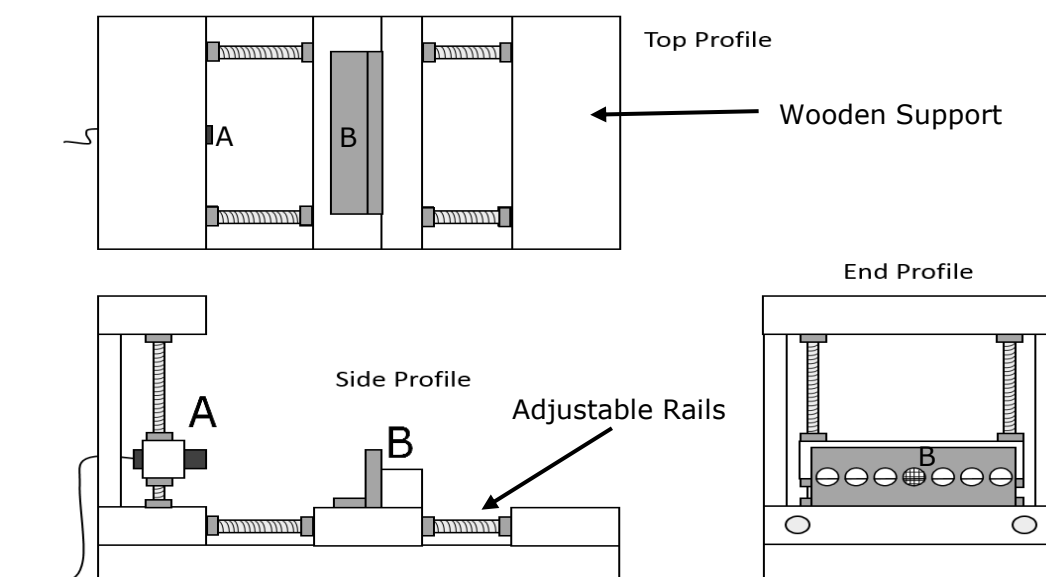


Figure 2.1 A schematic of the imaging station constructed for DART-MS ablation studies. A) USB Microscope and B) Sample rail. The rig was constructed to allow for accurate repositioning of the sampling rail in front of the USB microscope.

The evaluation study focused on comparisons between rhodamine B (Aldrich, 97% analytical standard) and benzil (Aldrich, 98%). These compounds were selected as they gave strong colours, large mass differences and were readily ionised. The DART was operated at a temperature of 150 °C (a commonly quoted DART operating temperature) in positive ionisation mode. Dominant selected ions of benzil and rhodamine B were chosen (211 Da $[M+H]^+$ and 443 Da $[M-Cl]^-$, respectively) and recorded as a function of time through their extracted ion chromatograms (EICs). Solutions of the two compounds were

prepared (1000 ppm in methanol) and loaded onto metal meshes held by the in-house constructed TM (transmission mode) rail developed in the previous study.¹

Most of the benzil was removed within the first few minutes of exposure to the DART stream as can be seen in Figure 2.2. Rhodamine B bound more strongly to the mesh surface and experienced a longer signal lifetime than that of benzil. A clear pattern can be seen from the removal of the rhodamine B directly from the centre of the mesh where the heat was most concentrated.

As the individual profile characteristics were obtained for both benzil and rhodamine B, a physical mixture was made of the two solutions and placed directly onto the mesh and allowed to evaporate. Benzil (E) appears to suppress the rhodamine B (F) in Figure 2.3 through the delay in the rhodamine B ion maximum. The individual profiles (Figure 2.2) show that the rhodamine B exhibits a gradual decline from the onset of the experiment as opposed to reaching a maximum later on as is observed with the mixture example.

In another experiment benzil (E) was then added to the mesh and allowed to dry. To this rhodamine B (F) was added and the mesh analysed (Figure 2.4). In this example it is evident that the upper layer of rhodamine B appears to 'protect' the lower layer of benzil extending the sampling lifetime. The images show the mesh appears more like the rhodamine B than the benzil.

The reverse profiles are shown in Figure 2.5 for a layer of rhodamine then benzil, in this example the mesh looks more benzil like showing more crystallisation. Benzil (E) appears to suppress the rhodamine B ion profile (F) for the duration of the experiment.

In terms of the current research, this preliminary study had three important conclusions:

- (a) Simple digital USB microscopes could provide useful ancillary information to complement DART mass spectra.
- (b) A more accurate control of the temperature than provided by the DART may allow thermal separation of mixtures with different physical properties such as melting points or decomposition temperatures.
- (c) Compounds adhering to meshes may have different binding affinities to the surface, this may result in different mass spectra depending on the type of mesh used.

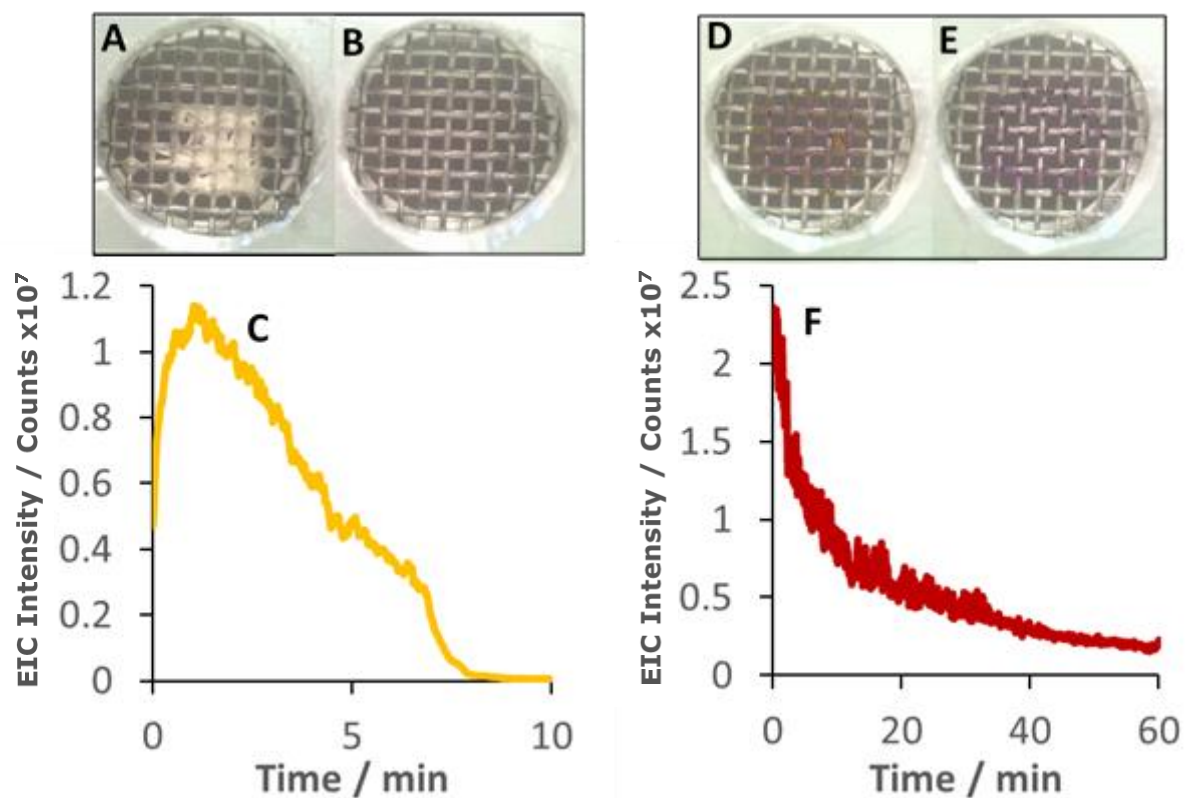


Figure 2.2 Individual component comparison. Removal of benzil from steel mesh A = benzil at 0 min, B = benzil at 10 min, C = EIC of benzil 211 Da $[M+H]^+$, D = rhodamine B at 0 min, E = rhodamine B at 60 min and F) EIC of rhodamine B 443 Da $[M-Cl]^+$.

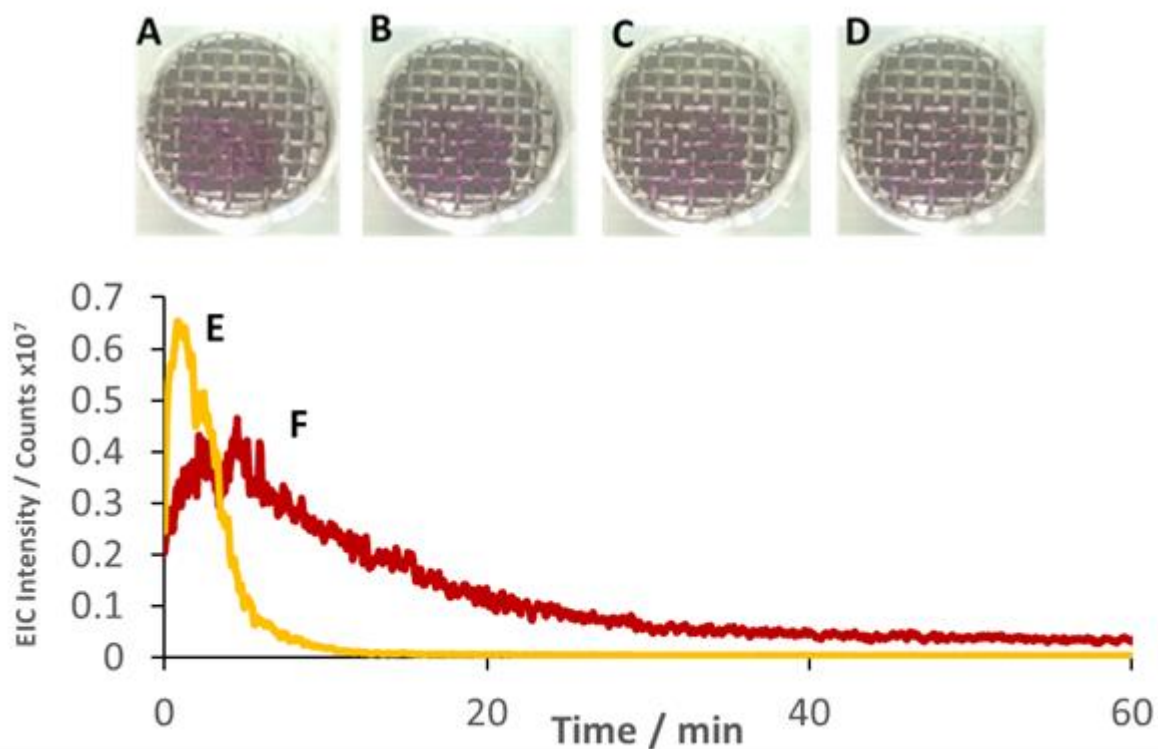


Figure 2.3 Mixture analysis of benzil and rhodamine B from a mesh surface. A = 0 min, B = 20 min, C = 40 min and D = 60 min. E = EIC of benzil 211 Da $[M+H]^+$ F = EIC of rhodamine B 443 Da $[M-Cl]^+$ plotted as a function of time.

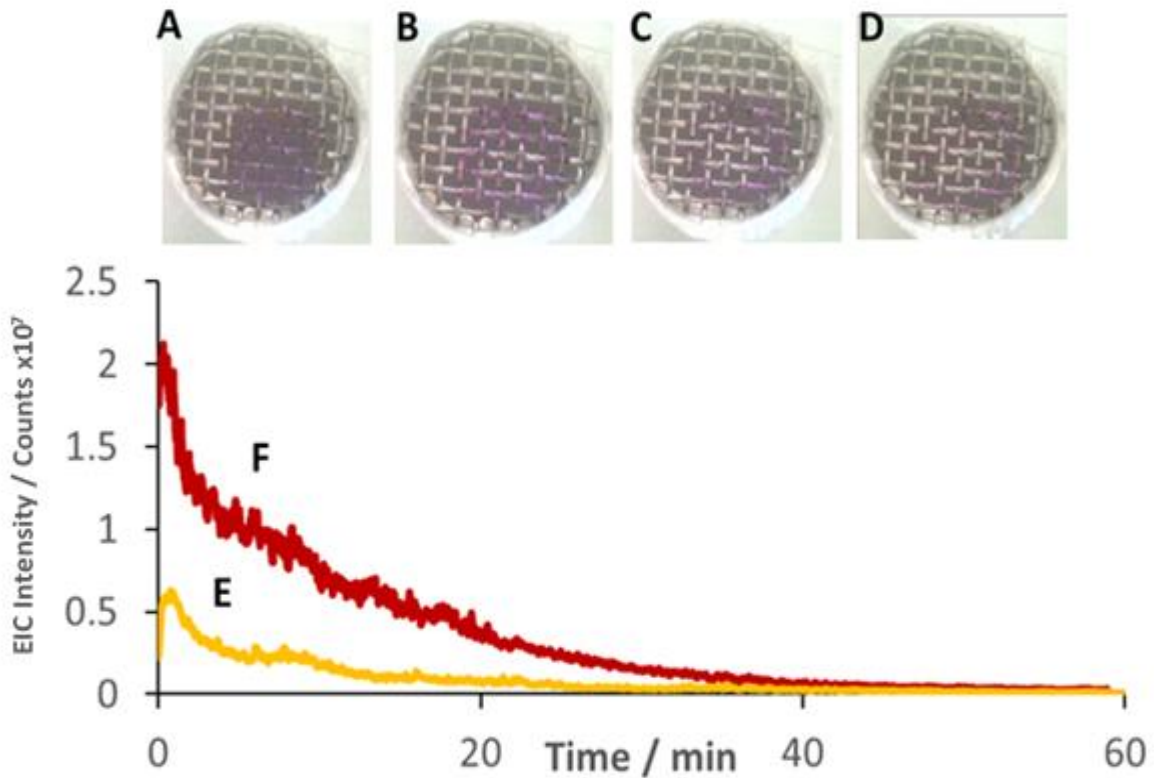


Figure 2.4 Layer analysis of benzil layered then rhodamine B on top. A = 0 min, B = 20 min, C = 40 min and D = 60 min. E = EIC of benzil 211 Da $[M+H]^+$ F = EIC of rhodamine B 443 Da $[M-Cl]^+$ plotted as a function of time.

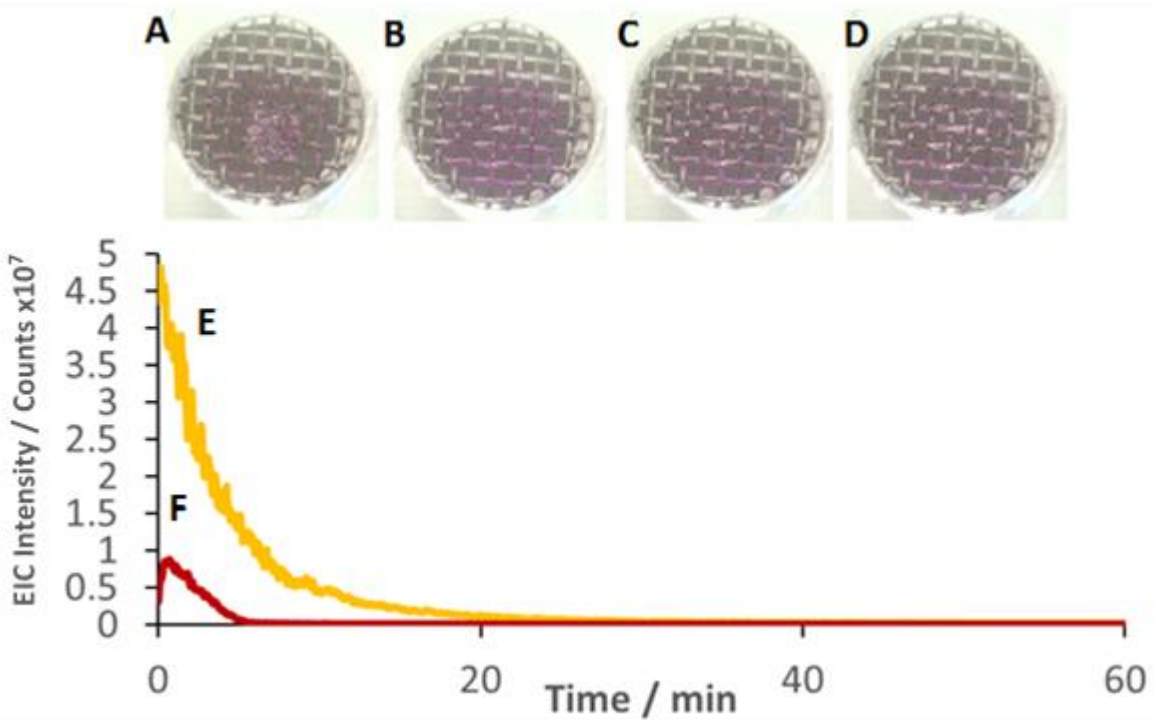


Figure 2.5 Layer analysis of rhodamine B layered then benzil on top. A = 0 min, B = 20 min, C = 40 min and D = 60 min. E = EIC of benzil 211 Da $[M+H]^+$ F = EIC of rhodamine B 443 Da $[M-Cl]^+$ plotted as a function of time.

2.2.2 DART-MS Temperature profiling

DART-MS users within the literature commonly quote mass spectral profiles achieved at the DART set temperature. It has been noted by several research groups that there is a significant temperature gradient between the DART outlet and the MS inlet.² The second preliminary study investigated this effect, noting the temperature gradients when using DART-MS, a feature that was hoped to be eliminated in the development of HDM.

DART has been shown to have a coronal type exit plume as was noted in earlier studies.³ The study had shown that the exit gas acts like a focused jet which aids with the idea that DART is actually mildly destructive causing sample ablation as was discussed in the previous section (Section 2.2.1). Thermal modelling of the DART exit gas plume was performed and confirmed with thermocouple measurements by Harris *et al.* the study shows the rapid decline of temperature within the sampling region and how the temperature models are affected by sample location within the gas stream.⁴

To evaluate the DART temperature plume an experimental rig was designed to profile temperature as a function of distance (see Figure 2.6). The rig consisted of an X-Y axial mount that held a low mass type K thermocouple connected to a thermocouple reader with 0.1 °C precision. The temperature per sampling position was taken by allowing the temperature reader to take the average reading over an arbitrary 10 second period.

The DART parameters were fixed to give a helium flow rate of 1.5 L min⁻¹ and temperatures were fixed at three set temperatures; 150, 250 and 350 °C. Sample measurements were taken once the DART temperature had stabilised itself according to the DART's own controller software. A fixed distance was selected at the midpoint between the DART outlet and the MS inlet (6 mm), from this distance sweeping measurements of temperature were taken 5 mm apart in two planes up to a radial distance of 20 mm from the midpoint.

Three set temperatures were selected to give a representation of standard operating temperatures used for DART analysis; 150, 250 and 350 °C. The raw values were recorded into a 2D plot and a colour gradient was applied to give a better visual representation of the temperature about the DART exit cap, shown in Figure 2.7.

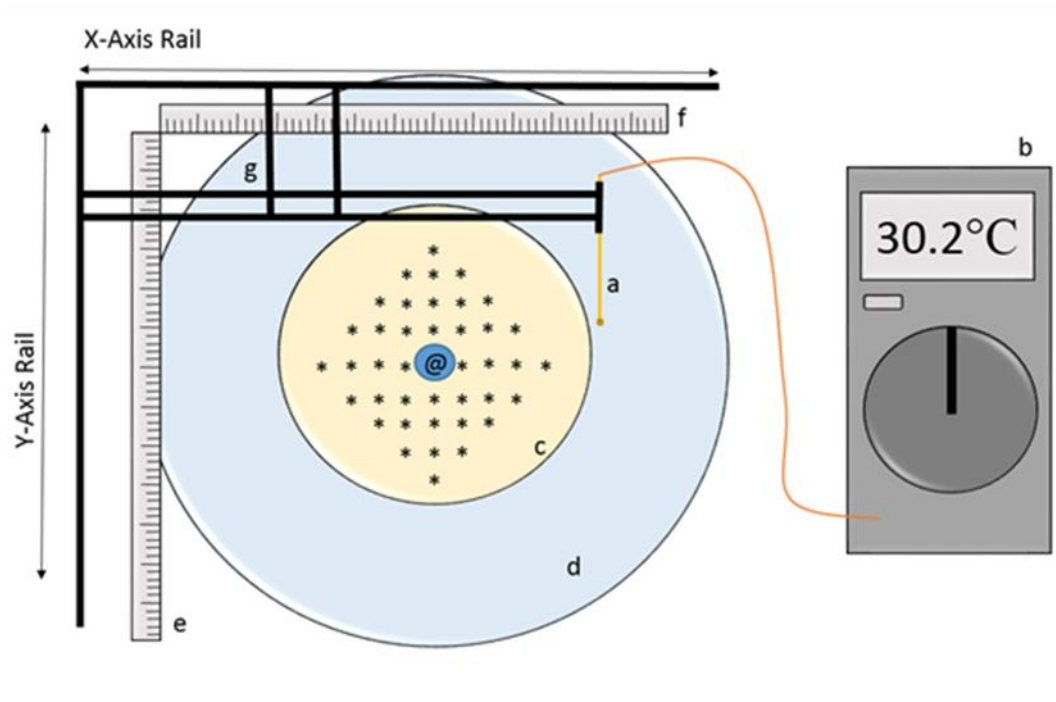


Figure 2.6 Temperature mapping rig for DART thermal profiling. a) Type K thermocouple (0.1mm), b) Thermocouple reader, c) Sampling within the discharge area, samples taken 5mm apart (*) from the centre of the DART source (@), d) DART source, e) Y-axis rail, f) X-axis rail, g) Thermocouple support.

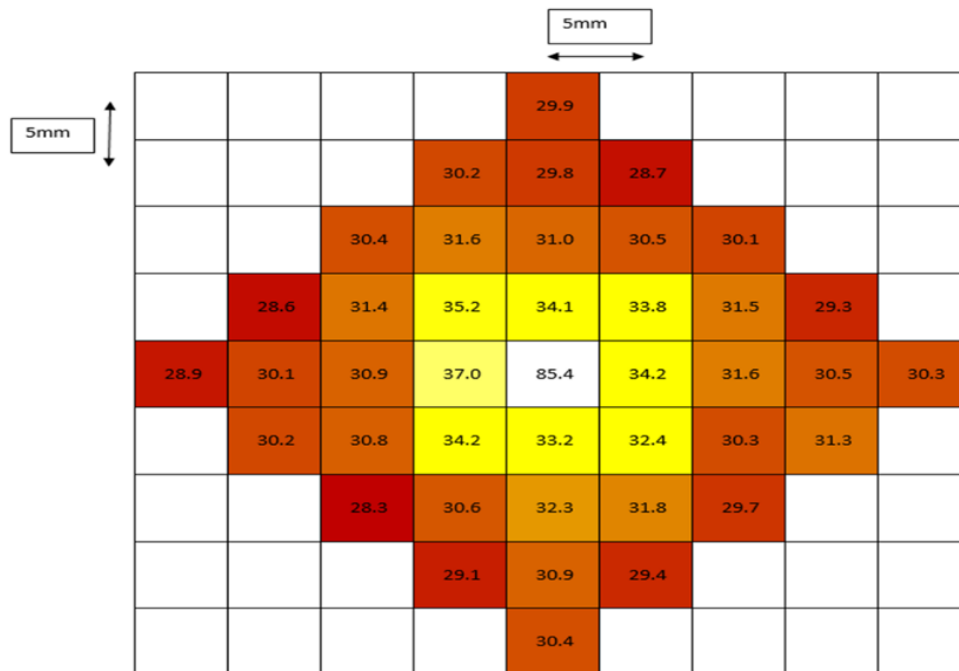


Figure 2.7 An example of thermal profiling of the DART outlet region at 150 °C, values shown are temperature obtained in °C.

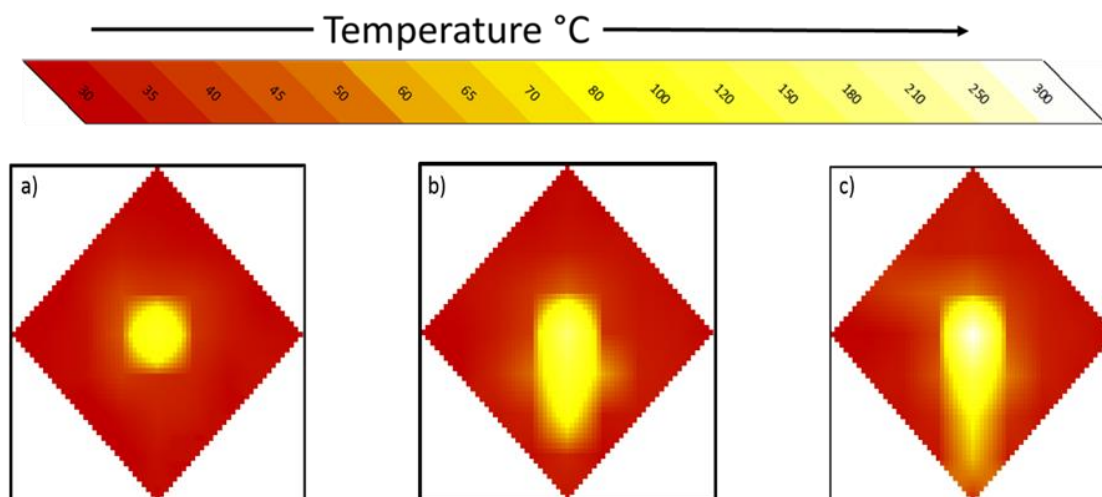


Figure 2.8 DART sampling region temperature profiles. a) 150 °C, b) 250 °C and c) 350 °C.

Using Microsoft Excel average colour plots were generated from the raw data (shown in Figure 2.8), these were generated by assigning a colour to temperature range, and then applying a series of averages between the points. The outlet has a focused temperature region of about 5 mm at the centre of the stream, and the temperature gradient rapidly falls away with distance away from the centre (Figure 2.8, a, b and c).

An inverted tear drop shape is shown in the higher temperature plots. This shape has arisen due to the thin thermocouple ceramic support beginning to heat up itself, the heat transmits down the ceramic towards the thermocouple tip, and hence the shape is only noted at higher temperatures in the lower sampling region. In an ideal design the point of the thermocouple would have been positioned coaxially into the DART stream to eliminate this effect, although the geometry did not allow for this.

The temperature gradient was approximately 70 to 80 °C lower than the set DART temperature, which is to be expected when the preheated gas stream hits the cold front of air within the sampling region. The difference in quoted against actual temperature has significant importance when quoting thermal based events, such as the sample desorption temperature.

In terms of current research, this preliminary study had two important conclusions:

- (a) The best results would be obtained if the sample was reproducibly positioned between the DART source outlet and the MS inlet, thus controlling metastable exposure and desorption temperature improving the reproducibility of MS profiles obtained.
- (b) A localised and controllable heating source would be desirable to heat the sample, as opposed to relying on the heated gas stream from the DART source. This method would be significantly more comparable to conventional thermal analysis and give more reliable results in general, improving reliability of data obtained.

2.3 Development of HDM

Partly as a result of the preliminary studies described previously, the potential benefit of a hyphenated hot-stage microscopy DART-MS system was recognised. The HDM went through several major design iterations both in terms of hardware and software, the following section describes these developments.

2.3.1 HDM Instrument Overview

A schematic representation of the current iteration (using hot-stage 2, introduced later) of the HDM system is shown in Figure 2.9. The system brings together three key pieces of instrumentation; a hot-stage microscope, a DART ionisation source and an ion trap mass spectrometer.

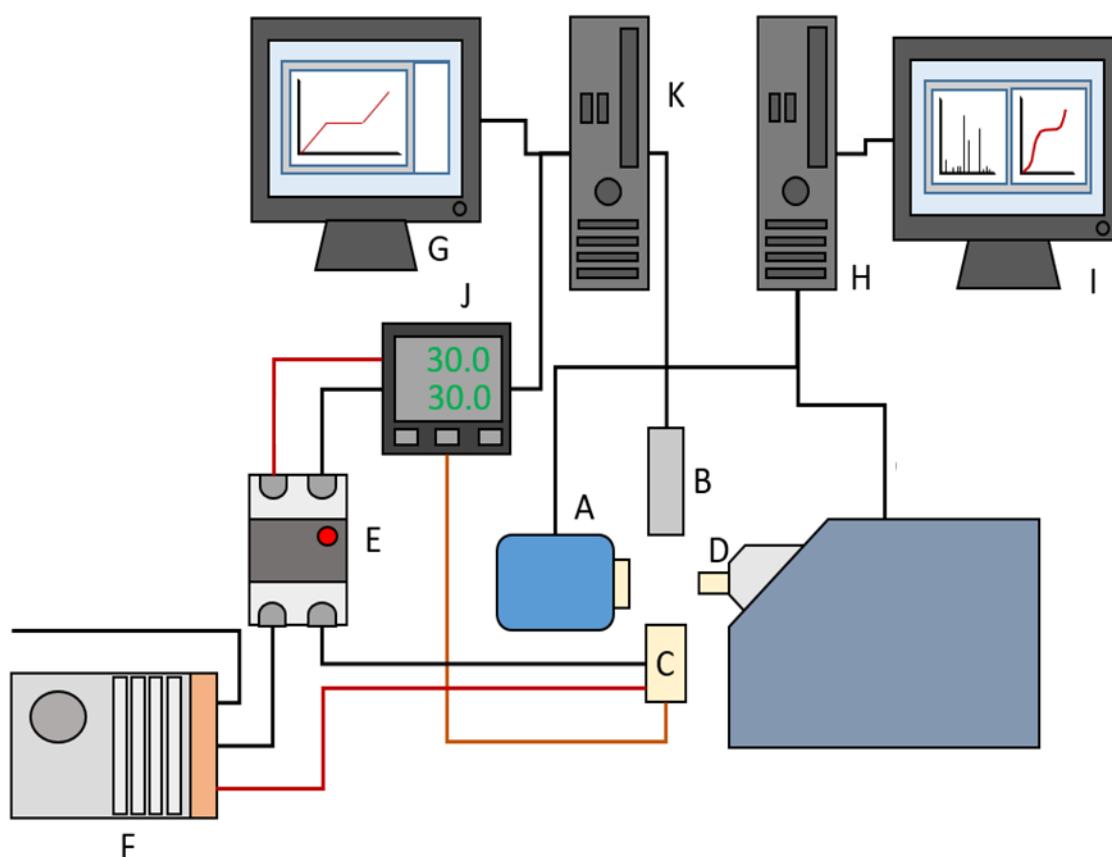


Figure 2.9 Schematic representation of the HDM system. A) DART, B) Digital Microscope, C) Hot-stage, D) Mass Spec., E) SSR, F) PSU, G) HSM Monitor, H) MS PC, I) MS Monitor, J) Eurotherm E818p, K) HSM PC.

The equipment can be considered from two separate viewpoints depending on the user; either a thermal analysis instrument with a high quality chemical detector attached or, alternatively, as a mass spectrometer with a multifunctional thermal desorption-ionisation source.

The core components of the HDM are:

(a) Hot-stage (C in Figure 2.9)

Various prototype hot-stages were constructed in-house but all were fundamentally similar. They consisted of a series of ceramic components, nichrome resistive heating wire and embedded low mass type K thermocouples for sample temperature measurement. Typically the hot-stages were designed to hold conventional thermal analysis pans between 5 and 6 mm in diameter. The hot-stages are discussed in greater detail in Section 2.4.

(b) Power-supply (F in Figure 2.9)

A variety of power supplies were trialled, the current iteration of HDM uses a switch-mode unit (TooGoo®, AD2410, 240W) capable of delivering 24 V DC and drawing a maximum current of 10A.

(c) Solid state relay (E in Figure 2.9)

An optocoupled solid state relay (FDTEK, SSR-25 DD) was used to switch the power supply. The solid state relay was controlled through logic level signal provided by the temperature programmer.

(d) Temperature programmer (J in Figure 2.9)

A Eurotherm® 818P temperature programmer was used and interfaced to a PC running the HDM controller and analysis software via a RS232C serial connection. The unit continuously measures the temperature of the hot-stage via the embedded thermocouple. Power is applied to the heating wire within the body of the hot-stage from the power supply using a technique known as pulse-width modulation described later in Section 2.3.2.

(e) Digital microscope (B in Figure 2.9)

A variety of digital USB microscopes were trialled (see Section 2.3.3) but generally a resolution of 800 x 600 was used. The focal length and magnification were adjusted so that the entire 6mm pan filled the image.

(f) Computers (H & K in Figure 2.9)

Two computers are used in the operation of HDM. The first runs the HDM software. The second controls the DART (Ionsense, DART control) and the mass spectrometer software (Bruker, esquire control).

(g) DART source (A in Figure 2.9)

The DART-100 source serves as the ionisation source in the HDM system. The DART voltages were fixed at needle voltage 3 kV, discharge and grid electrode 400 V. The gas flow rate through the DART source was controlled through a needle valve and measured using a digital flow meter (Omega, FMA3109) and calibrated using a positive volume displacement method.⁵

The temperature of the DART source was typically set to operate at a fixed temperature of 30 °C so that any heating was solely provided by the hot-stage. The DART source may be operated in either positive or negative polarity mode, selected through the DART controller software depending on the nature of analysis.

(h) Mass spectrometer (D in Figure 2.9)

The ion trap mass spectrometer (Bruker, esquire HTC) was used to analyse samples in either positive, negative or alternating polarity modes depending on the nature of analysis. The mass spectrometer was operated using the dedicated controller software. The mass spectrometer was optimised for DART analysis and the method was fixed throughout the research project using the following parameters unless otherwise stated: analysis was typically collected over a mass range of 50-2800 Th, the source temperature was set to 300 °C, an accumulation time of 200 ms was used, a Smart target of 200, 000 was set and the capillary voltage was set to 4kV.

(i) HDM controller software

This was developed from existing software written within the University of Huddersfield by Dr Gareth Parkes using VB.NET. The software controls the temperature programmer, records and processes images from the microscope and saves the data in the CSV format, allowing post-acquisition processing. A review of the software is given in Section 2.5.

A flow diagram of the operation of HDM is given in Figure 2.10.

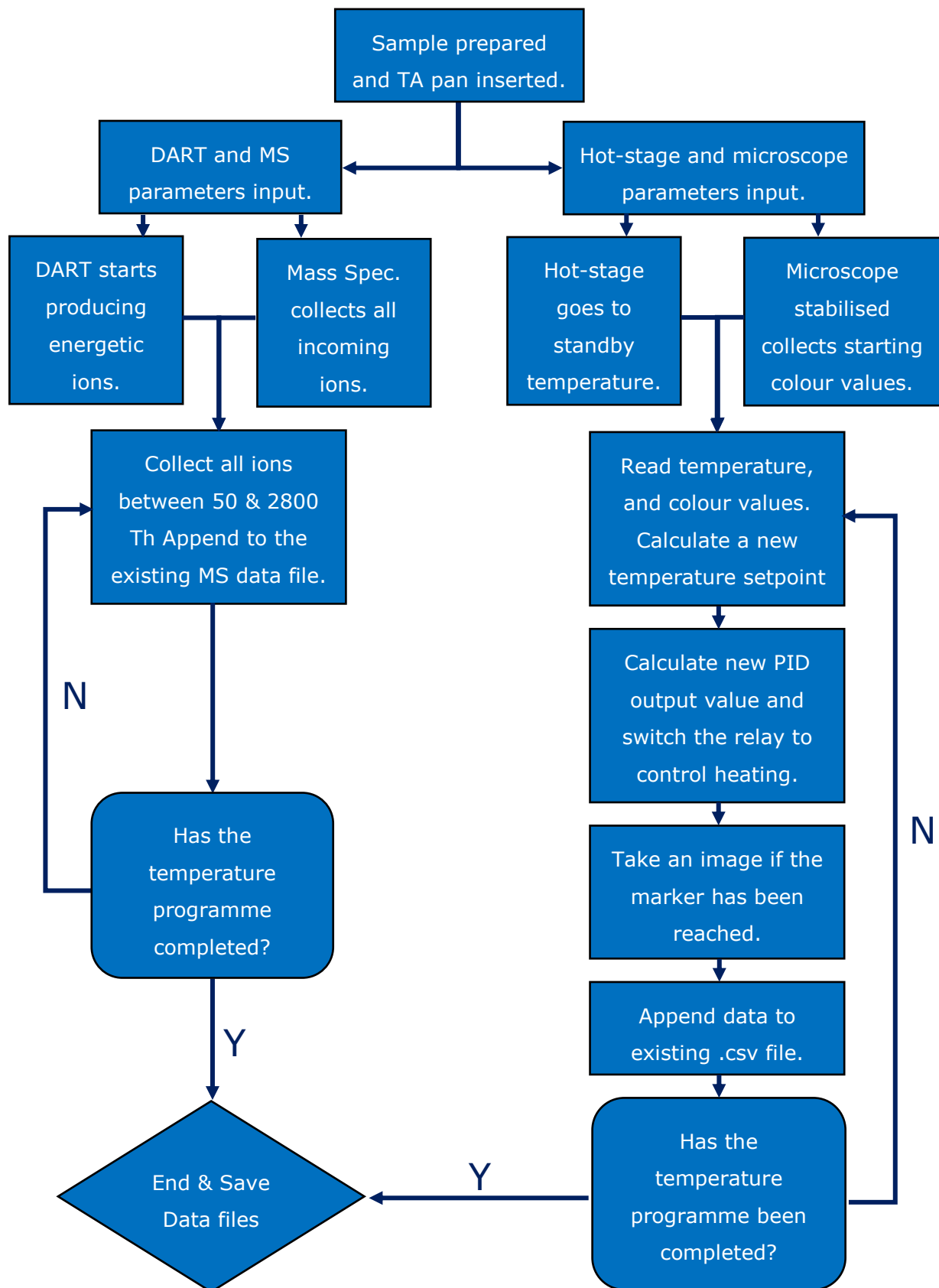


Figure 2.10 Flow diagram of the operation of HDM.

2.3.2 Temperature control - PID algorithm and pulse width modulation

Accurate control of the temperature of the sample heater is a vital part of any thermal analysis instrument. To achieve this there needs to be a link between the temperature and the electrical power being supplied to the heater.

Four terms are considered:

- (a) The process variable (PV), in HDM this is the actual temperature.
- (b) The setpoint (SP), the temperature the HDM should be.
- (c) The error (e), the difference between PV and SP.
- (d) The Output, the measure of power being supplied to the heater.

In temperature control systems the error is continuously calculated and used to modify the output. If $e = 0$ ($PV = SP$), that is if the actual temperature is equal to the setpoint the output remains unchanged. If $PV > SP$ ($e < 0$) then the output is decreased, contrastingly if $PV < SP$ ($e > 0$) then the output is increased. The aim of any controller is to attempt to maintain the error, at, or near, 0 even if the SP is changing with time (as would be the case during a linear heating experiment). There are many mathematical relationships (algorithms) linking the output and error but the most common used is called 'PID' where P stands for proportional, I for Integral and D for derivative.⁶ This type of control is shown in Figure 2.11. The PV (actual temperature) is represented by the blue trace and the setpoint (SP) is given by the red dashed line. The PID algorithm reduces the error over time until the error becomes 0 when $PV = SP$, ideally the time should be as short as possible whilst retaining good control (minimal overshoot).

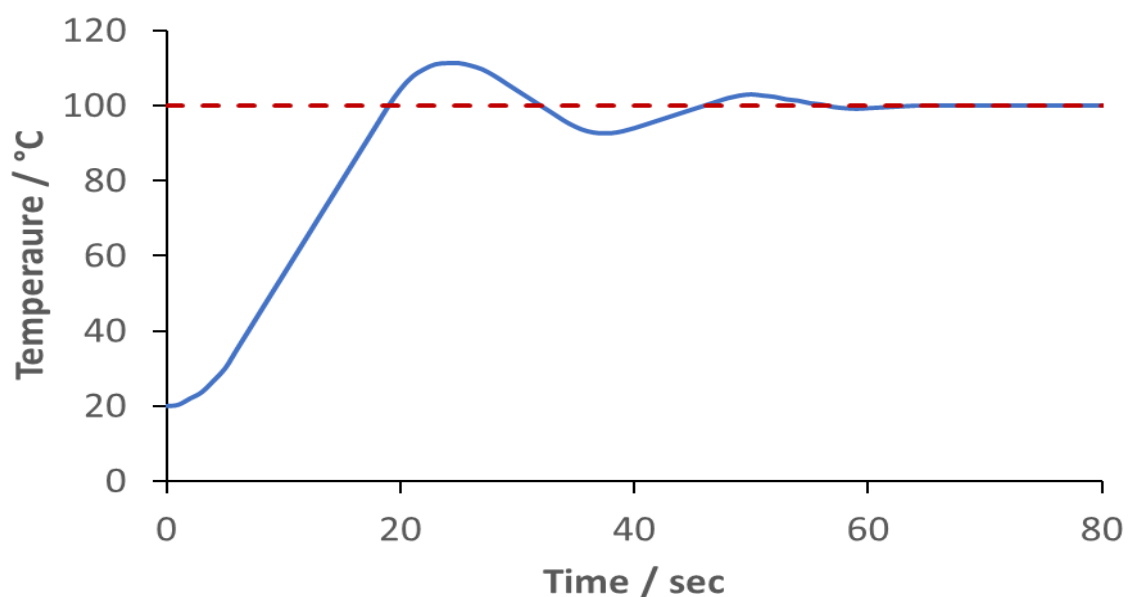


Figure 2.11 Representation of how PID temperature control works, aiming to get the temperature (blue line) to match the setpoint (red dashes).

Within the HDM system PID controllers (Eurotherm and Arduino, Section 2.7.2.1) incorporate the individual terms to evaluate how the error may be change over time and how best to control the output to maintain the best possible temperature control. The PID terms act as follows:

(P or K_p) Proportional. This term is directly proportional to the magnitude of the error. This is usually the main controlling term used in the algorithm but if used solely can induce major oscillations of the PV about the SP.

(I or K_i) Integral. This term is proportional to the magnitude of error over a selected period of time (denoted as $e(t)$). The integral term usually compensates for the 'undershoot' found when the PV lags behind the SP.

(D or K_d) Derivative. This term is linked to the rate of change in error over a selected period of time. The derivative acts like a dampener, slowing how rapidly PV approaches SP, and can minimise induced oscillations of the PV around SP.

The three terms are individually weighted and then summed to produce the output value. The values for the weightings are crucial for good control which is essential for thermal analysis. These values are dependent on how responsive the sample heater is and usually dictated by how good a heat path exists between the heater and thermocouple.

Other terms may be incorporated into the basic PID algorithm to further improve the control and responsiveness of the system. The two most common are:

(P_{band}) The proportional band is used to account for any large differences between PV and SP which may occur, particularly when the controller is initialised. A basic description is it allows regions of coarse and fine PID values to be set. Should e lie outside of the P_{band} coarser weighting values are applied, this minimises control and focuses on making the PV come close to SP as quickly as possible. Once e lies within the P_{band} finer weighting values are used, aiming for better control over speed, this ensures minimal overshoot of PV against the SP. Typically, the Eurotherm system uses P only if the error is greater than the P_{band} , and introduces I and D when $e < P_{band}$ to regain control.

(P_{gain}) The proportional gain is used to account for significant differences between PV and SP by scaling the response of the P term by applying a multiplication factor.

A typical PID algorithm (incorporating the P_{band}) is shown as a block diagram in Figure 2.12.

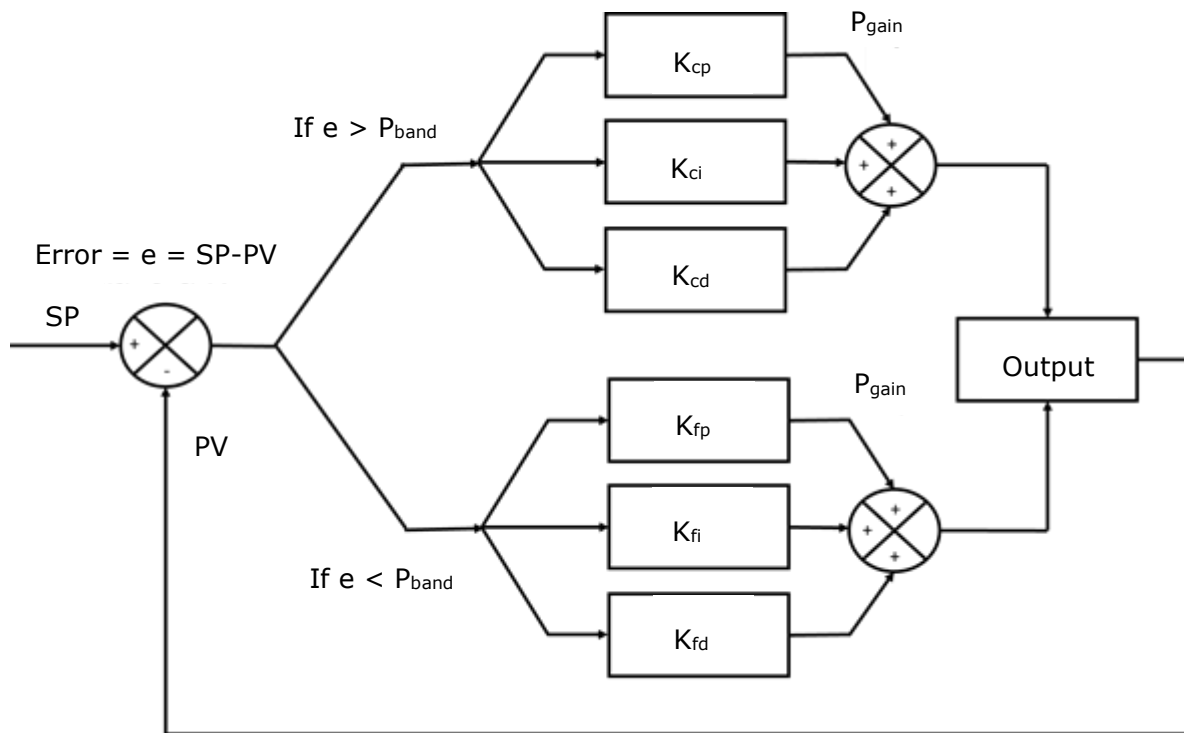


Figure 2.12 PID block diagram used in the temperature control of the hot-stage.

The output is calculated according to the following algorithms (Figure 2.13) based on the block diagram in Figure 2.12. The Eurotherm controller uses the proportional only term when the error is outside of the P_{band} ($e > P_{band}$), when the error is within the P_{band} ($e < P_{band}$) the D and I terms are included. As was introduced in the description of the individual algorithm terms, I and D have a time component (t). Time is used in this algorithm to monitor how the error is changing within a certain time period.

This approach is used by the Eurotherm, later, the Arduino microcontroller is introduced (Section 2.7.2.1) which uses PID continuously regardless if the error is above or below the P_{band} . Instead, the Arduino PID utilises fine (K_{fp} , K_{fi} and K_{fd}) and coarse (K_{cp} , K_{ci} and K_{cd}) values depending on if the error is within the P_{band} or not.

$$\text{If } e > P_{band}$$

$$\text{Output} = K_p \cdot e \cdot P_{gain}$$

$$\text{If } e(t) < P_{band}$$

$$\text{Output} = (K_p \cdot e P_{gain}) + (K_i \int_0^t e \cdot \Delta t) + (K_d \frac{\Delta e(t)}{\Delta t})$$

Figure 2.13 P_{band} based output algorithm selection

Although theoretically the output from the PID controller could be amplified and fed directly into the sample heater it is more common (and electrically simpler) for the output to be converted proportionately into on and off states using Pulse Width Modulation (PWM). PWM is readily adaptable for use with solid state relays which are capable of switching the high currents often required for heating applications.

In PWM an overall cycle time is selected and this is divided into on and off periods. If the cycle time was 1000 ms then an output from the PID algorithm of 50% would be 500 ms on and 500 ms off, likewise for an output of 60%, 600 ms is spent on and 400 ms off. This is shown graphically in Figure 2.14. Long cycle times can result in poorer control as the temperature may fall during extended off times hence the reason for using shorter times. Although shorter cycles put more strain on the electronic components shortening the lifetime of the system so an appropriate balance must be found.

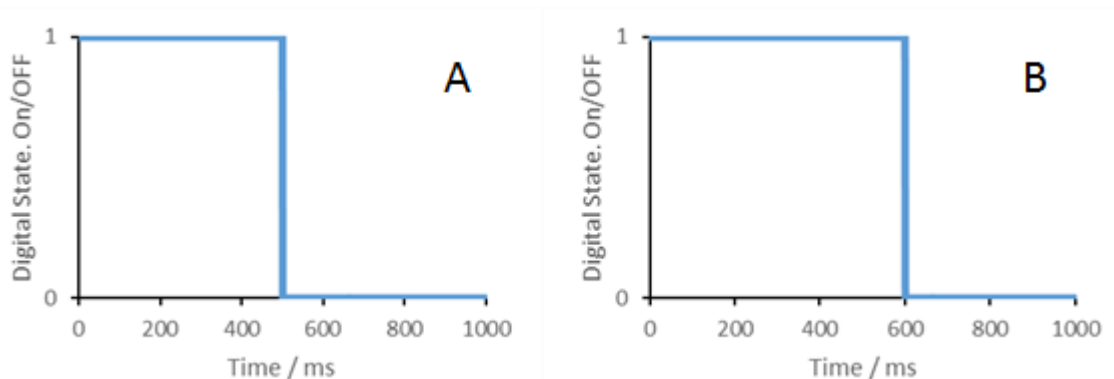


Figure 2.14 PWM control examples over a fixed 1000 ms loop. A) 50 % applied power over 1 cycle of 1000 ms, B) 60 % applied power over 1 cycle of 1000 ms.

The Eurotherm has a useful feature that allows the controller to auto tune for a specified temperature range. Tuning is used to achieve maximum control over temperature changes. A well-tuned system will respond to changes in temperature rapidly, with minimal over or undershooting effects, whilst a poorly tuned system will struggle to ensure stable control and will often lead to temperature oscillations and steps in the output. PID values were tuned in for each hot-stage constructed to ensure reproducibility in temperature control.




The majority of the results presented in this thesis were produced using a version of the HDM incorporating a commercial temperature controller (818P, Eurotherm) which has its own internal PID routines. However, the most recent forms of the instrument utilise micro-controllers (as part of a move towards a cheaper, 'open source' approach to HDM) which required the development of code to implement PID (see Section 2.7.4.2) as the main temperature control routine.

2.3.3 HDM – Digital microscopy and image processing

One design aim for HDM was to have flexibility in the software, allowing the use of different digital microscopes with the ability to switch between them relatively easily.

Individual microscopes were evaluated separately from the HDM but utilising the HDM software (see Section 2.5). Several digital microscopes were trialled but the three principal types used during this project were the Supereyes-B008, MAOZUA-MI001 and the Teslong-MS100 (see Table 2.1).

Table 2.1 Comparison table of the three main USB microscopes used & evaluated during this project.

Microscope	Supereyes B008	MAOZUA MI001	Teslong MS100
Image			
Dimensions	Length = 126 mm O/D 17 mm	Length = 110 mm O/D 33 mm	Length = 147.0 mm O/D = 8.0 mm
Magnification	1-500X	20-300X	10-200X
Lighting	8 Bright White LEDs.	8 Bright White LEDs.	8 Bright White LEDs.
Camera Resolution	5.0 Megapixel CMOS sensor	5.0 Megapixel HD CMOS Sensor	1.0 Megapixel CMOS sensor
Focal Distance	3 -'∞' mm	0- 150 mm	10-500 mm

One important criterion in the selection of the digital microscope was the focal distance which needed to be out of the DART stream. It was noted in the preliminary studies that should the microscopes be introduced too close to the hot-stage the combined additional heat rising from the hot-stage and the ionisation potential of the DART would lead to an increase in background peaks, mainly in the form of phthalate plasticisers from the plastic body of the microscope itself.

An additional consideration was the possible effect of temperature on the digital microscope optical sensor as it is well-known that the performance of camera electronics is inversely proportional to temperature,⁷ with higher temperatures inducing increased

levels of noise superimposed on the image. Although not currently implemented, future developments of HDM may incorporate a cooled microscope to maximise image quality.

In addition to the actual camera there was also a requirement for the images to be available for processing by the main HDM software (developed using Visual Studio (Microsoft, ed, 2013 – 2017)). Although all the digital cameras came with basic software provided by the manufacturers these were 'self-contained' and not possible to integrate with the HDM software. After an online search for possible solutions, a webcam library called Touchless⁸ was identified as being the most appropriate for this project.

The Touchless software library is a community run project and has not been updated recently. However, it has the advantages that:

- (a) It is designed specifically to work with Visual Studio
- (b) It operates seamlessly with the majority of USB microscopes and provides a measure of 'plug and play' allowing different cameras to be quickly evaluated.
- (c) It has user selectable control of parameters such as image resolution and image capture rate
- (d) It is freeware.

There are, however, some problems with the Touchless library partly that it was being developed by a small team but mainly from its primary aim of being used with webcams and not microscopes. USB cameras come with an array of controllable parameters such as hue, saturation, sharpness and auto-brightening. The latter parameter, while useful for a webcam, proved to be problematic as it cannot be disabled. In effect, a sample may undergo a variety of colour and brightness changes during an experiment which may trigger the auto-brightness feature causing a sequence of images to appear non-uniform with step changes in brightness. The effect has a particular impact on a feature incorporated into the HDM software for real-time monitoring of the colour of a selected part of the image (see below). Currently, these effects are manually removed after an experiment but software routines to account for these step changes in brightness are being developed.

In the longer term, an alternative camera library may need to be used or even developed in-house.

In operation, the HDM software (see Section 2.5) collects between 1 to 3 images (800 x 600 pixels), via Touchless, over approximately 200 ms. These images can be averaged, pixel by pixel, to reduce noise before being displayed on the screen together with superimposed information (typically time, temperature and sample name). The final image

is displayed on screen and updated once per second. Images are saved to disk in jpeg format at user-selectable intervals of time or temperature.

In addition to the images, real-time information relating to changes in the total colour of selected rectangular regions ('colour monitoring boxes') of the image are also recorded. The average colour value for the box is taken by averaging the RGB (red, green and blue) values for each pixel within the selected region as shown schematically in Figure 2.15

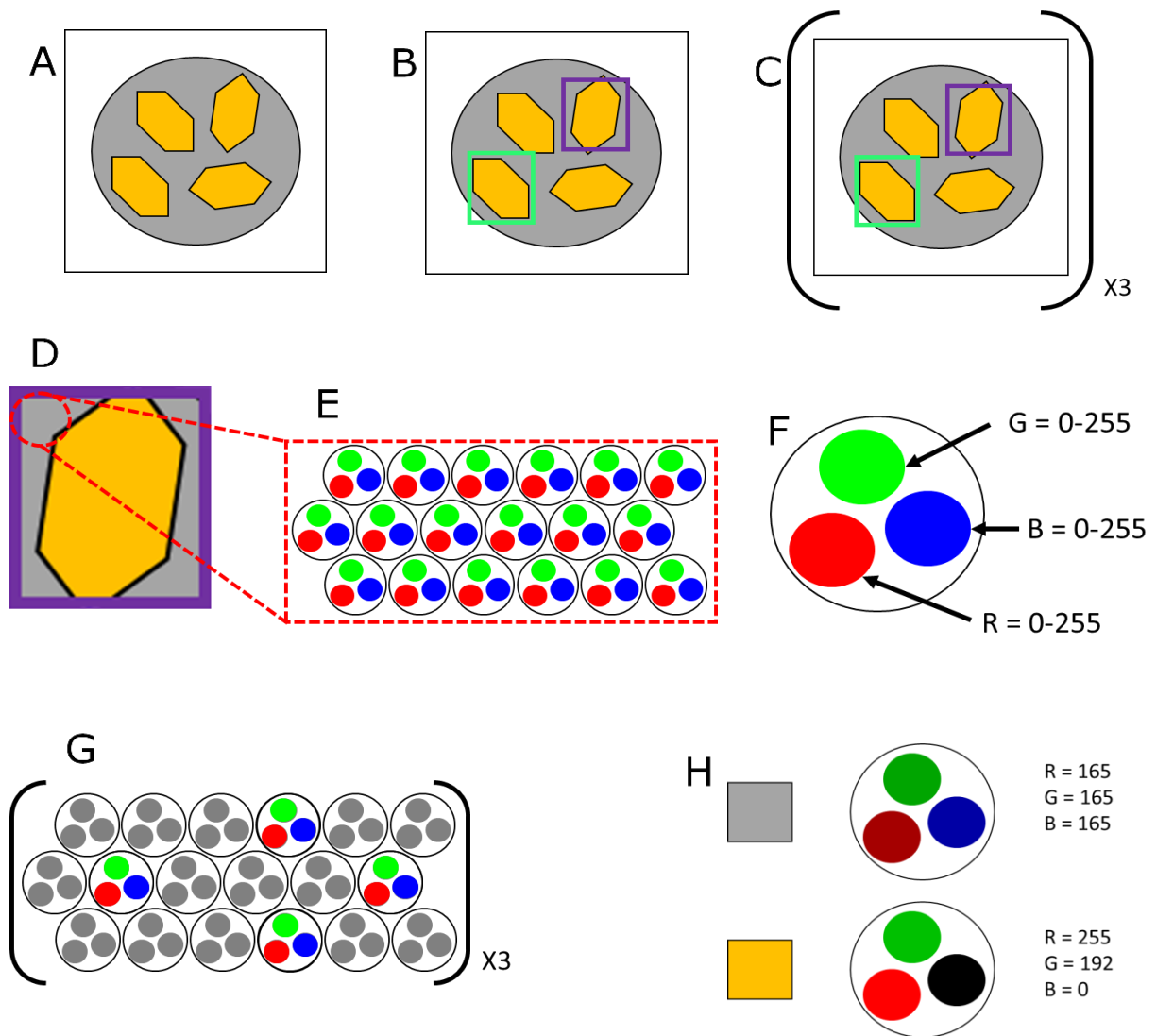


Figure 2.15 Graphical explanation of how RGB colour scores are achieved from user defined areas. Firstly an image is taken (A), and from this the user defines an area of interest (B). The camera captures 3 images within a few milliseconds of each other (C). The images are then broken down into their individual 8-bit colour values, each RGB term is represented by an integer between 0-255. D represents the sampling region, E shows the expanded individual colour components into the pixels (exaggerated) and F shows one pixel's individual RGB components.

An average integer is inbuilt into the code to choose how many pixels to take an average from (G); in this example the sampling integer is four. H shows how RGB colours vary across the sample, RGB values of 165 are obtained for the grey background but for the orange sample RGB scores of 255, 192 & 0 are obtain respectively. For best results and sample representation the user boxes should overlay as much sample as possible, the larger the box the more representative the result is of the true overall colour. In the 8-bit colour scale the closer the three components are to 0 the closer the sample in to black, is contrast as the 3 values come closer to 255 the sample appears white.

Gamma (another pixel collected term) corrects for non-linearity within the obtained images and gives a depth property but is not an active property that is monitored during HDM analysis, instead the primary RGB values are focused on.

The RGB values are processed in a number of ways either using the individual colour components red, green and blue, the summated score which is defined as $\sum RGB$ or as the difference in colour from the starting colour (ΔRGB) viewed as a sample colour history profile. They both produce subtly different plots, $\sum RGB$ is good for broad colour changes whilst ΔRGB is good at highlighting sharp events.

The most recent version of the HDM software incorporates a feature called 'in range pixel counting' (IPC). IPC sums the total number of pixels that are 'in range' of an upper and lower threshold level for a particular colour. This allows a measure of, say, the change in the number of green pixels in a selected region. IPC was used as a means of determining changes in size of a polymer due to thermal expansion and contraction (see Chapter 4, Section 4.4).⁹ The operation of IPC is shown schematically in Figure 2.16. As the size of the selected region of the image is known in terms of height and width of pixels IPC can be expressed as a percentage.

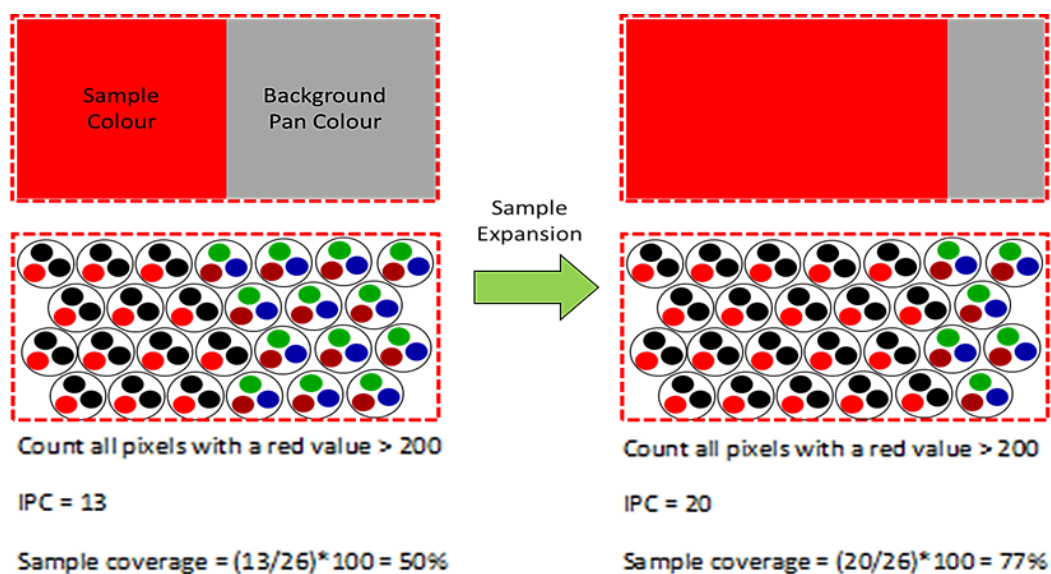


Figure 2.16 Schematic representation of IPC monitoring of a sample during expansion.

A stable lighting source is crucial for any form of microscopy. During the initial development of HDM, a variety of lighting sources were evaluated by comparing the noise and stability of the calculated ΔRGB values obtained when a thermally inert sample (silicon carbide) was heated (see Figure 2.17).

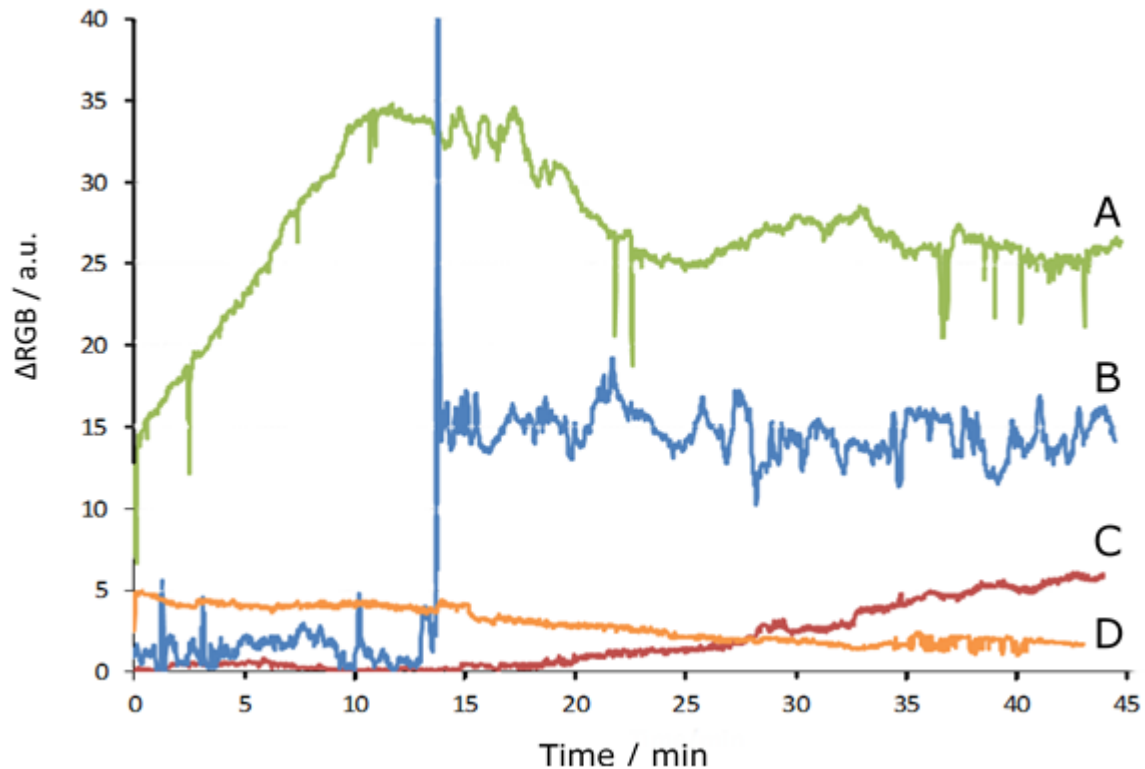


Figure 2.17 HDM lighting comparison evaluated against thermally inert silicon carbide. A) No additional lighting, B) Lamp, C) inbuilt LEDs & D) LEDs and Lamp.

Optimum lighting would give a desired profile that contained minimal spikes (large random fluctuations), and retained a relatively stable background throughout the run.

Lighting based on 240 V filament bulbs was found to produce the least consistent lighting and the decision was made to use the simple white LED lighting inbuilt into most of the digital microscopes (in combination with the overhead fluorescent lighting within the laboratory). This combination provided minimal noise spikes within the colour traces, whilst keeping shadowing effects, caused by lighting position bias, to a minimum. Overall profile C shows a very gradual drift but retains minimal noise throughout on the ΔRGB trace.

2.3.4 HDM – Temperature measurement

As described in Section 2.3.2 the control of the temperature of the hot-stage is facilitated by the Eurotherm temperature programmer, under control of the HDM software.

The various hot-stages developed as part of the project will be discussed in detail below but in all cases they utilised a low mass type K thermocouple for temperature measurement. This is then fed into the Eurotherm and then read by the HDM software. The choice of type K thermocouples was based on from a combination of factors; affordability, compatibility with the Eurotherm (and later Arduino) and an excellent temperature range (sub-ambient to >1000 °C).

Each of the stages was calibrated for the desired working range for each block of experiments and validation checks were performed at least every few weeks. Accurate temperature measurement is a critical factor in any thermal analysis technique and thus a standard method for temperature calibration was developed for all the hot-stages.

A common practice with thermal analytical techniques such as DTA and DSC is to calibrate for temperature through the detection of the phase change(s) in well characterised materials.¹⁰ These include solid to liquid transitions in metals (e.g. indium, tin and lead)¹¹ and organic materials (e.g. diphenylamine, m-dinitrobenzene and benzoic acid)¹² or solid to solid phase changes (e.g. potassium nitrate, ammonium nitrate and caesium chloride).¹³ For hot-stage microscopy, materials with transitions resulting in colour changes (thermochromics) have been suggested (e.g. mercury (II) iodide, vanadium dioxide and ammonium metavanadate).¹⁴ In all cases, the transition needs to be detectable and repeatable.

Indium, tin, bismuth and lead were used throughout the project for temperature calibration for all hot-stages. The method used to calibrate HDM utilised a combination of the micrographs and monitoring the colour change during the melt (see Section 2.3.3). Typically, a sample of the metal to be used for calibration was pressed using ridged pliers both to give a flatter sample that has small indentations on it. These indentations produced sharpened edges whose disappearance as the metal melted was clearly visible optically. In addition, the average RGB values for the pixels in two regions of the image were recorded (see Section 2.3.3). One region comprised the entire field of view while the second was positioned directly over the indented metal, both were recorded during calibration. Graphs of measured melting temperatures against literature values were plotted and fitted with second order polynomial curves. Values from the polynomial curves were stored within the HDM software and used to apply a real-time temperature correction during the operation of the instrument, typical offsets between 1 and 10 °C were noted between measured and literature melting points prior to correction.

The ΔRGB values proved an effective means of detecting the melting point with a step being seen between the values before and after melting (see Figure 2.18 for a sample of indium). This change was not truly the result of a change in colour but rather a change in reflectance of the metal with the indentations serving to create a fresh piece of exposed metal which was lost as the sample melted. The final value for the melting point was taken by extrapolating the colour baseline before the melt and the colour step change itself, standardising on the onset of the melt for calibration values.

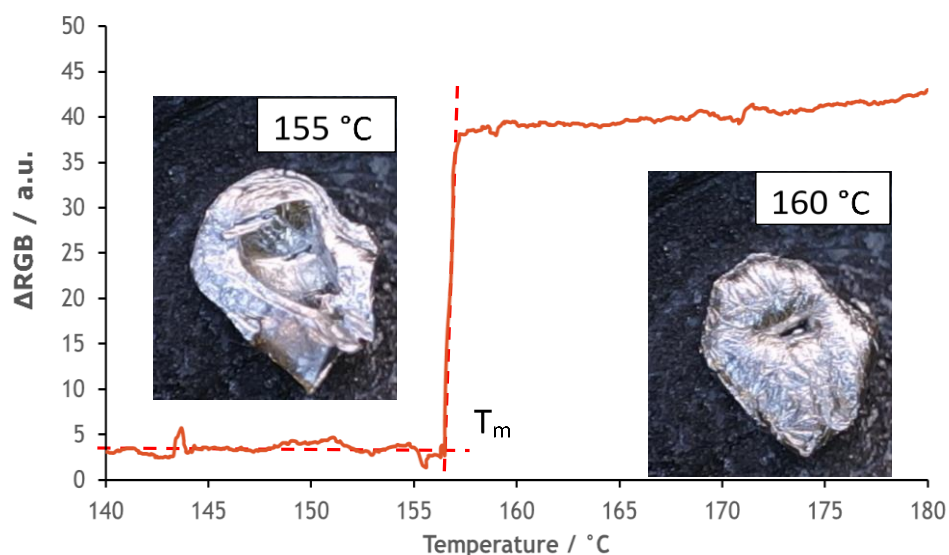


Figure 2.18 HDM temperature calibration example using indium on a graphite insert (to maximise optical contrast) analysed with hot-stage 2. Images shown before and after the melt.

The 'indentation' method was developed to increase the sensitivity of the melting event, as other metallic samples such as bismuth are subject to high levels of oxidation. The oxides of bismuth are highly coloured and produce large variations in the RGB baseline, so the edges of freshly revealed metal aids the detection of the melting point.

Currently the HDM software only supports two pixel monitoring boxes although this can be readily expanded to several more. It is hoped that a later development would be to have, say, four metals in the same pan, to use as a standard calibration pan with the RGB values of each metal being monitored independently during a temperature calibration.

In an ideal situation, simultaneous temperature and mass spectrometer calibration would be achieved. This may be possible through the thermal degradation of PEG (polyethylene glycol) which is already the 'unofficial standard' for DART-MS calibration.¹⁵ The molecular mass of the polymer chains observed with the DART-MS increase with temperature over the range 50 to 350 °C due to increasing thermal lability, so it may be possible to use the first appearance of certain mass fragments as diagnostic of a given temperature. Although it is likely that an accurate temperature measurement would not be possible through this approach it may be a useful rough guide to validate the hot-stage temperature.

2.3.5 HDM – DART and MS

Although an integral component of the HDM system very little DART-MS optimisation was required after the initial evaluation experiments to obtain sufficient MS spectra using the DART source.

A standard DART-MS method, previously developed by Dr Lindsay Harding at Huddersfield was used throughout the course of the study with minor changes made depending on the sample being studied. Generally, initial wide mass scans were performed when evaluating unknown material, with later focusing around the target mass region for the ion of interest.

Small molecule analysis was optimised using the mass spectrometer's inbuilt 'smart parameters' settings with the mass spectrometer focusing on masses typically below 500 Th. This method was mainly employed in the reactions and desorption chapters, Chapters 3 and 5 respectively.

In contrast, a large molecule DART-MS method was utilised mainly for polymer analysis. This method was developed to focus the mass spectrometer to the middle-high end of detection range of the spectrometer, typically above 1000 Da. This method provided most useful for polymer studies in which broad spectrum analytes are noted with significant variety of ions observed during decomposition (see Chapter 4, polymers).

Depending on the nature of the sample, the ionisation polarity chosen is important as certain analytes may not be ionisable in certain polarities. The DART-100 source can be set to operate in either positive or negative polarity mode, and takes several seconds (approximately 10-15) to switch. The mass spectrometer also operates in either positive or negative polarity mode and it can operate almost simultaneously sampling both positive and negative modes within the space of a few hundred milliseconds. Unfortunately since the DART-100 source was relatively slow at switching polarities (when compared to the spectrometer) dual polarity mode was not able to be used and single polarity mode experiments were performed when using the DART-100 source. This dual polarity feature was later exploited during the development of the μ -DART (see Section 2.6).

The following DART and MS parameters were used for the majority of experiments unless otherwise stated in the individual experimental sections.

Flow rates of helium between 1.0 and 1.5 L min⁻¹ controlled by a needle valve and monitored using a flow sensor were used for the ionisation gas. The operating temperature was fixed at 30 °C when used in conjunction with the hot-stage. The DART-100 used grid and discharge voltages of ± 400 V and the needle voltage was set to ± 3 kV (depending on the polarity used). The mass spectrometer (Bruker, Esquire HCT ion trap) analysed over a range 100-2800 Th. Accumulation times of 200 ms were set with a Smart Target of 200,000. Capillary voltage was set to 4 kV with a source temperature of 300 °C.

2.3.5.1 MS Inlet heater

A heater was constructed to fit around the length of ceramic that protrudes from the gist adapter on the mass spectrometer.

It was noted during the analysis of some samples that material condensed on the inlet ceramic to the mass spectrometer. Such condensation is inevitable when large molecular masses are released from samples on the hot-stage at higher temperatures, although the immediate interior of the mass spectrometer is operating at temperatures of 250-350 °C, the inlet ceramic itself is marginally above ambient temperature.

To address the issue of condensation which, if at a sufficient level, could increase the level of background peaks observed in the mass spectra a simple experiment where the inlet ceramic was covered in an insulating material was trialled. The additional insulation did appear to delay or reduce the condensation problems presumably by increasing the heating effect produced by the heated gases leaving the hot-stage and maintaining the inlet temperature set by the spectrometer. The insulating material itself presumably obtained some condensation also, hence the noted delay.

Based on the initial insulation experiments a heater was developed, constructed in a similar manner to the hot-stages themselves (Section 2.4) and comprised of a series of windings of nichrome heating wire wrapped around an electrically insulating material, similar to the interfaces used in other TA-MS instrumentation¹⁶ (used to prevent condensation) with adjustable power being supplied by a standalone microcontroller. This inlet heater reduced the overall signal intensity observed in the mass spectrometer which was attributed to the face plate of the heater being exposed metal which may have provided a surface on which ions could have been grounded before entering the mass spectrometer.

To overcome this, an inert ceramic based paint was applied to electrically insulate the heater. Initial experiments showed that this modification was successful in maintaining signal intensity and that no additional background fragments were observed from the paint. The heater was utilised continuously in the later stages of the project reducing condensation build up from volatiles. Typically a temperature of 250 °C is used (the maximum is around 400 °C) and has been shown to minimise condensation from most samples. Figure 2.19 shows a schematic of the inlet heater and a photograph of it installed.

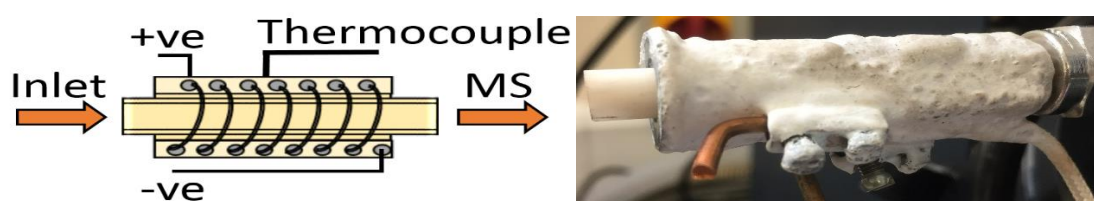


Figure 2.19 Left) Inlet ceramic heater schematic & Right) photograph of the installed unit.

2.4 Hot-stage designs

The hot-stage design went through many development stages. Initially, these were variations of types and geometry of heater and microscope and are described in this section. However, more recent developments have considered other methods for heating samples and passing vapours into the DART stream and these are discussed in Section 2.7.

2.4.1 Hot-stage design 1

The first prototype HDM system is shown schematically and photographically within Figure 2.20. The design mainly was developed to use the Supereyes B008 USB microscope (see Section 2.3.3) situated above the sampling region. The aluminium rig was designed to fit directly onto the standard DART-100 MS coupling flange.

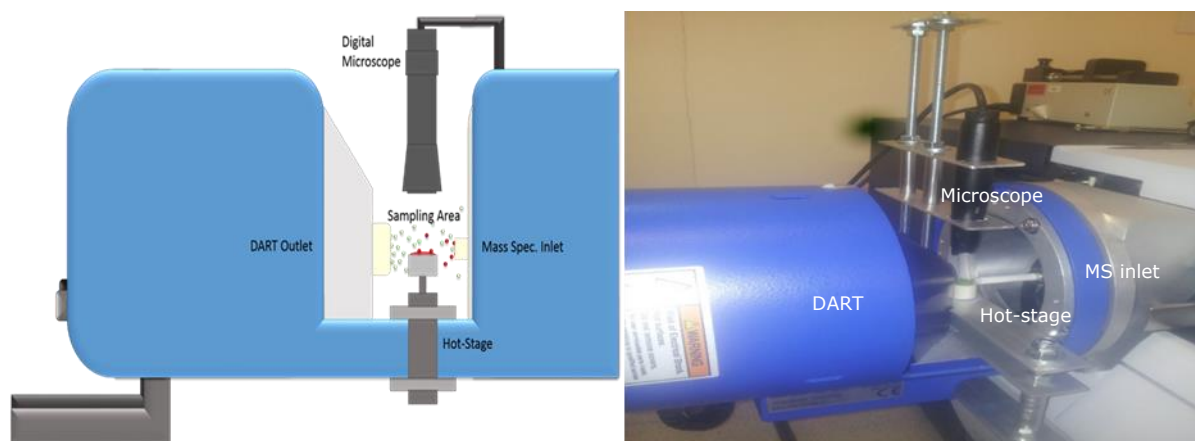


Figure 2.20 The first HDM prototype. A) HDM schematic and B) Photograph of the completed HDM.

The hot-stage was held in place using an aluminium framed rig that could be adjusted in all three axial directions by using a series of nuts and M6 threaded rods. A linear rail was added for the microscope to adjust the focal length, and focusing was achieved using the focusing wheel itself on the camera (see Figure 2.21).

The hot-stage consisted of a ceramic body (Alumina tube, Almath, OD = 12 mm, l) with a DSC pan (Mettler, 27311) added into the top surface and held in by silicate adhesive. The Type K thermocouple (Omega, Type K, 0.1 mm) was then threaded into a twin bore ceramic rod (Almath, OD = 0.5 mm, l = 15 mm) and fed out through a hollow threaded rod, later used to fix the hot-stage to the aluminium rig. Around the thermocouple ceramic was a length of electrical resistance wire (nichrome, l = 10 cm, 2.4 Ω) that was led out of the side of the ceramic stage. The interior was filled with silicone carbide which is both an excellent conductor of heat and provides sufficient electrical insulation between the resistance wire windings (see Figure 2.21).

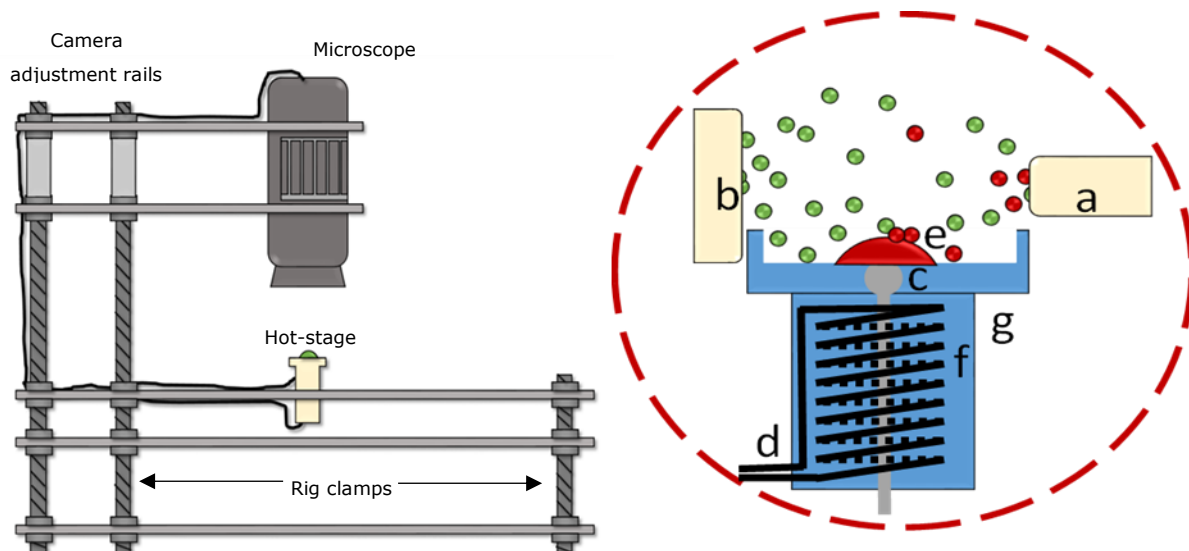


Figure 2.21 Hot-stage design 1 rig and cutaway. a) MS inlet, b) DART-100, c) Type K thermocouple, d) resistive wire windings, e) DSC sampling plate, f) Silicone carbide infill and g) Ceramic body.

The strength of this design was the high level of reproducibility in positioning the sample in the DART stream as the hot-stage was locked in place and the sample was contained within the area of the shallow DSC pan (Metler, Aluminium 27311).

However, this design has a major drawback in that the hot-stage was so rigid that when it need to be cleaned (due to excessive contamination) the whole rig required dismantling.

The aluminium DSC pan used for the hot-plate design had two major flaws that were addressed in the next design. Firstly the pan was too shallow, meaning that most crystalline samples could easily be blown directly into the mass spectrometer inlet.

The second major design flaw was that the use of aluminium restricted the maximum operating temperature to roughly 600 °C (aluminium melts at 660 °C). Although many experiments typically never needed to reach this temperature it did restrict 'baking out', a decontamination step used to destroy most organic based residues where temperatures higher than 600 °C are sometimes desirable.

Sections covered using this edition of the hot-stage;

- Section 4.2, 4.3.1- 4.3.4
- Section 5.2

2.4.2 Hot-stage design 2

To address some of the issues and limitations noted during the operation of the first hot-stage a new design was developed.

The major constraint for development of HDM was the small working area in which the hot-stage needed to fit. The typical height from the baseplate of the DART to the sampling region is ca. 40 mm. Within this height the hot-stage and appropriate wiring needed to be installed, although it was achieved using the first stage more space was desired for design two. Since it was less desirable to drill a hole straight through the DART's baseplate it was decided to modify the interface to orientate the DART 90 ° from its original position.

Feasibility studies (not shown) were performed by clamping the DART to the MS interface and no notable signs of performance loss were noted, therefore a new permanent steel adapter was machined (by Dennis Town of the University of Huddersfield, School of Computing and Engineering) as shown in Figure 2.22. Additionally the steel adapter had holes drilled in the top section of the steel. These holes served as anchors for a motorised rail for the various microscopes, with the intention of later software developments for focusing control.

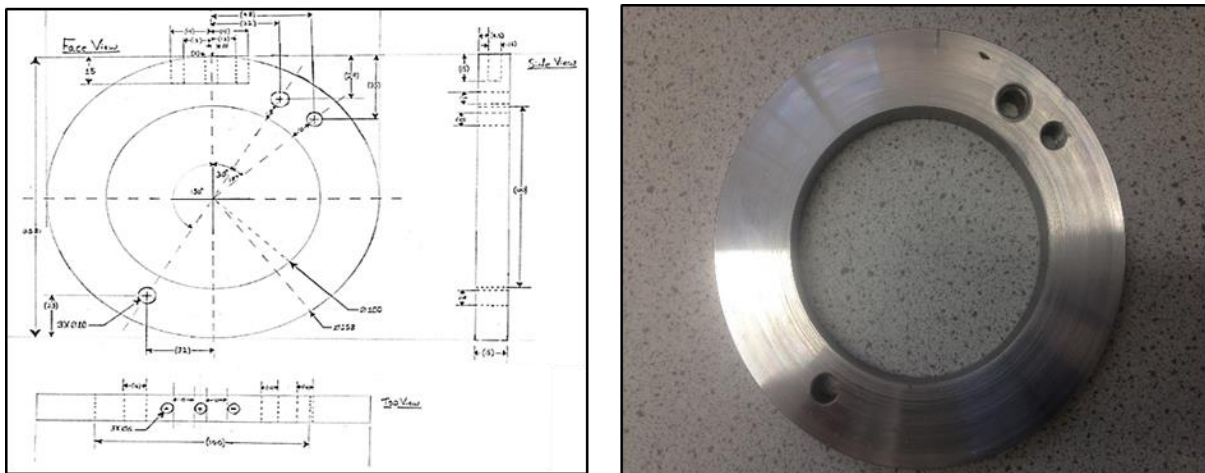


Figure 2.22 Technical drawing of the desired adapter and photograph of the final machined part.

A larger working area had been generated using the DART in this orientation, allowing for the hot-stage to be constructed in a completely linear fashion as shown in Figure 2.23.

Hot-stage two was similar in construction to its predecessor having similar key components. The main body is a ceramic crucible (Almath, TGA175, OD 12.5 mm, 20 mm) hosting the thermocouple/heater assembly. The central assembly consists of the same thermocouple in a ceramic rod construction as before, but with the modification of a second thin ceramic tube to enable more turns of heating wire. This design enables greater uniformity of heating across the stage. The heating wire used was nichrome ($l = 16 \text{ cm}$, 3.8Ω) and the stage itself was filled with silicon carbide powder as in the original design.

A brass collar (1/4", brass ferrule, Swagelok) was added in the top of the stage to transmit heat further up the walls of the pan enabling further uniformity of sample heating. The Inconel pans were then placed within the well of the brass as shown in Figure 2.23.

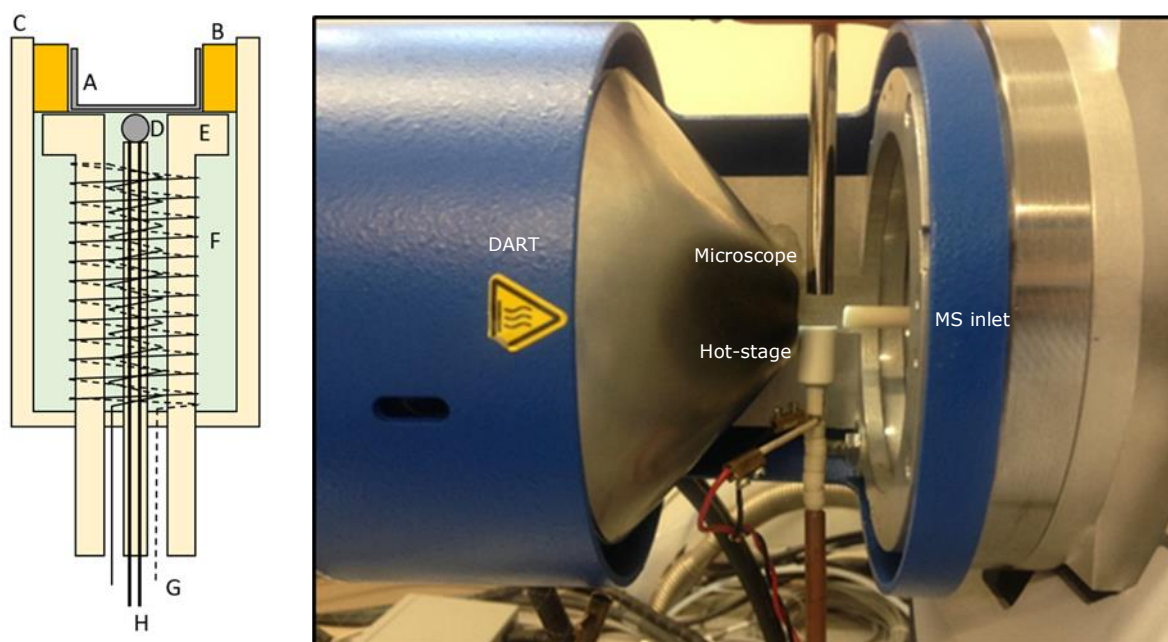


Figure 2.23 Hot-stage rig and stage design two. Left) Schematic of hot-stage two A) Removable sample pan, B) Removable brass collar, C) Outer ceramic, D) Type K thermocouple in twin bore ceramic, E) Secondary ceramic stage, F) Silicone carbide infill, G) Resistive heating wire & H) Thermocouple leads. Right) Photograph of the finished hot-stage two.

A much higher temperature range (approximately 750 °C) could be achieved using this stage whilst still retaining excellent temperature control (± 0.1 °C). The removable brass collar and selectable pan allowed for less 'down time' due to the reduced need for cleaning of the stage should it become contaminated.

A wide range of microscopes was evaluated in this orientation, but typically the unit was fixed with the Teslong microscope to keep with the 'small form factor' of the stage. The reduction in bulk of the rig overall made it much easier to place and remove samples without sacrifice of reproducibility of positioning.

Sections covered using this edition of the hot-stage;

- Section 3.2 - 3.10
- Section 4.3.5 - 4.4.6
- Section 5.3

2.5 Software

The HDM software was developed and extended from prototype software written in Visual Basic 6.0 (Microsoft) by Dr Gareth Parkes at Huddersfield University for Windows XP. The current software utilises the more powerful Visual Studio (Microsoft) programming platform designed for Windows 10.

This section describes the basic operation of the HDM software and shows a selection of screen shots of some of the key interfacing windows.

2.5.1 Experimental header editor

Details relating to the sample and experimental parameters are stored in 'header' files. Figure 2.24 shows the experimental header editor window. Each experimental header is stored on a disk as a text file and can be loaded for examination or as a template for subsequent experiments.

The screenshot displays the 'HSM - Edit Header' window with the following sections and controls:

- A (Sample Information):** Sample: Polystyrene, Filename: Poly1, Sample mass: 1.1 mg, Atmosphere: Static air, Operator: GPA, Date: 30-May-18, MS file: 13579, Comment: (two empty text boxes).
- B (Experiment Type):** Manual control (selected), Temperature program, Sample controlled.
- C (Acquisition Trips):** Temperature: 400.0 °C, Time: 30.0 min.
- D (Settings under development):** Separate sample T? (checked), RLI enabled? (unchecked), Start on MS activated? (unchecked).
- E (Image Capture):** Capture on time, Capture on temperature (selected), Use values from data file (unchecked), Start capture time: 2.0 min, End capture time: 25.0 min, Capture time interval: 0.5 min, Start capture temp.: 50.0 °C, End capture temp.: 250.0 °C, Capture temp. interval: 10.0 °C, Pseudo video mode (unchecked).
- F (RGB Pixel Monitoring):** Monitor RGB pixels in full image (checked), Total RGB = change from start (checked), Monitor RGB pixels in box 1 (checked), Box 1 RGB = change from start (checked), Monitor RGB pixels in box 2 (checked), Box 2 RGB = change from start (checked).
- G (Temperature Calibration):** Temperature calibration active? (checked), Calibration Values button.
- H (Experiment Control):** Edit Flags button, Edit IPC button.
- I (Microscope):** Magnification: 20x, Brightness: 2 on dial.
- J (Control buttons):** Load Header, Temp. Program, Additional Parameters, EXIT, SAVE and EXIT.

Figure 2.24 HDM screenshot - experimental setup window. A) Sample information, B) Experiment type, C) Acquisition trips, D) Settings under development, E) Image capture, F) RGB Pixel monitoring, G) Temperature Calibration, H) Experiment control, I) Microscope, J) Control buttons

2.5.1.1 Sample information (A)

This section is used to store information about the sample such as what the sample is, the quantity and any additional information is added in the comments box. A file name is chosen here, the data collected from the experiment and micrographs will then be stored under this file name.

2.5.1.2 Experiment type (B)

Two experimental types can be currently run: manual control and linear heating. The manual control experiments allow the user to input a fixed set point at any moment during the operation of HDM, power is adjusted accordingly to reach the setpoint. Temperature program experiments follow a series of pre-set heating or cooling rates (Figure 2.25) to predefined setpoints and may dwell there for a fixed amount of time. The third experimental option 'sample controlled' will be discussed further in Section 2.7.4.1.

2.5.1.3 Acquisition trips (C)

As a safety precaution all instrumentation has trip values included to prevent damage to the instrument, these are shown as an upper temperature limit and upper time limit. If either of these values are reached during an experiment, the instrument returns the setpoint below room temperature (10 °C), ceases applying power to the hot-stage and stops the data acquisition.

2.5.1.4 Developments (D)

This section is used for the coding sections under development. A development for having a separate sample thermocouple (as opposed to using a furnace alone thermocouple) is shown. The possibility of having RLI (reflected light intensity) measurements was included but so far has not been significantly developed. Finally, a development to start the MS directly through the HDM controller software was included (better experiment synchronisation).

2.5.1.5 Image capture (E)

The software is instructed to save an image depending on either time or temperature although the microscope image is continuously updated throughout the experiment, images files (.jpeg) are only saved at these predefined intervals.

2.5.1.6 RGB pixel monitoring (F)

This section allows the user to turn on and off the recording of Red, Green, Blue, Σ RGB and Δ RGB values for the whole image or the two pixel monitoring boxes. The pixel monitoring boxes setup is shown later (see Section 2.5.3)

2.5.1.7 Temperature calibration (G)

This window allows the calculated second order polynomial temperature calibration values (see Section 2.3.4) to be added. The calibration factor can be toggled on or off, to allow the raw data to be saved.

2.5.1.8 Experiment control (H)

This section allows the operator to set 'flags' which tell the software to do something when a certain criterion is met, such as *'take more images if the colour becomes more red'*. The second set of parameters to be set relates to the IPC (In-range pixel counting) function. Values can be stored to count the number of pixels within, below or above a selected threshold (see Section 2.3.3)

2.5.1.9 Microscope parameters (I)

This section is used to store values obtained from the microscope itself. These are manually input by reading off the values from the digital microscopes themselves, this is again stored to the header file and is useful for comparative studies, ensuring the same level of brightness and magnification is used.

2.5.1.10 Control buttons (J)

The final section shows a series of control buttons that allow the operator to load existing headers (from previous experiments), save the current header and modify the temperature programme.

2.5.2 Temperature programme editor

Shown in Figure 2.25 is a screenshot of the temperature programme editor window. This version is currently used to modify the existing Eurotherm temperature programme.

The Eurotherm has a maximum of 8 temperature ramps that can be used to either controllably heat or cool the sample between 30 and 750 °C (based on hot-stage 2). Very slow heating and cooling rates less than 1 °C min⁻¹ may be used (tested down to 0.1 °C using the HDM), contrastingly relatively quick heating rates may be used of up to 50 °C min⁻¹, faster heating rates can be achieved but this has been limited to 50 °C min⁻¹ to prevent damage to the hot-stage through thermal shock.

Typically, very few experiments need more than 8 temperature ramps so the use of the Eurotherm has been more than sufficient for the development of the HDM.

A similar window used to control the Arduino microcontroller temperature programmer is introduced shortly in Section 2.7.

Eurotherm Temperature Programme								
Eurotherm Temperature Program								
Ramp 1	5.0	°C/min	Level 1	700.0	°C	Hold 1	0.0	min
Ramp 2	STEP	°C/min	Level 2	30.0	°C	Hold 2	END	min
Ramp 3	STEP	°C/min	Level 3	30.0	°C	Hold 3	END	min
Ramp 4	STEP	°C/min	Level 4	30.0	°C	Hold 4	END	min
Ramp 5	STEP	°C/min	Level 5	30.0	°C	Hold 5	END	min
Ramp 6	STEP	°C/min	Level 6	30.0	°C	Hold 6	END	min
Ramp 7	STEP	°C/min	Level 7	30.0	°C	Hold 7	END	min
Ramp 8	STEP	°C/min	Level 8	25.0	°C	Hold 8	END	min

Figure 2.25 HDM screenshot – temperature program window.

2.5.3 Pixel monitoring window

The pixel monitoring functionality is set up in another window shown as a screenshot in Figure 2.26. In this mode the pixel monitoring boxes (shown as the green and purple squares) are adjusted and moved to the desired location of the image in which representative colour values are taken.

HSM - Pixel Value Monitoring

Whole image
 Select Box 1
 Select Box 2

> Get Image <

Width	Height
+ -	+ -
800	600

Whole image	
Red	117.1
Blue	96.0
Green	102.7
Total	315.9

X 779 Y 387

Figure 2.26 HDM screenshot – Pixel monitoring window.

The pixel monitoring boxes are selected by toggling the radio buttons in the upper right hand side of the window. The pixel monitoring boxes are then dragged into place (X and Y coordinates are also shown) over a region of interest and the size is adjusted accordingly using the height and width buttons. The individual red, green, blue and total (Σ RGB) values are shown in a table to the right hand side of the screen, these values are mainly used to set the IPC parameters prior to analysis.

2.5.4 Acquisition window

Figure 2.27 shows a screenshot of the display when a typical experiment is running. Key information is displayed to the right hand side of the main image relating to the colour of the image and corresponding boxes. The values for the current second's red, green, blue and Σ RGB for the whole image and the two pixel monitoring boxes are displayed. The IPC value is then expressed as a percentage based on the previously input IPC thresholds.

Images are overlaid with key information (sample name, time and temperature) set in the experiment header. A setpoint temperature control input used in a manual control experiment can be seen. Buttons to control the main experiment are shown, 'Start' starts the experiment and runs the temperature programmer, 'Stop' stops saving data and returns the setpoint to 10 °C, 'Hold' holds the temperature at the current temperature, inducing an isothermal hold and 'Exit' stops the experiment and returns to the main screen.

A burst image mode (used to take and store images, typically at intervals less than 1 second) was developed to capture events that occur between the predefined values set in the experimental setup, to ensure maximum flexibility of the image capturing control. This feature provides very useful for fast transitions such as the melting of pure compounds.

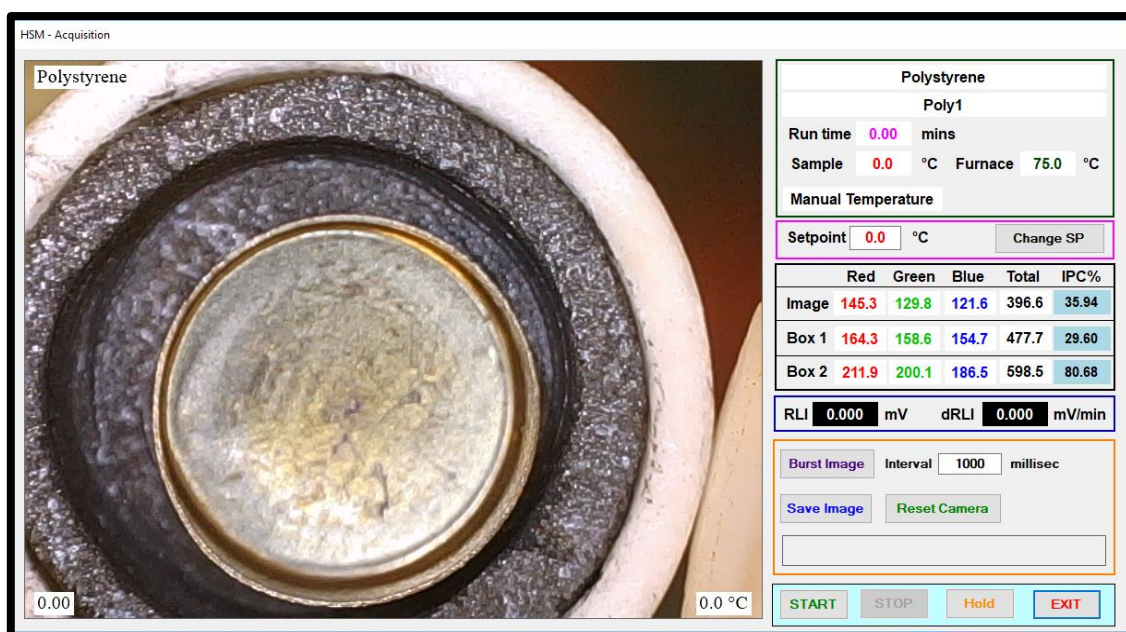


Figure 2.27 HDM screenshot – Experiment acquisition window.

2.5.5 Data extract

A separate programme called DataExtract was developed in-house to decrease the time needed to process mass spectral data collected during an experiment. This was necessitated by the limited data manipulation capabilities of the inbuilt mass spectrometer data analysis software. In particular, it was desirable to be able to extract individual ions (or range of ions) from each mass scan to allow 'thermographs' relating to a particular chemical species to be obtained as a function of time or temperature. As a one hour experiment could create several hundred megabytes of data corresponding to over 50 million data points an automated method was essential. The main program window is shown in Figure 2.28.

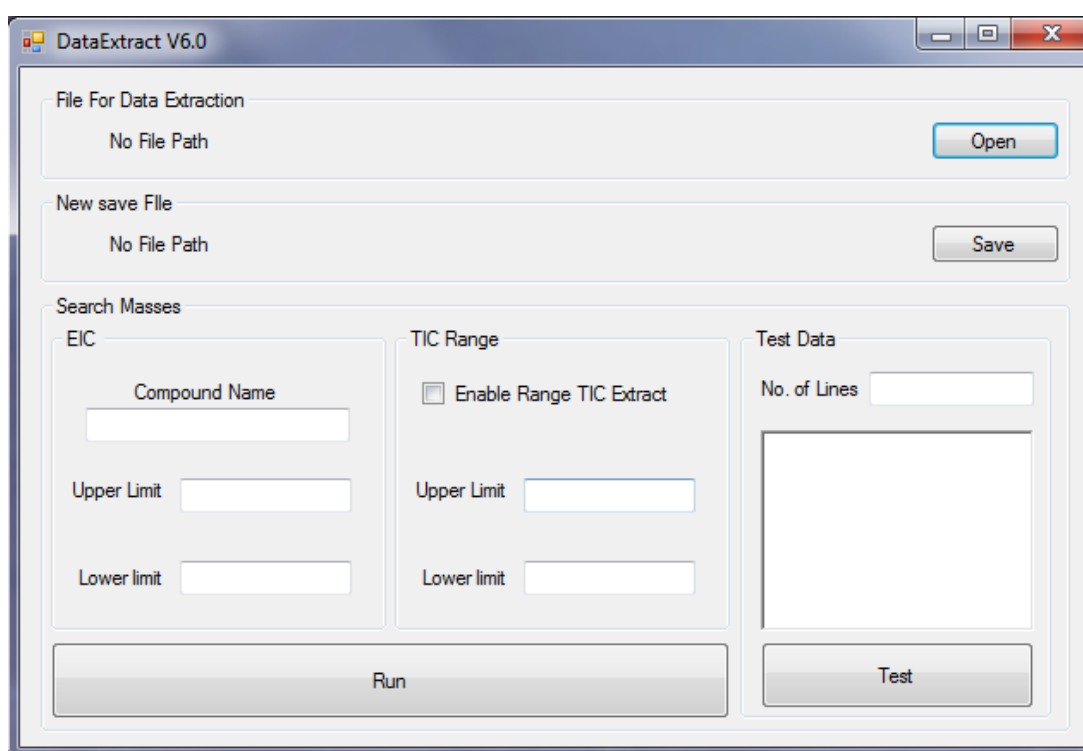


Figure 2.28 Data Extract version 6.0, used for chromatogram extraction of raw MS data.

In essence, a data file corresponding to all the mass scans in an experiment is selected and the mass range of ions of interest chosen. The data file is read line by line (where each line represents a string of numbers representing the magnitude of each ion detected in one scan) and any ions within the selected range recorded. The program then produces a separate output data file in .csv format ready for processing further using Excel.

In Excel, the data file from the Data Extract and the corresponding HDM data file are combined using the VLOOKUP function so that they share the same time base. Once this has been done mass spectral data can then be plotted as a function of either time or temperature.

2.6 Development of an alternative ion source (μ -DART)

One of the major constraints of the HDM system was the overall size of the DART-100 source which as can be seen from Figure 2.23 dwarfs the hot-stage. The most recent commercial versions of the DART have seen a significant reduction in size although the instrumental rig that accompanies the DART is still relatively large.¹⁷ One factor that determines the overall size of the DART source is that it has to incorporate heating elements used to raise the temperature of the ionisation gas – a feature not required with the use of a hot-stage. In addition, the DART source has additional circuitry used for ion filtering, which is used to change the ionisation polarity. This is useful when coupled to some mass spectrometers but the Bruker Esquire HCT ion trap mass spectrometer used in this project can be operated in positive, negative or in simultaneous modes, allowing for selective charge monitoring even if the source of ions is not filtered.

As part of the longer-term aim of simplification of the HDM system, the idea of producing a smaller, simpler DART source was investigated. Using a range of source materials including the original patent documents,¹⁸ photographs of Cody's own prototype¹⁹ and other literature²⁰⁻²¹ an ion source termed ' μ -DART' was developed.

μ -DART is possibly the simplest form of DART as it does not contain an ion filter or a heater. The μ -DART (see Figure 2.29) comprises a PTFE T-piece (Swagelok) used as the main body (A) that houses the electrodes used for plasma generation (E). High voltage wires are fed through a blanking plate on one end of the T-piece which are connected to the electrodes. The electrode assembly consists of an outer steel electrode housing a ceramic guide (that is non-electrically conductive) and protruding from the ceramic guide is the counter electrode, the distance of which can be adjusted. The ionisation gas is passed through the 'bottom' of the T-piece junction. The final junction of the T-piece is used as the outlet, the outlet itself is a glass tube that tapers down to an outlet size of 1 mm in diameter.

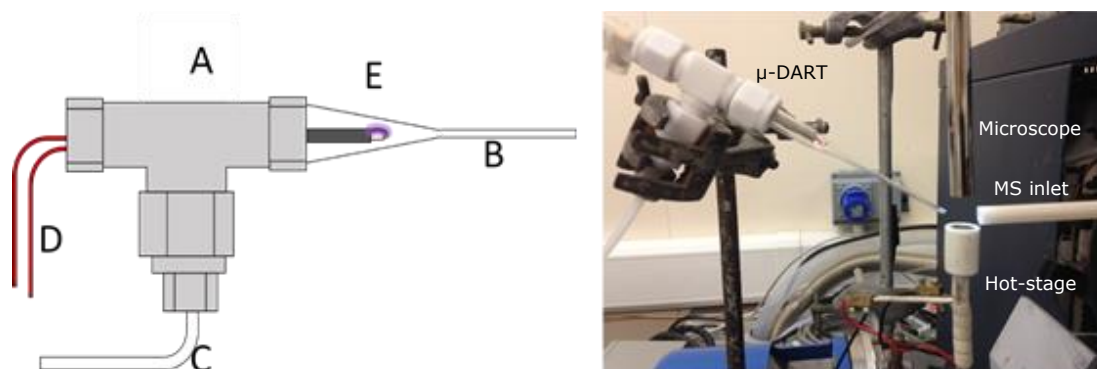


Figure 2.29 μ -DART development. Left) μ -DART schematic A) Swagelok PTFE T-piece, B) Glass ion guide, C) Gas inlet, D) HV connections, E) Plasma region & Right) Photograph μ -DART in operation.

The μ -DART operates using high DC voltage and low currents which leads to the formation of the classic corona-to-glow discharge in the carrier gas. The metastable ions are generated within the low temperature plasma which are focused by the glass ion guide towards the sample on the hot-stage. The plasma itself is highly localised and does not extend into the sampling region.

To ensure the μ -DART could not be classified as another ambient ionisation technique (many of which share a lot of similarities) comparisons were made with DART, FAPA (flowing atmospheric pressure afterglow) and LTP (low temperature probe) based on information from the literature (see Table 2.2).

In appearance μ -DART looks very similar to some versions of the LTP, however the LTP uses higher AC voltages and relies on direct sample contact with the plasma, unlike the μ -DART which is a non-contact plasma. The FAPA source operates at low voltages and higher currents than the μ -DART, with a higher temperature plasma extending into the sampling region. However, μ -DART, LTP and FAPA contain no ion filtering unlike the DART source. μ -DART is more DART like than FAPA like.²⁰

Table 2.2 μ -DART comparison against similar plasma based techniques.

	DART	FAPA	LTP	μ-DART
Voltage Type	DC	DC	AC	DC
Voltage of plasma	0-5 KV	-ve 400-500 V	11-18 KV	Fixed at 9 KV
Current of plasma	2-5 mA	25 mA	160-270 μ A (calc. from 3W)	500 μ A (calc. from $P_{in} = 5W$)
Type of plasma	Corona-to-glow	Glow-to-Arc	Dielectric barrier discharge	Corona-to-glow like
Electrode types	Pin cathode to grounded disk	Various, pin-plate, halo	Dielectric barrier	Pin-Pin
Filtering	Bias electrode to select polarity	No filtering	No filtering	No filtering
Exit Gas Temperature	30-35 $^{\circ}$ C Up to 500 $^{\circ}$ C with additional heating.	235 $^{\circ}$ C	Ca. 30 $^{\circ}$ C	30-40 $^{\circ}$ C
Contact Type	Non-contact	Semi-non-contact. The plasma plume extends into the sampling region	Plasma Contact	Non-contact

To fully characterise the plasma a number of techniques can be used including optical emission spectroscopy which monitors the energetic states generated by the plasma itself.²² Alternatively, the formation of charged water clusters produced by DART (but not FAPA) can be detected by low range mass spectrometric analysis.²³

Another documented method used to evaluate the plasma types is through the comparison of 'survival yields' which is the ratio of the molecular ion / most abundant ion and its fragments.²⁰ Generally, the harsher the experimental conditions the more analyte fragmentation is observed, resulting in a lower survival yield.

Since DART is typically classified as a soft ionisation technique, the molecular ion or molecular adducts will be in higher abundance than that of the fragments leading to higher survival yields.

A series of experiments was undertaken to directly compare the performance of the DART-100 and the μ -DART using the desorption of tetryl (2,4,6-trinitrophenylmethylamine, see Chapter 5.0). The most abundant ion for tetryl was the nitrated molecular adduct $[M+NO_3]^-$ at 349 Da with the main fragment ion $[M-NO]^-$ found at 257 Da. The second compound evaluated was methyl salicylate, observed as the protonated ion $[M+H]^+$ 153 Da and a single demethoxylated fragment $[M-OCH_3]^+$ 121 Da.

Figure 2.30 shows the average mass spectra for tetryl using the DART-100 and the μ -DART source. The fragmentation patterns for both sources are broadly similar. The intensity of the signals when using the μ -DART appears to be greater but the background level is also higher. Figure 2.31 shows the average mass spectra for methyl salicylate using the DART-100 and the μ -DART source, again the mass spectra look very similar, the μ -DART source does show one extra peak at 129 Da, but this was apparent in the background before sample analysis.

Based on the ratio of the ions at 349 Da and 257 Da the survival yield for the DART-100 was 59% while that of the μ -DART was 67% when analysing tetryl. Survival yields of 91 and 93 % were achieved for the DART-100 and μ -DART respectively when the ratio was based on the ions 153 Da and 121 Da using methyl salicylate. Shelley *et al.* have reported that the harsher FAPA source generally leads to more analyte fragmentation than the DART source resulting in lower survival yields.²⁰ Encouragingly, the values obtained for the μ -DART are significantly higher than those reported for the FAPA source.

The combination of operating conditions, sample interaction methods and survival yields clearly shows that not only can μ -DART be viewed as having the same form of ionisation as DART but that it operates sufficiently well to act as a replacement.

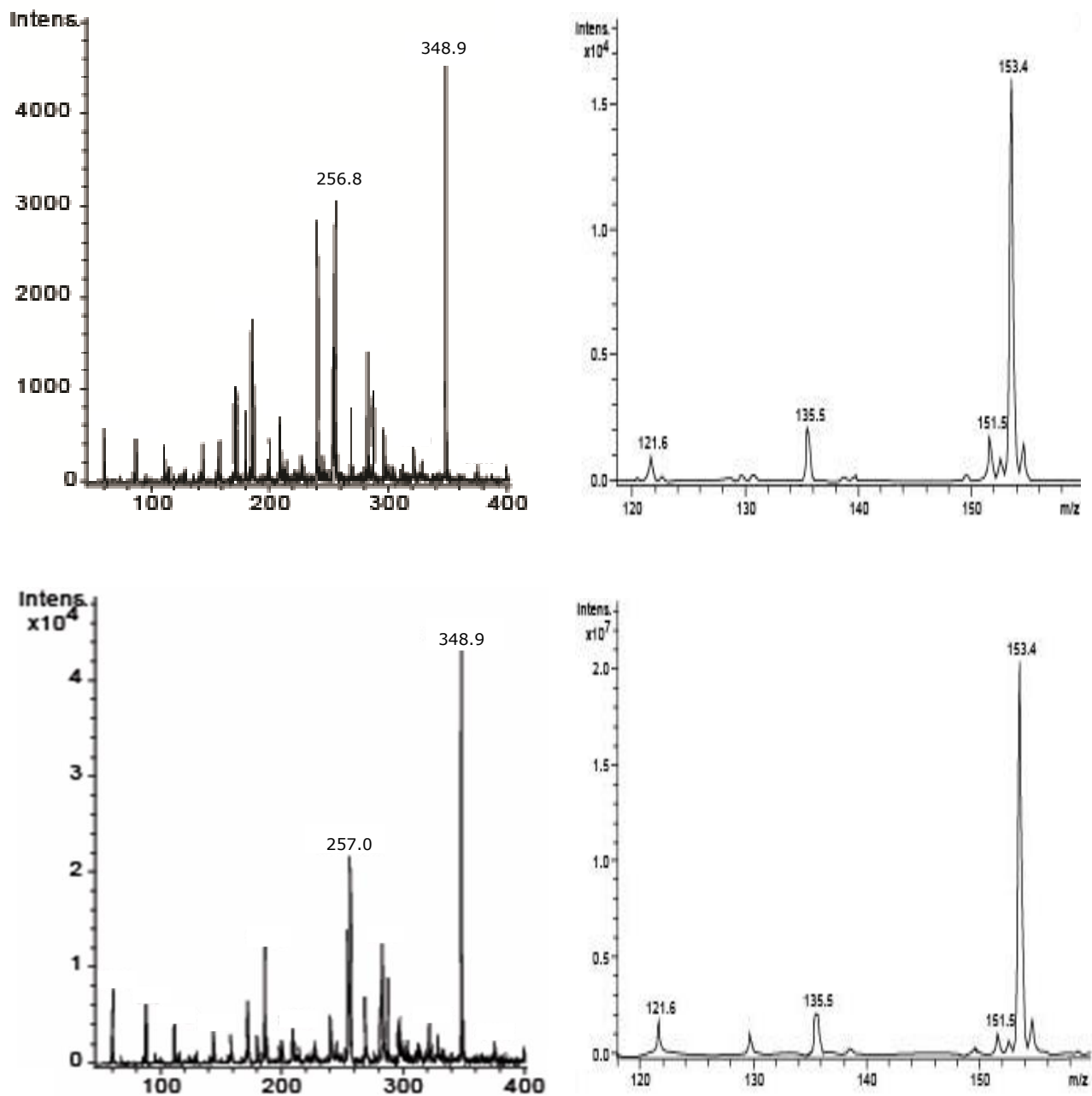


Figure 2.30 Top Left) DART-100 analysis of tetryl & Bottom Left) μ -DART analysis of tetryl.

Figure 2.31 Top Right) DART-100 analysis of methyl salicylate & Bottom Right) μ -DART analysis of methyl salicylate.

The μ -DART was used within the following sections:

- Section 2.7.4.4
- Section 3.4 & 3.9
- Section 4.3.5 - 4.4.6
- Section 5.3.3 - 5.3.5

2.7 Current and Future developments

As with any instrumental development project the process is dynamic and ever evolving to suit the requirements of analysis. The project as a whole was focused on the evaluation of the combination of HSM with DART-MS. However, it soon became apparent that a wide variety of techniques involving controlled heating of the sample and DART-MS of either sample itself and/or evolved material was possible. Some of these techniques would be modifications or adaptations of the basic HDM design while others would move away from the microscopy aspects of the current project. This section describes some of these designs which are in various stages of development and also describes planned developments to the software. A longer term aim beyond the current HDM is to have a more modular approach to the instrumentation with more standardised components.

2.7.1 DTA hot-stages

A logical development of the current hot-stage is to incorporate some form of differential thermal analysis (DTA). This would add information about enthalpic changes in a sample to the chemical and optical information HDM already provides.

There are two approaches possible. One is to have separate thermocouples for both the hot-stage and the sample and then process the difference in software – an approach some thermal analysis instrument manufacturers adopt. The other is to have separate sample and reference thermocouples and amplify the differential signal which gives a 'true' DTA as described in Chapter 1.

A schematic of the prototype DTA stage is given in Figure 2.32. It features three thermocouples, one connected to the main body of the stage for heating control, whilst the other two thermocouples are used to measure sample and reference temperatures. The main body of the DTA stage is constructed from metal, in the first iteration of the prototype (see Figure 2.33) aluminium was used for ease of machining, again this does limit the upper temperature range to around 600 °C. The metal body has excellent thermal conduction properties and ensures fast heat flow through to the sample from the external heater windings. The heaters windings (nichrome) are separated by a thin layer of mica, an electrically insulating material. The heater will be driven in the same way as the hot-stages described in Section 2.4. The outer layer is coated with thermally and electrically insulating paint to prevent damage to the instrument, protect the operator from live wires and also force the heat inwards towards the sample pans. The sample wells drilled out are flat, to ensure good thermal contact with standard TA pans up to 6 mm in diameter.

The key to any differential temperature analysis is balance, both in terms of instrumental mechanical symmetry between the sample and reference and a temperature balance to compensate for any drift within the differential signal. High quality amplification of the DT

signal is also necessary to ensure sensitivity as typically the difference is in the order of a few microvolts.

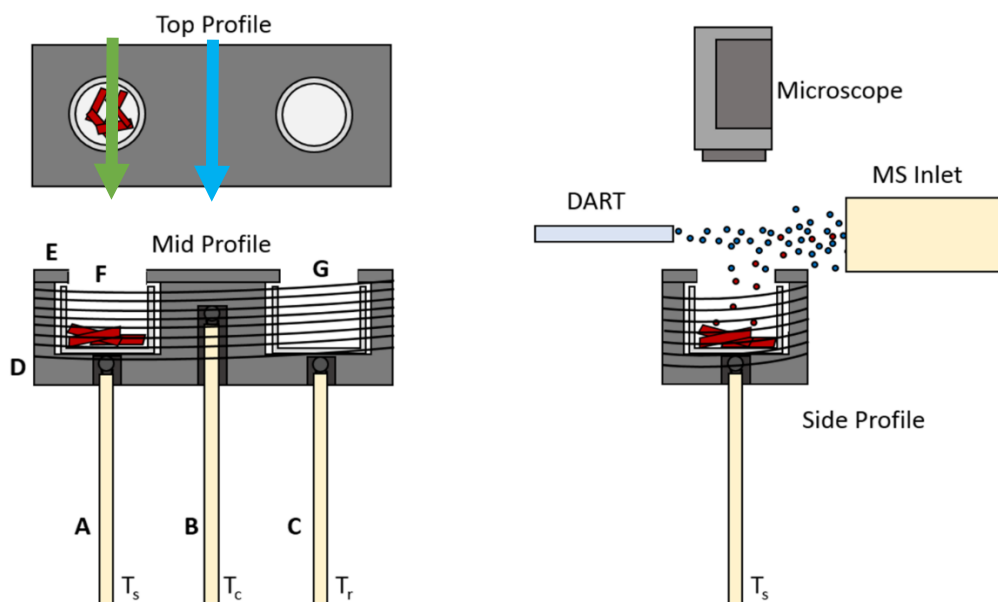


Figure 2.32 Schematic profiles of the constructed DTA stage. A) Sample thermocouple, B) Stage control thermocouple, C) Reference thermocouple, D) DTA stage, E) Insulating cap with viewing points, F) Sample well and G) Reference well. (Not to scale)



Figure 2.33 Photograph of the prototype DTA stage.

Initial tests with a prototype show that although the temperatures are being read accurately an improved preamplification circuit for the DT signal is required.

The location of the DTA stage in the DART-MS ionisation stream will also be a crucial factor. Locating the stream immediately above the sample pan (green arrow, Figure 2.32) would lead to the most sensitivity in terms of mass spectrometry, but is likely to lead to a temperature imbalance on the sample side of the DTA stage itself.

Alternatively, the DTA stage could be positioned with the DART stream passing down the central axis (blue arrow, Figure 2.32). This would ensure maximum temperature balance as the DART's cooling effect is equal on both sides of the stage. But, as was shown earlier in this chapter (see Section 2.2.2) the DART outlet stream is typically quite narrow, and a significant reduction in sensitivity in terms of mass spectrometry is likely.

Nonetheless, the use of a DTA stage would be a clear step forward for the instrument as a whole and enhance the aspects of HDM.

2.7.2 Desorption stage

Although desorption experiments have been done using the current HDM (see Chapter 5) there would be benefits in having a system capable of controlled desorption of samples collected from a variety of 'swabbing' materials. Here, the microscopy component would be redundant as samples are typically at trace levels from which no useful optical information can be gained.

The proposed desorption stage is shown schematically in Figure 2.34 and the first prototype photographically in Figure 2.35. The design is primarily for use with cotton tipped swabs although other adsorbent matrices could be used. The stage would use a 'twin thermocouple' approach with one thermocouple used as the source of control of the main body of the desorption stage and a separate thermocouple to monitor the sample temperature.

The prototype design consists of the main body being constructed out of aluminium (around 35 mm long), with resistive heating wires wrapped around the main body (around 15 mm in diameter). An inner glass sleeve would contain the swab resting on a sintered frit with an embedded thermocouple.

The carrier gas (matching the ionisation gas) would be passed over the sample to aid with the transport of analytes into the ionisation stream of the DART. At the base of the desorption stage connected to the protruding glass sleeve would be a PTFE T-piece used to connect two gas flows, the actual carrier gas and the optional inlet for a source of 'dopant'. Dopants are introduced to increase sensitivity of analytes (see Chapter 5, Section 5.3.5) which is particularly useful for trace analysis.

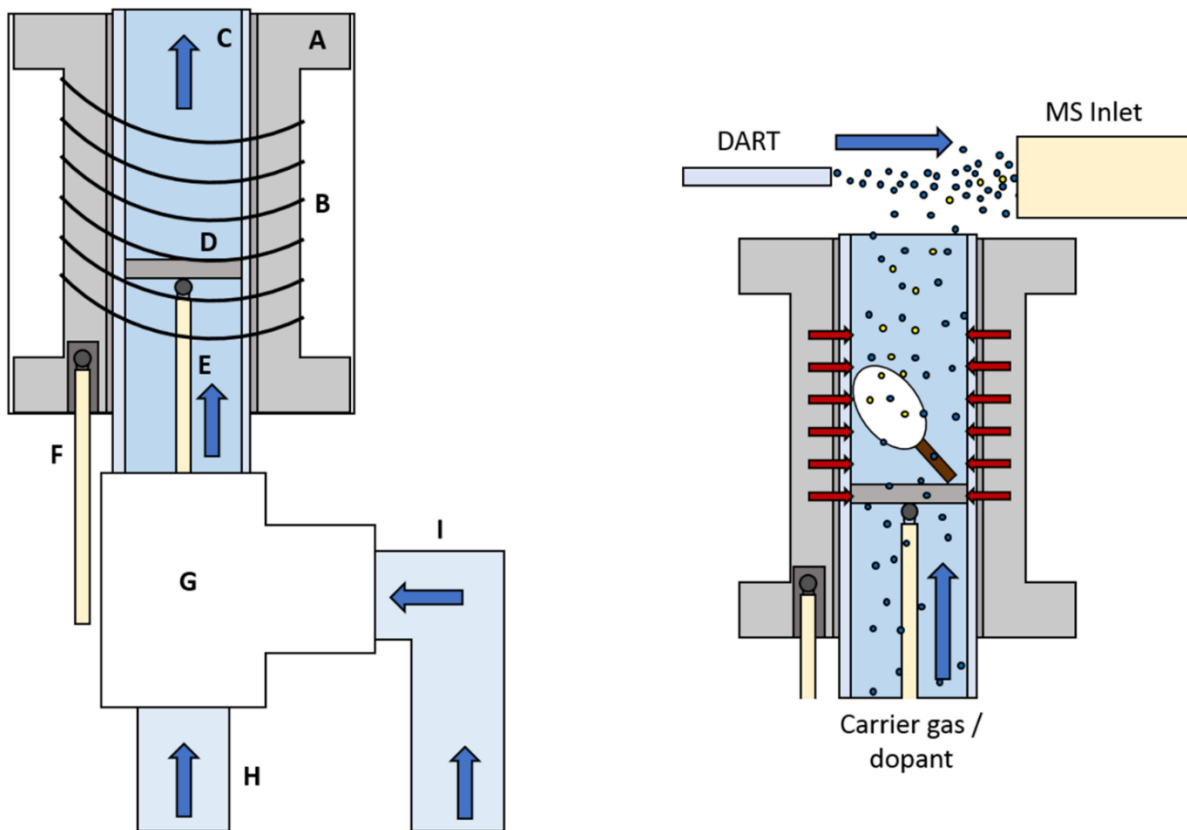


Figure 2.34 Schematic representation of the flow through stage and operation. A) Aluminium body, B) Resistive heating wire, C) Quartz glass insert, D) Porous platform, E) Sample thermocouple, F) Hot-stage thermocouple, G) PTFE T-piece, H) Carrier gas inlet and I) Dopant inlet. (Not to scale)

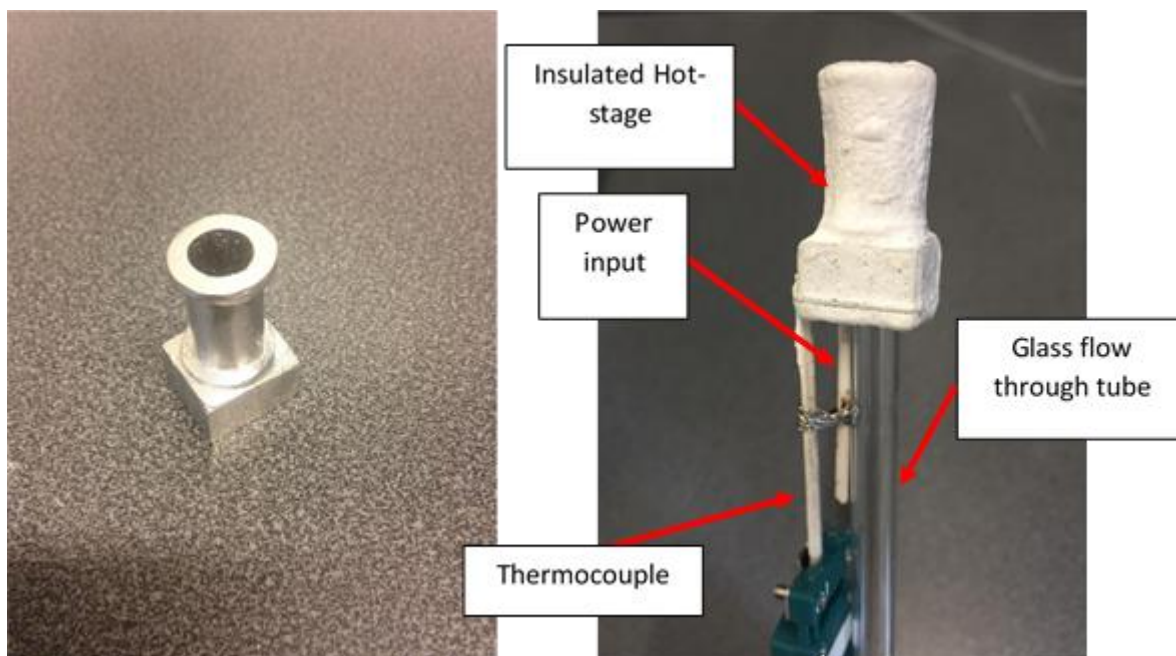


Figure 2.35 Photographs of the prototype desorption stage, Left) the bare stage and Right) the completed prototype.

2.7.3 Induction heating thermal desorption DART-MS

Another approach to desorption studies being planned by the group involves a combination of commercial thermal desorption tubes and induction heating.

TD-GC-MS (Thermal desorption gas chromatography mass spectrometry) is an existing commercialised technique that separates analytes chromatographically where vapours from the area of interest are pulled by vacuum onto a sorbent material contained within a metal tube. If required, these desorption tubes can be sealed for longer term storage so that sampling can be done away from the analytical laboratory. During analysis the tubes are heated rapidly while a carrier gas passes through them to transport the vapours onto a GC column to be separated and then analysed by a mass spectrometer.

TD-GC-MS has shown to be a powerful technique in the investigation of a wide range of analytes including accelerants associated with arson,²⁴ foods²⁵ and energetic materials analysis.²⁶

Combining the flexibility of the thermal desorption tube approach with ambient ionisation techniques such as DART offers many benefits especially if the complexities of the standard thermal desorption unit and gas chromatography could be removed. In an earlier project at the University of Huddersfield, the use of induction heating has been investigated as the basis of a novel thermal analysis technique. Induction heating occurs through the use of high frequency oscillating magnetic fields to drive currents through a material to generate heat. The metal TD tubes are very amenable to induction heating and as it is a direct form of heating, no furnace is required. In addition, induction heating circuitry is relatively cheap and simple. We have demonstrated that induction heating can support rapid but controlled temperature rates of up to several hundred degrees a minute.

A schematic representation of the IHTD-DART-MS system is shown in Figure 2.36. The technique comprises an oscillator circuit (A) attached to the working coil (B) that provides the oscillating magnetic field and in turn the induced currents in the TD tube (or work piece). The TD tube is placed axially within the copper coil so that the tube sits within the highest magnetic flux region ensuring even heating throughout the body of the TD tube. Temperature is measured using a thermocouple situated between the coil and the TD tube, the thermocouple must touch the body of the TD tube for accurate temperature measurement. A gradual flow of carrier gas applied to the base of the TD tube provides a positive flow transporting desorbed vapours into the ionising DART stream. The heating is controlled using a temperature programmer and is switched using PWM circuitry demonstrated earlier in Section 2.3.2.

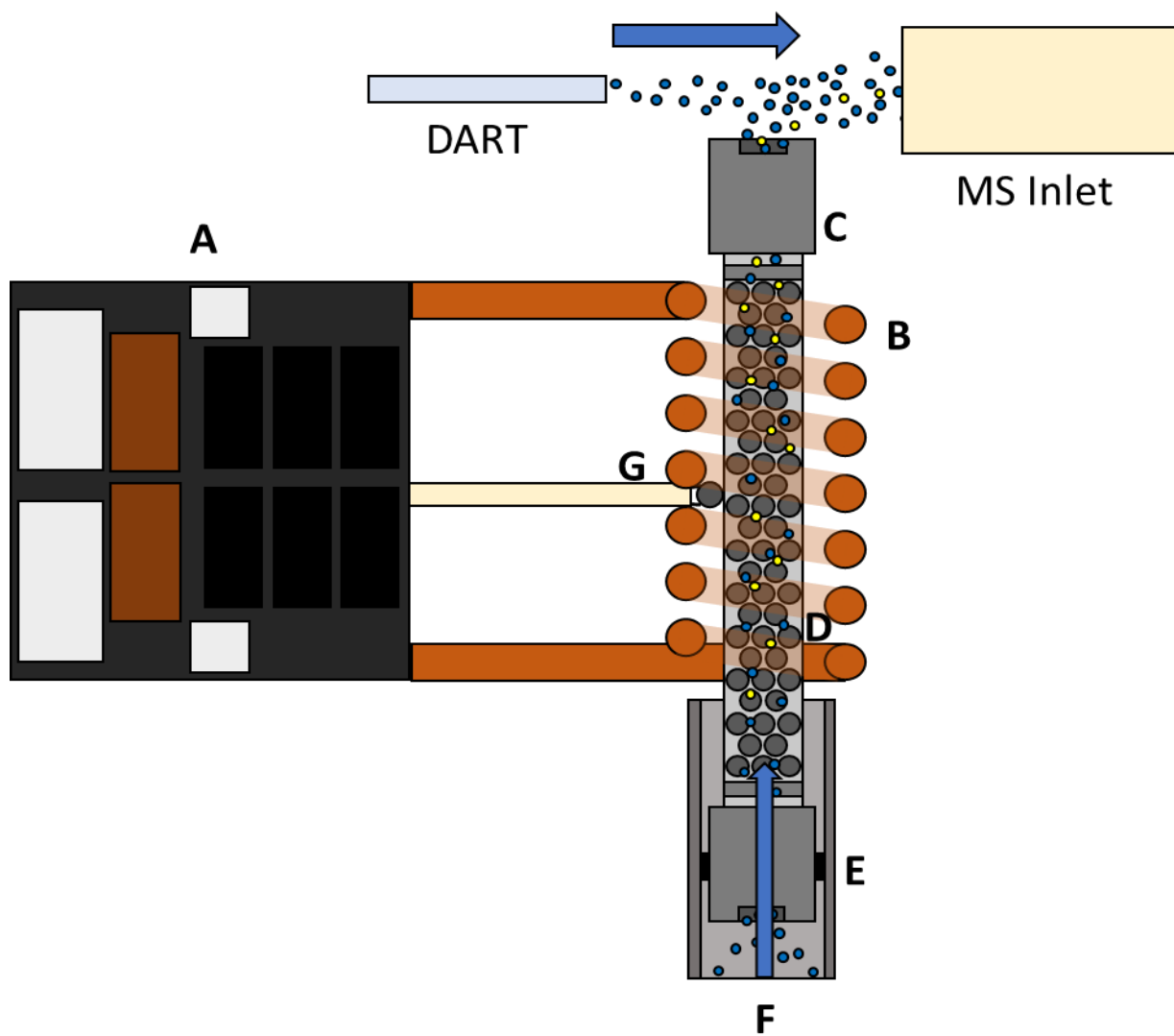


Figure 2.36 Schematic representation of the proposed Induction heating thermal desorption direct analysis in real-time mass spectrometry system. A) Induction heater driver, B) Induction working coil, C) TD tube, D) sorbent material, E) TD tube holder, F) Carrier gas and G) TD tube thermocouple.

2.7.4 Software developments

In addition to the hardware, there are also developments to the HDM software in progress. This falls into two main categories. Firstly, there are modifications to the existing HDM software to provide more capabilities and, secondly, there is a move towards micro-controllers to remove the reliance on commercial temperature programmers.

2.7.4.1 SCTA applied to HDM

Sample Controlled Thermal Analysis (SCTA) is a family of techniques that use feedback algorithms that alter the heating rate of the sample depending on some measured response of some property of the sample. SCTA aims to increase thermal resolution of overlapping events by heating slowly *through* events and more rapidly *between* them. SCTA can help resolve processes which may be missed when performing standard isothermal or linear heating rate experiments. In addition, the near isothermal conditions that can be achieved under SCTA conditions can be useful. Commonly, SCTA has been applied to DSC²⁷ and TGA²⁸ using heat flow or mass loss respectively as the source of control.

Two of the signals monitored by HDM, colour and ion intensity, are potentially amenable to SCTA. Although reflected light intensity (RLI) used in hot-stage microscopy has combined with SCTA,²⁹ colour itself has not been used although it has been shown to relate directly to the extent of reaction for some processes.³⁰ SCTA can be used to control the temperature as a function of rate of colour change, this approach would be interesting to apply to some of the highly pigmented reactions discussed in Chapter 3.

The benefits of combining mass spectrometry with SCTA have been realised by other workers.³¹⁻³² Virtually every system studied using HDM produces a MS profile so, in many cases, a specific ion intensity that uniquely corresponds to a material can be extracted. Controlling temperature following a specific ion allows processes to be investigated in terms of reactants, products and possibly even intermediates. This method could help in the study of complex processes such as the thermal degradation of polymers. A similar approach was used by Sánchez-Jiménez *et al.* who found that using SCTA with TGA in the study of the thermal degradation of PVC (polyvinyl chloride) gave a clearer separation of the mass losses arising from the plasticiser and the polymer itself.³³

2.7.4.2 Incorporation of Arduino microcontrollers

Microcontrollers miniaturised computers on a single integrated circuit board. They are cheap, relatively powerful and an increasing variety of supporting circuitry is available that make them ideal for interfacing to scientific instruments.

One of the most popular microcontroller manufacturers is Arduino. They produce a wide range of boards offering different capabilities and have their own IDE (integrated development environment) based on the programming language 'C'. As an 'Open Source' environment with a large user base there is a lot of software freely available for use. Several key electronic manufacturers have realised the potential of this platform and offer high grade peripherals to allow voltages and thermocouples to be monitored, control motors, etc. These attachments invariably come with full software support. In addition, Arduino microcontrollers are easy to interface to Windows PCs using a standard USB connection.

The initial interest in Arduino microcontrollers was driven by the desire to replace the Eurotherm 818P temperature programmers used in the HDM. Although the Eurotherm 818P is a high quality controller it is now obsolete and can only monitor a single thermocouple. There are newer models but they often cost many hundreds of pounds. In principle, an Arduino could form the basis of a temperature programmer and also allow for other peripherals to be added for monitoring other sensor inputs. This would provide flexibility allowing adaptations to the basic HDM with minimum need for additional components or software changes.

The current prototype is shown in Figure 2.37. The hardware consists of the Arduino board (Nano, Uno or Mega), a 16 bit analogue to digital converter (ADC) breakout board (Adafruit, ADS1115) and high resolution universal thermocouple reader breakout boards (Adafruit, MAX31856). One of the digital outputs on the microcontroller board is dedicated for use for on/off PWM control of a solid state relay. Code was written in both the Arduino IDE (C, V1.5-1.8) and Visual Studio (VB.net, 2013-2017) to develop a controller that can support the hardware developed shown in Figure 2.37.

The resolution of the thermocouple reader boards is (at least theoretically) 0.0078 °C which is of sufficient quality for most thermal analysis work. The accuracy of temperature is typically dictated by the thermocouple itself and will have an error of about ± 2 °C, although this is readily calibrated using the methods described earlier (see Section 2.3.4).

Software developed with the Arduino IDE and embedded on the controller board uses the MAX31856 library³⁴ to read the thermocouples at 200 ms intervals and then averages 5 measurements to reduce noise and produces a value expressed to a resolution of 0.01 °C. One of the two thermocouples is used as an input to a PID routine adapted from an open

source PID library to allow temperature control of a hot-stage using pulsed width modulation period of 1 second. The 4 channel 16 bit ADC with inbuilt amplifier circuit monitors voltages with a maximum resolution of ca. 80 μV per bit, and is run through the ADS controller library.³⁵ Although these inputs could be used to connect to many signal sources, its initial intended use is for measuring RLI (reflected light intensity) a signal from an optical detector mounted into the eyepiece of a microscope.

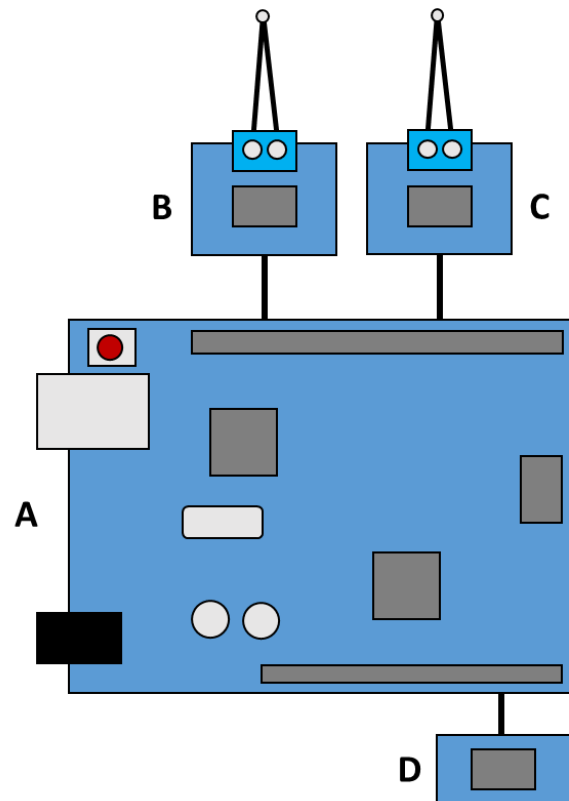


Figure 2.37 Schematic representation of the hardware used in the microcontroller temperature controller. A) Arduino board, B) MAX31856 thermocouple reader Temp 1, C) MAX31856 thermocouple reader Temp 2 and D) ADS1115 16-bit ADC.

Figure 2.38 shows a screenshot of a form used to interface with the Arduino board. The window is designed to be embedded into the existing HDM software and is has been developed as a replacement for the Eurotherm controller.

The form acts as a bridge between the main HDM software and the Arduino and allows values and control parameters to be sent from to and from the microcontroller. The form comprises key sections, connection, output, input and functions. The connection function allows the form to be connected to any available Arduino devices. The output section, contains all the values 'output' from the Arduino, these are mainly in the form of sensor values such as temperature or ADC readings, but also include stored parameters such as the temperature setpoint. The input section 'inputs' instructions to the Arduino, currently this is used to update either a setpoint or a percentage power. Finally, functions are extra routines that the form recognises to either save the data or reset the Arduino board.

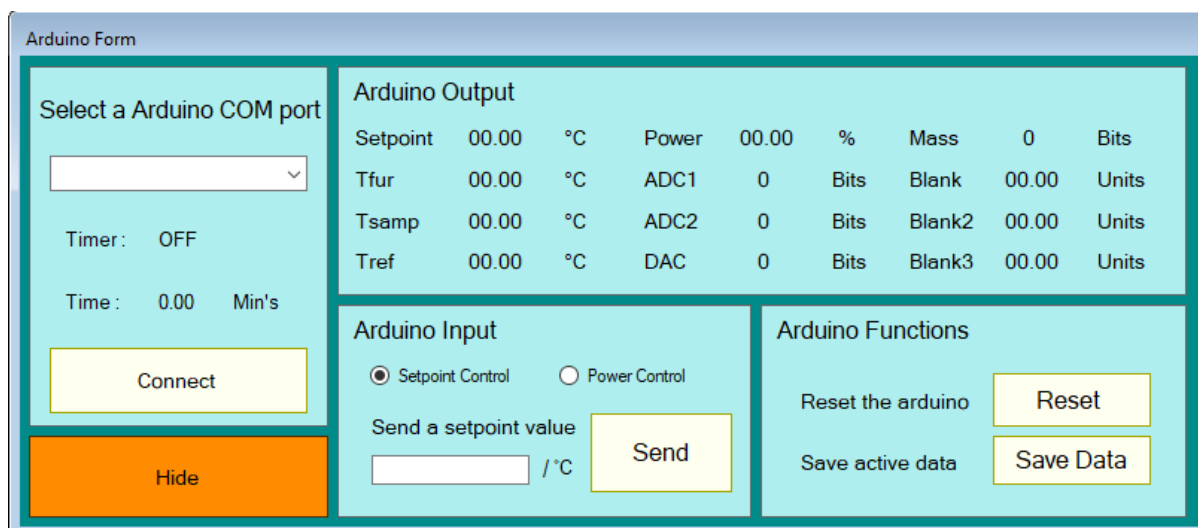


Figure 2.38 A screenshot of the standalone form used to interface to the Arduino microcontroller.

An example of a test linear heating experiment ($10\text{ }^{\circ}\text{C min}^{-1}$) is shown in Figure 2.39. The Arduino PID routine controls the output (expressed as percent power, blue trace) to make the furnace thermocouple (PV, process variable, orange trace) follow the setpoint (SP, green trace) as closely as possible. So far excellent control has been achieved using this approach with a maximum error (SP-PV) of around $0.1\text{ }^{\circ}\text{C}$. A secondary sample thermocouple (red trace) is recorded simultaneously.

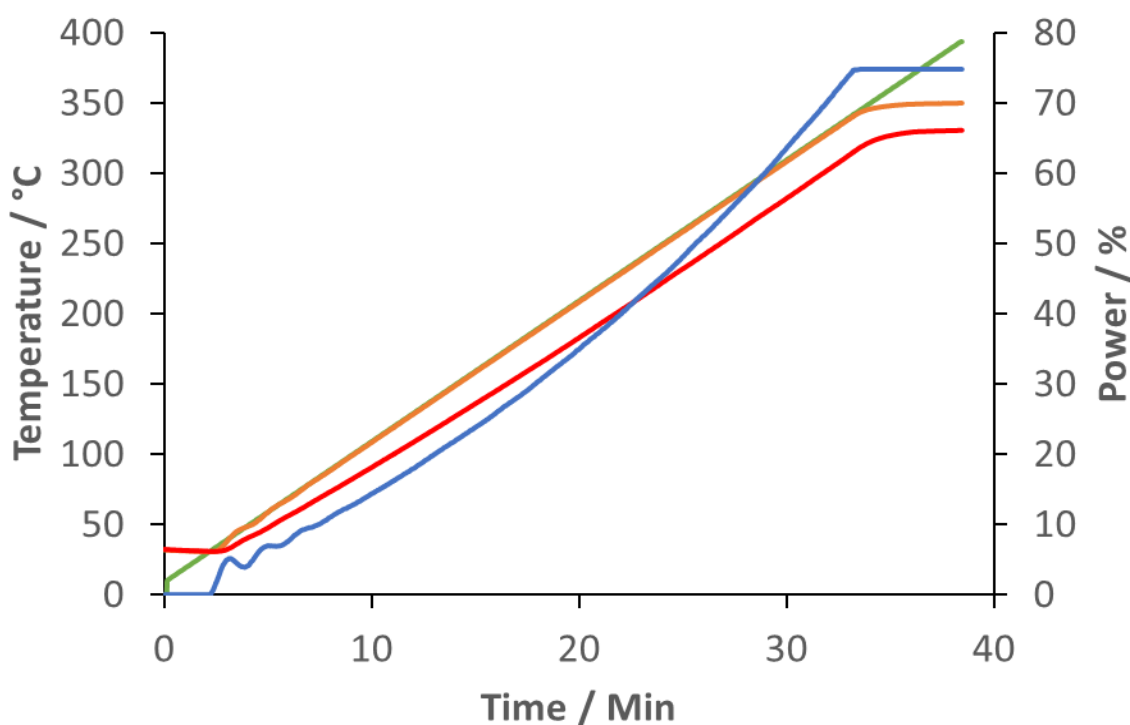


Figure 2.39 A selected example of PID control using the Arduino microcontroller system. Green) setpoint, Orange) furnace thermocouple, Red) sample thermocouple and Blue) PWM power output.

2.7.4.3 Automated positioning of the hot-stage

The HDM stage may need to be moved away from its position in the DART stream for a variety of reasons, when the stage becomes significantly contaminated, when the mass spectrometer needs servicing or generally when prototype stages need short evaluations. This requires frequent manual positioning of the stage which can be time-consuming and fiddly, and ensuring accurate repositioning is paramount.

To address this problem a two axis motorised stage mover has been developed using a selection of aluminium rail and custom made 3D printed parts as shown in Figure 2.40.

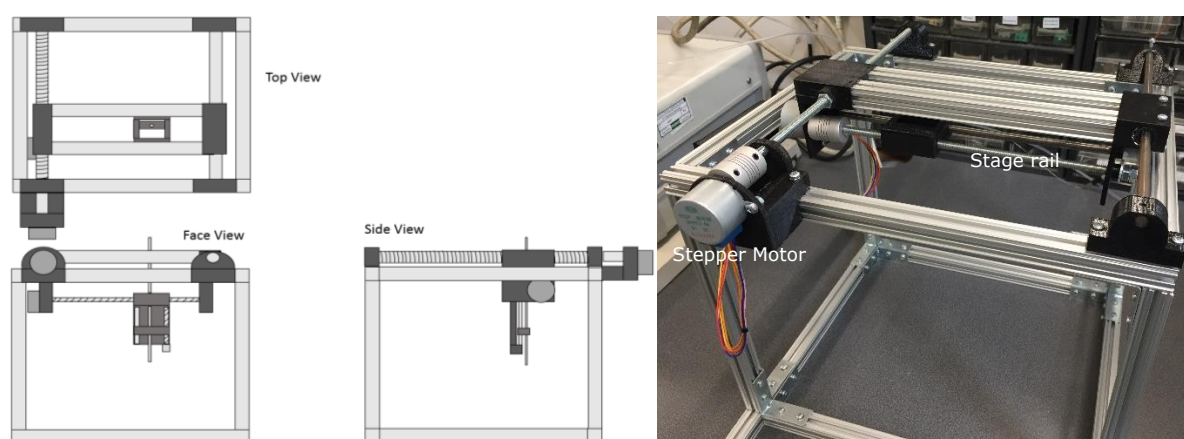


Figure 2.40 Schematic (Left) and photograph (Right) of the motorised stage mover.

The stage mover comprises of a mount that holds the hot-stage in position and two rails which are each driven by a stepper motor (28 BY J-48) under control of an Arduino and corresponding stepper driver boards (ULN2003). The stepper motors allow repeatable positioning of the hot-stage (measured to within 200 μm). A separate interface window, similar in concept to that described in Section 2.7.4.2, is being developed in-house to embed in the main HDM software to allow simple commands such as move a fixed distance, 'load' and 'run'. These commands allow accurate positioning of the stage mover, moving from a loading sample position to a run position situated within the ionising stream. A further development is to add a Z-axis so that the hot-stage may be moved up and down axially.

It is the intention is to use the motorised stage mover in the projects incremental work to return to some of the fundamental studies based on how position distance and position of the sample in the DART stream affects the ion profiles obtained from the mass spectrometer.

2.7.4.4 Automated positioning of the μ -DART

The commercial DART used in this work has a fixed orientation with the ionising stream in line with MS inlet and passing over the top of the sample on the hot-stage. The newer DART models (DART-SVP) does allow the angle at which the ionising stream hits the sample to be changed between 45° and 0° (flat) but this has to be done manually. It has been reported in the literature that changing the angle at which the ionising stream hits the sample was found to alter the extent of surface ionisation and affected the profiles obtained from the mass spectrometer.³⁶

The small size and low mass of the μ -DART lends itself to automated positioning and a second motorised rig has been developed for controlling an arm holding the μ -DART so that it can be quickly set to any angle with respect to the sample (even below 0°) see Figure 2.41. This positioning could be rapid enough to allow the angle to be changed even in the middle of an experiment allowing volatiles vs sample ablation sampling to be performed.

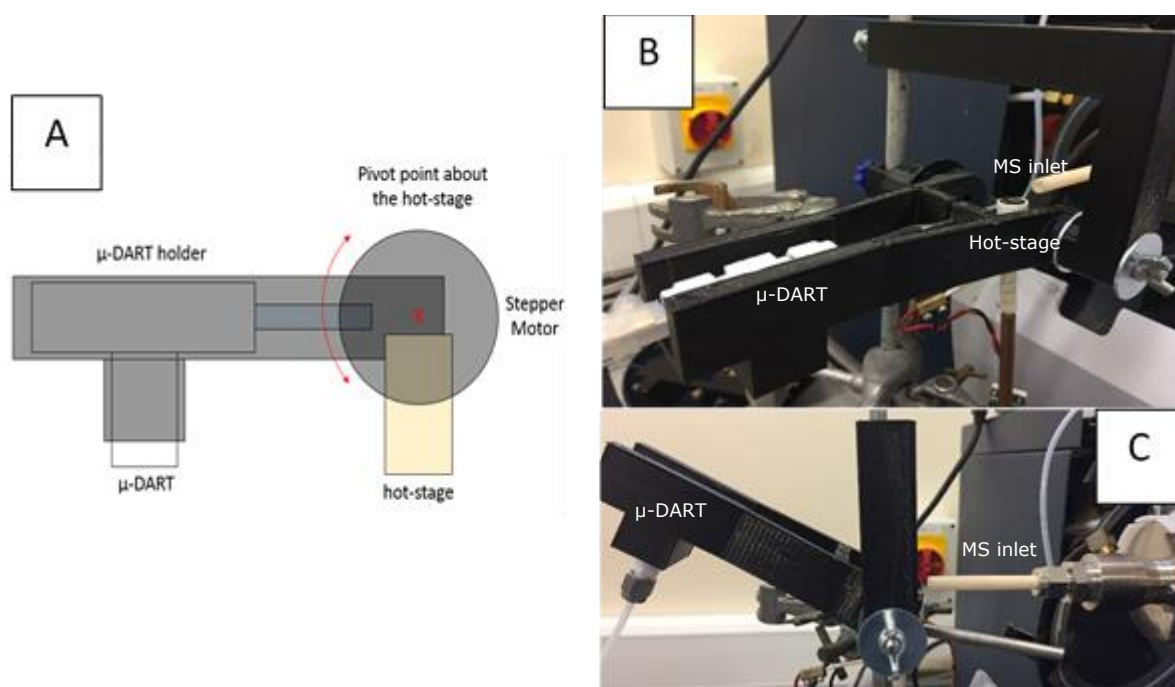


Figure 2.41 Schematic (A) and photographs (B & C) of the μ -DART in the motorised holder at 0° and 45° respectively.

By using the μ -DART in combination with the hot-stage the surface/thermally desorbed ionisation effects could be investigated more thoroughly. Standard models of DART rely on the thermal desorption process to aid with the removal of analytes from the surface of an introduced sample, for this reason it would be difficult to differentiate completely the difference between surface sampling and volatiles analysis within a single experiment.

Figure 2.42 shows a graphical representation of the types of experiment possible with an angled μ -DART. (A) shows the most aggressive type of experiment, with the ionising stream directed at 45° to the sample giving a combination of thermal desorption ionisation and surface sampling ablation effects. (B) shows the standard configuration used currently with an angle of 0°. Mostly, only material desorbed from the sample would be ionised but the ionisation stream may be broad enough for some surface ionisation to occur. (C) shows the DART angled below the horizontal. In such a position only desorbed species would be expected to be ionised. The μ -DART arm could be swept from low to high angles throughout the experiment during a temperature programme, possibly aiding with surface/desorption processes which may be useful in matrix effect studies.

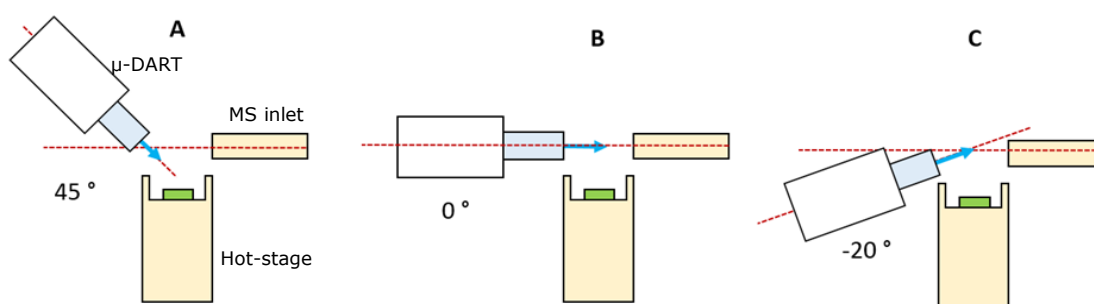


Figure 2.42 Sampling angle effects of μ -DART with HDM. A) 45° towards the surface, B) 0° across the surface and C) -20° below the surface.

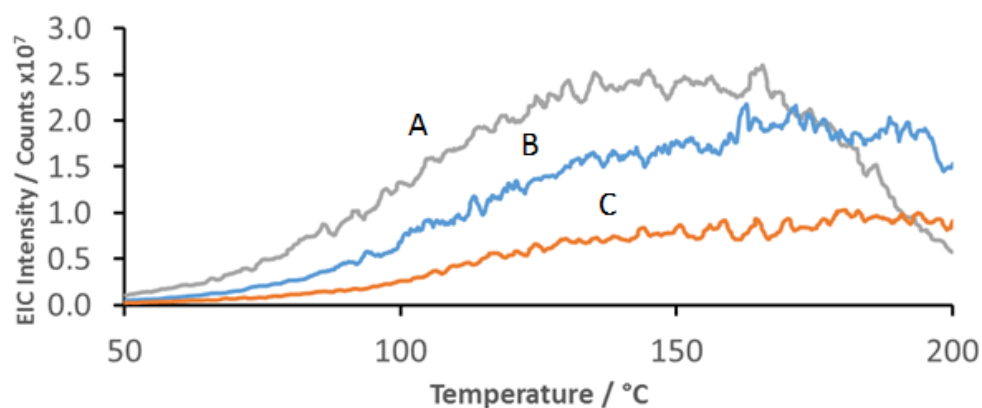


Figure 2.43 Angle comparison using the μ -DART stepper monitoring ammoniated benzil evolution. A) 228 Da $[M+NH_4]^+$ -10°, B) 228 Da $[M+NH_4]^+$ 0° and C) 228 Da $[M+NH_4]^+$ 45°.

Figure 2.43 shows the results of the analysis of benzil (Aldrich, 5mg) at a variety of angles (see legend) heated at 5 °C min⁻¹ between 50 and 200 °C in a standard Inconel pan. When the μ -DART stream is below the hot-stage (-10°) benzil is still observed. Ionisation is taking place solely through sample volatiles opposed to sample ablation. The harshest analysis (45°) shows a reduction in intensity of benzil potentially arising from physically 'blowing' the powdered sample from the analysis pan, and/or creating disruption to the air currents about the inlet of the spectrometer through direct impact with the hot-stage. Further investigation is needed into the effects of angle position, this was included to show how the angle effect may be utilised.

2.8 Conclusions

Investigations were conducted using microscopy to evaluate DART's ionisation and suppression properties. It was found that simple digital microscopes could provide complementary information to DART mass spectra. Commonly during DART analysis samples are introduced on a mesh after first being deposited, compounds may readily be 'blown' from these meshes reducing the amount of analyte being analysed during DART analysis indicating the need for a more stable sample holder.

The DART source temperature was found to vary significantly between measured and set temperatures. Thermal inconsistencies may exist through conventional DART sample introduction methods. Preliminary studies revealed the need for accurate and controllable heating of samples so that correct thermal conditions could be quoted and evaluated with greater certainty.

This chapter has described the design and development of a hyphenated TA-MS technique; hot-stage microscopy direct analysis in real-time mass spectrometry abbreviated to HDM. The system can relate physical processes such as melting, geometry changes and colour changes to chemical signals observed by a mass spectrometer as either a function of time or temperature.

Software has been developed to control the instrument and collect data (such as time, temperature and RGB values from selected regions of the image) as well as the images themselves in .jpeg format.

A miniaturised DART source termed μ -DART has been developed in tandem with the main HDM project. The μ -DART source has been characterised by comparing electronic characteristics and chemical tests utilising survival yields for ionisation source assignment and shown to be a soft ionisation technique most DART-like as opposed to similar plasma based ambient ionisation sources.

Throughout possible improvements and developments on the basic HDM have been identified and these are at different stages of implementation. These range from modifications to the current hot-stage to incorporate DTA, new approaches combining desorption with DART-MS through to the use of micro-controllers to allow flexibility and facilitate further development. The HDM software is also continuously evolving with additional features such as support for sample controlled thermal analysis has been planned.

2.9 Instrumentation Development References

- ¹ L.P. Harding, G.M.B. Parkes and J.D. Townend, *Analyst*, 2014, **139**, 4176-4180.
- ² G.A. Harris, C.E. Falcone and F.M. Fernandez, *J. Am. Soc. Mass Spectrom.*, 2012, **23**, 153-161.
- ³ M. Curtis, J.D. Keelor, C.M. Jones, J.J. Pittman, P.R. Jones, O.D. Sparkman and F.M. Fernandez, *Rapid Commun. Mass Spectrom.*, 2015, **29**, 431-439
- ⁴ G.A. Harris and F.M. Fernandez, *Anal. Chem.*, 2009, **81**, 322-329
- ⁵ C. Pinho, *Applied Thermal Engineering*, 2012, **41**, 111-115.
- ⁶ W. Altmann, *Practical process control for engineers and technicians*, Oxford, Newnes, 2005.
- ⁷ E.D. Salmon, S.L. Shaw, J.C. Waters, C.M. Waterman-Storer, P.S. Maddox, E. Yeh and K. Bloom, *Methods Cell Biol.*, 1998, **56**, 185-215
- ⁸ CodePlex Archive, <https://archive.codeplex.com/?p=touchless>, (accessed June 2018)
- ⁹ S.E. Pownall, *An investigation into the thermal behavior of polymer cookware using conventional and novel thermal analysis techniques*, submitted as final year MChem project dissertation, University of Huddersfield, 2018.
- ¹⁰ Y.A. Abdelaziz, E.M. Ibrahim & M.M. Mekawy, *International Journal of Pure and Applied Physics*, 2010, **6**(4), 429-437
- ¹¹ D.G. Archer & S. Rudtsch, *J. Chem. Eng. Data*, 2003, **48**(5), 1157-1163
- ¹² S.F. Wright, P. Phang, D. Dollimore and K.S. Alexander, *Thermochimica Acta*, 2002, **392**, 251-257
- ¹³ A. Shimkin, *Thermochimica Acta*, 2013, **566**, 71-76
- ¹⁴ P.J. Haines, *Thermochimica Acta*, 1999, **340**, 285-292
- ¹⁵ R.B. Cody & J. Dane, *Rapid Commun. Mass Spectrom*, 2016, **30**, 1206-1212
- ¹⁶ W. Xie and W.-P. Pan, *Journal of Thermal Analysis and Calorimetry*, 2001, **65**, 669-685
- ¹⁷ Ionsense, https://www.ionsense.com/Products/DART/DART_SVP/en, (accessed June 2018)
- ¹⁸ R.B. Cody and J.A. Laramee, 2003, US6949741B2
- ¹⁹ SlidePlayer, <http://slideplayer.com/slide/6492883/>, (accessed June 2018)
- ²⁰ J.T. Shelley and G.M. Hieftje, *J. Anal. At. Spectrom.*, 2010, **25**, 345-350
- ²¹ K.T. Upton, K.A. Schilling and J.L. Beauchamp, *Anal. Methods*. 2017, **9**, 5065-5074
- ²² V. Poenariu, M.R. Wertheimer and R. Bartnikas, *Plasma Process. Polym.*, 2006, **3**, 17-29
- ²³ G.A. Newsome, L.K. Ackerman and K.J. Johnson, *J. Am. Soc. Mass Spectrom.*, 2016, **27**, 135-143
- ²⁴ M. Kärkkäinen, I. Seppälä and K. Himberg, *Journal of Forensic Sciences*, 1994, **39**(1), 186-93
- ²⁵ D. Klein, S. Maurer, U. Herbert, J. Kreyenschmidt and P. Kaul, *Food Analytical Methods*, 2018, **11**(1), 88-98
- ²⁶ M.E. Sigman, C- Ma, R.H. Ilgner, *Analytical Chemistry*, 2001, **73**(4), 792-8
- ²⁷ E.L. Charsley, P.G. Laye, G.M.B. Parkes and J.J. Rooney, *Journal of Thermal Analysis and Calorimetry*, 2011, **105**, 699-703
- ²⁸ T. Arii, T. Taguchi, A. Kishi, M. Ogawa and Y. Sawada, *Journal of the European Ceramic Society*, 2002, **22**, 2283-2289
- ²⁹ O.T. Sørensen & J. Rouquerol, *Sample Controlled Thermal Analysis*, Springer Science, 2013, 54-55
- ³⁰ J.C.J. Bart, *Plastics Additives*, IOS Press, 2006, 210
- ³¹ M.J. Tiernan, P.A. Barnes & G.M.B. Parkes, *J. Phys. Chem. B*, 1999, **103**(33), 6944-6949
- ³² L.A. Pérez-Maqueda, J.M. Criado & F.J. Gotor, *Int. J. Chem. Kinet.*, 2002, **34**(3), 184-192
- ³³ P.E. Sánchez-Jiménez, L.A. Pérez-Maqueda, J.E. Crespo-Amorós, J. López, A. Perejón, and J.M. Criado, *Anal. Chem.*, 2010, **82** (21), 8875-8880
- ³⁴ Github, https://github.com/adafruit/Adafruit_MAX31856, (accessed June 2018)
- ³⁵ Github, <https://github.com/br3ttb/Arduino-PID-Library>, (accessed June 2018)
- ³⁶ E.S. Chernetsova, A.I. Revelsky and G.E. Morlock, *Rapid Commun. Mass Spectrom.*, 2011, **25**, 2275-2282

3.0 Reaction Profiling

3.1 Introduction

The ability to monitor chemical reactions in real-time is an important tool for both industry and synthetic chemists developing or optimising processes. Such work requires a valid method to monitor the formation of intermediates and undesired side products, detect energetic events that might cause thermal run away and overall ensure the reaction is being driven in the most efficient and economical way. It can take a considerable amount of time to optimise all the different conditions needed to drive even the simplest reactions to completion without sacrificing yields. The analytical information and good temperature control that HDM can provide make it an ideal method to study complex reactions that are thermally driven.

Today the synthetic chemist has a large range of analytical tools to aid with reaction monitoring with techniques such as TLC,¹ UV-VIS,² FTIR³ and NMR⁴ commonly being used either offline or inline. As with all techniques, they have both strengths and weaknesses, TLC suffers with poor optimisation and requires complete manual input, UV-Vis can require a lot of sample preparation and NMR requires expensive solvents and clean material. The majority of these techniques cannot be employed in real-time. Thermal analysis can also be used as a reaction profiling tool but is generally better suited towards the study of thermal decompositions. Standard thermal techniques, particularly TG, can be coupled with mass spectrometry or FTIR for studies of any volatiles produced by a reaction. These combined methods are excellent for interpreting complex TG mass loss curves during reactions (commonly in the form of decompositions) and provide an extra level of discriminatory power directly relating a quantitative component to a qualitative one.⁵

Conventional chromatography - mass spectrometry systems are less suited for reaction profiling as, although they combine separation with identification, they are not real-time techniques. In addition, the state of the sample must be considered to avoid damaging the equipment or producing high levels of instrument contamination.

Ambient MS, however, has offered a rapid sampling technique for the synthetic chemist with numerous publications demonstrating the use of DART⁶ for reaction monitoring. Illustrated in Figure 3.1 are two literature methods for reaction monitoring using ambient MS showing how setups can be made for reaction monitoring using ambient ionisation. The attraction is many mass spectrometers are readily adaptable for ambient ionisation studies and data can be obtained very quickly. Users of ambient MS for reaction profiling typically analyse a representative sample of the whole reaction medium and acquire all the resulting data, which may result in very complex spectra. Some workers have attempted to overcome this by chromatographic separation using TLC and analysing each spot on the plate separately. Both DART and DESI have been highly successful for

monitoring reactions directly from TLC plates⁷ although the ability to detect transient intermediates may be lost.

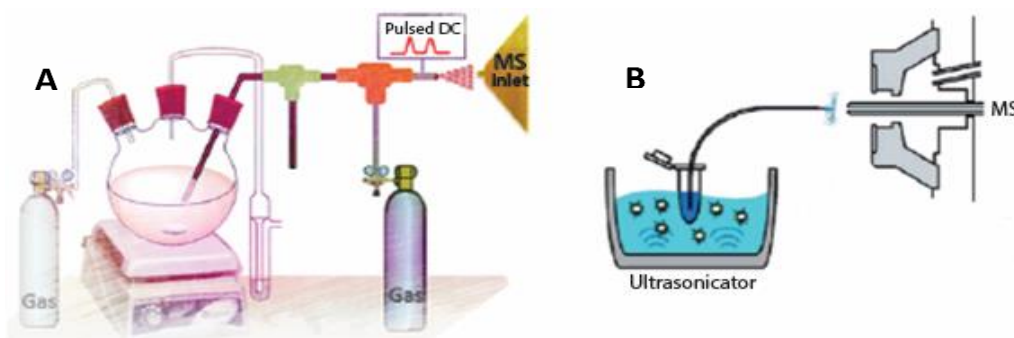


Figure 3.1 Selected ambient ionisation reaction monitoring techniques. Figure modified from; (A) Inductive ESI-MS⁸ (B) Ultrasonic assisted reactions⁹

Ray *et al.*, amongst others, have shown that DART itself suffers immensely as an online reaction monitoring tool due to the current sample introduction methods and the overall geometry of the source when compared to other ambient ionisation methods.¹⁰ Several authors¹¹⁻¹² have reported the use of DART for reaction monitoring but mainly in an 'offline' way, typically relying on manual input from the user with a reaction mixture being introduced on the Dip-it[®] tip (similar to a glass tube). To date it is because of these reasons DART is arguably one of the weaker ambient methods for online reaction monitoring, when other methods are much more applicable.

Research published by Song *et al.* demonstrated a pseudo online reaction monitoring system that was used to analyse a batch slurry reaction. The authors had constructed a mechanical rig that continuously introduced Dip-it[®] tips loaded with a fraction of the collected reaction mixture directly into the DART-100 stream (see Figure 3.2).¹³ This work provides an excellent example of what can be achieved using an automated online system.



Figure 3.2 DART-MS batch slurry reaction instrumental rig, used to analyse samples in a pseudo online method, individual samples are gradually moved into the DART stream.¹³

Due to the size of the HDM system many experiments can be carried out with relatively low quantities of sample (compared with standard synthetic practices), the amounts used within the following reactions typically fall between 5 and 25 mg. This can prove to be a useful probing tool should there be limited quantities of any reagent used in the synthesis.

Importantly due to the use of a reaction pan (as opposed to the standard mesh or Dip-it[®] introduction methods), reactions can be evaluated as either solids or liquids, making it applicable to heterogeneous systems. The volume of the pan used is around 70 μL meaning that only very small quantities of solvent might need to be used when studying a reaction. HDM can, therefore, be viewed as a 'green chemistry' technique concerning the reaction profiling. The extraction process usually requires much more solvent should a final product wish to be extracted for further analysis but the aim is to have a system that allows reaction profiling and not preparation.

3.1.1 Green Chemistry

Green chemistry is defined as '*the utilisation of a set of principles that reduces or eliminates the use or generation of hazardous substances in the design, manufacture and application of chemical products*'.¹⁴ In terms of synthetic chemistry the practice is often applied to either reducing solvent use and/or using ones which are less environmentally damaging.

However, optimisation of industrially important chemical reactions so as to optimise yield or use less energy would also fall under the umbrella of 'green chemistry' and it is this aspect for which HDM is particularly suited.

This chapter describes the use of HDM as a reaction profiling technique, although it does not include any quantitative analysis or exploration of yields. Instead, the work was designed as an illustration of the possible benefits of HDM to a wide range of organic reactions compared to more conventional methods and that of standard DART-MS.

Solvent free synthesis has been a major synthetic principle that has been adhered to within the following reactions, typically no auxiliary solvents have been added (those not considered a reactant themselves). For this study, all the reactions investigated utilised the precise temperature control of the HDM and were 'thermally driven' although, some of the reactions are typically performed at room temperature.

3.1.2 Aims

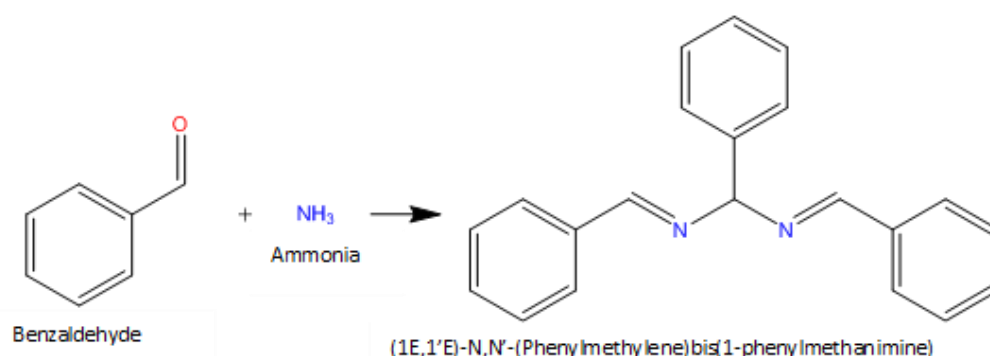
The aims of this work were:

- To evaluate HDM as a technique for thermally profiling organic reactions.
- To trial reactions in a variety of reaction states (heterogeneous and homogeneous reactions) evaluating breadth of the technique.
- To evaluate reaction temperature and its relation to reaction progression.
- To evaluate the relationship between reaction images and colour (physical information) to mass spectral profiles (chemical information).
- Confirmatory studies are used to evaluate HDM findings.

3.2 Hydrobenzamide Synthesis

Hydrobenzamide can be synthesised from a two component liquid state reaction between aqueous ammonia and benzaldehyde. The system was selected to demonstrate HDM's capabilities of profiling reactions in the liquid state with the product forming a white powder.¹⁵

Although no longer a commonly used compound the synthesis of (1E, 1'E)-N, N'-(phenylmethylene) bis (1-phenylmethanimine) (commonly known as hydrobenzamide), serves as an excellent example of an aldol condensation reaction (see Schematic 3.1). Hydrobenzamide was historically investigated for use medicinally,¹⁶ more recently it has been used within the nanotechnologies industry.¹⁷

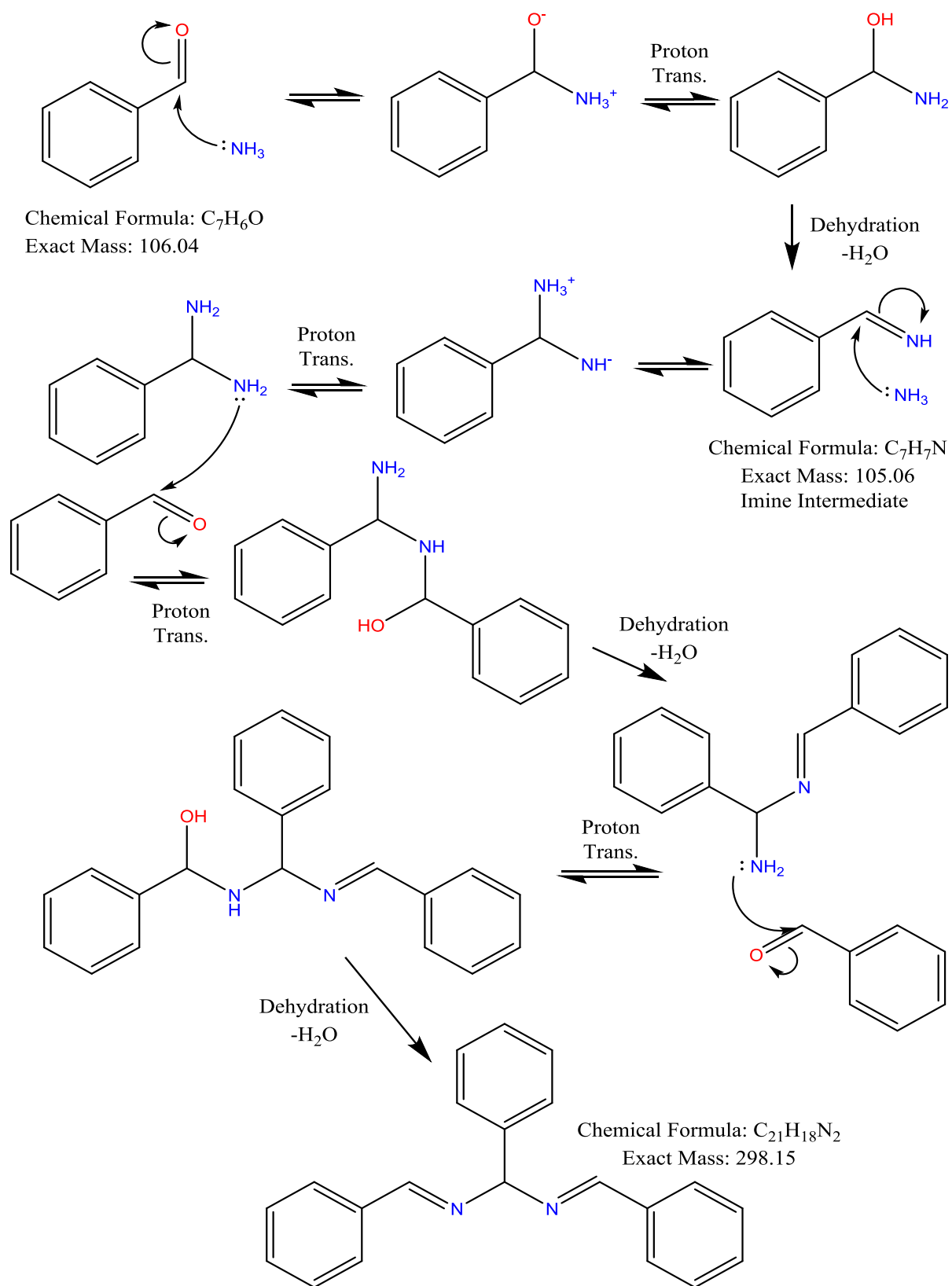


Schematic 3.1 Overall synthesis of hydrobenzamide from benzaldehyde and aqueous ammonia.

Standard synthesis methods report stirring the two components together for 24-48 hours at room temperature.¹⁸ The HDM study the following experimental parameters were used:

To a standard thermal analysis reaction pan (6mm, Inconel) was added benzaldehyde (30 μ L, Aldrich) and aqueous ammonia (35%, 150 μ L, excess, Aldrich). A linear heating rate of 10 $^{\circ}$ C min^{-1} from 30 to 400 $^{\circ}$ C was used. The DART source and mass spectrometer were operated in positive mode only with all resultant mass spectral profiles being acquired. Scan ranges were set between 100 and 2800 Da with an accumulation time of 200 ms.

Based on the mass spectra obtained in combination with existing literature the reaction scheme shown in Schematic 3.2 has been proposed.¹⁹ The reaction is initiated by the nucleophilic ammonia attacking the carbonyl carbon of benzaldehyde. After rearrangement and self-condensation a reactive imine is formed (phenylmethanimine, intermediate). The imine undergoes further nucleophilic attack from another free ammonia molecule, after rearrangement a diamine (phenylmethanediamine) is formed yielding the central backbone of the final hydrobenzamide product. Each of the amine arms then undergoes nucleophilic attack of benzaldehyde carbonyl carbons and, after rearrangement and dehydration, the final product is obtained. An average mass spectrum of the reaction process is shown in Figure 3.4 with key signals marked.



Schematic 3.2 Proposed mechanistic pathway of hydrobenzamide synthesis from benzaldehyde and aqueous ammonia.

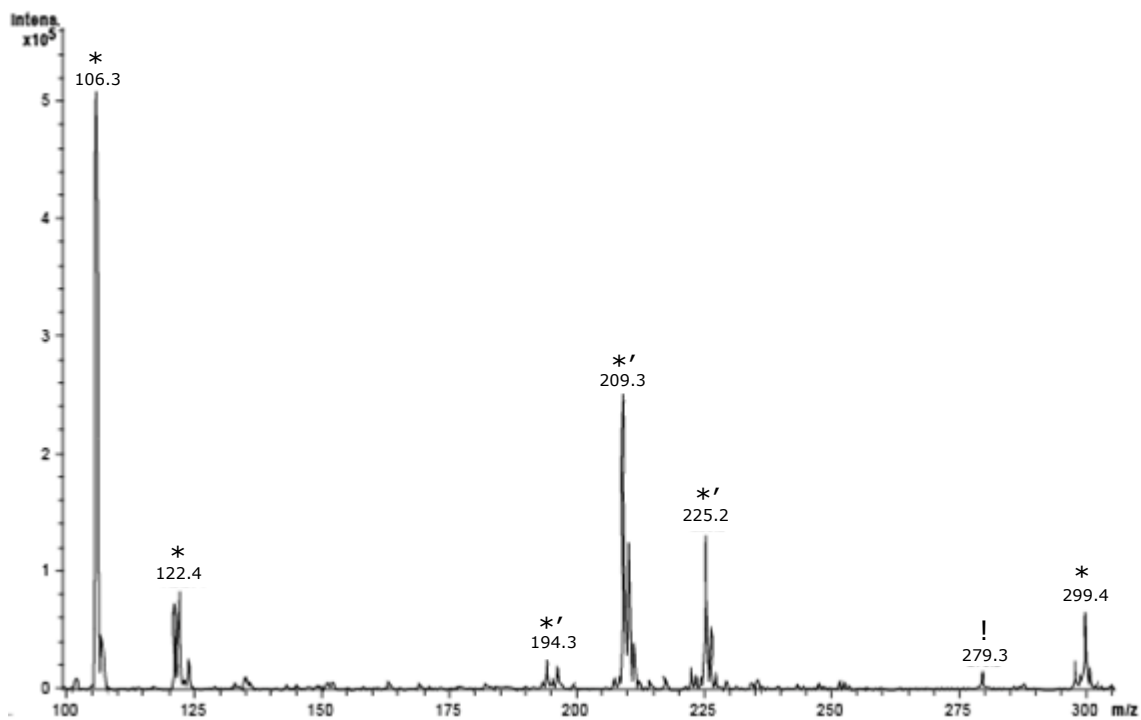


Figure 3.3 Average mass spectrum over the full duration of the hydrobenzamide reaction *) Assigned Reaction peaks, *) Unassigned reaction peaks, !) Contaminant peak

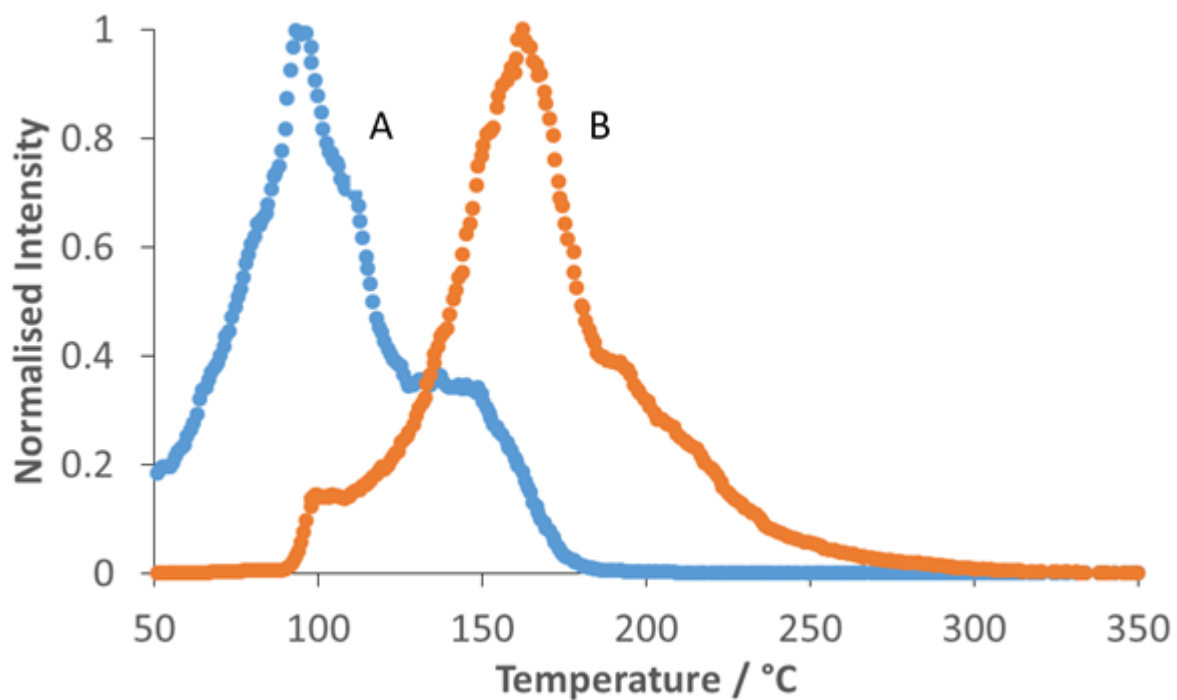


Figure 3.4 Reaction profiling for the formation of hydrobenzamide from benzaldehyde and aqueous ammonia. A) 106 Da [Benzaldehyde + H]⁺, B) 299 Da [Hydrobenzamide + H]⁺.

The reaction profile for the reactant (benzaldehyde, 106 Da [M]⁺) and product (hydrobenzamide, 299 Da [M+H]⁺) is shown in Figure 3.5. The ion intensities have been normalised for clarity.

The blue trace (A) in Figure 3.4 shows an initial rise in profile intensity as the benzaldehyde is heated up (attributed to evaporation) until 95 °C when it suddenly begins to decline in intensity as the product becomes evident. This decline in reactant intensity has been tentatively attributed towards reaction consumption. The reactant continues to decline up until 127 °C when a plateau is observed with the shoulder being attributed to the presence of another compound of the same nominal mass. Schematic 3.2 shows that the imine intermediate has a mass of 105 Da, the charged protonated molecular ion $[M+H]^+$ would also appear at 106 Da. After this event around 150 °C the final decline of the reactant is observed. Product evolution is shown between 100 and 165 °C up until the final decline of the reactant the onset is tentatively attributed towards the melting of the product. Since all the reactant has been either evaporated or consumed the product formation declines due to exhaustion of the benzaldehyde.



Figure 3.5 Micrographs of the hydrobenzamide reaction. A) 50 °C, B) 100 °C and C) 150 °C

Figure 3.5 shows the micrographs of the reaction process. Since the reaction is based on two clear liquids reacting to form a white product the overall process is quite subtle. Image A shows the liquids beginning to react as a slightly cloudy solution starts to form. Image B sees the reduction in volume associated with the evaporation of the benzaldehyde and correlates well with the rise in intensity of the product seen in Figure 3.4. The melting point of the hydrobenzamide product is close to this temperature (102-105 °C)²⁰ and links to the step rise for the hydrobenzamide protonated molecular ion profile. As the temperature is increased further the remaining solution is forced towards the edges of the pan (Image C) this remains until all the solution becomes exhausted or evaporates away.

Figure 3.6 is a plot of the overall reaction's total colour change as a function of temperature, this value is a summated colour score ($\sum RGB$) as was discussed in Chapter 2. The trace mainly illustrates the removal of the liquid reactants from the pan between 50 and 120 °C. The dip in the signal at 120 - 145 °C was caused by the loss of the reflection from the LED lighting from the microscope itself (the 'halo' type effect in Figure 3.5 image B) and the loss of this reflectance in image C. The faint decline in colour signal has been attributed towards the final removal of sample from the pan as the remaining liquids are removed between 150 - 250 °C complimenting the reaction profile in Figure 3.4. The final section (250 °C onwards) is essentially a steady signal produced by an empty pan.

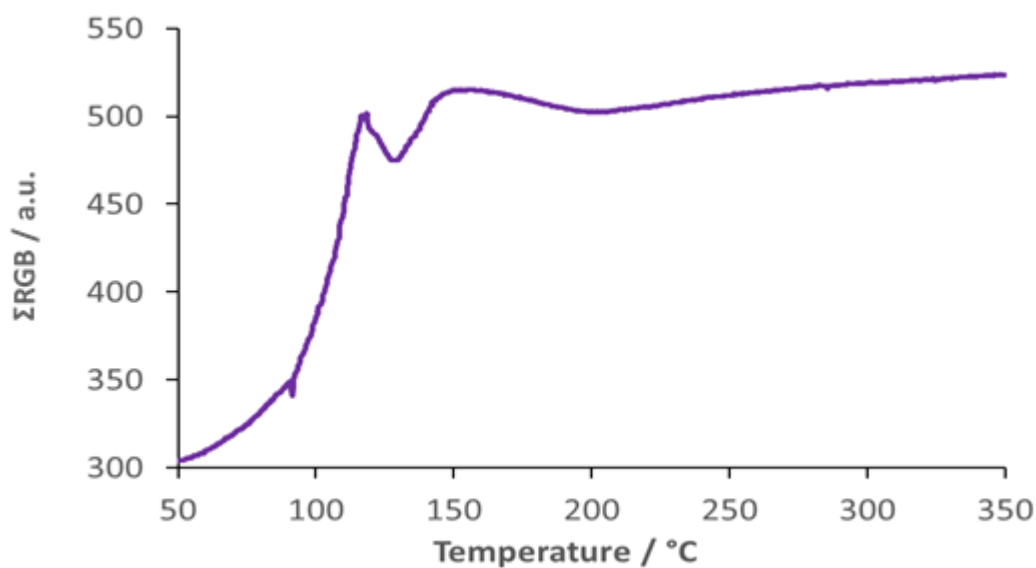


Figure 3.6 Colour profiling of the hydrobenzamide reaction, colour of the reaction plotted as a function of temperature.

Confirmatory studies were done using DSC and NMR on products from the same reaction but on a slightly larger scale

The reactive mixture was placed within a temperature controlled furnace and the temperature ramped to a maximum of 130 °C so sufficient product was formed without risk of depletion or decomposition.

The product was then purified by allowing the solution to cool and rest until a precipitate of hydrobenzamide was noted. The crude product was then isolated and washed with cold distilled water under vacuum. The final washed product was then recrystallised from minimal hot ethanol to yield white crystals. The sample was then analysed for purity by using proton NMR analysis and DSC.

Figure 3.7 shows the proton NMR spectrum of the hydrobenzamide product, the sample was prepared in deuterated chloroform. The NMR assignment is within good agreement to the existing literature.²¹

δ_{H} (400 MHz; CDCl_3 ; Me_4Si) 7.314(2H, m, Ar-H), 7.404(2H, t, Ar-H), 7.461(4H, m, Ar-H), 7.553(2H, d, Ar-H), 7.899(4H, m, Ar-H), 8.623(2H, s, N=CH).

Figure 3.8 shows the melting of the purified hydrobenzamide product using DSC (performed to evaluate the purity of the final product). A linear heating experiment was set up at a rate of $5\text{ }^\circ\text{C min}^{-1}$ between 30 and 200 °C, the mass of the product was approximately 10 mg. As can be seen a sharp melt is observed at $T_{\text{onset}} = 101.6\text{ }^\circ\text{C}$, which is very close to the literature melting range of 102-105 °C.²⁰ The DSC 'fit' has been included for illustrative purposes.

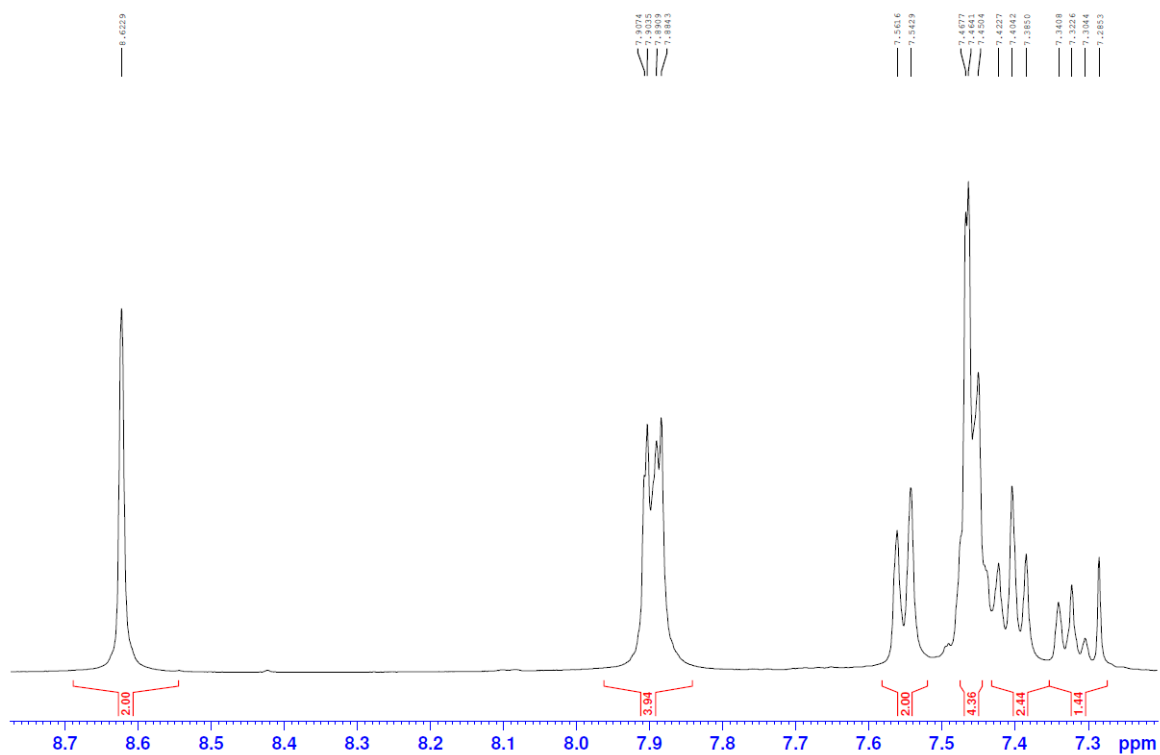


Figure 3.7 Proton NMR spectrum of synthesised hydrobenzamide product.

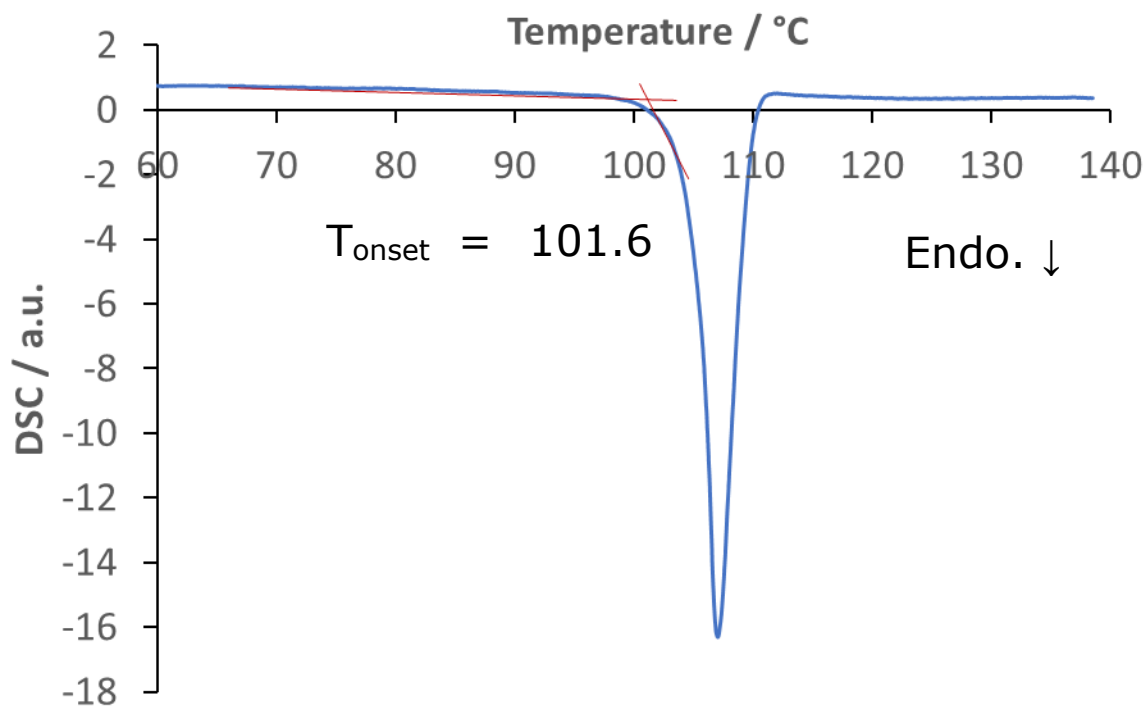
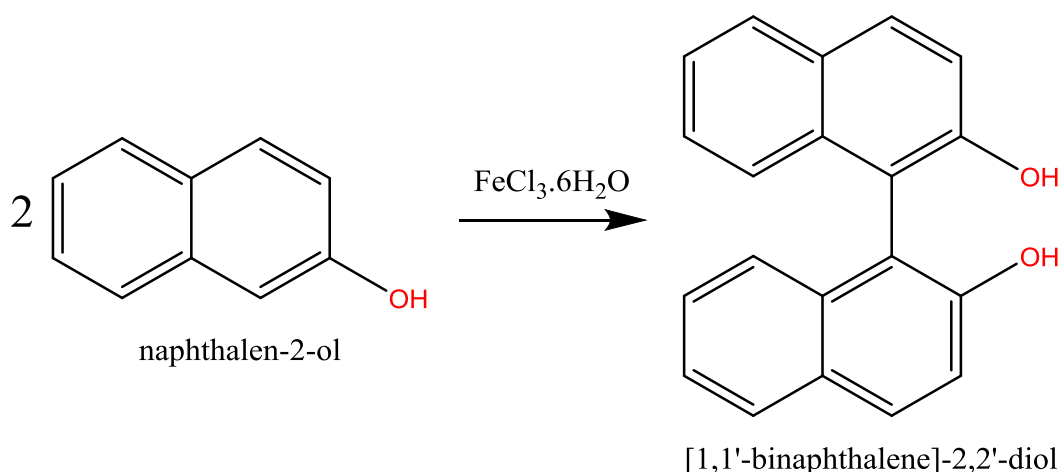


Figure 3.8 DSC analysis of synthesised hydrobenzamide product.

3.3 Binol Synthesis

[1,1'-Binaphthalene]-2,2'-diol (commonly known as binol) can be produced by the reductive coupling of 2-naphthol. The reaction is known as the Scholl reaction,²² and is an important synthetic reaction used for forming carbon-carbon bonds within substituted aromatic rings primarily belonging to the phenol and naphthol families.²³ The system was selected to demonstrate HDM's capabilities for profiling reactions within the solid state.

The reaction relies on the reductive catalyst inducing radical recombinations yielding the final product. An overview of the reaction is shown in Schematic 3.3.

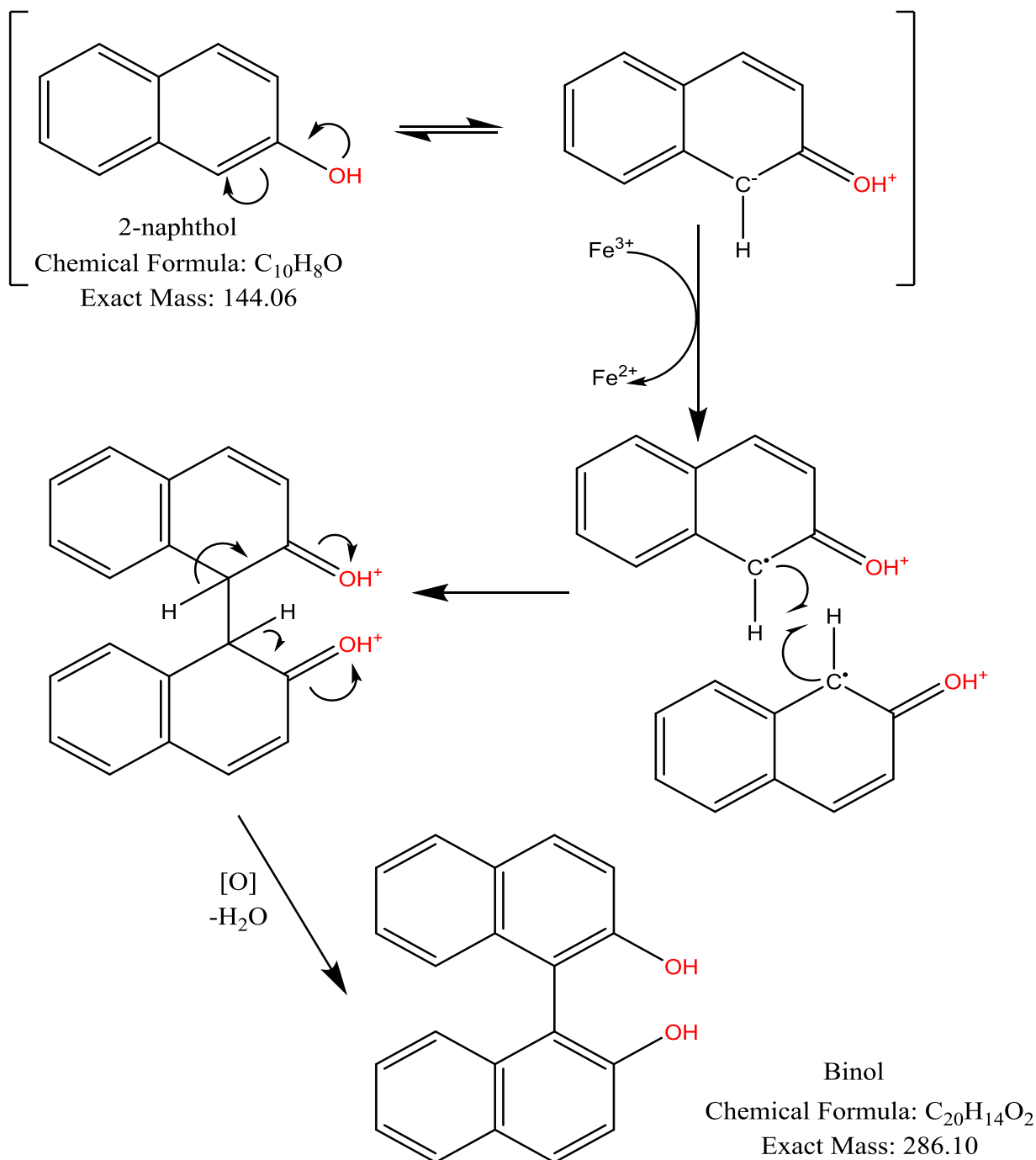


Schematic 3.3 Overall synthesis of binol from 2-naphthol and ferric chloride hexahydrate.

The reaction has been extensively studied with primary focus on solvent free synthesis that can be achieved with careful selection of reagents. Many of the literature methods evaluate the effect of the addition of various catalysts such as $\text{FeCl}_3 \cdot 6\text{H}_2\text{O}$,²⁴ MnO_2 ²⁵ and TiCl_4 ²⁶ on the yield. Binol itself serves as a useful synthetic building block primarily used within the formation of organometallic catalysts²⁷ and as a chelating compound for fluorescence studies.²⁸

The synthetic pathway shown in Schematic 3.4 is based on the existing literature.²⁷ The reaction is induced by the reductive ferric ion removing an electron from the resonant form of the 2-naphthol. This electron removal yields a naphthol radical species based at the β -carbon. A radical pairing occurs to produce the penultimate binol product. Final oxidative rearrangement is most likely initiated by atmospheric oxygen removing the hydrogens at each of the β -carbons, (driven by aromatic stabilisation) yielding the final racemic binol product. Although many authors²⁹⁻³⁰ claim that this reaction is a solid-solid reaction they often neglect the fact that the waters of crystallisation in the ferric chloride hexahydrate are lost at *ca.* 37 °C, so slight heating results in a heterogeneous state reaction.

Based on the work of Toda *et al.* the experimental parameters for the HDM were as follows; β -naphthol (8 mg, 55.5 μ mol, Aldrich, beige solid) and iron (III) chloride hexahydrate (30 mg, 111 μ mol, Aldrich, light yellow solid) were 'loosely' ground together before addition to the sample pan. The stage was heated at 1 $^{\circ}\text{C min}^{-1}$ from 30 to 250 $^{\circ}\text{C}$. Full mass scans were acquired in positive ion mode.



Schematic 3.4 Proposed mechanistic pathway of binol synthesis from 2-naphthol and ferric chloride hexahydrate based on work of Toda *et al.*²⁹

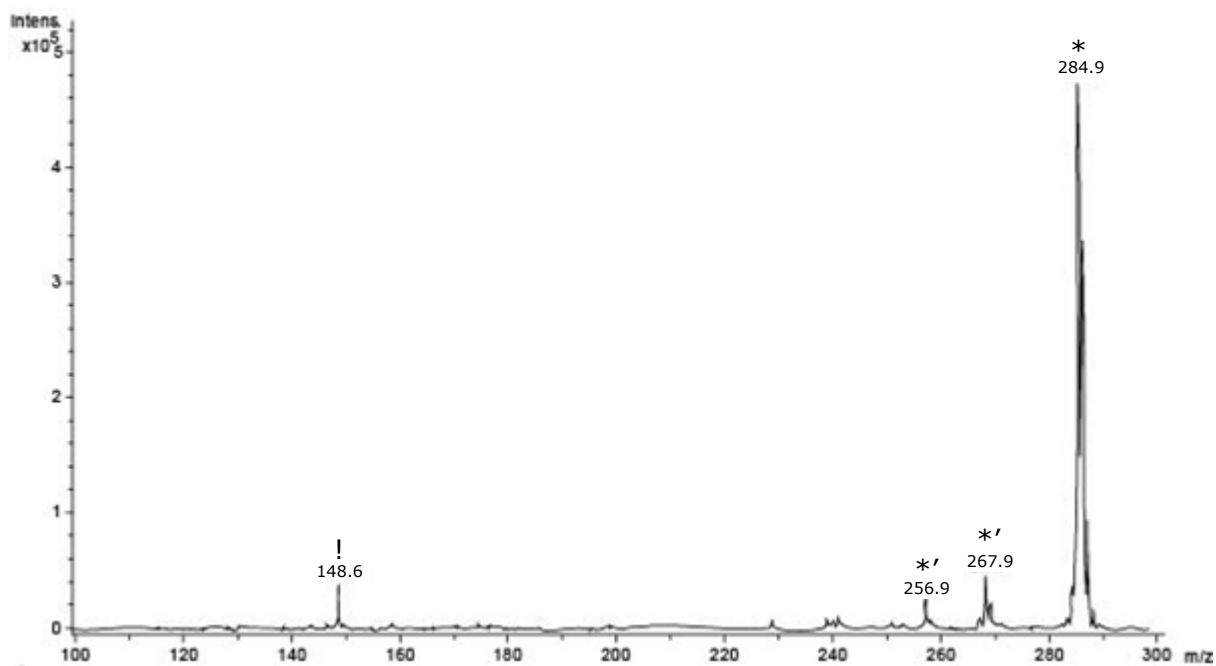


Figure 3.9 Average mass spectrum over the full reaction period for the synthesis of binol. *) assigned reaction peaks, *) Thermal rearrangement peaks, !) Common contaminant peak

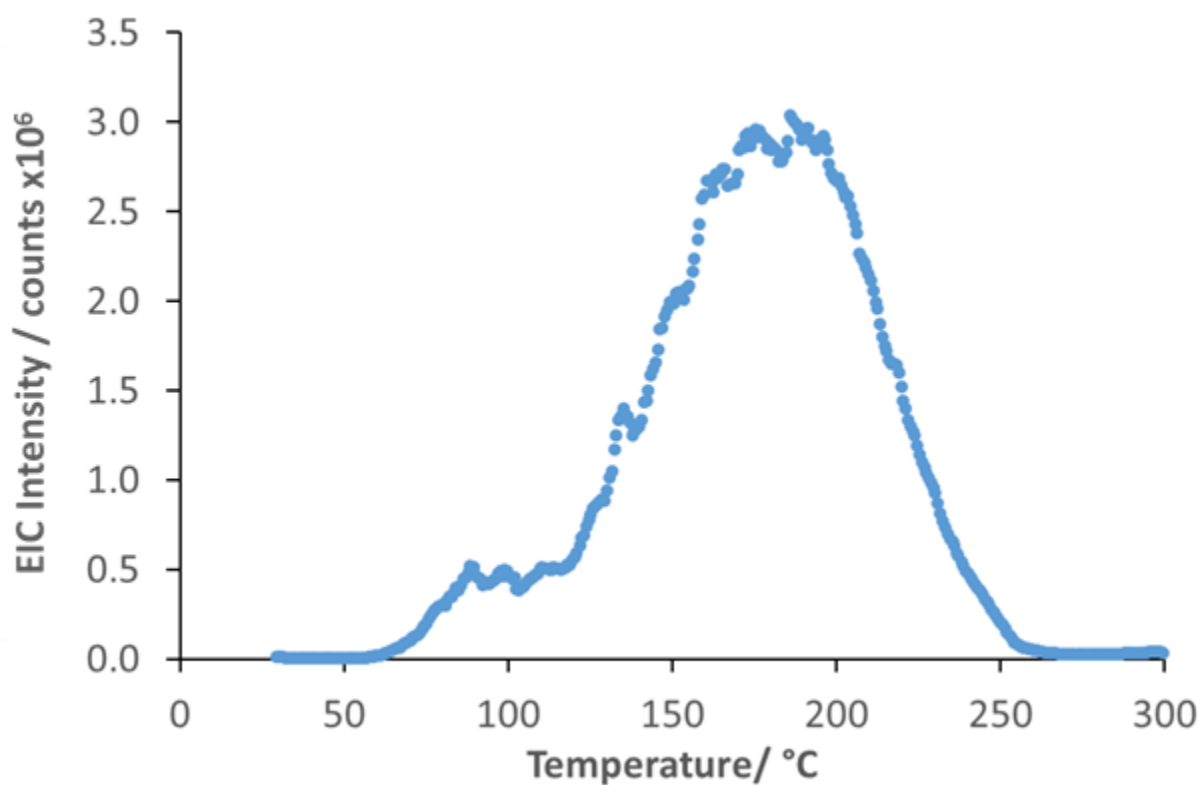


Figure 3.10 Reaction profiling for the synthesis of the binol product, as a function of temperature.

Figure 3.10 shows the formation of binol as a function of temperature. In this example the EIC of binol (286 Da, $[M]^+$) is shown exclusively as no sign of reactive intermediates (see Figure 3.9) was detected. Extra signals observed are assumed to be the thermal rearrangement products of binol.

A sample of 2-naphthol was tested individually as a separate experiment and was observed as the protonated form 145 Da $[M+H]^+$ but more readily as its dimer 299 Da $[2M+H]^+$. From this brief experiment the complexation of the iron in the reaction experiment is expected to have reduced the ease of ionisation existing as an iron complex, the literature has very few examples of DART-MS applied to coordination complexes.

The profile in Figure 3.10 shows a series of key steps. Nothing is observed until above 70 °C when there is the first indication that product is being formed. A plateau in the profile is shown from *ca.* 90 to 120 °C which is tentatively attributed towards a steady state condition where the rate of product formation is matched by the rate of loss through thermal desorption. The rise in binol shown from 120 °C can be directly correlated to the melting of the 2-naphthol reactant, at this moment the reaction rate significantly increases due to more intimate mixing between liquid reactant and the iron chloride. Product is continuously evolved up until 185 °C after which the decline in signal is assigned to the depletion of the reactant.

For this reaction, the optical component of HDM yields very useful complimentary data to the EIC profile.

Figure 3.11 shows micrographs of the reaction at a range of temperatures. The most striking change is between images A and B going from a light yellow to a dark brown attributed to the dehydration of ferric chloride hexahydrate (commonly referred to as the melting as the salt dissolves in its own waters of crystallisation) around 37 °C. The dark colour itself most likely has two components, the actual 'wetting' of the 2-naphthol and also from the iron-naphthol complex that can be formed. This dark brown colour is used as a common indicator as a 'wet test' to show the presence of phenol and naphthol based compounds.³⁰ The colour profile (obtained from the overall colour change ΔRGB) shown in Figure 3.12 also reveals this sharp colour change clearly.

Secondly, key events the melting of the 2-naphthol and the rapid onset of product formation which is clearly observable in both the colour profile and micrographs. Images C and D show a clear difference, the beige coloured spots of the 2-naphthol disappear during the melting and the colour profile shows a corresponding step change in total RGB change of 30 a.u.. A final event relates to the melting of the binol product revealed by another step change in colour between 200 and 216 °C which correlates to the known melting point of the product.³²

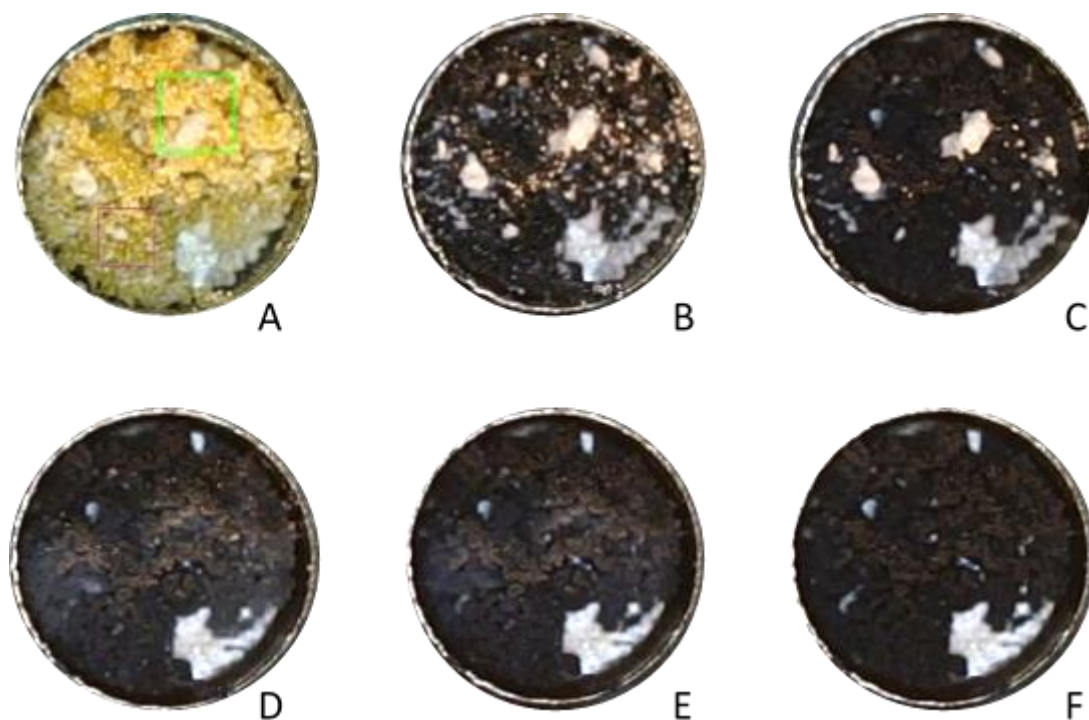


Figure 3.11 Micrographs of the synthesis of binol. A) 30 °C, B) 50 °C, C) 100 °C, D) 150 °C, E) 200 °C, F) 250 °C

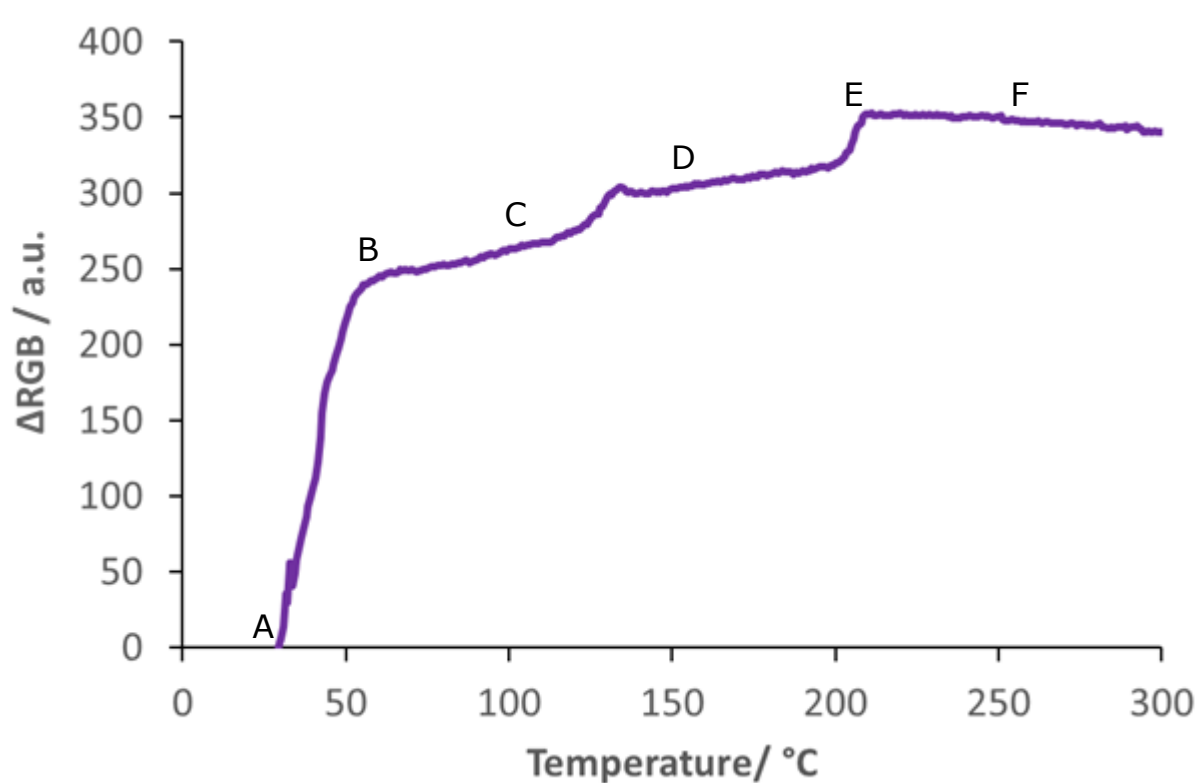


Figure 3.12 Colour profiling of the binol synthesis. Reaction colour change plotted as a function of temperature. Labels correlate to micrographs in Figure 3.11.

Micrographs E and F show a very gradual change between brown and black as the product melts (images E and F), but this is very difficult to observe with the human eye and interpretation could be somewhat subjective. However, interpretation of the binol profile is aided by the colour profile data provided by HDM.

Again, confirmatory studies were done using DSC and NMR on products obtained from the same reaction but on a larger scale. *A 1 °C min⁻¹ heating rate was applied with the maximum temperature restricted to 150 °C. The product was purified by washing with cold water to remove the various iron salts and then recrystallised to obtain a white/beige powder.*

Figure 3.13 shows the NMR spectrum of the binol product (the insert shows expansion of the aromatic region) and is in good agreement with the literature.³³

δ_{H} (400 MHz; CDCl₃; Me₄Si) 5.057 (2H, s, -OH), 7.181 (2H, d, Ar-H), 7.326 (2H, td, Ar-H), 7.387 (4H, td, Ar-H), 7.412 (2H, d, Ar-H), 7.920 (2H, d, Ar-H), 8.002 (2H, d, Ar-H).

Figure 3.14 shows the DSC thermogram of the purified binol. *The product (ca. 5 mg) was heated using a linear heating rate of 5 °C min⁻¹ from 30 to 300 °C. A sharp melt is observed at T_{onset} = 216.2 °C, agreeing closely with literature ranges published between 215 and 217 °C.*³²

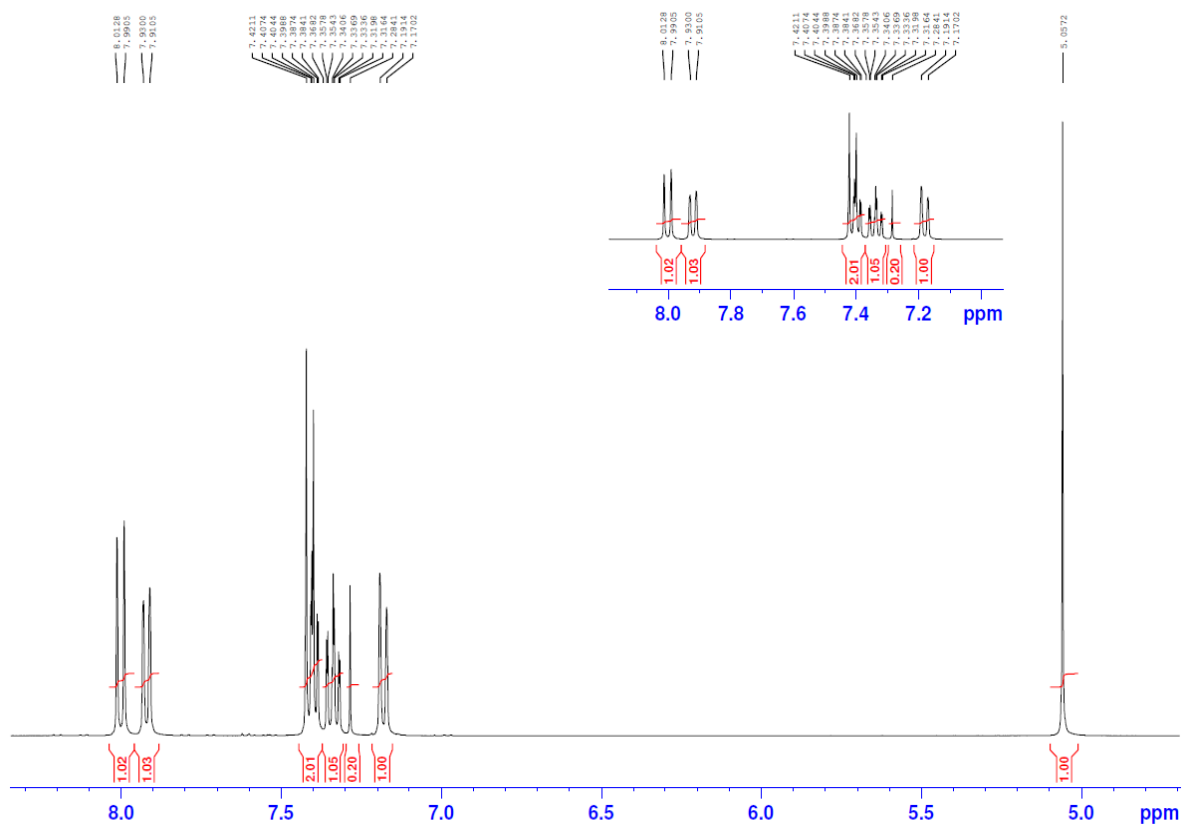


Figure 3.13 proton NMR spectrum of the synthesised binol product, insert focusing on the aromatic region.

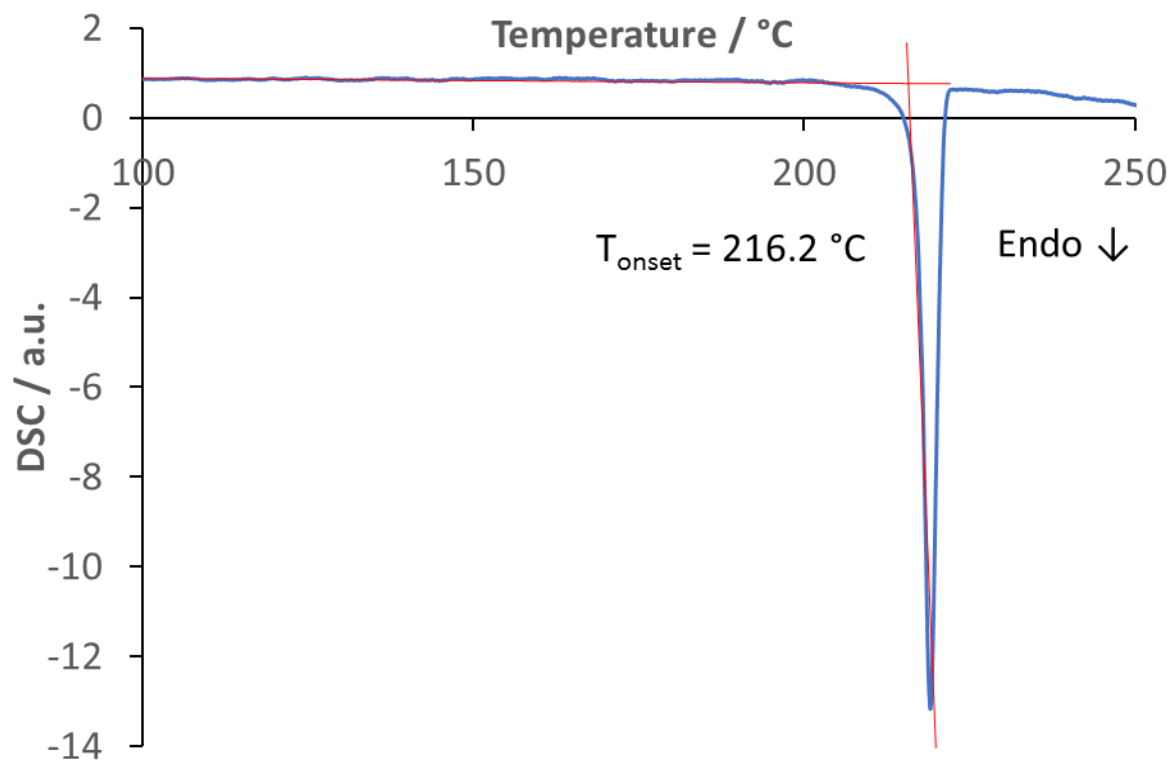
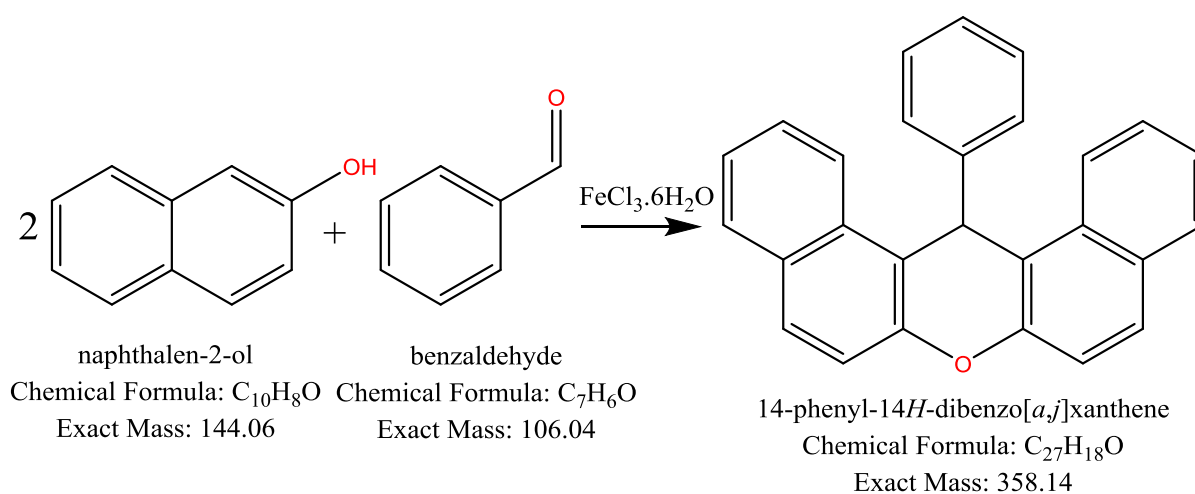


Figure 3.14 DSC analysis of the synthesised binol product.

3.4 14-Aryl Xanthene Synthesis

For this study, the μ -DART (Chapter 2, Section 2.6) was used to simultaneously sample in both the positive and negative mode utilising the ion trap's fast polarity switching mode. The synthesis of 14-phenyl-14H-dibenzoxanthene (aryl xanthene) is similar to the binol carbon coupling reaction described previously. This reaction is multicomponent, using the same components (2-naphthol and ferric chloride hexahydrate) together with an aromatic aldehyde, benzaldehyde. Schematic 3.5 shows an overview of the reaction: 2 equivalents of 2-naphthol react with 1 equivalent of benzaldehyde to form the product 14-phenyl-14H-dibenzoxanthene.



Schematic 3.5 Overall synthesis of aryl-xanthene from 2-naphthol, benzaldehyde and ferric chloride hexahydrate.

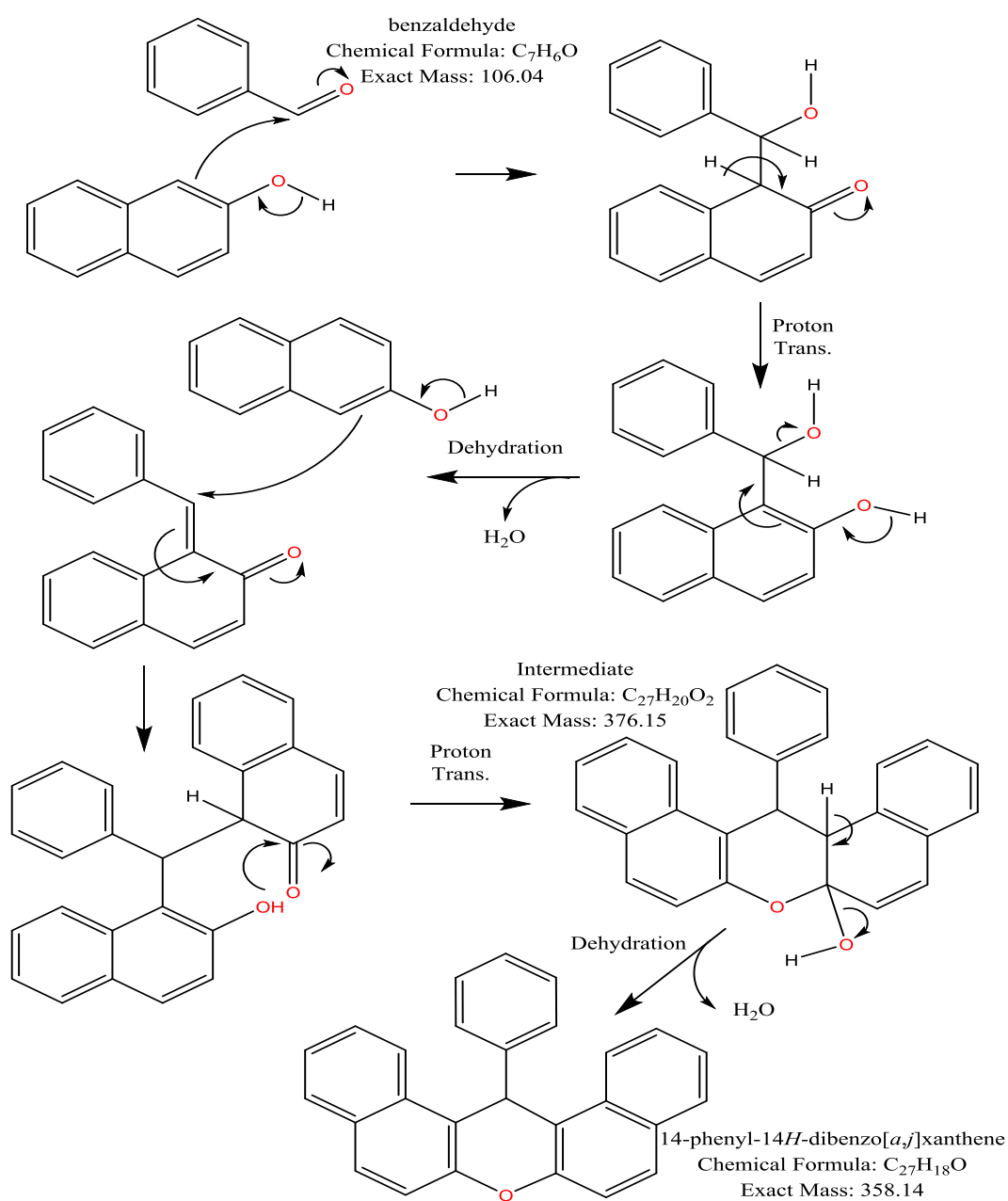
The reaction was considered a good test of HDM due to the greater complexity of the system (being multiple component). Aryl-xanthenes themselves find uses primarily within the dyes and pharmaceutical sectors, with many research articles reporting on their use within lasers,³⁴ anti-viral activity³⁵ and solar materials.³⁶

Much current research focuses on ways of making the synthesis 'greener' primarily through the use of modified clay catalysts,³⁷ non-conventional heating methods such as microwave heating³⁸ and with metal salts as catalysts.³⁹

The experimental conditions used were:

2-naphthol (16 mg, 111 μmol , Aldrich) and iron (III) chloride hexahydrate (30mg, 111 μmol , Aldrich) were premixed before the addition of the benzaldehyde (5.1 μl , 50 μmol). The reaction mixture was heated at 5 $^\circ\text{C min}^{-1}$ from 30 to 400 $^\circ\text{C}$. Simultaneous positive and negative spectra were obtained using the μ -DART and the mass spectrometer was set to alternating polarity mode for dual polarity data collection.

Schematic 3.6 shows the reaction scheme based on existing literature.⁴⁰ The reaction forms a complex between the solvated iron and the benzaldehyde although, as 2-naphthol is also present, the iron-naphthol complex will also form resulting in a dark coloured solution as noted in the binol example. Through nucleophilic attack by the 2-naphthol on the benzaldehyde the first intermediate is formed, which is stabilised by proton transfer. The intermediate then undergoes dehydration to form the second intermediate which is subjected to further nucleophilic attack with a second 2-naphthol molecule. The penultimate intermediate self-cyclises and dehydrates to finish the reaction process forming the aryl-xanthene.



*Schematic 3.6 Proposed mechanistic pathway of aryl-xanthene synthesis from 2-naphthol and ferric chloride hexahydrate.*⁴⁰

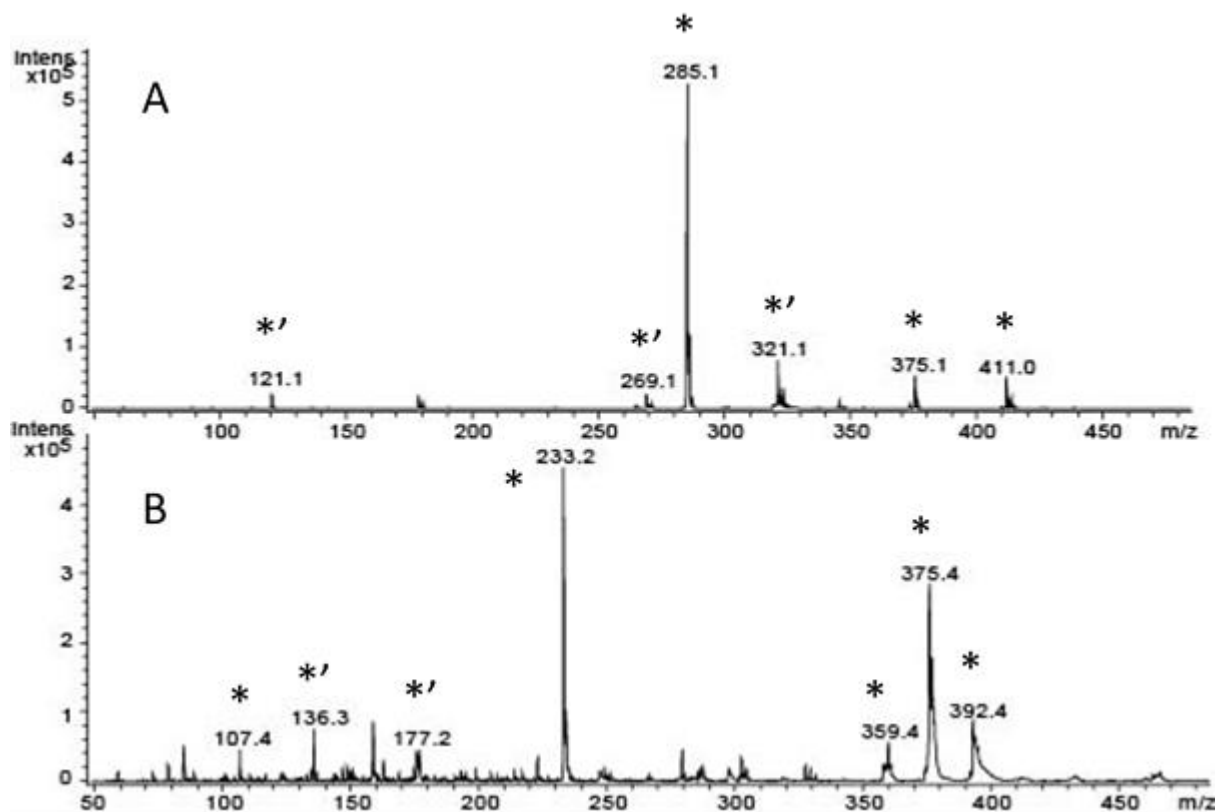


Figure 3.15 Averaged mass spectrum across the aryl-xanthene reaction. A) Negative mode, B) Positive Mode. *) Reaction signals, *') unassigned reaction signals. Thermal degradation peaks were not highlighted for clarity,

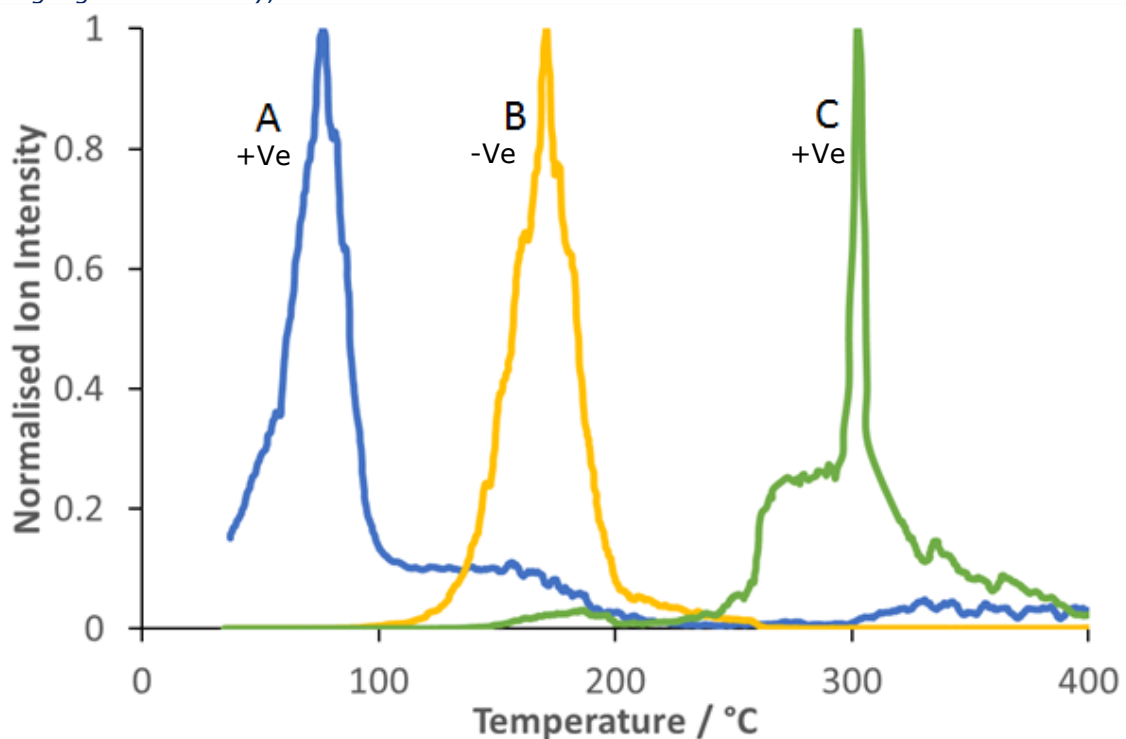


Figure 3.16 Reaction profiling for the synthesis of aryl-xanthene shown as a function of temperature. A) Benzaldehyde 107 Da $[M+H]^+$, B) Reaction intermediate 375 Da $[M-H]^-$ and C) Aryl-xanthene 358 Da $[M]^+$.

Figure 3.15 shows the average mass spectra obtained in both negative (A) and positive (B) modes. Increasing the number of reaction components also increases the number of possible side reactions and, since this is a temperature driven reaction, the number of thermal re-arrangement and decomposition products also may increase. In positive mode more side reactions and decomposition stages are apparent. In negative mode mass spectra are simpler mainly because fewer analytes are amenable to negative mode ionisation. Many intermediates are shown within the proposed reaction scheme, and the average mass spectra in both modes appear to reflect this, as opposed to the relatively simple spectra noted in other examples.

Figure 3.16 was constructed using both positive and negative mode signals from the μ -DART as some key intermediates may be missed if the experiment is operated in one ionisation mode solely. Although commercial DART systems have the ability to switch ionisation mode (between positive and negative) it is still slow (some seconds) and ionisation quantity is expected to be reduced due to the 'down time' taken to switch the module. In the case of the ion trap this switching capability is a relatively quick MS allowing virtually simultaneous recording of both polarities when using the μ -DART.

Profile A in Figure 3.16 follows the release of the protonated molecular ion of benzaldehyde. As in previous examples, this compound is released from the onset of heating and comes to a maximum level around 75 °C. A sharp decline is observed after the signal maximum which is attributed to the initiation of the reaction between 80 and 100 °C. Between *ca.* 100 and 170 °C the level of benzaldehyde plateaus and coincides with the formation of intermediate (B). As the intermediate profile declines the first signs of product release are seen. The product profile (C) has an unusual shape that has arisen from several ions being formed for one analyte, product C is observed as both the molecular ion 358 Da $[M]^+$ and the protonated molecular ion 359 Da $[M+H]^+$ that take preference during different temperature regions. Although both signals are present the molecular ion 358 Da $[M]^+$ observed the greatest profile stability so was used as a representative profile for the aryl-xanthene product. A sharp increase in profile C is seen at 250 °C which correlates to a change in colour and micrographs discussed later. The final sharp increase and then decline in profile C *ca.* 295 °C correlates to the final drying of the reaction when the final oily components are removed leaving behind a solid char that appears to gradually oxidise and results in a loss of profile intensity. The apparent gain in benzaldehyde (A) during the later stages has most likely arisen from lower molecular weight thermal decomposition products sharing the same nominal mass as several new signals are also observed.

Figure 3.17 shows the colour profile of the reaction. For this reaction the profile is difficult to interpret partly due to the complex nature of the trace. However, with the aid of the

micrographs in Figure 3.18 some features of the trace can be evaluated. 80-100 °C shows a sharp step in colour ($\Sigma\text{RGB} = \text{ca. } 220 \text{ a.u.}$), the step arises from the dehydration of the majority of liquid components in the reaction pan, mainly the benzaldehyde (micrographs A-B, Figure 3.21) profile A.

A gradual darkening is noted before another step change between 145-170 °C, micrographs C-D show the remaining liquid begins to turn slightly matte in finish, coinciding with the intermediate formation (B). The reaction darkens gradually between 180 and 250 °C, ΣRGB changes by *ca.* -250 a.u.. The surface becomes reflective, linked to the sharp rise in product signal (C). During this temperature range the remaining organic products are assumed to have reached a boiling point and boil away. The remaining solid gradually oxidises under the harsh conditions between 250-400 °C leaving behind the char (see micrograph F).

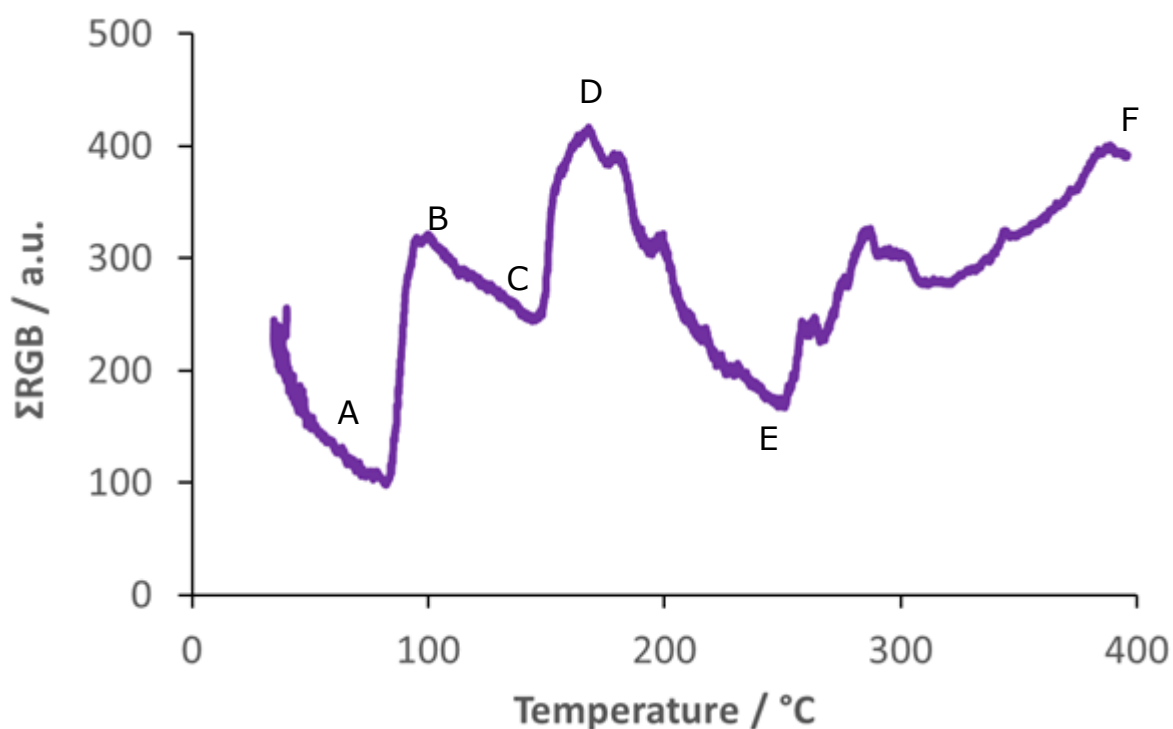


Figure 3.17 Colour profiling of the aryl-xanthene synthesis. Labels correlate to the micrographs in Figure 3.18.

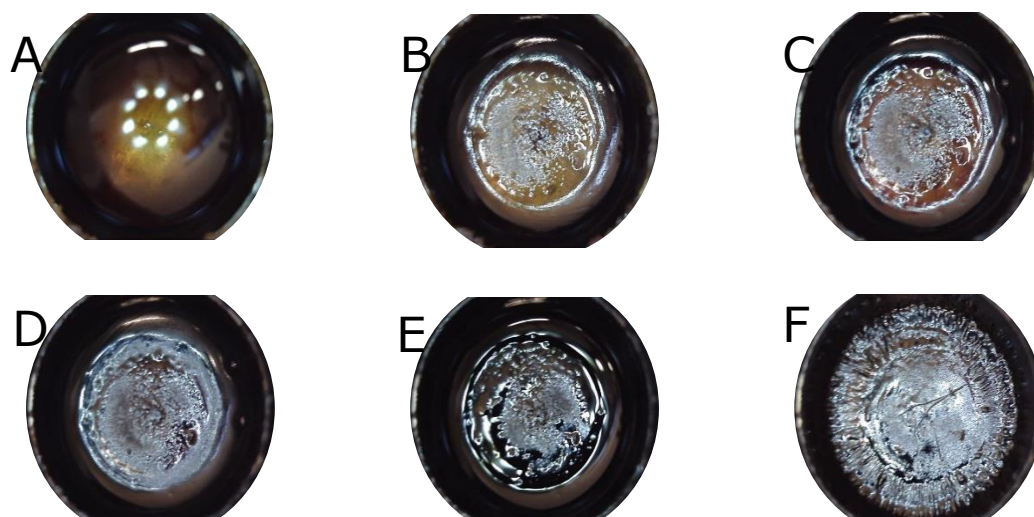


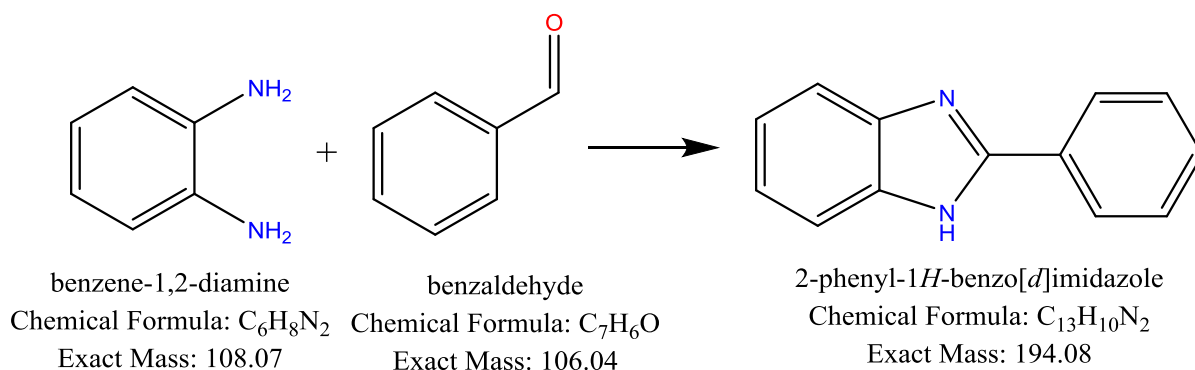
Figure 3.18 Micrographs of the aryl-xanthene synthesis, A) 80 °C, B) 100 °C, C) 145 °C, D) 170 °C, E) 250 °C and F) 400 °C.

The reaction was repeated but on a slightly larger scale so that DSC and NMR confirmatory studies could be performed. *The scaled reaction was heated at 5 °C min⁻¹ between 30 and 170 °C, the reaction was held in this temperature region for 10 minutes so product formation occurred without risk of significant thermal decomposition. The reaction mixture was washed with cold deionised water to remove the remaining iron salts and the crude product was recrystallised from hot ethanol to afford a beige powder.*

Unfortunately, the beige powder requires further purification after the original NMR analysis suggested that multiple chemical species were still present. The intention would be to return to the powder and purify through column chromatography.

3.5 2-Phenylbenzimidazole Synthesis

A heterogeneous reaction between the liquid benzaldehyde and solid o-diaminobenzene was selected to be monitored using HDM, selected as many reactions rely on heterogeneous synthesis. The reaction itself has been extensively reviewed within the literature yielding the product 2-phenylbenzimidazole.⁴¹ Commonly phenylbenzimidazoles are produced through reactions of primary amines and carbonyl-containing phenyl compounds such as benzaldehyde or benzoic acid as outlined in Schematic 3.7.



Schematic 3.7 Overall reaction between benzene-diamines and phenyl-aldehydes yielding substituted phenylbenzimidazoles.

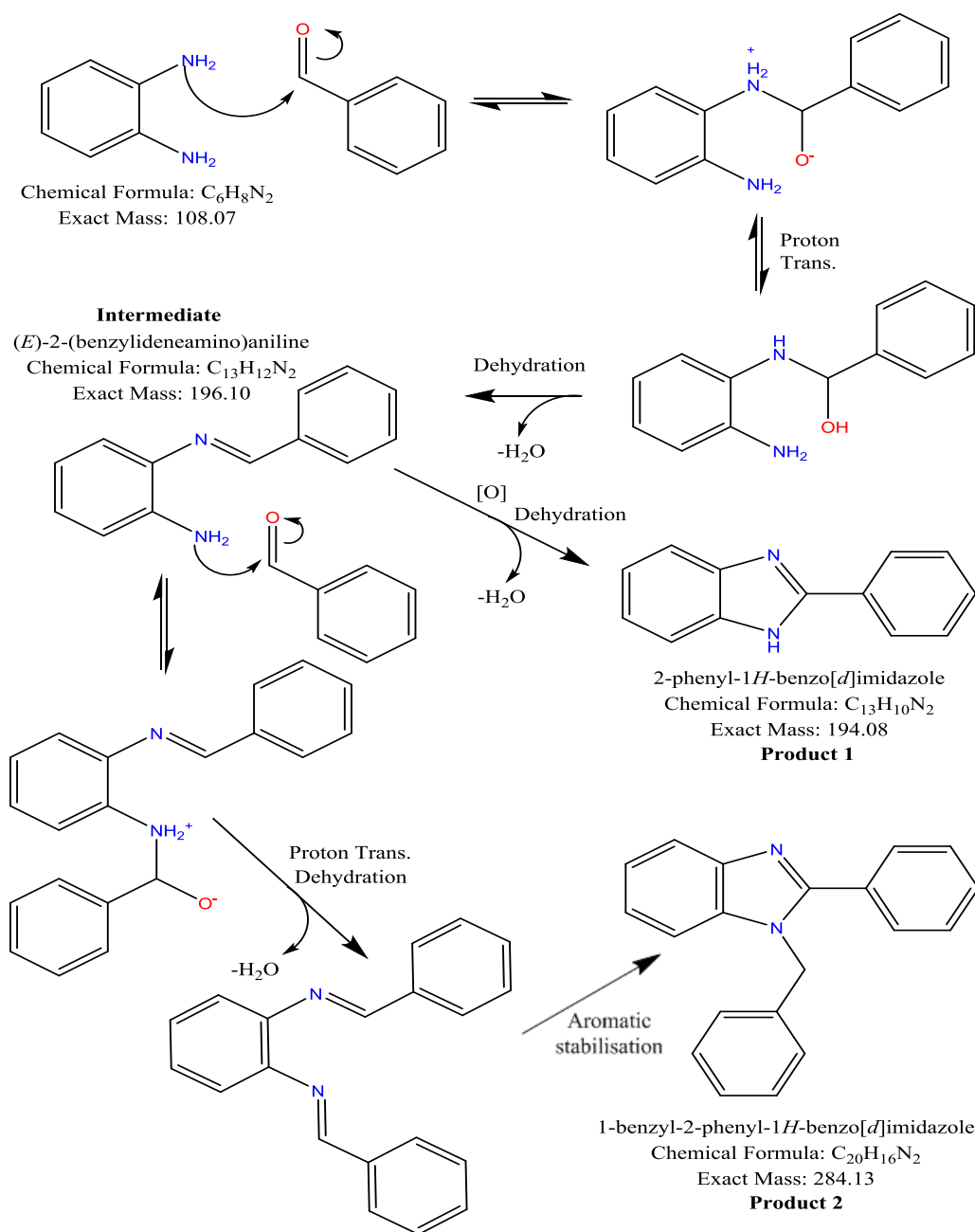
Phenylbenzimidazole and its various substituted analogues are of great interest for current research for their use within a wide range of applications including as antimicrobial,⁴² antiviral⁴³ and anticancer⁴⁴ compounds. Many literature methods report the use of reaction of these compounds within solvents usually refluxing under oxidative and acidic conditions as originally reported by Phillips,⁴⁵ and the method of synthesis is now commonly known as the Phillip's benzimidazole synthesis.

Schematic 3.8 shows a proposed synthetic pathway based on existing literature.⁴⁶⁻⁴⁷ The reaction can follow one of two routes, the formation of the target molecule 2-phenylbenzimidazole and the second route yields the product 1-benzyl-2-phenyl-1H-benzo[d]imidazole. The reaction proceeds through nucleophilic attack between the amine group of o-diaminobenzene and the carbonyl carbon of the benzaldehyde. After proton transfer and dehydration the key intermediate ((*E*)-2-(benzylideneamino)aniline) can follow one of two pathways. If sufficient oxygen is present the intermediate may undergo a final dehydration to yield the 2-phenylbenzimidazole product.

Should the reaction be oxygen deprived or if higher amounts of benzaldehyde are used the synthetic pathway preferentially follows a second nucleophilic attack from the primary amine towards another benzaldehyde molecule. Another condensation reaction follows to produce the penultimate product. The final step is the self-cyclisation driven by aromatic stabilisation producing the secondary product 1-benzyl-2-phenyl-1H-benzo[d]imidazole.

The following experiments were setup to evaluate the synthesis without solvent (common synthetic method) and as a function of temperature, the driving force is expected to be the removal of water at elevated temperatures preventing the reverse reaction:

Benzaldehyde (20.4 μL , 200 μmol , Aldrich) was deposited onto 1,2-diaminobenzene (21.6 mg, 200 μmol , Aldrich) in the reaction pan. A linear heating rate of 5 $^{\circ}\text{Cmin}^{-1}$ was applied to the sample between 30 and 300 $^{\circ}\text{C}$. The reaction was also repeated keeping everything constant other than using benzaldehyde in excess. The DART and MS combination were operated in positive mode only.



Schematic 3.8 Proposed mechanistic multi-route synthesis between benzaldehyde and o-diaminobenzene. Based on literature.⁴⁶⁻⁴⁷

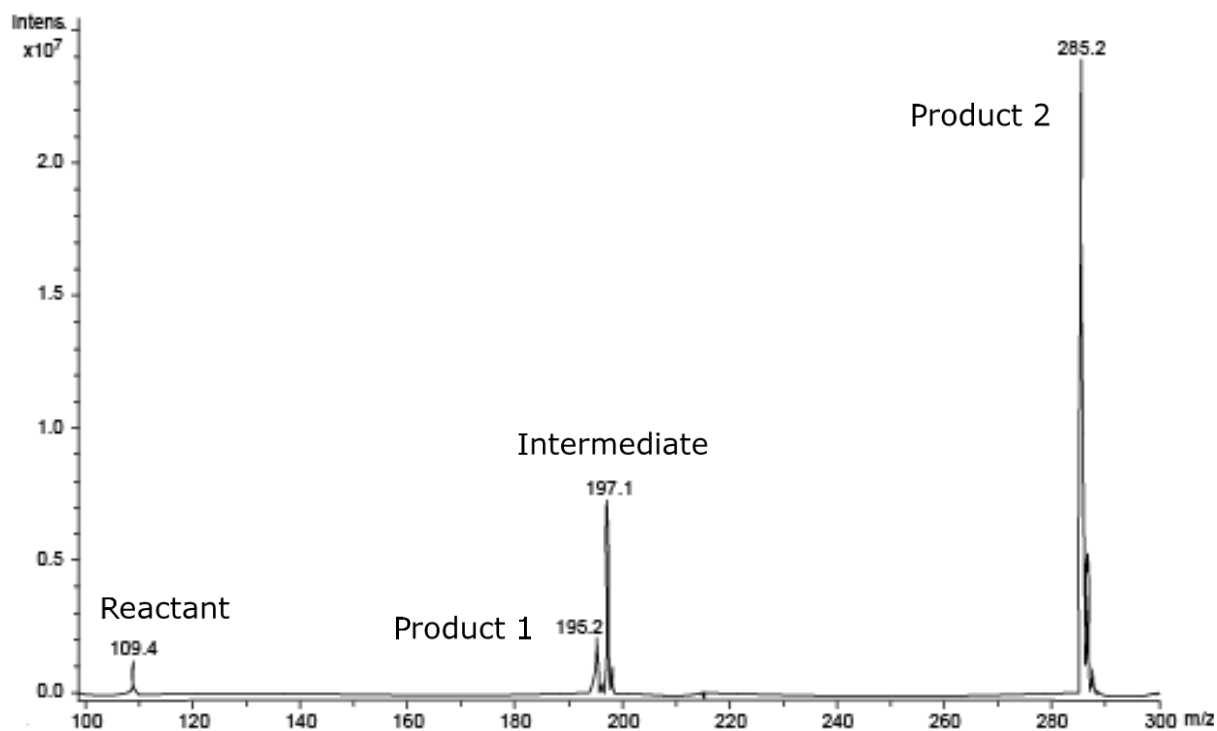


Figure 3.19 Average mass spectrum over the full reaction duration for phenylbenzimidazole. All major peaks have been assigned.

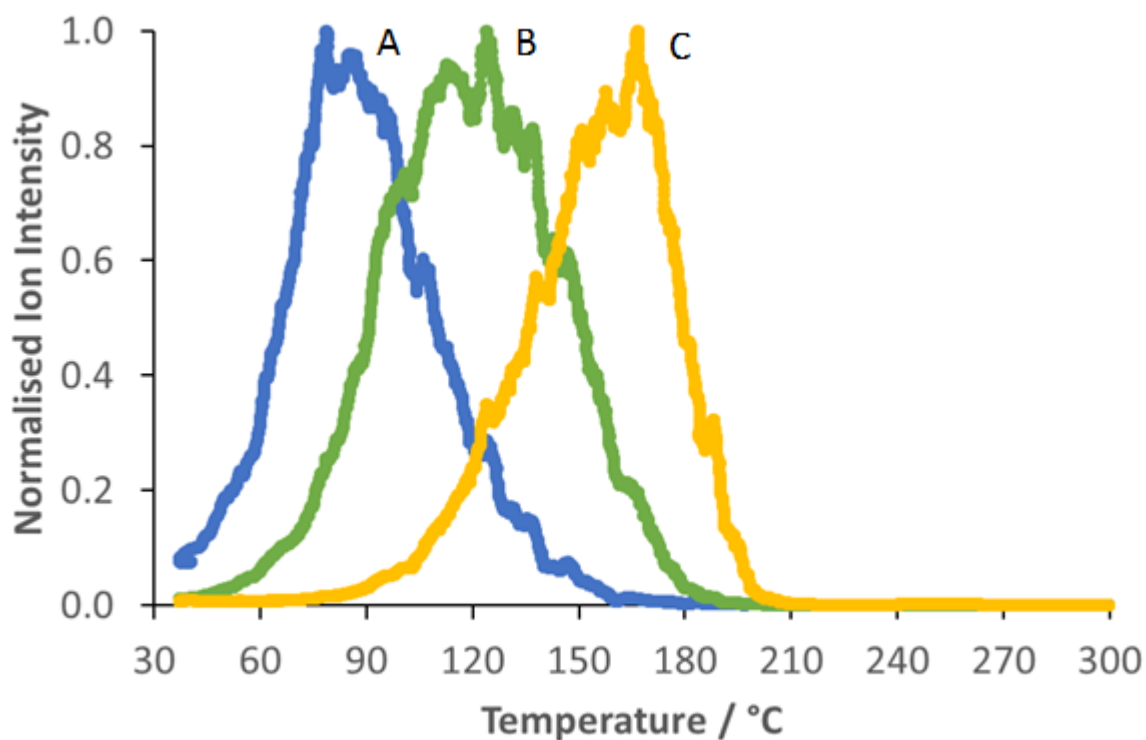


Figure 3.20 Reaction profiling normalised ion intensities plotted as a function of temperature for reaction pathway one. A) o-diaminobenzene 109 Da [M+H]⁺, B) Intermediate 197 Da [M+H]⁺, C) Product one 195 Da [M+H]⁺.

Reaction pathway 1 from Schematic 3.8 is profiled (see Figure 3.20), the large differences in ion intensity (shown in Figure 3.19) resulted in the reaction profile being normalised for clarity. Figure 3.20 profiles the conversion from reactant (*o*-diaminobenzene, 109 Da, $[M+H]^+$), to intermediate ((*E*)-2-(benzylideneamino)aniline, 197 Da, $[M+H]^+$) to product (2-phenylbenzimidazole, 195 Da, $[M+H]^+$).

The onset of heating releases the *o*-diaminobenzene, around 85 °C the peak maximum is noted. The highest rate of intermediate formation (B) is shown between 70 and 105 °C coinciding with the maximum of *o*-diaminobenzene. The same trend is observed between intermediate and product formation between 120 and 150 °C. A significant amount of water is removed during these reaction pathways potentially explaining the exclusivity of the protonated signals as discussed in the introduction.

Comparisons of the micrographs and colour (Figure 3.21 & Figure 3.22 respectively) to the reaction profile show some key steps. Micrographs A-C show the conversion from a liquid state to a semi-solid reaction mixture as the benzaldehyde reacts with the *o*-diaminobenzene. The colour profile within this temperature range shows a gradual increase in total colour, arising from the shift in yellow liquid to the more reflective solid bed that formed. The development of the semi-solid correlates well with the rise in product 1 profile (C). The decline in product 1 (C) from 170 °C appears to arise from the onset of thermal decomposition as the colour also begins to darken. The final darkening (see micrograph E) is the thermal decomposition monitored between 200 and 300 °C as a brown oil remains, from a variety of thermal decomposition products which formed, the step change in colour around 270 °C appears to be an underlying eutectic melt of the product mixture.

This was the first example in which reaction intermediates had been noted in significant quantities resulting in mass spectrum signals. (*E*)-2-(benzylideneamino)aniline is an isolatable transient intermediate although under these reaction conditions it will be driven towards either product as shown in Schematic 3.4. As intermediates reach the gas phase prior to MS analysis it is reasonable to assume that the environment they exist within at this stage is unfavourable for further reaction (primarily oxidation), this combined with the short transit time from reaction pan to the mass detector may help suggest why these reaction intermediates can be seen, further demonstrated across a wider range of reactions discussed within this chapter.

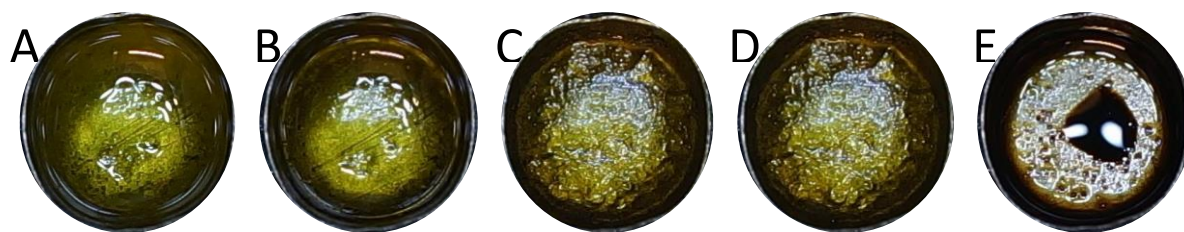


Figure 3.21 Micrographs of the phenylbenzimidazole reaction progression A) 30 °C, B) 100 °C, C) 150 °C, D) 200 °C and E) 300 °C

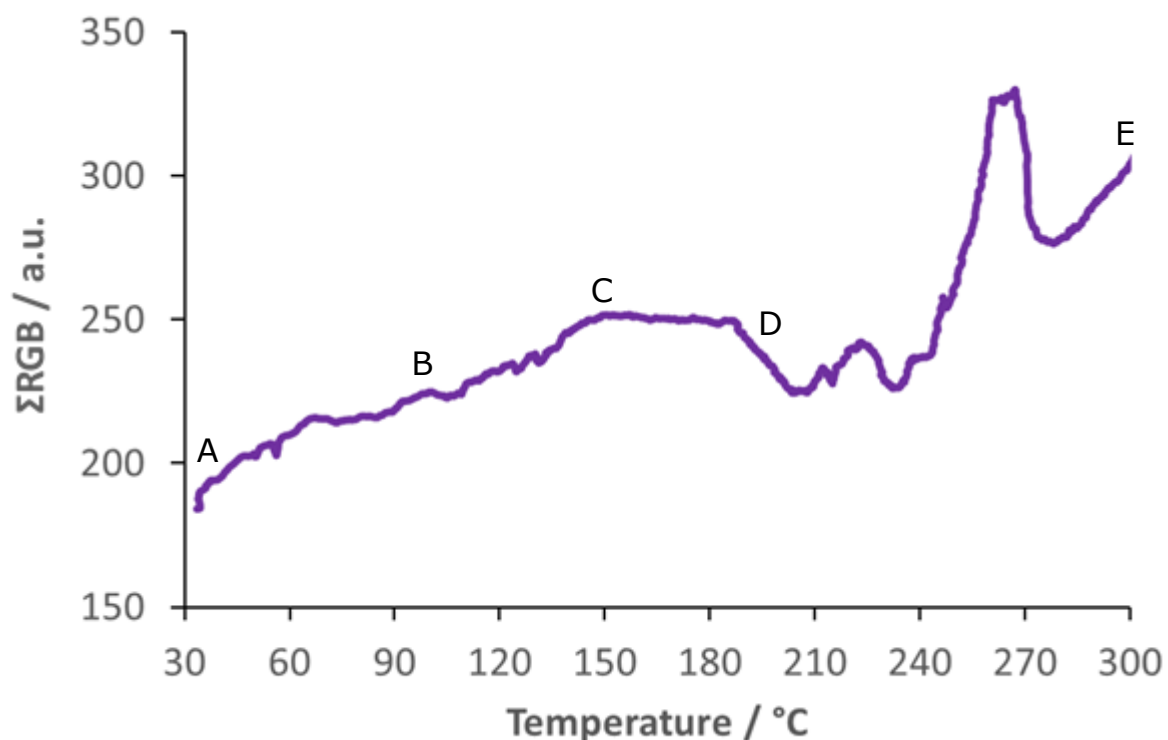


Figure 3.22 Colour profiling of the phenylbenzimidazole reaction progression, total colour plotted as a function of temperature. Labels correlate to the micrographs in Figure 3.21

Figure 3.23 demonstrates the same reaction but using an excess of benzaldehyde since a 1:1 stoichiometry would limit the amount of secondary product formed when following pathway 2. The excess benzaldehyde used in this example does appear to drive further formation of the secondary product (comparing average MS profiles). Benzaldehyde (A) and intermediate (B) profiles follow closely to the 1:1 example having a similar shape. The secondary product forms shortly after the intermediate's onset of formation, the rate of secondary product release is constant until around 130 °C.

Investigation within this region shows that product one is also released resulting in an apparent slowdown in rate of product two between 135 and 160 °C; this has been tentatively attributed to a signal suppression effect. After this temperature the reaction appears to undergo thermal decomposition again with a corresponding loss of ion signal. The slight peak shown around 270 °C had arisen from deposition of the product on the MS

inlet ceramic, with further heating this is removed and thus is considered an artefact of the experiment. This was the primary reasoning for the construction of the inlet ceramic heater to prevent further sample deposition as this had been noted previously in Chapter 2.

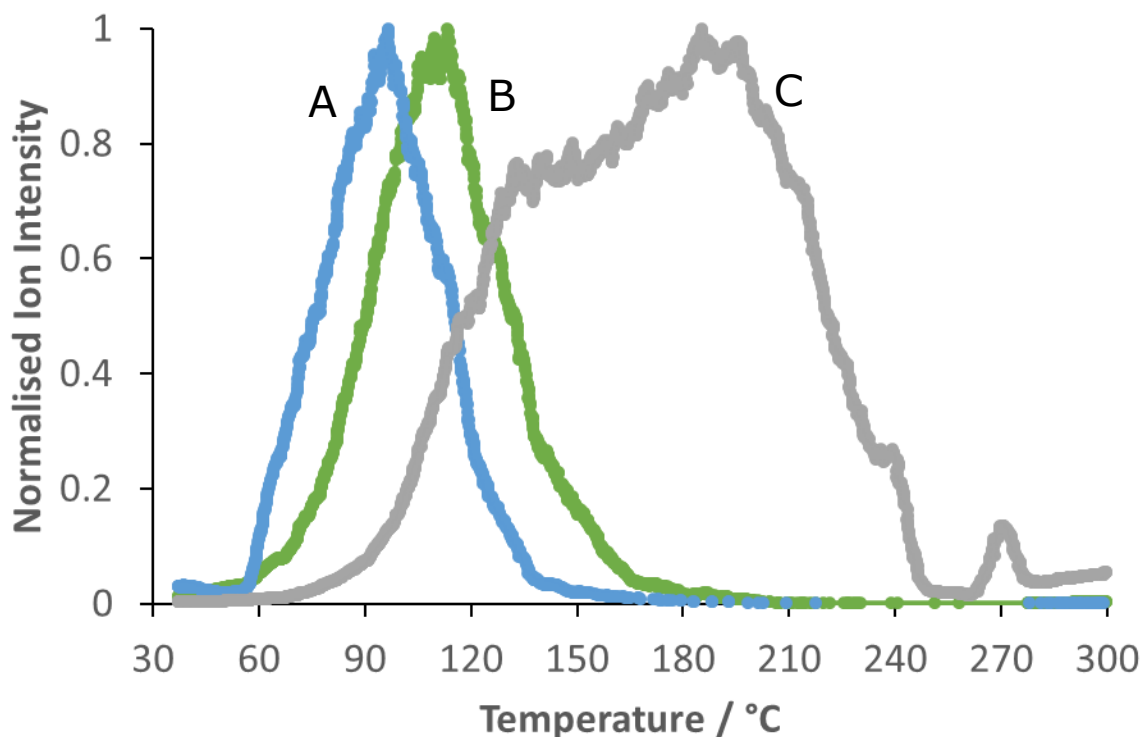


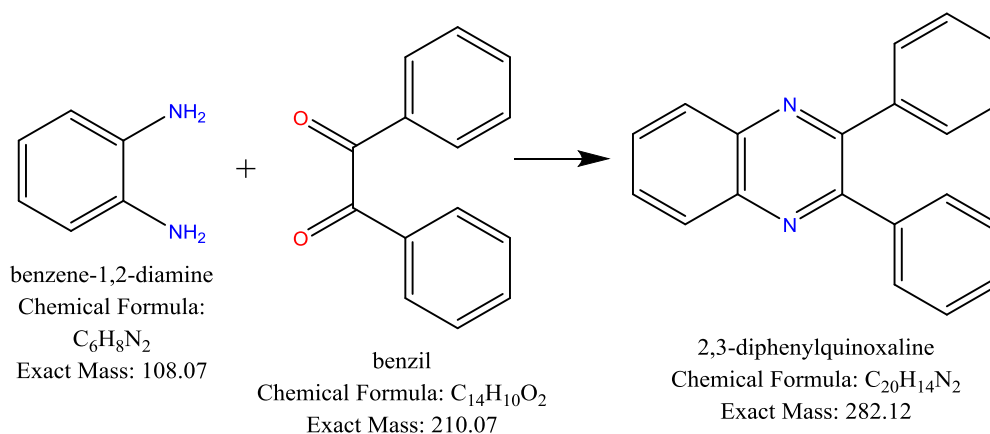
Figure 3.23 Reaction profiling normalised ion intensities plotted as a function of temperature for reaction pathway two. A) o-diaminobenzene 109 Da $[M+H]^+$, B) Intermediate 197 Da $[M+H]^+$, C) Product 285 Da $[M+H]^+$.

It has been noted by several authors that if this particular reaction is starved of oxygen then the yields of product one are reduced.⁴⁸ The DART source constantly creates a curtain gas (typically inert He) across the sample, the reduced oxygen atmosphere helps to explain why preferential formation of product pathway two is noted in both examples. By increasing the proportion of the benzaldehyde the reaction can be pushed almost exclusively towards reaction pathway two.

The products have not been formulated on a large scale for NMR and DSC analysis. Again, the intent would be to characterise these materials through other instrumental means to strengthen the assignment of the signals obtained by HDM in future work.

3.6 2,3-Diphenylquinoxaline Synthesis

Two different experiment types were trialled for the diphenylquinoxaline synthesis, a simple linear heating experiment and an isothermal temperature hold experiment. The profile of 2,3-diphenylquinoxaline was monitored using HDM to monitor the melt reaction between benzil and o-diaminobenzene. The overall reaction is outlined in Figure 3.28, essentially a double dehydration reaction forming a heterocyclic pyrazine ring.



Schematic 3.9 Overall reaction between o-diaminobenzene and benzil yielding phenyl substituted quinoxaline.

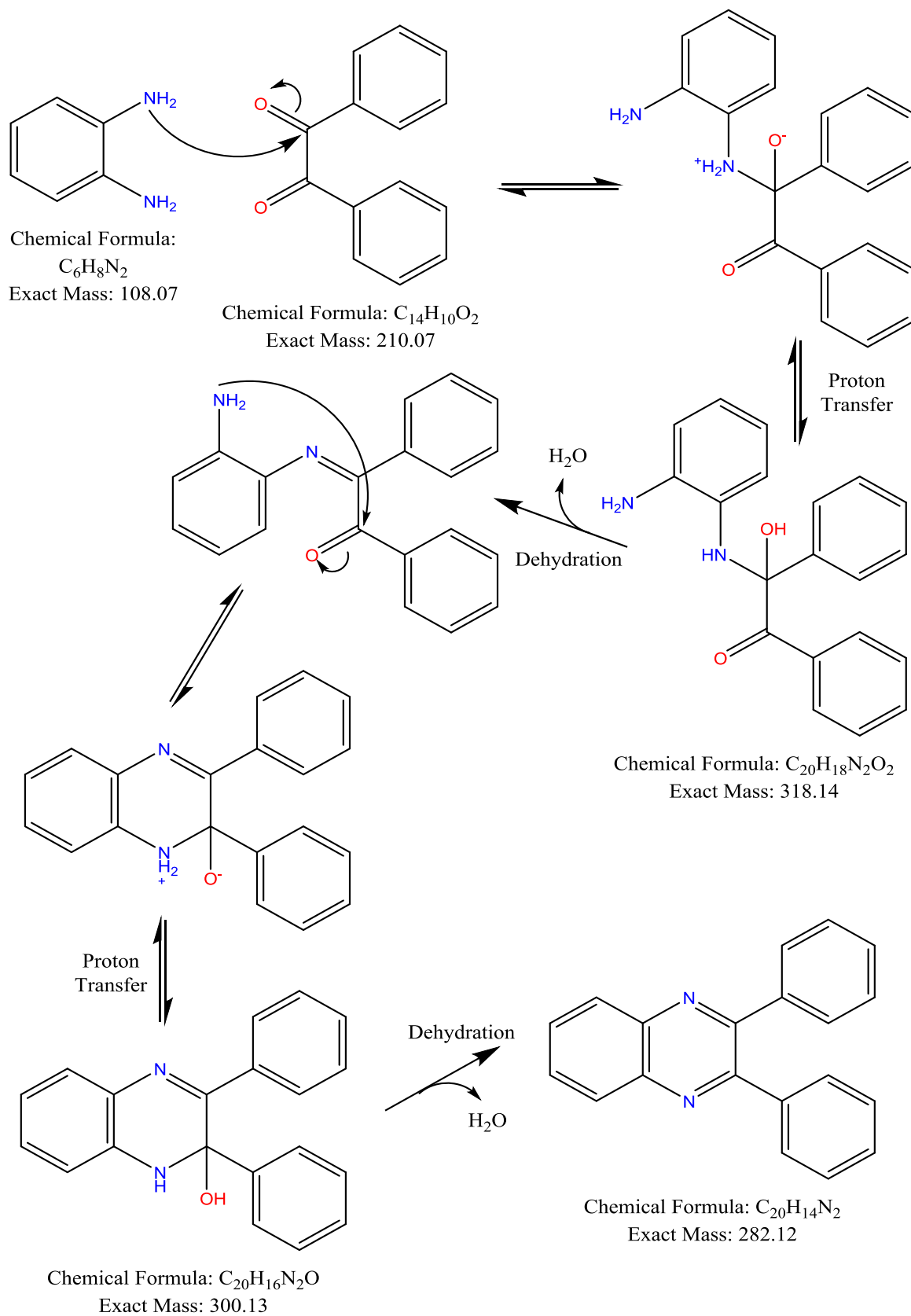
The quinoxaline family of compounds serve major roles biologically and are being extensively researched for use within the following areas: selective protein inhibitors,⁴⁹ antioxidants⁵⁰ and cytotoxicity.⁵¹ Chemically quinoxalines serve as excellent backbones for photoactive compounds used within electroluminescence⁵² and as chromophores.⁵³

Schematic 3.5 shows the proposed mechanistic pathway based on the existing literature.⁵⁴ The reaction follows a series of dehydrations and final aromatic stabilisation as the driving force behind this reaction. An amine of o-diaminobenzene attacks a carbonyl carbon of benzil, followed by proton transfer and dehydration. The final condensation is intramolecular, with the free terminal amine attacking the second carbonyl carbon, the intramolecular reaction is likely to be quick and driven by aromatic stabilisation upon formation of the final product. The water from the dehydration reactions is being driven off by the elevated temperatures preventing possible reverse reactions.

Both experiments followed the same sample preparation:

Equimolar amounts of o-diaminobenzene (10.8 mg, 100 μ mol, Aldrich) and benzil (21 mg, 100 μ mol, Aldrich) were slightly ground before addition to the analysis pan.

The linear heating experiment followed a temperature program of 5 $^{\circ}$ C min⁻¹ between 30 and 300 $^{\circ}$ C. The isothermal experiment used a 5 $^{\circ}$ C min⁻¹ heating rate, held isothermally at 100 $^{\circ}$ C for 30 mins and continued linearly heating at 5 $^{\circ}$ C min⁻¹ up to a maximum temperature of 250 $^{\circ}$ C. The DART and MS were operated in positive mode.



Schematic 3.10 Proposed mechanistic synthesis between benzil and *o*-diaminobenzene forming 2,3-diphenylquinoxaline.

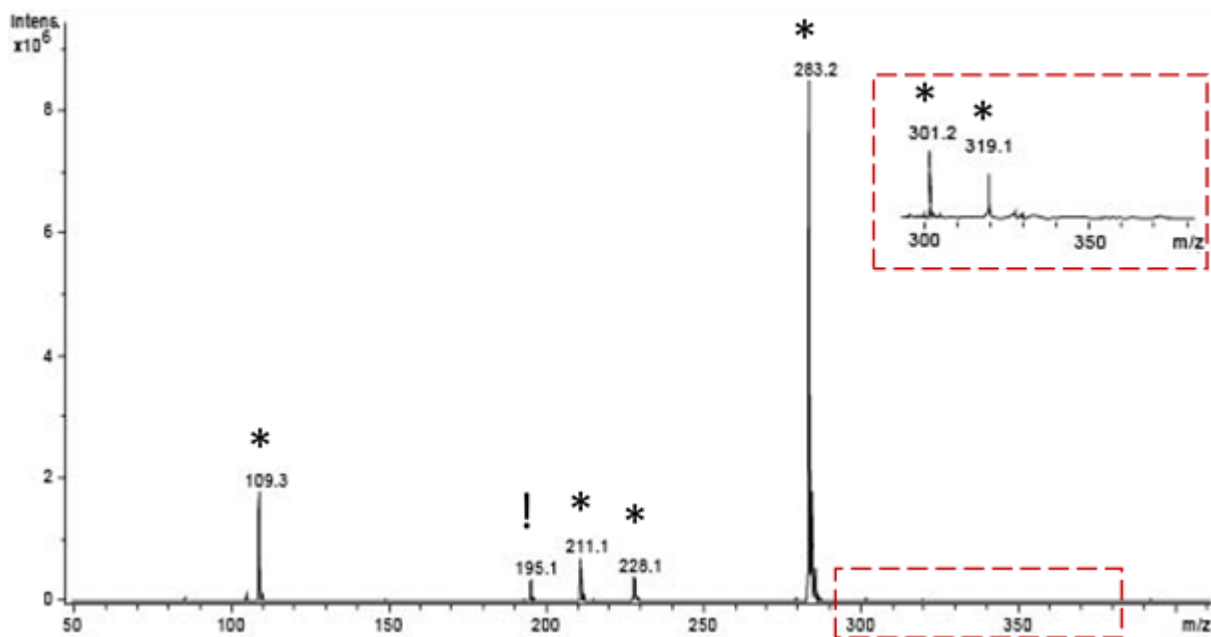


Figure 3.24 Average mass spectrum over the entire reaction duration (linear heating experiment) for diphenylquinoxaline, insert shows scaled intermediate region. *) Assigned Reaction peaks and !) Carry over peak.

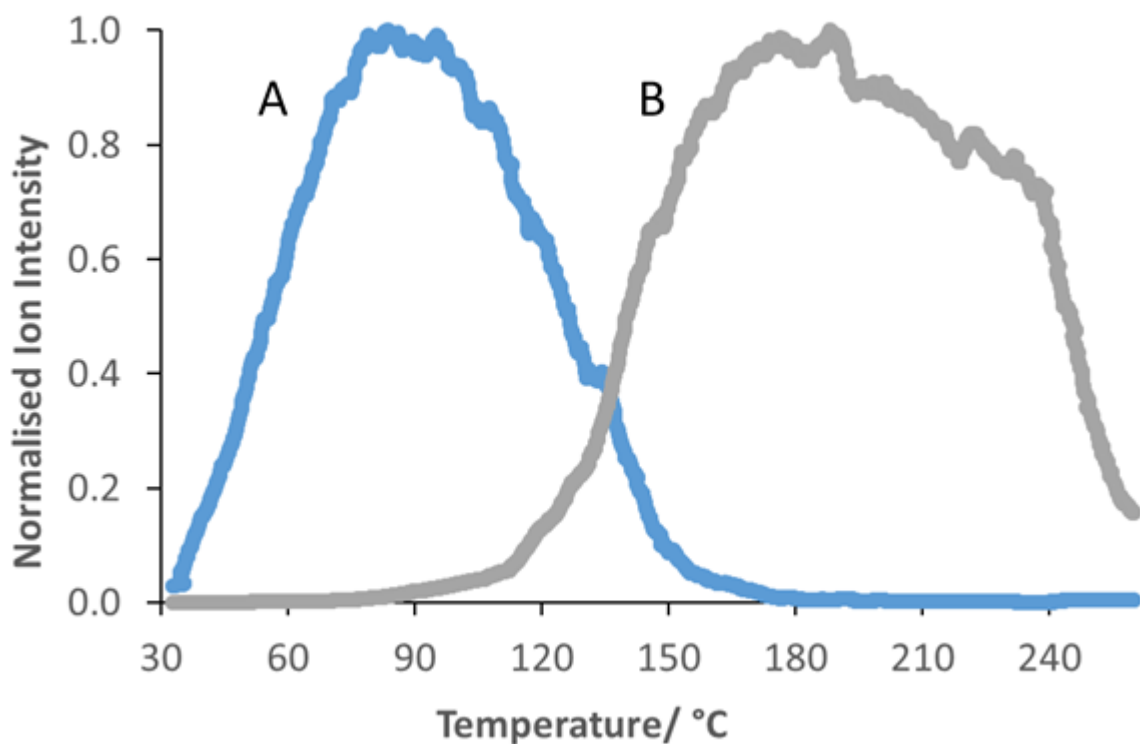


Figure 3.25 Reaction profiling normalised ion intensities plotted as a function of temperature. A) *o*-diaminobenzene 109 Da $[M+H]^+$, B) diphenylquinoxaline 283 Da $(M+H)^+$.

Shown in Figure 3.24 is the average mass spectrum for the linear heating experiment, although both reactant signals *o*-diaminobenzene 109 Da $[M+H]^+$ and benzil 211 Da $[M+H]^+$ are noted the trace for benzil has been omitted from Figure 3.25. The choice to omit the benzil profile was due to inconsistencies within the signal arising from apparent signal suppression of the *o*-diaminobenzene and diphenylquinoxaline product 283 Da $[M+H]^+$. Reaction intermediates (Figure 3.24, insert) had been noted but in relatively low quantities. The apparent reduced intensity is most likely due to the speed at which intramolecular reactions can occur.

Figure 3.25 shows a selected reaction profile from reactant (*o*-diaminobenzene 109 Da $[M+H]^+$) through to the final product (diphenylquinoxaline product 283 Da $[M+H]^+$), the profiles have been normalised. *O*-diaminobenzene (A) is gradually evolved with heating until a maximum of 90 °C, coinciding closely with the secondary reactant benzil ($T_m = 95-96$ °C).⁵⁵ As profile (A) reaches its maximum the molten benzil begins to react with the *o*-diaminobenzene, the profile decline is attributed to the reactants being consumed. During the decline of *o*-diaminobenzene (A) the rise of diphenylquinoxaline profile (B) is shown with an increase in rate of release around 110 °C as the entire reaction is now within the liquid state. Continued heating drives off the product over a broad temperature range *ca.* 100 °C. The sharp decline of profile (B) at 240 °C is caused by complete depletion of products from the analysis pan. The profile was concluded at 260 °C for profile clarity as inlet ceramic contamination (from condensation) was a major issue during this experiment, giving rise to apparent prolonged profiles.

This reaction demonstrates some interesting physical processes as can be viewed by comparison of micrographs (Figure 3.26) and colour profiles (Figure 3.27). Micrograph A shows the two reactants in the pan with an off-white colour, with minimal heating the reaction becomes a faint yellow see micrograph B, an associated colour change in the colour profile is seen around 50 °C. The colour profile becomes slightly noisy between 50 and 90 °C as the reactants begin to move around and shrink exposing more of the metallic pan underneath. A step change is noted about 90 °C for the onset of melting of the benzil, micrographs B-C. The colour profile stabilises between 90 and 130 °C, although the colour trace did not reveal too much within this region, comparison between micrographs C and D shows that the reaction mixture had crystallised most likely due to supersaturation of the solution. A sharp step is shown in the colour profile at 130 °C, linked to the micrographs D and E as the reaction mixture melts. The melt coincides with the maximum rate of evolution of the quinoxaline product in Figure 3.25. The colour profile remains relatively stable over the next 100 °C until a final sharp step is observed at 240 °C as all the liquid state evaporates from the pan.



Figure 3.26 Micrographs of the synthesis of 2,3-diphenylquinoxaline. A) 30 °C, B) 50 °C, C) 95 °C, D) 120 °C, E) 150 °C.

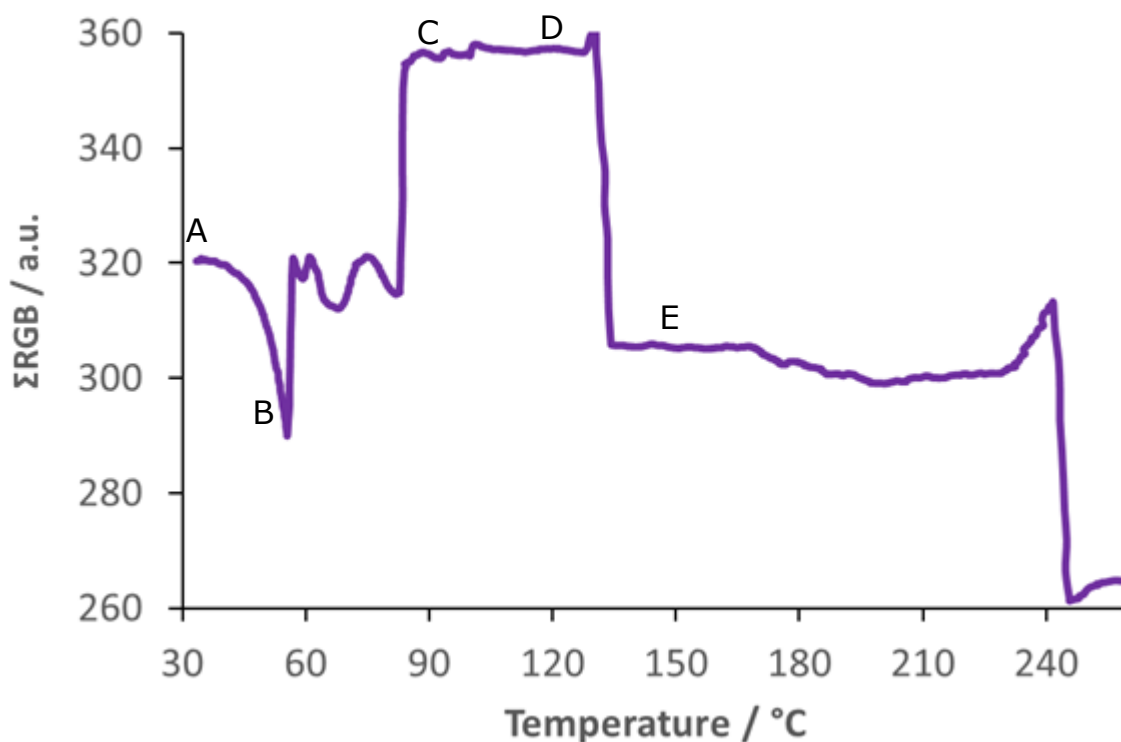


Figure 3.27 Colour profiling of 2,3-diphenylquinoxaline synthesis (linear heating), total reaction colour plotted as a function of temperature. The labels correlate to the micrographs in Figure 3.26..

To evaluate the reaction and primarily the *in situ* crystallisation process further the reaction was held isothermally at 100 °C for 30 minutes to allow further reaction conversion. The isothermal temperature was selected to be between the melting of the reactants and melting of the product to induce the crystallisation shown earlier in Figure 3.26. A series of micrographs are shown in Figure 3.28 and Figure 3.29 has been split into three profiles (EICs, differential colour and temperature).

The differential colour (Δ RGB) shows sharper signals most notably around the melting events. During the first heat ramp the colour profile is similar to Figure 3.27 (the linear

heat example). A series of noisy spikes are shown due to movement, colour change and the onset of melting around 85 °C, slightly earlier than in the linear heating example.

The colour remains constant during the isotherm, with no clear sign of crystallisation in this period. Further heating forces the melt at 130 °C, and the final boil away of the sample is shown by a sharp peak around 245 °C in a similar manner to the linear heating example.

In the isothermal example the profile for benzil has been included. The increase in reaction time gave sufficient resolution between reactant profiles that it was decided that the benzil could be included. During the isothermal period the benzil profile dominates the mass spectra, likely owing to the fact it is molten by this point. The benzil signal gradually falls away during the isotherm, a combination of evaporation and reaction consumption will be occurring during this stage. The o-diaminobenzene profile is evolved in a similar manner to Figure 3.25 during the initial heat, and falls away during the isothermal period, again when combinations of evaporation and reaction consumption are occurring. The quinoxaline product shows the onset of formation during the same temperature region as the decline of o-diaminobenzene.

During the isothermal period a steady profile is achieved for the quinoxaline, until the second heat when a rapid evolution is noted. Both benzil (B) and o-diaminobenzene (A) show a brief rise in intensity about the melting of the reaction mixture, suggesting that some of the unreacted components may have been trapped within the solid that formed. The product continues to be released until product depletion beyond 180 °C and reaction termination at 250 °C.

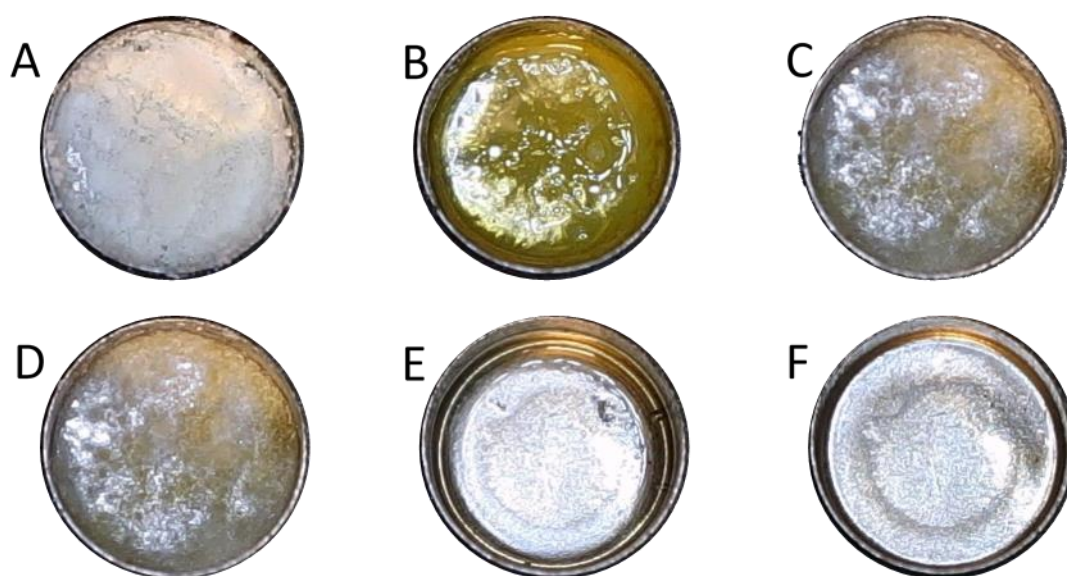


Figure 3.28 Micrographs of the synthesis of 2,3-diphenylquinoxaline during isothermal synthesis. A) 0 min, B) 15 min, C) 18 min, D) 48 min, E) 58 min, F) 88 min.

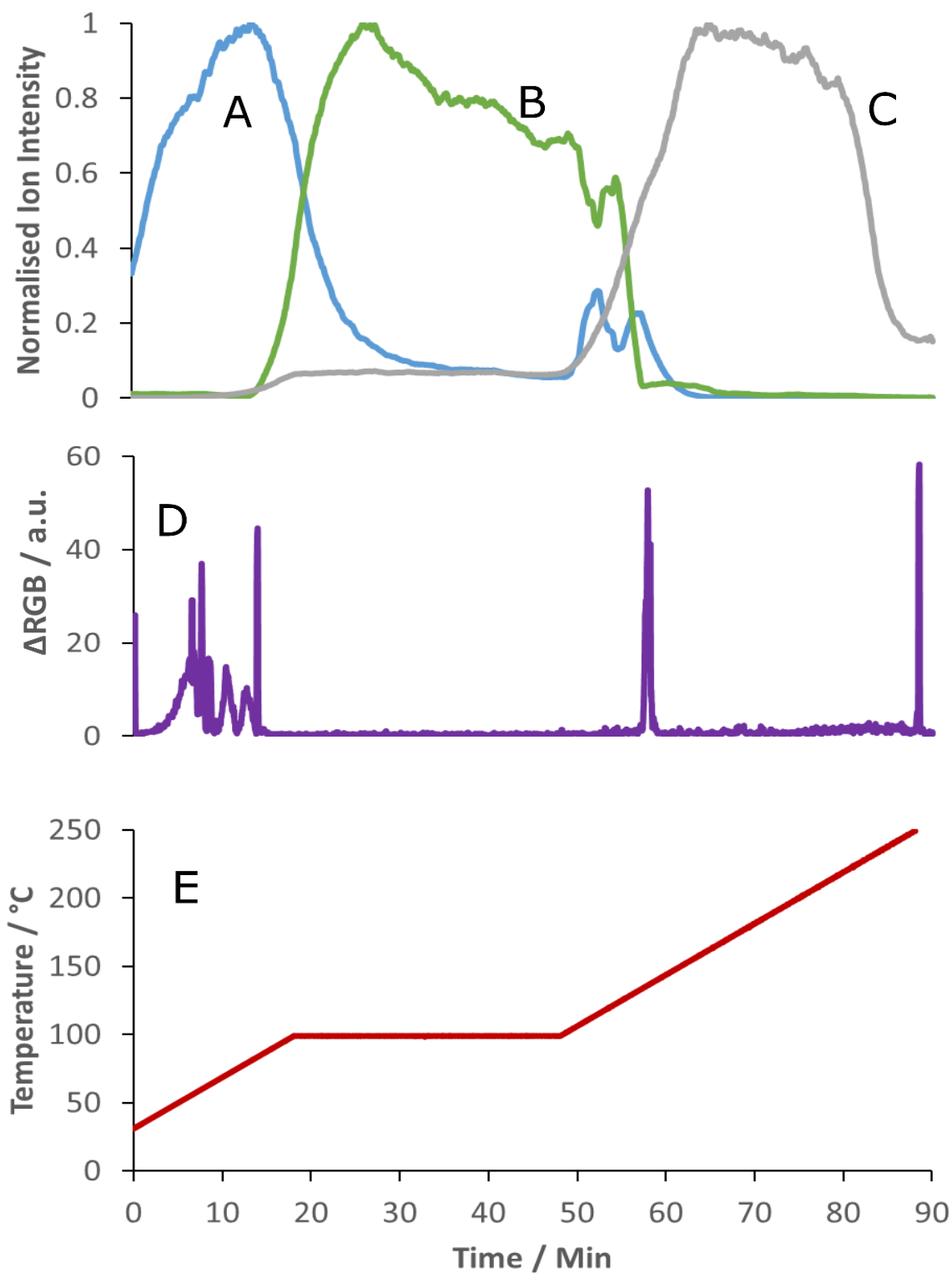


Figure 3.29 Isothermal profile of 2,3-diphenylquinoxaline synthesis. A) *o*-diaminobenzene 109 Da $[M+H]^+$, B) benzil 211 Da $[M+H]^+$, C) diphenylquinoxaline 283 Da $[M+H]^+$, D) Differential colour and E) Temperature.

The micrographs in Figure 3.28 follow closely to the micrographs obtained during the linear heating experiment in Figure 3.26. The same key features are noted, conversion from white to yellow, with an eventual melt (micrographs A-B). During the isotherm the reaction crystallises and continues to solidify removing any resulting liquid components through reaction and evaporation (micrographs C-D). Micrographs D-E show the rapid melt of the reaction mixture at 130 °C. The final micrograph F shows the boil away of the final components around 250 °C.

The reaction was scaled up to perform both DSC and NMR analysis on the final product.

The temperature of the reaction was ramped at 5 °C min⁻¹ to 100 °C and held isothermally for 30 minutes in the same manner as the isothermal HDM experiment. The product was allowed to cool and the solid product was removed from the crucible. The crude product was ground, washed and recrystallised from hot ethanol, to yield white crystalline needles.

Figure 3.30 shows the NMR spectrum of the final 2,3-diphenylquinoxaline product, the peaks appear in good agreement with the literature.⁵⁶ The spectrum shows no evidence of residual starting material (aryl-amine shifts between 3-5 ppm) and all peaks are assigned within the aromatic region.

δ_{H} (400 MHz; CDCl₃; Me₄Si) 7.287 (s, res. solvent), 7.379 (6H, m, Ph-*H*), 7.541 (4H, dd, Ph-*H*), 7.807 (2H, m, Ar-*H*), 8.211 (2H, m, Ar-*H*).

Figure 3.31 shows the melting of the purified 2,3-diphenylquinoxaline product as monitored using DSC analysis. A linear heating experiment was set up at a rate of 5 °C min⁻¹ between 30 and 300 °C. A melt is observed at $T_{\text{onset}} = 125.6$ °C, close to literature ranges of 123-124 °C.⁵⁷

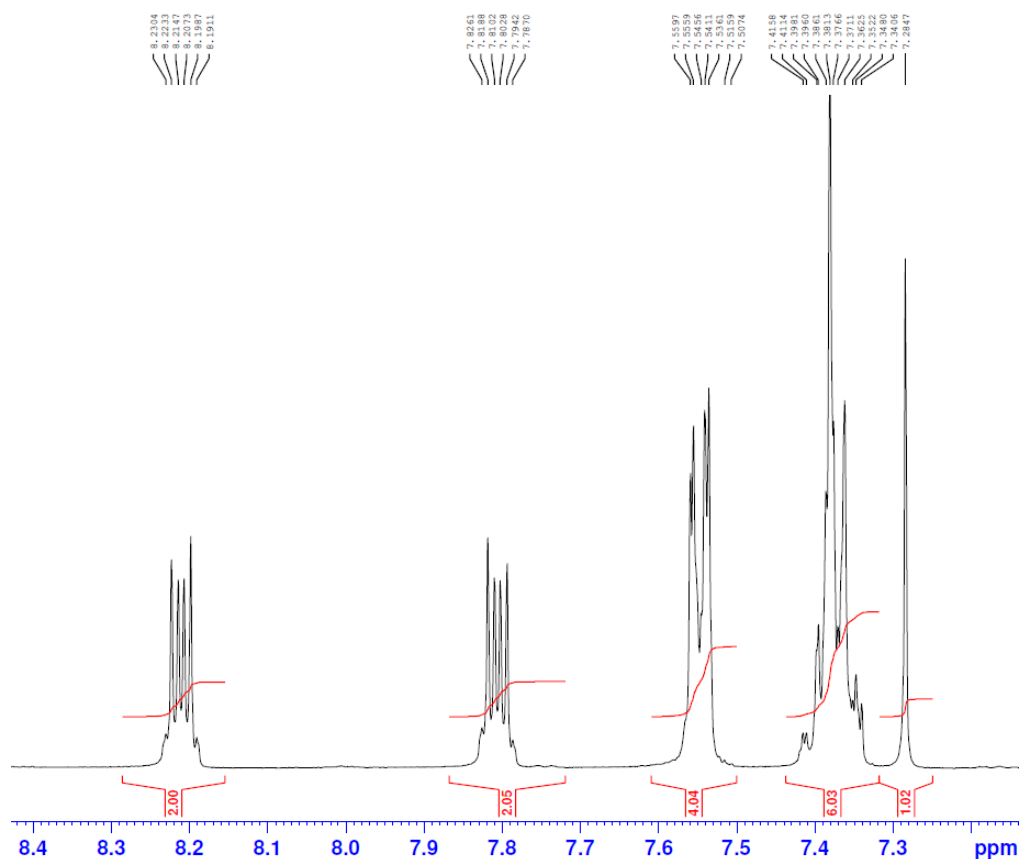


Figure 3.30 Selected region of the proton NMR spectrum of the synthesised diphenylquinoxaline product.

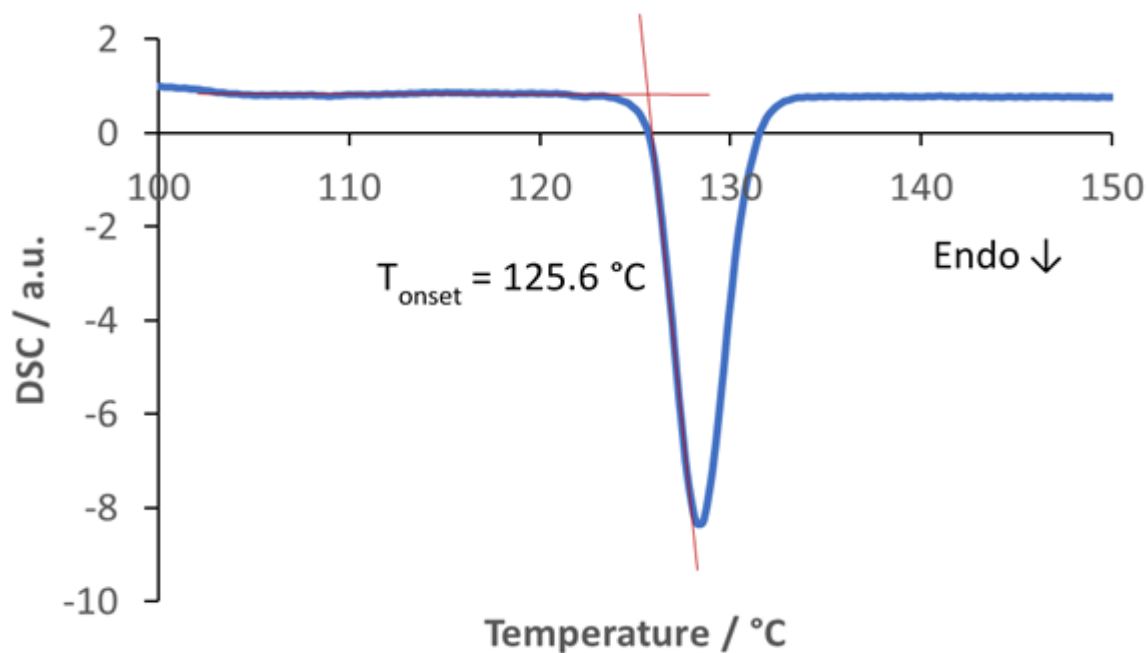
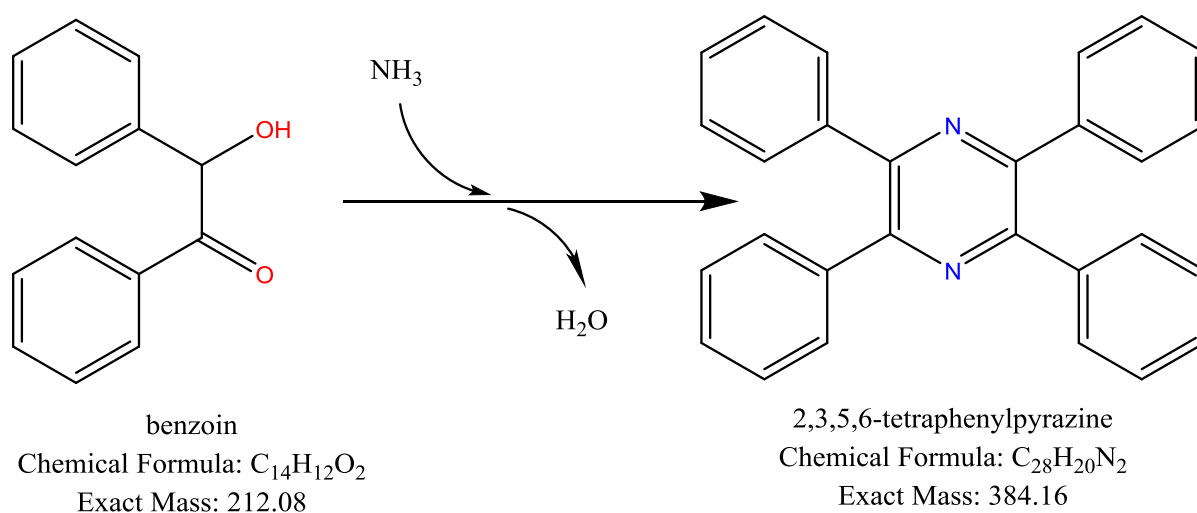


Figure 3.31 DSC analysis of the synthesised diphenylquinoxaline product.

3.7 Tetraphenylpyrazine Synthesis

As highlighted previously the study of solid state reactions typically proves troublesome for many techniques, for this reason it was decided to investigate HDM's capabilities with solid state reaction profiling with a focus on multicomponent reactions. The synthesis of tetraphenylpyrazine uses solid components (benzoin, ammonium acetate and anhydrous zinc chloride) and relies on the liberation of ammonia (from an ammonium salt) to initiate the reaction as shown below in Schematic 3.11.



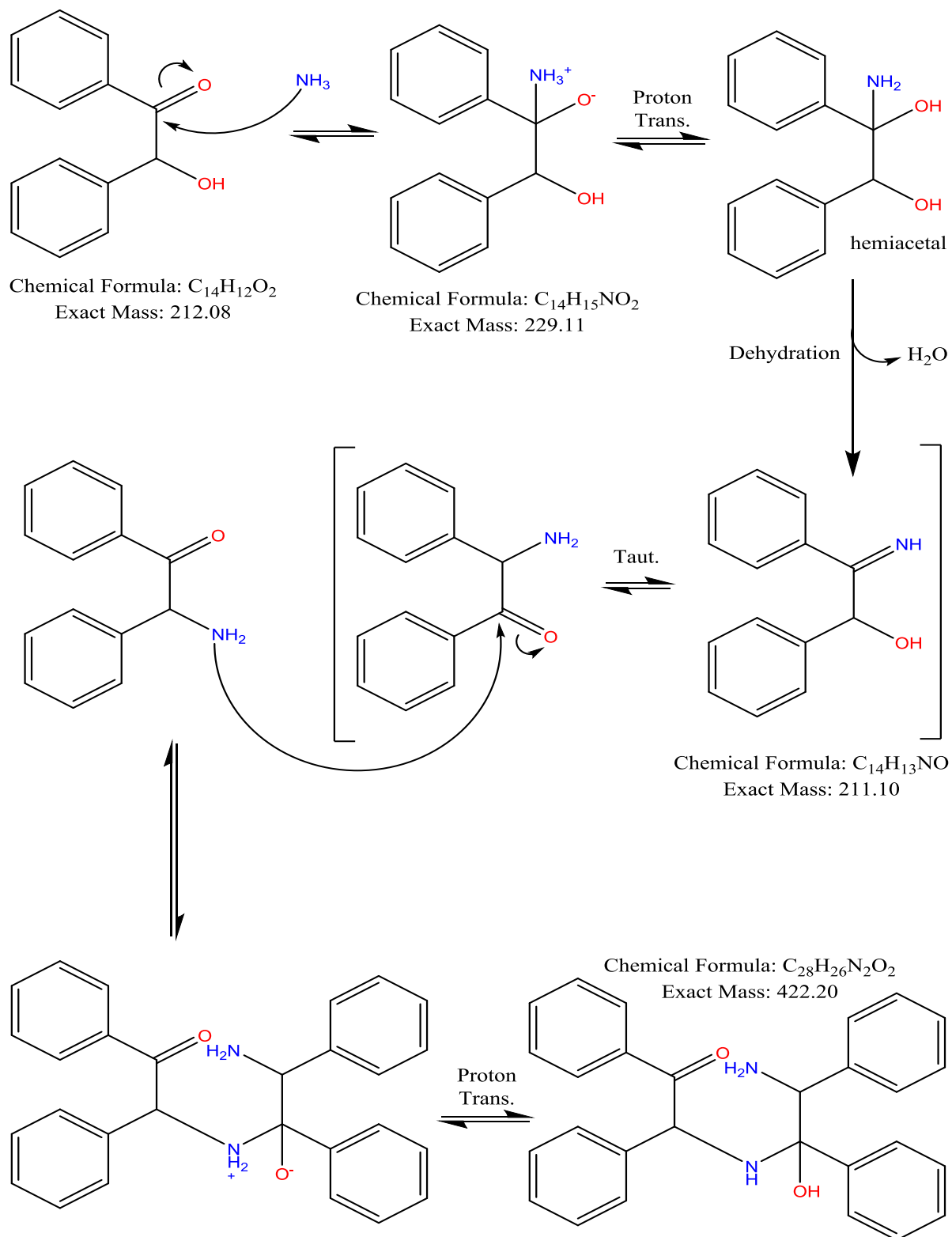
Schematic 3.11 Overall reaction between ammonia and benzoin forming the tetraphenylpyrazine product.

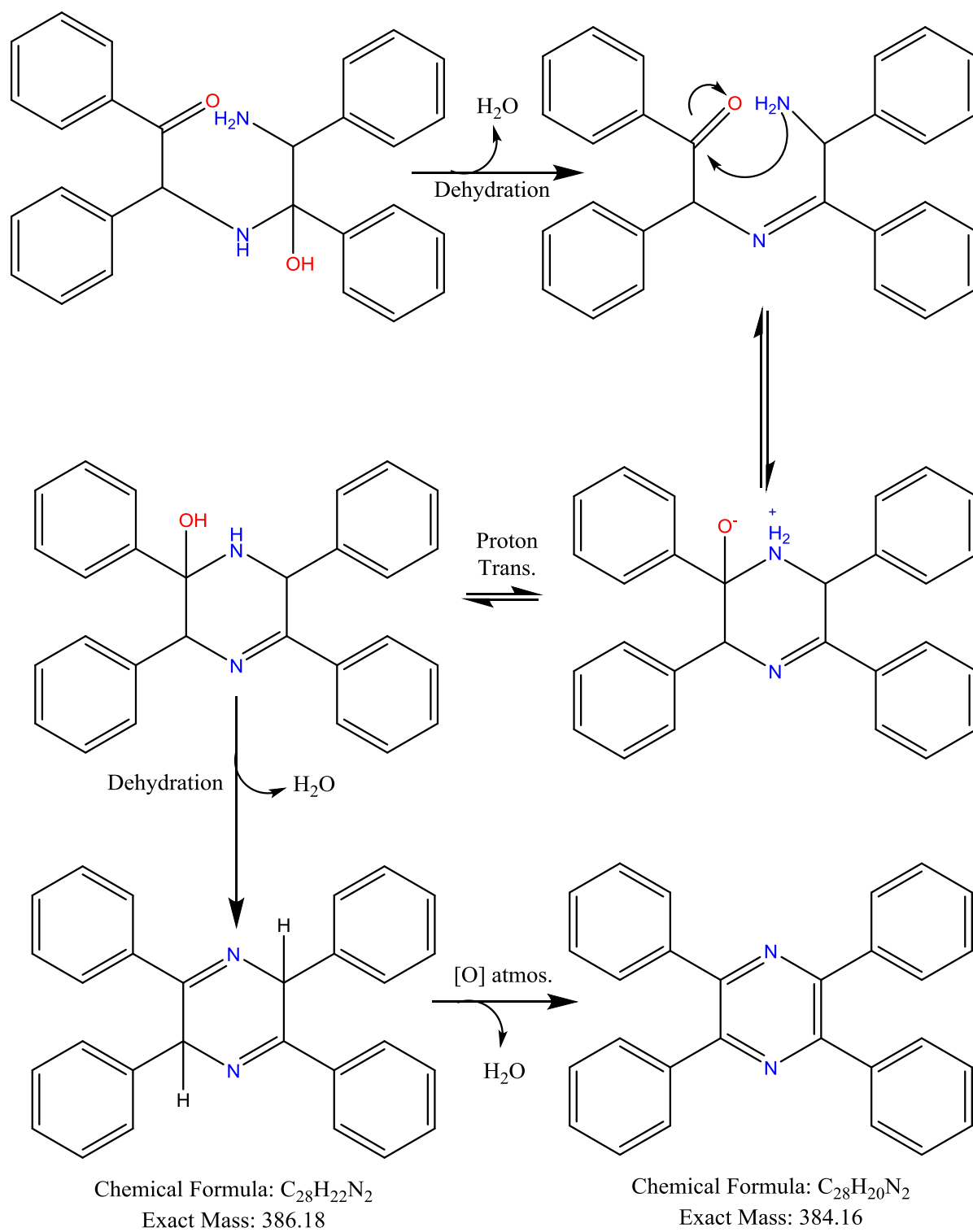
Benzoin is commonly used as an organic building block finding particular use within pharmaceutical formulations,⁵⁸ although many synthetic procedures usually oxidise it to benzil at some point during the reaction.⁵⁹

Pyrazines as a class of compounds find major importance in the food⁶⁰ and perfume industries.⁶¹ Recently studies into wines have shown how pyrazine compounds play a major role in the overall flavour and authenticity, and how instrumental techniques are being used to detect these compounds to prove adulteration of products.⁶²

In the following example benzoin undergoes nucleophilic attack from ammonia liberated through the thermal decomposition of ammonium acetate, yielding ammonia and acetic acid. A hemiacetal intermediate that is formed undergoes dehydration yielding a Schiff base as in the earlier examples. The tautomeric amino-ketone form may then react with another equivalent of itself undergoing cyclisation through a double dehydration. The final step relies on oxidation from the atmosphere to remove the remaining central hydrogens and forms the aromatic stabilised pyrazine ring. This has been demonstrated through a proposed mechanism in Schematic 3.12 based on existing pyrazine literature.⁶³ The nature of the multicomponent system leads to obvious side reactions, some of these side reactions will be evaluated alongside the main tetraphenylpyrazine reaction.

Benzoin (10.5 mg, 50 μmol , Aldrich), ammonium acetate (7.4 mg, 100 μmol , Aldrich) and zinc chloride anhydrous (0.6 mg, 5 μmol , Aldrich) were ground prior to the addition to the sample pan. A linear heating rate of 5 $^{\circ}\text{C min}^{-1}$ was applied to the sample between 30 and 350 $^{\circ}\text{C}$. The DART and MS were operated in positive mode.





Schematic 3.12 Proposed mechanism for the synthesis of tetraphenylpyrazine from benzoin and ammonia.⁶³

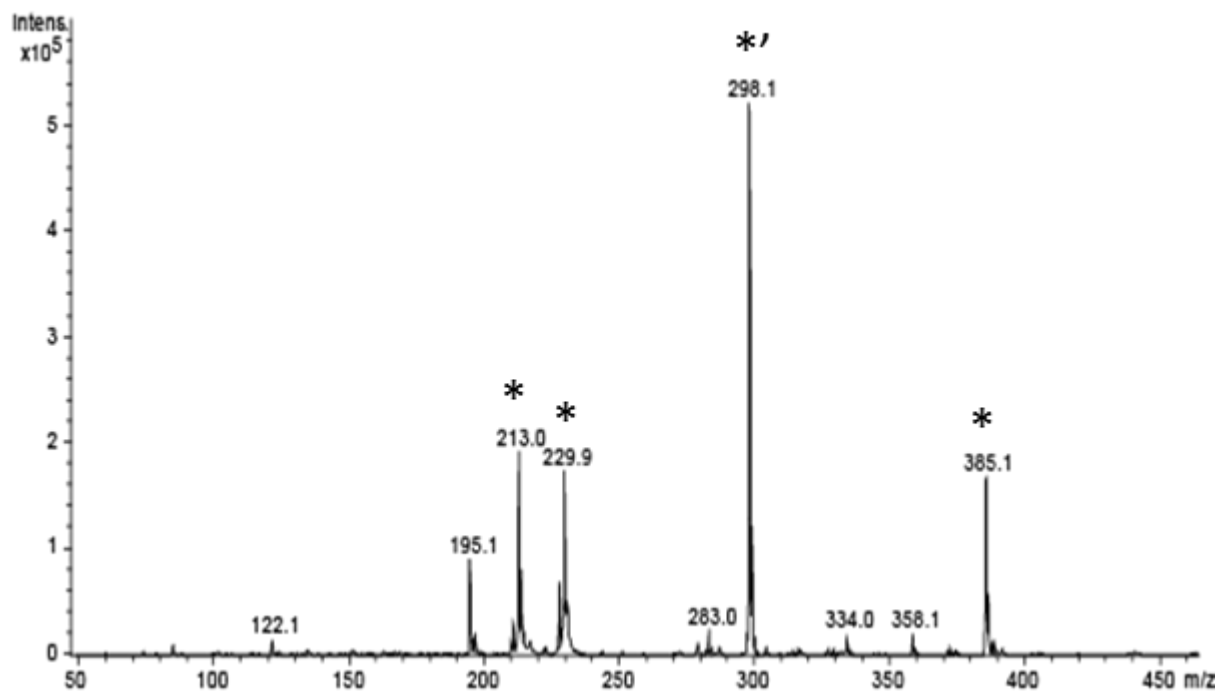


Figure 3.32 Average mass spectrum over the entire reaction duration for tetraphenylpyrazine synthesis. *) Assigned Reaction peaks and *) Side product.

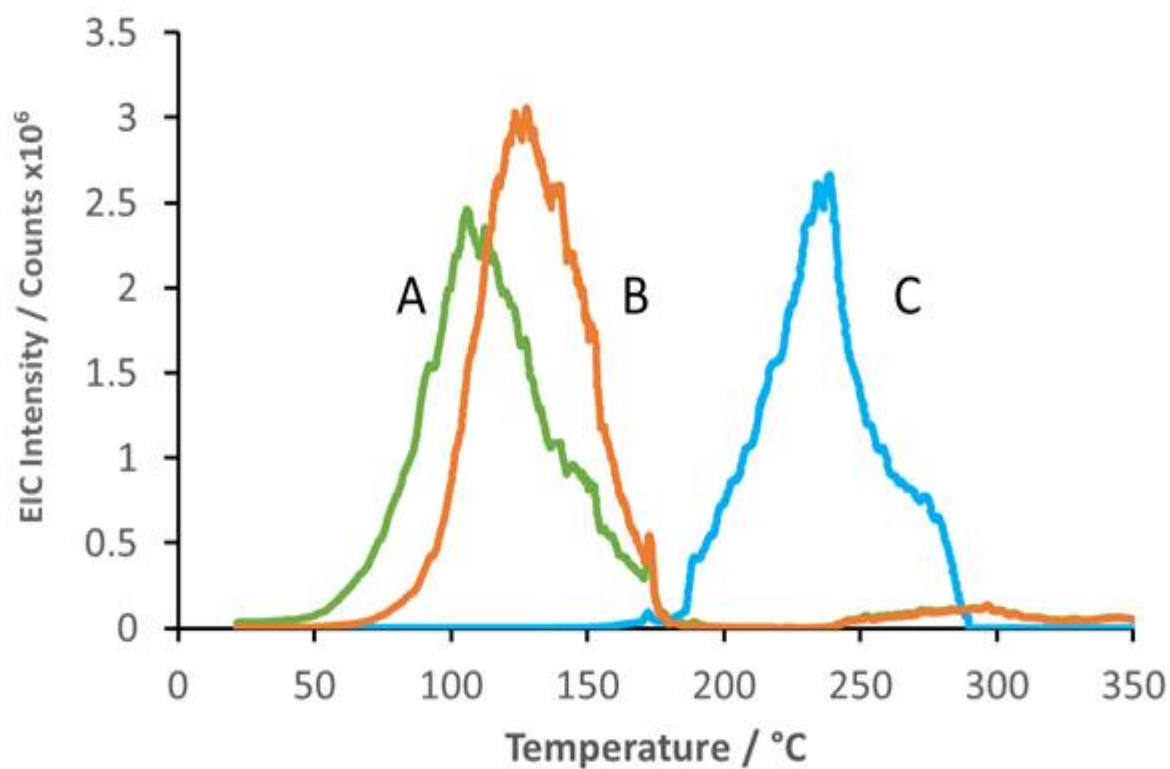
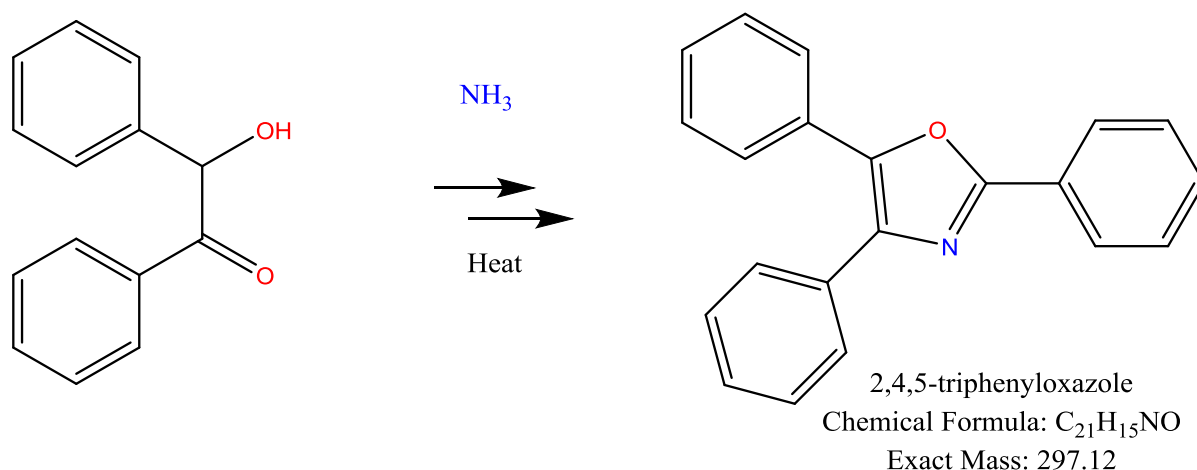


Figure 3.33 Reaction profiling of tetraphenylpyrazine synthesis plotted as a function of temperature. A) Benzoin 213 Da $[M+H]^+$, B) hemiacetal intermediate 230 Da $(M+H)^+$ and C) tetraphenylpyrazine 385 Da $[M+H]^+$.

Key ions are noted having direct relation to the tetraphenylpyrazine synthesis, along with several other ions most likely arising from side reactions. Although this exact reaction hasn't seen much development in nearly a century preliminary work was undertaken to elucidate possible structures of these products.⁶⁴ Figure 3.32 shows the average mass spectrum over the entire course of the reaction, the key signals being monitored are the protonated molecular ion of benzoin 213 Da $[M+H]^+$, the protonated molecular ion of the hemiacetal intermediate 230 Da $[M+H]^+$ and finally the protonated molecular ion of tetraphenylpyrazine 385 Da $[M+H]^+$.

Since the ammoniated molecular ion of benzoin forms a signal at 230 Da $[M+NH_4]^+$ a separate experiment was trialed to identify the proposed analyte. A dopant experiment was set up by adding an open bottle of concentrated ammonium hydroxide near the instrument, resulting in a rise in the concentration of ammoniated signal through increase in liberated gaseous ammonia. The protonated and ammoniated signals of benzoin could not be resolved by temperature ramping the stage, suggesting that since thermal separation of the two signals could be achieved in Figure 3.33 this is indeed related to the hemiacetal intermediate and not the ammoniated form of benzoin. Dopants are discussed in more detail in Section 5.3.5.

The peak that dominated the mass spectrum is a signal at 298 Da, this has been attributed to the product of a side reaction shown in Schematic 3.13. Early work performed by Leslie *et al.* noted the formation of quantitative yields of 2,4,5-triphenyloxazole along with tetraphenylpyrazine.⁶⁵ Should the reaction be performed using benzil as opposed to benzoin a chemically luminescent material lophine (2,4,5-triphenylimidazole) is formed instead forming a central imidazole ring.



Schematic 3.13 Side product formation during tetraphenylpyrazine reaction, proposed origin of the 298 Da signal.

Figure 3.33 profiles the reaction from benzoin to tetraphenylpyrazine via the hemiacetal intermediate. Since the reaction is initiated by the decomposition of the ammonium salt it is reasonable to assume this initiation won't be until higher decomposition temperatures. The first stages of heating see the release of benzoin (A) up to around 100 °C, the signal maximum of benzoin relates closely to the highest rate of evolution of the intermediate at $2.26 \text{ counts} \times 10^6 \text{ } ^\circ\text{C}^{-1}$ around 105 °C. The maximum intensity of the protonated hemiacetal intermediate (B) is noted around 130 °C. Both benzoin and the hemiacetal decline until an abrupt end at 180 °C. Unlike other reactions discussed previously the product signal does not begin to evolve until the apparent end of the intermediate signal, as opposed to during the decline of the intermediate. This proves quite difficult to explain through the EICs alone but a much simpler explanation is found when looking at the micrographs in Figure 3.34.

The tetraphenylpyrazine profile (C in Figure 3.33) shows a sharp rise in signal intensity at around 185 °C, with continuing release until a peak maximum around 240 °C. The decline of the product signal arises from a combination of sample exhaustion and decomposition at elevated temperatures.

The optical data obtained by HDM excel within this example showing how physical sample information can be collected during the reaction processes. Figure 3.34 shows an array of micrographs from key points during the reaction. Micrograph A shows the starting point of the reaction, a partially ground mixture of white compounds, transitioning to B the onset of colour formation is shown with hints of red during the formation of the intermediate hemiacetal. As the temperature reaches 130 °C (see micrograph C) the whole reaction pan becomes red in colour at the same temperature the maximum of the intermediate is shown. Micrographs C-E show the red product begin to melt, the melt correlates well with the 'take off' of the tetraphenylpyrazine profile. Although a melt is shown it is significantly lower than the literature melting point for tetraphenylpyrazine, so the reduction in melting has been tentatively attributed to a mixture of impurities, similar to what is noted in the analysis of mixtures melting. The final micrograph (F) shows the dark black tar that has formed during oxidation of the reaction after the pyrazine signal has been reduced into background levels.

The ΔRGB profile (see Figure 3.35) documents the processes occurring during the reaction. The profile remains stable until around 70 °C at the same temperature that the intermediate signal is noted in Figure 3.39. The colour increase (white to red) follows closely with the intermediate signal between 80 and 130 °C, the sharp step in the colour trace is not an artefact of the system but is actually related to the reaction appearing more reflective at this temperature before returning to a base line around 500 a.u. at 150 °C.

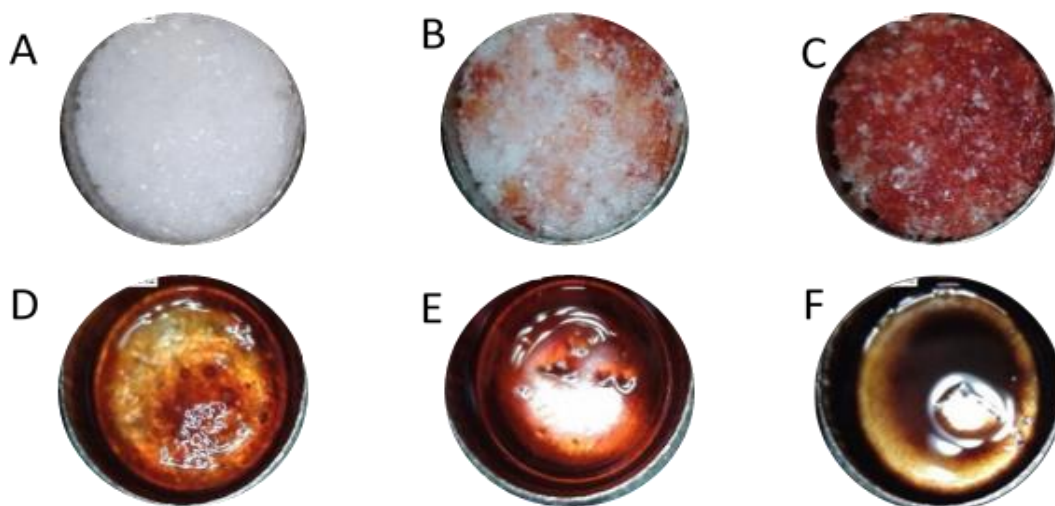


Figure 3.34 Micrographs of the tetraphenylpyrazine synthesis. A) 30 °C, B) 100 °C, C) 130 °C, D) 180 °C, E) 190 °C, F) 250 °C.

A process relating to the melt is shown between 150-200 °C. A decline in colour value is noted between 500 and 350 a.u., under the gradual decline a subtle melt can be shown between 180-190 °C. The remaining colour profile monitors the decomposition process primarily within the 200-240 °C region as decomposition products remain in solution resulting in the stable baseline. The final step at 280 °C is related to a loss in liquid volume as the products begin to boil away at the elevated temperatures, with the remaining noise coming from breakdown of semi-solid decomposition char beyond see (micrograph F).

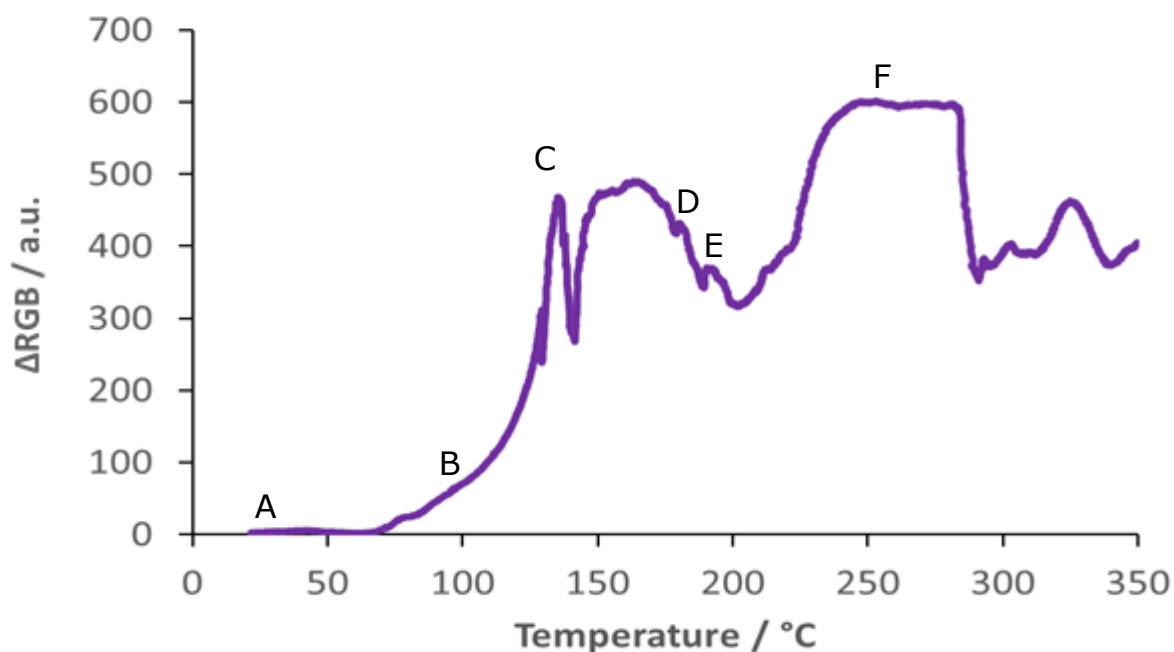


Figure 3.35 Colour profile for the tetraphenylpyrazine synthesis. Labels correlate to micrographs in Figure 3.34

To authenticate the reaction process and isolate the tetraphenylpyrazine product for further analysis (DSC and NMR) the reaction was scaled up as in previous examples.

A scaled up equimolar reaction was added to a temperature controlled furnace. This time air was pumped through the furnace to ensure complete conversion to the reduced product, as typically the furnace is under a stagnant air atmosphere. The temperature was ramped at a rate of 5 °C min⁻¹ between 30 and 200 °C.

The solid red mass was removed and washed through with iced deionised water to remove the water soluble zinc chloride and any other water soluble side products. The crude product was then purified through column chromatography (silica, 5% methanol: dichloromethane). The crude product was then triple recrystallised from hot glacial acetic acid to yield fine white needles.

Interestingly the product was pure white, so the red colour of the reaction must arise from one of the reaction intermediates, thus the colour is not related to product formation within this example. The colour has been tentatively attributed to a potential bathochromic shift caused by reaction intermediates possibly complexing with the zinc.⁶⁶

Figure 3.36 shows the melting of the purified 2,3,4,5-tetraphenylpyrazine product using DSC. A linear heating experiment was set up at a rate of 5 °C min⁻¹ between 30 and 200 °C using ca. 5 mg of sample. As can be seen a sharp melt is observed at $T_{\text{onset}} = 246.9$ °C. The synthesised product shows good purity with the agreement to existing literature melting of 246 °C.⁶⁷

However, although the DSC indicates purity (through lack of other thermal events and a sharp melting peak) the proton NMR suggests evidence of impurities (remaining from recrystallisation solvent) indicated by extra signals in the spectrum and was not included.

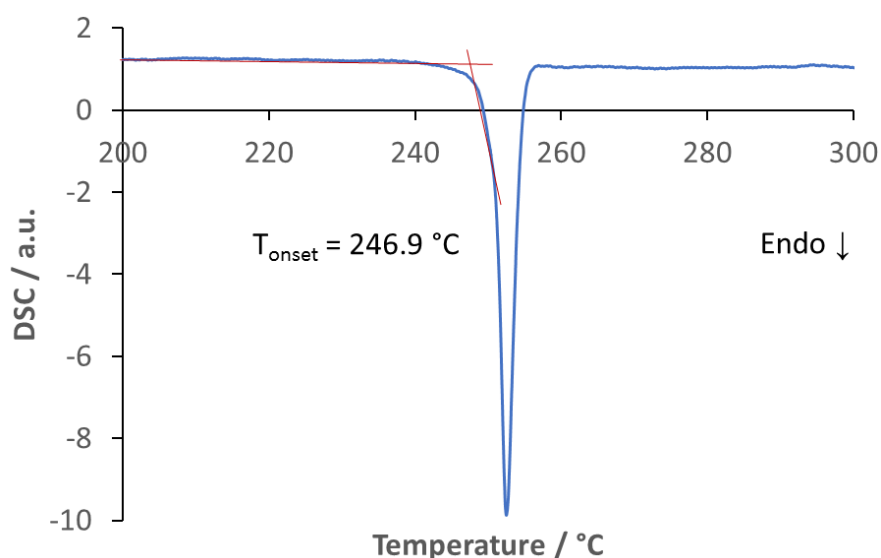
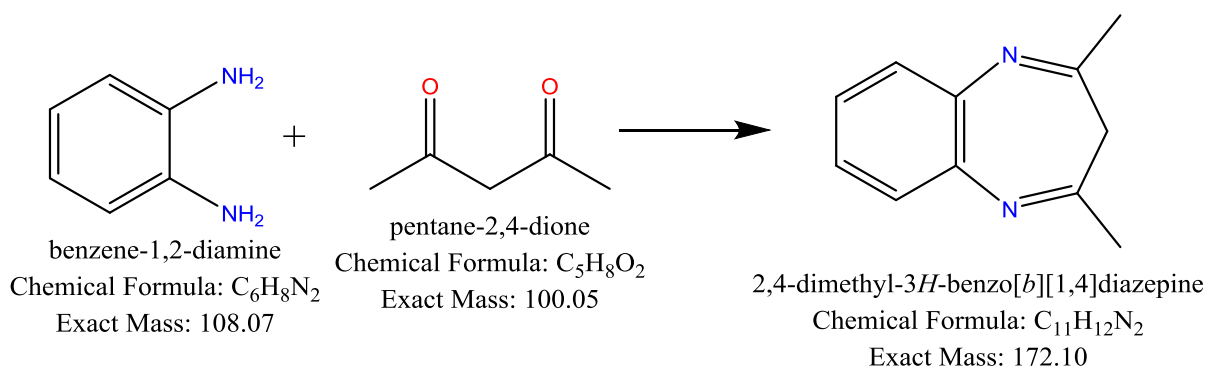


Figure 3.36 DSC analysis of the synthesised tetraphenylpyrazine product.

3.8 Benzodiazepine Synthesis

A reaction between *o*-diaminobenzene and pentane-2,4-dione was trialed to see if the HDM synthesis of 2,4-dimethylbenzodiazepine outlined in Schematic 3.14 could be achieved. Typical literature synthesis of benzodiazepines relies on the coupling reaction between substituted 1,2-diamines and 1,3-dicarbonyls, usually under the influence of acid,⁶⁸ base⁶⁹ or a catalyst.⁷⁰ In the nature of HDM the reaction was trialed without any further additives and was evaluated as a thermally driven reaction.



Schematic 3.14 Overview reaction for benzodiazepine synthesis between diamines and dicarbonyls.

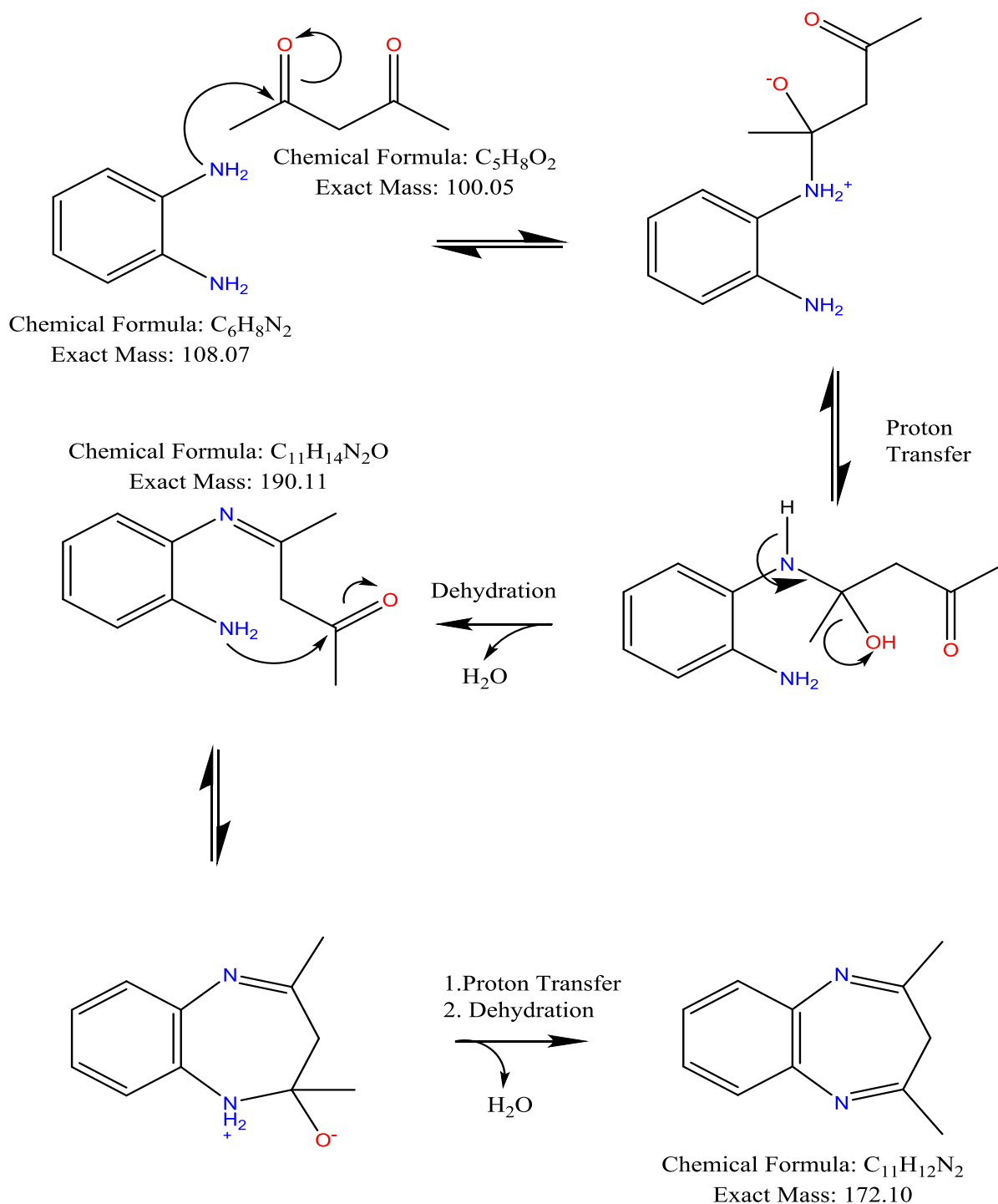
The class of compounds known as benzodiazepines is of critical importance pharmaceutically with selected compounds having medicinal properties to aid with anxiety,⁷¹ insomnia⁷² and depression.⁷³ Immense research is currently being undertaken to synthesise these compounds due to the limited supply of these drug compounds that are found without major side effects.

The following reaction is heterogeneous between solid *o*-diaminobenzene and the liquid state pentanedione and is mechanistically following the same theme as many of the previous reactions forming Schiff base complexes through dehydration. Schematic 3.15 shows an overview of the mechanism of reaction. The amine attacks one of the carbonyls of the pentanedione, followed by proton transfer and resulting in dehydration, forming the mono-substituted intermediate. The intermediate can undergo further self-condensation between the remaining carbonyl and amine, forming the final benzodiazepine product.

The following reaction conditions were setup:

To a reaction pan (6mm, Inconel) was added o-diaminobenzene (10.8 mg, 100 μmol) and pentane-2,4-dione (excess). A linear heating rate of 5 °C min⁻¹ was applied to the hot-stage between 30 and 350 °C. The DART source and mass spectrometer were operated in positive mode only with all resultant mass spectral profiles being acquired.

Figure 3.37 shows the average mass spectrum of the entire reaction, with the insert showing the reactant peaks mainly observed during the low temperature range, product formation is noted almost instantly. The key signals are marked but consist of the protonated molecular ions of *o*-diaminobenzene 109 Da [M+H]⁺, pentane-2,4-dione 101 Da [M+H]⁺, mono-substituted intermediate 191 Da [M+H]⁺ and the dimethyl benzodiazepine product 173 Da [M+H]⁺.



*Schematic 3.15 Mechanism for the synthesis of dimethyl benzodiazepine from *o*-diaminobenzene and pentanedione.*

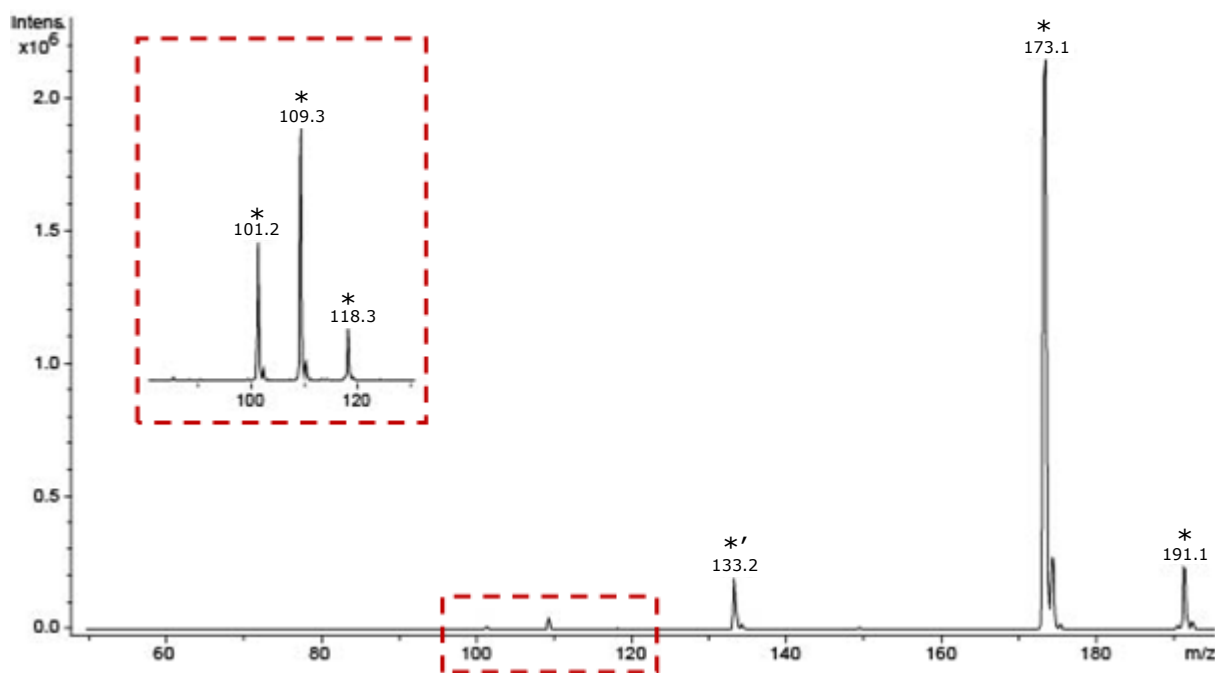


Figure 3.37 Average mass spectrum over the entire benzodiazepine reaction, insert shows reactant signals that are noted in the initial stages of analysis. *) Reaction signals, *) Side product signal.

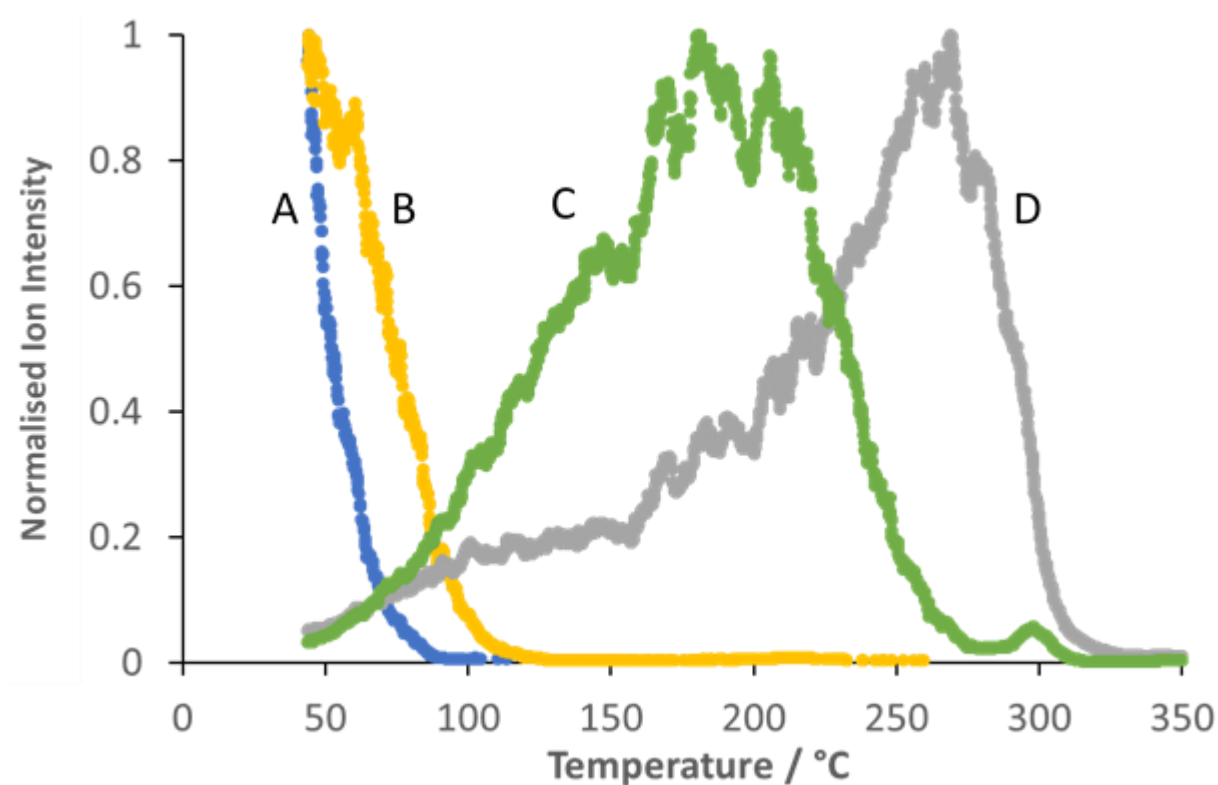


Figure 3.38 Reaction profiling of the benzodiazepine synthesis. A) 101 Da [pentane-2,4-dione + H]⁺, B) 109 Da [o-diaminobenzene + H]⁺, C) 191 Da [mono-sub intermediate + H]⁺ and D) 173 Da [benzodiazepine + H]⁺.

The reaction between *o*-diaminobenzene (B) and pentanedione (A) appears to proceed both quickly and cleanly, this is similar to literature findings obtaining both high yields and relatively short reaction times.⁷⁴

Figure 3.38 monitors the reaction process as a series of EICs with relation to reaction temperature. From the onset of heating there is a clear decline for both reactant profiles A and B (pentanedione and diaminobenzene respectively) until around 100 °C. Pentanedione itself is extremely volatile so the sharp loss is expected to be some reaction consumption, but largely evaporation. Both the reaction intermediate and product are observed from the start of the experiment.

The reactive intermediate (C) begins to increase in signal intensity at much lower temperatures than the final product (D) until 157 °C. The reaction intermediate reaches a maximum signal intensity between 165-220 °C forming a steady signal during a linear rate of signal evolution for the product, possibly reaching a steady state within this region of intermediate formation and intermediate evaporation and consumption. Continued heating shows decline of the intermediate (C) upwards of 220 °C; the rate of product evolution reaches its highest rate around 250 °C, until the product finishes being released at 270 °C. The product profile then sharply falls away between 270-300 °C, as the reaction remnants boil away and thermal decomposition starts.

The micrographs in Figure 3.39 and the total colour (Σ RGB) profile in Figure 3.40 appear to correlate well with the reaction profile in Figure 3.38. The underlying crystal formations of *o*-diaminobenzene can be seen within the pentanedione in micrograph A, the decline can be shown between micrographs A-C up to 150 °C as shown by the EIC profiles in Figure 3.46. The colour profile remains almost constant until the release of the diazepine product around 150 °C, comparing micrographs C-D the colour actually darkens from yellow to orange possibly with the onset of decomposition. Further heating shows the decomposition (see micrographs D-F) and the colour step between 200 and 300 °C. The final boil off of the remaining materials can be shown between 300-350 °C within the curves of both the product profile and the colour profile, micrographs F-G show the liquid reduced down to an oil/char.

A signal was shown at 133 Da which did not relate to any of the proposed intermediates, fragments or adducts. A secondary product 2-methylbenzimidazole has been assigned to this signal as its protonated molecular ion. Schematic 3.16 provides a brief proposal of the origin of this signal, arising from the second amine attacking the hydroxyl-carbon and not the carbonyl carbon before imine formation. HDM may allow for identification of these side reactions aiding with explanations to reduced reaction yields.

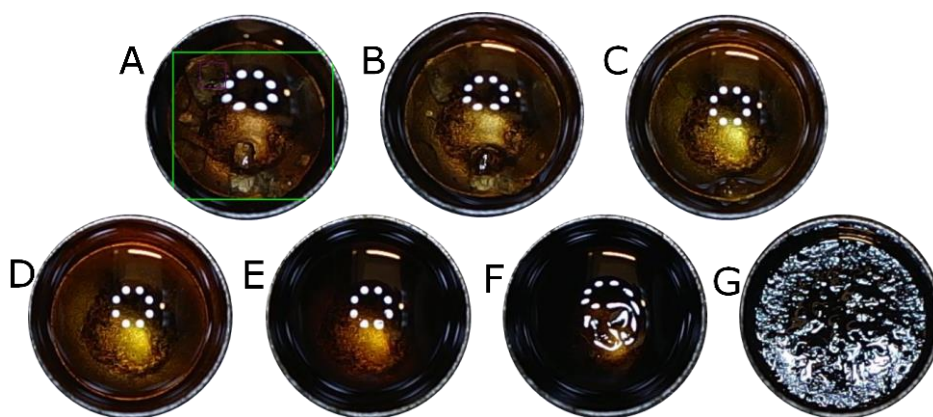


Figure 3.39 Micrographs of the benzodiazepine synthesis. A) 30 °C, B) 100 °C, C) 150 °C, D) 200 °C, E) 250 °C, F) 300 °C, G) 350 °C. Green square pixel monitoring region, white spots are lighting reflection from the USB microscopes inbuilt lighting.

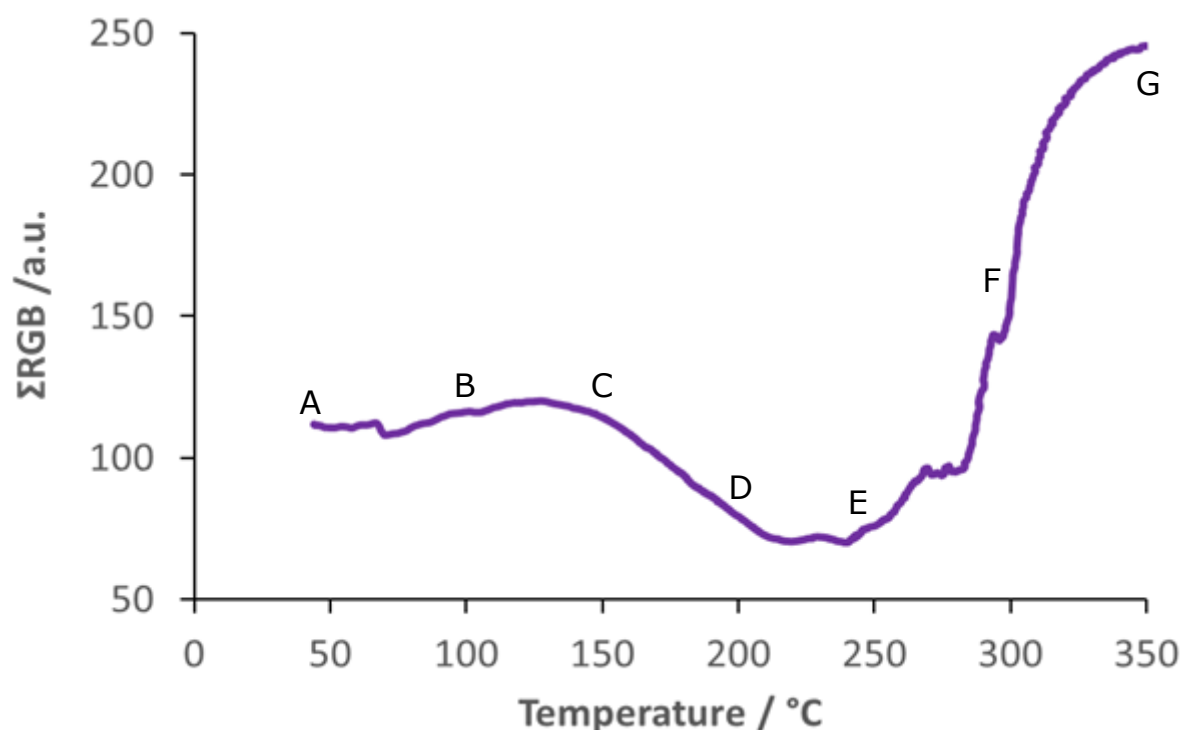
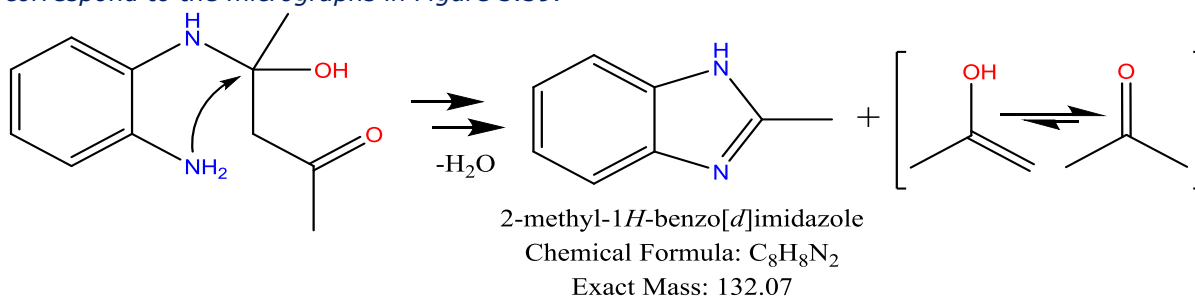


Figure 3.40 Colour profiling of the benzodiazepine synthesis as monitored using HDM. Labels correspond to the micrographs in Figure 3.39.

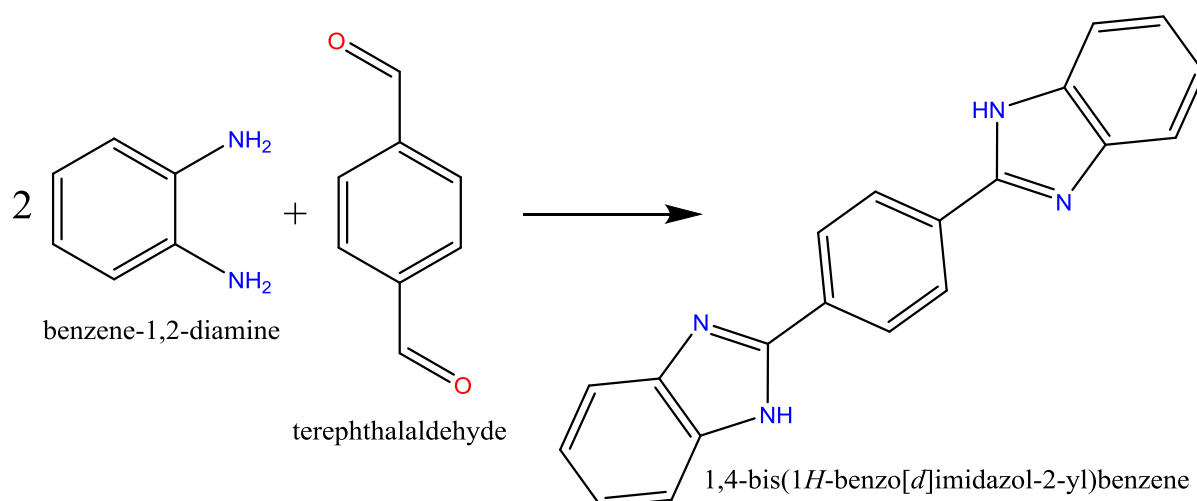


Schematic 3.16 Proposed side reaction giving rise to the unidentified signal at 133 Da.

The reaction wasn't scaled up within the time frame of the investigation so no complimentary NMR or DSC data was obtained.

3.9 Phenylbisbenzimidazole Synthesis

After the successful reaction between *o*-diaminobenzene and benzaldehyde (Section 3.5) a reaction based on this but in the solid state was trialled. Since benzaldehyde is a liquid at room temperature a solid aldehyde was required to evaluate this reaction. The compound terephthalaldehyde was investigated for this reaction as it is very similar in structure to benzaldehyde and only differs by having two aldehyde groups in the para position. Terephthalaldehyde offered a solid material at room temperature⁷⁶ and added another level of reaction complexity by forming two terminal benzimidazole groups as opposed to the one afforded by benzaldehyde itself. The overall reaction is shown in Schematic 3.17 forming the product commonly known as phenylbisbenzimidazole (1,4-bis(benzimidazolyl)benzene).



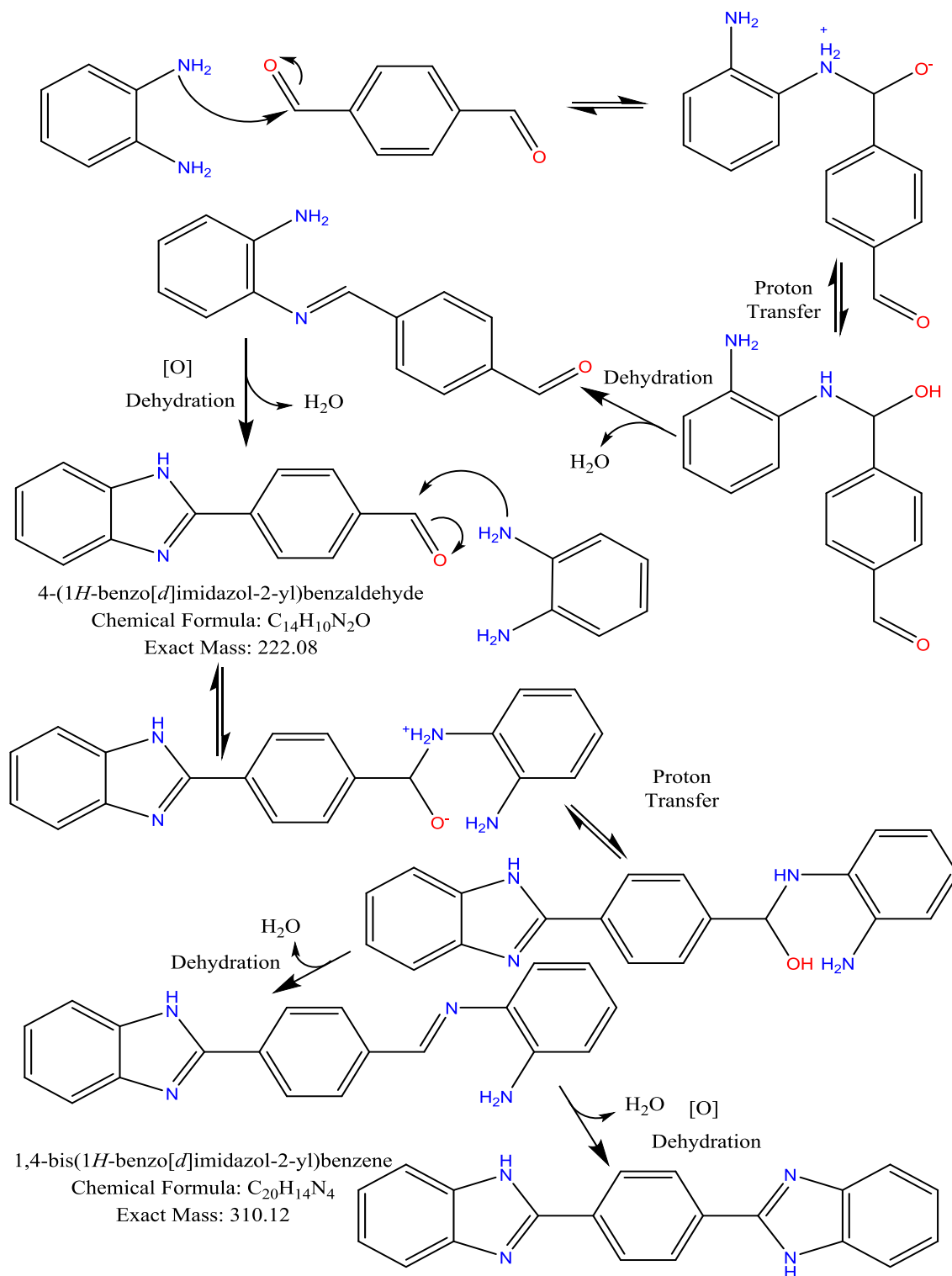
Schematic 3.17 reaction overview for the synthesis of phenylbisbenzimidazole.

A review of the literature did not reveal too much about the applications of phenylbisbenzimidazole other than its inclusion as a reaction analogue within the phenylbenzimidazole papers.⁷⁷ Literature mainly shows the compound has been studied crystallographically with investigations into its various forms.⁷⁸

The proposed reaction mechanism is outlined in Schematic 3.18 and was based on the mechanism from the phenylbenzimidazole example (Schematic 3.8). The reaction route is expected to favour the less sterically hindered phenylbisbenzimidazole as opposed to the more complex structures that may form further reactions at the secondary amine similar to reaction pathway 2 in Schematic 3.8. The mechanism in summary has several key steps, nucleophilic attack between an amine and one side of the aldehyde, followed by imine formation via dehydration. The intramolecular oxidation reaction occurs forming a mono-substituted intermediate. The process is repeated at the remaining terminal aldehyde, resulting in the formation of the final product.

The experiment was set up as follows:

1,2-diaminobenzene (21.6 mg, 200 μmol , Aldrich) and *terephthalaldehyde* (13.4 mg, 100 μmol , Aldrich) were layered side by side in the reaction pan. A linear heating rate of 5 $^{\circ}\text{C min}^{-1}$ was applied to the sample between 30 and 350 $^{\circ}\text{C}$. All resulting mass spectra were collected in positive ion mode.



Schematic 3.18 Proposed mechanism for the synthesis of phenylbisbenzimidazole.

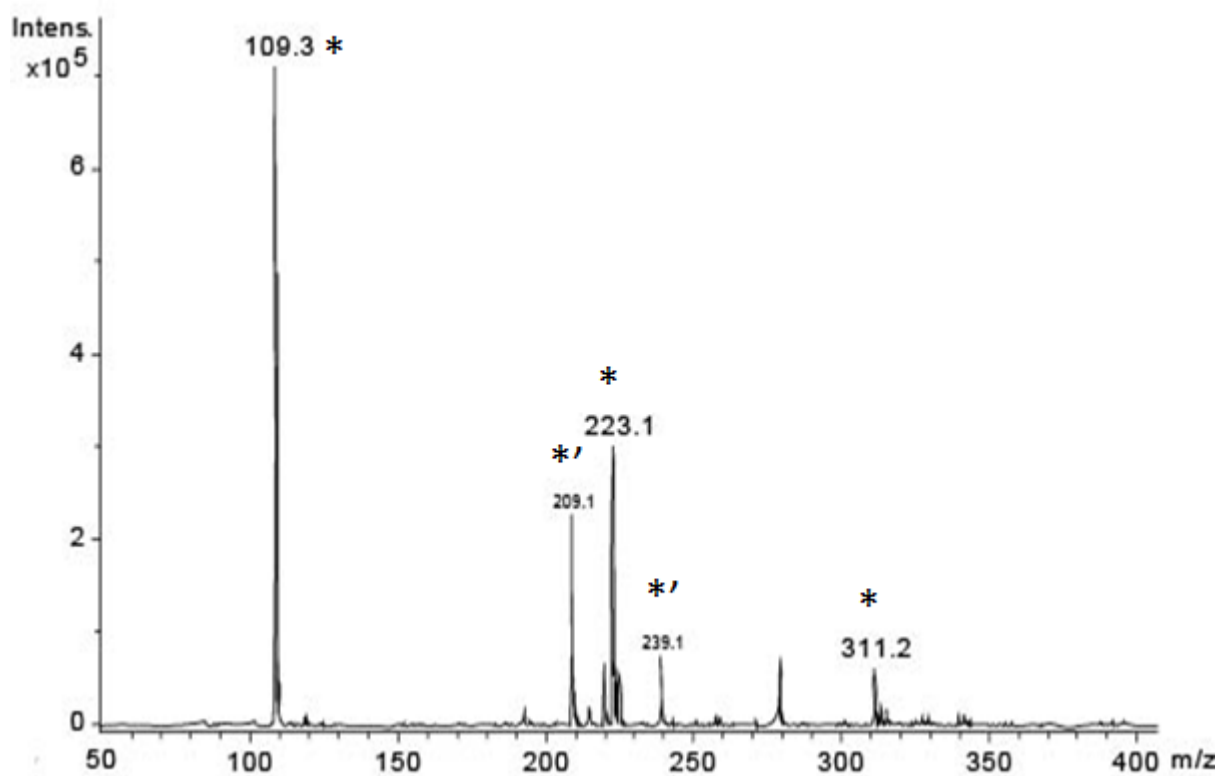


Figure 3.41 Average mass spectrum of the phenylbisbenzimidazole synthesis. *) Key reaction signals, *) Unassigned signals. Reaction carry over was not labeled for clarity.

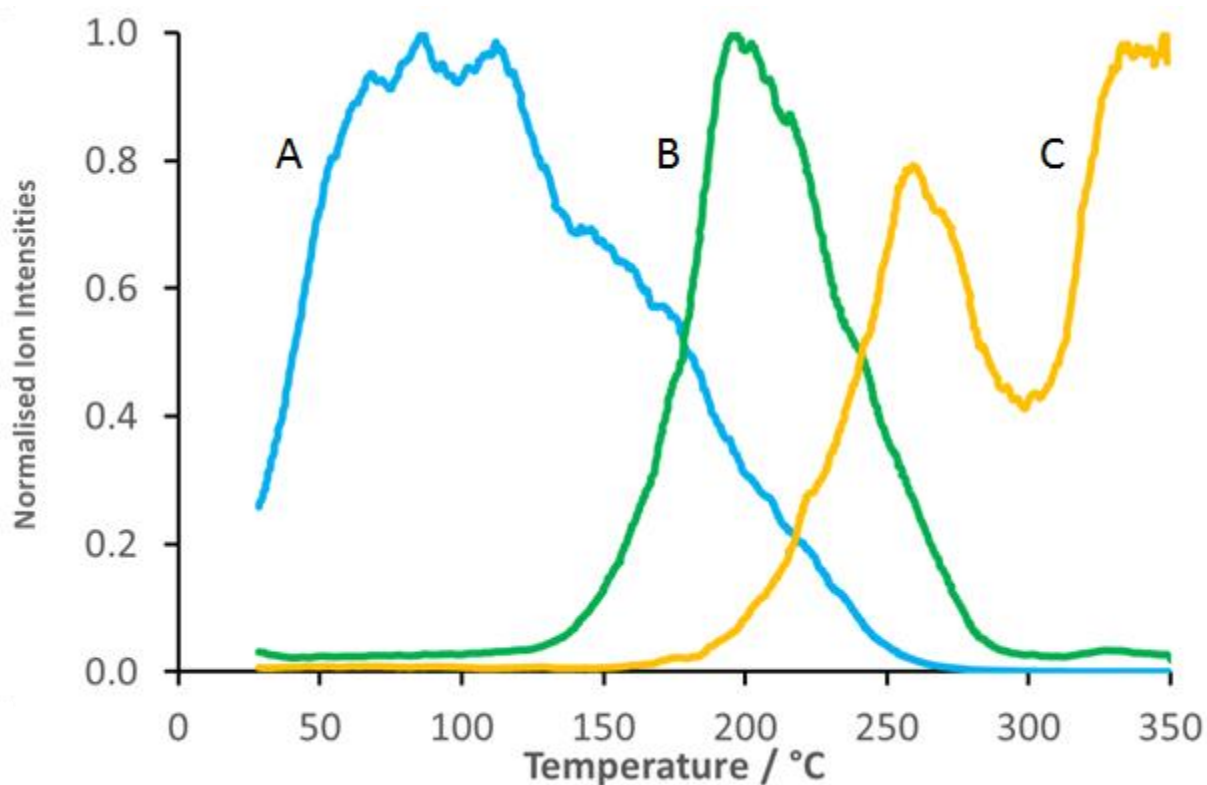
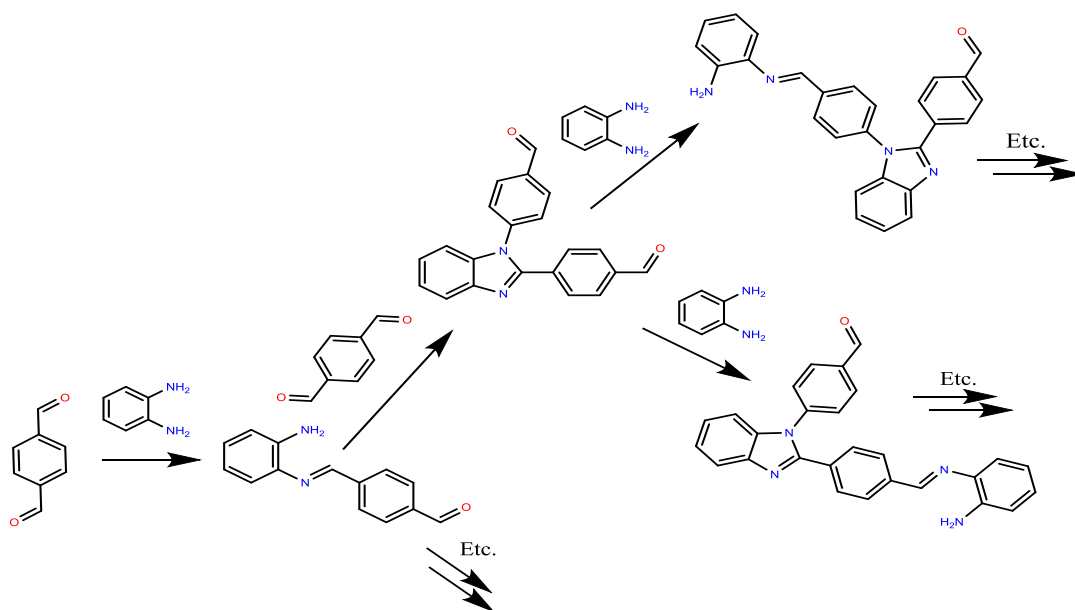


Figure 3.42 EICs for the synthesis of phenylbisbenzimidazole monitored as a function of temperature. A) *o*-diaminobenzene 109 Da $[M+H]^+$, B) Monosubstituted intermediate 223 Da $[M+H]^+$ and C) bisbenzimidazole product 311 Da $[M+H]^+$.

Figure 3.41 shows the average mass spectrum over the full duration of the reaction, the major reaction signals are marked. The three signals of interest are of the protonated molecular ions for *o*-diaminobenzene 109 Da $[M+H]^+$, the monosubstituted intermediate 223 Da $[M+H]^+$ and the phenylbisbenzimidazole product 311 Da $[M+H]^+$, the EICs of these signals are displayed in Figure 3.52.

Figure 3.42 shows the normalised signals plotted as a function of temperature. The *o*-diaminobenzene (A) is observed from the onset of heating reaching a signal maximum soon after the start of the experiment levelling in intensity between 70 and 115 °C. No substantial quantities of intermediate or product are shown until the *o*-diaminobenzene profile begins to decline. A linear evolution of intermediate profile (B) is observed from 135 °C until the maximum around 200 °C, during the release of the intermediate the reactant profile is almost completely lost and the product (C) is shown. Product (C) evolution increases between 150 and 250 °C and goes through a trough (between 250 and 300 °C) before reaching the highest level of signal above 340 °C. The sudden decline in the profile has been attributed to the surface of the reaction forming a 'crust' as the surface appears to solidify and all MS ions show intensity losses within this region. Further heating appears to melt the surface thus showing a return in the product (C). Within the trough it is worth noting that a few unassigned higher molecular weight species were observed, it is expected that some polymeric system had formed that caused the brief surface effect.



*Schematic 3.19 Possible polymeric chain reaction between terephthalaldehyde and *o*-diaminobenzene.*

In the previous reaction example 3.5 for the synthesis of phenylbenzimidazole two possible reaction pathways were noted. It is reasonable to assume that the secondary reaction route could follow in the same way as in Schematic 3.4 although the products that would

be formed would continue to have terminal aldehydes leading to possible polymeric reactions as illustrated in Schematic 3.19. The higher molecular weight species noted within the 250-300 °C region could have been related to these undesired reactions although no signals were formally assigned.

It is worth noting that the reason the two components were layered and not physically ground/mixed is due to the apparent highly reactive nature of the process. Initially upon trialling these experiments the powders were weighed and ground, from the start of grinding the colour evidently changes from white to yellow to a vibrant orange. A quick analysis using DART in the standard mode (300 °C, introduced on a melting point tube) revealed that the product had indeed been formed through mechanical synthesis - as has been noted in similar reactions by other authors.⁷⁹ Although this discovery was interesting it was not the focus of this study as the evaluation is focused on the thermally driven reaction. The two compounds were then layered to ensure minimal mechanical reactions would proceed before the analysis could begin.

The micrographs in Figure 3.43 show the vibrant colour changes across the entire reaction. The two light powders have been layered in micrograph A. The colour dramatically changes to deeper yellows and oranges as the heating has commenced at 100 °C (see micrograph B). Micrograph C shows a melt at the maximum formation of the intermediate around 200 °C, this is much higher than either of the reactants' melting points so is a good indication that the reaction is proceeding and forming higher melting products. The colour is lost between micrographs C and D as the onset of decomposition is likely to have started. Micrograph D shows the 'crusting' type effect on the surface, the matte colouration is lost with further heating at 300 °C (micrograph E), correlating well with the return of the product (C) in Figure 3.42. The final micrograph (F) shows the reaction at 350 °C with the remaining oil (assumed to be polymeric) with a dark colour due to thermal decomposition products.

Figure 3.44 shows the Δ RGB profile of the reaction. The signal changes rising in intensity to 105 °C as the yellow-orange colour is formed. A small peak is shown after 105 °C up to 130 °C as the reactants begin to melt together revealing some of the metallic pan. The colour remains quite constant from 130 - 300 °C, a slight drift is shown for the melting at 205 °C and the surface 'crusting' at *ca.* 265 °C. The next major event is the step change at 300 °C when the surface melts and becomes more reflective. 300-350 °C monitors the thermal decomposition as the reaction goes from brown to black.

Although an upscaled synthesis was achieved, during the purification step using column chromatography the product appeared to decompose between elution and recrystallisation indicated by more than one product using TLC. Since this was not the main focus of the study the upscaled synthesis was abandoned for other pursuits.

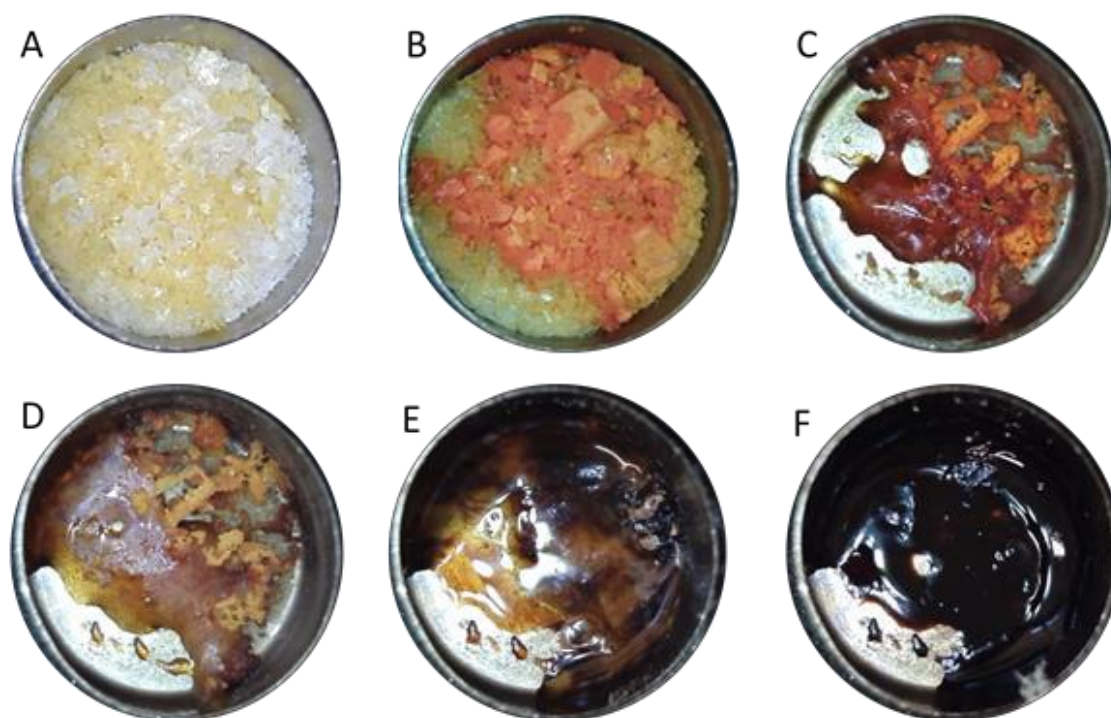


Figure 3.43 Micrographs of phenyl-1,4-bisbenzimidazole synthesis. Key; A) 30 °C, B) 100 °C, C) 200 °C, D) 250 °C, E) 300 °C, F) 350 °C.

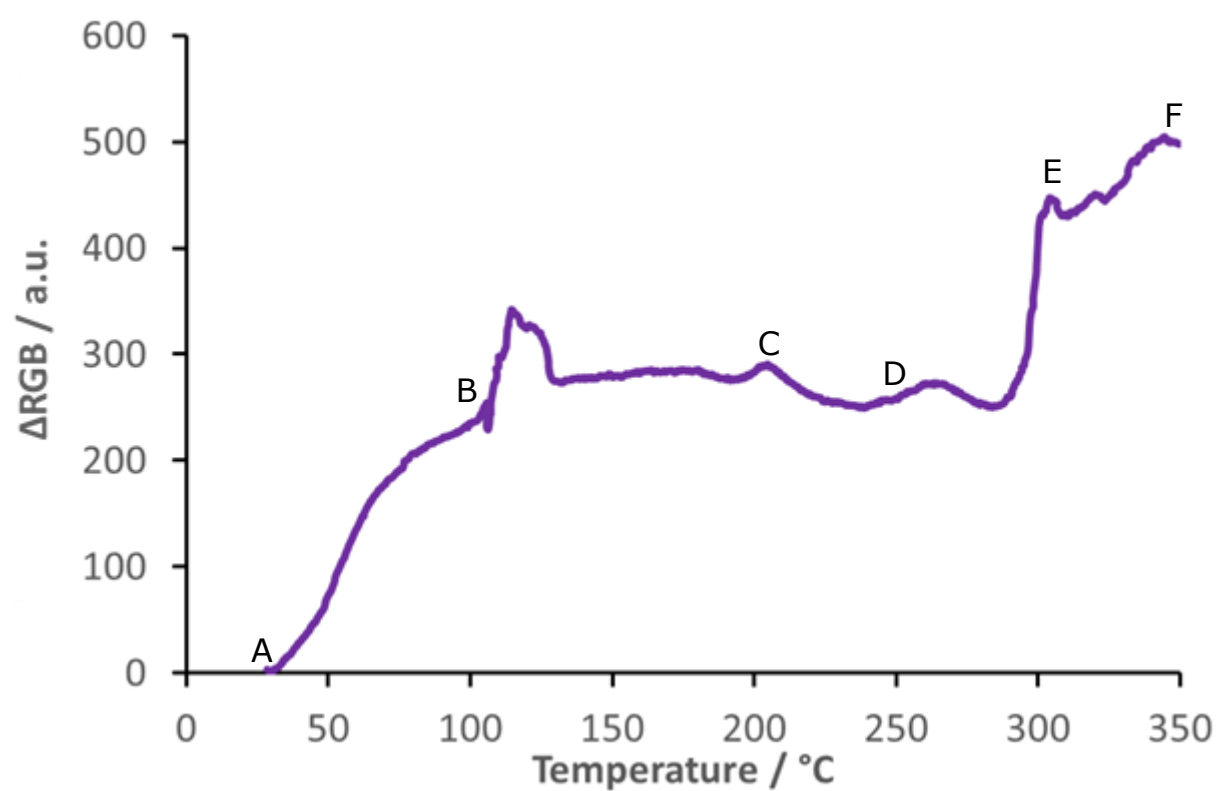


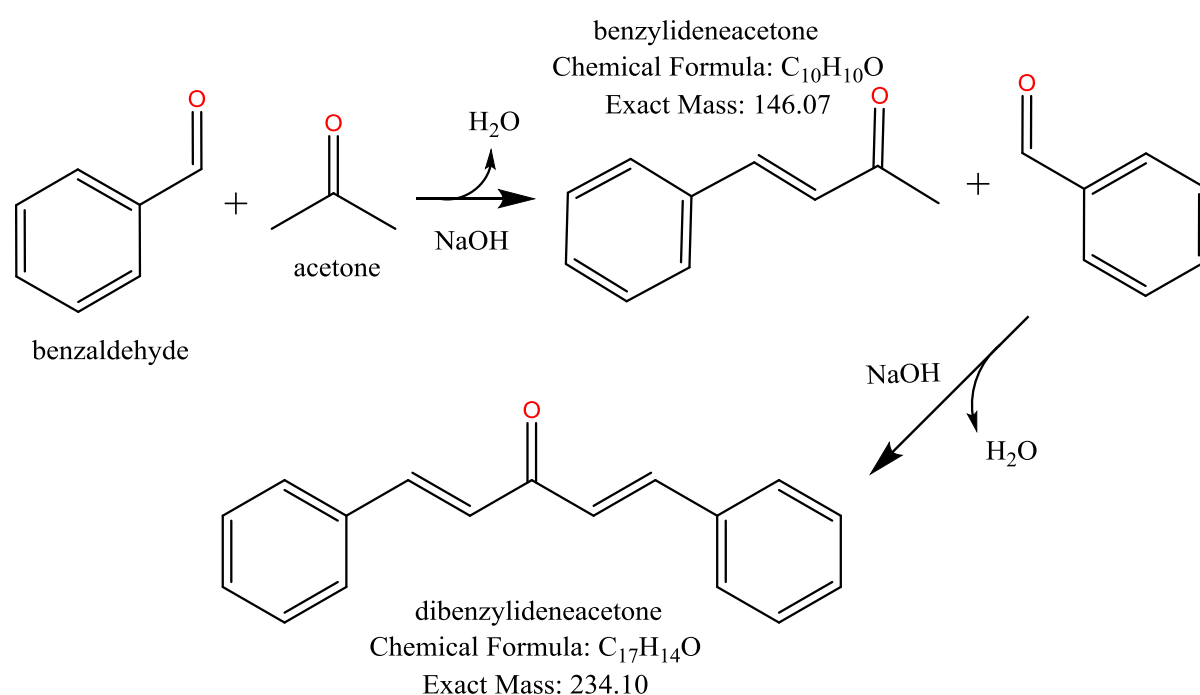
Figure 3.44 Colour profiling of the synthesis of phenylbisbenzimidazole. Labels correspond to micrographs in Figure 3.43.

3.10 Incomplete Reactions

The following reactions have been included to demonstrate some of the weaknesses of the current HDM system and include a brief discussion about the reactions as a whole and how they may be addressed in future work.

3.10.1 Dibenzylideneacetone

Following the initial success of the hydrobenzamide example (Section 3.2) a similar synthesis was attempted with the formation of the compound dibenzylideneacetone. The synthesis is base catalysed and undergoes a double dehydration to form the final compound via a transient intermediate benzylideneacetone as shown in Schematic 3.20.



Schematic 3.20 Overall reaction progression from benzaldehyde and acetone forming dibenzylideneacetone.

The reaction was initially trialled using a solution of sodium hydroxide added to a mixture of acetone and benzaldehyde. Although the reaction did appear to progress the volatile nature of the acetone meant that it was rapidly removed with mild heating (30-50 °C) meaning one of the reactants had been depleted without being consumed within the reaction.

The reaction was commonly used to teach kinetics as the rate of the reaction can be directly related to the concentration of the sodium hydroxide within the system. Experiments were trialled by forming basic alumina (Al₂O₃ soaked in sodium hydroxide for 24hrs) to act as both a catalyst and a support for the reaction. The milder reaction conditions were hoped to increase the longevity of the reactant signals. The temperature

ramping always removed the acetone from the reaction typically within a minute or two, so an isothermal experiment was designed to hold the temperature at 30 °C to allow the reaction to progress without exhausting the acetone reactant. Unfortunately, the volume of helium across the sample assisted with the evaporation process and without a complete redesign of the HDM it appeared that this reaction type (those with extremely volatile solvents) was unfavourable in the current method of HDM analysis. Although the reactants themselves could not be followed accurately both the intermediate and the product were noted.

The reaction shown in Figure 3.45 was set to a gradual heating rate of 1 °C min⁻¹, from 30 to 120 °C. The slow rate was set to increase the thermal resolution between the signals as most were noted pre-100 °C.

The benzylideneacetone intermediate (A) was noted from the onset of heating the reaction and shows brief evolution across a narrow temperature range (30-40 °C) associated with its low melting point. The intermediate is expected to have reacted further with the slightly more thermally stable benzaldehyde forming the final dibenzylideneacetone product (B). The product evolution temperature (>90 °C) suggests that the more sterically favoured isomer (Z-Z) had formed (The evolution of the E-E isomer is expected to be earlier melting around *ca.* 60 °C), resulting in higher thermal stability as evolution of the product hasn't finished within this temperature range. Acetone and benzaldehyde have been omitted due to inconsistencies of their profiles, as no meaningful trace with relation to the reaction was obtained.

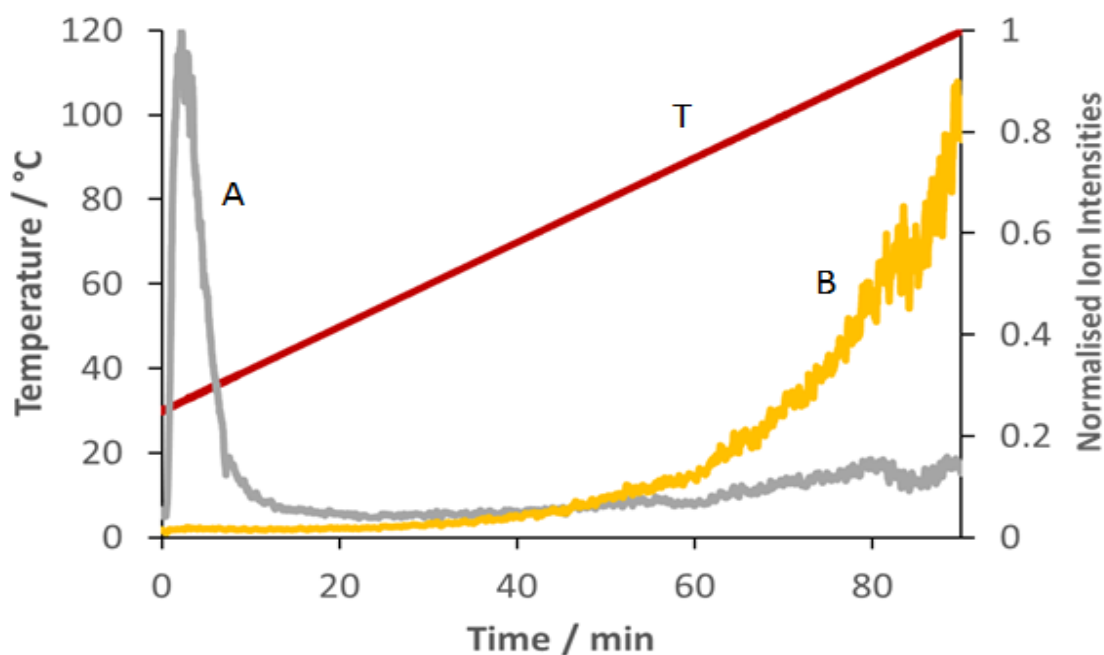


Figure 3.45 HDM reaction monitoring of dibenzylideneacetone synthesis. A) Intermediate 147 Da [M+H]⁺, B) dibenzylideneacetone 235 Da [M+H]⁺ and T) Temperature.

Micrographs of the reaction are shown in Figure 3.46. Micrograph A ($t = 0$ min) shows a white reaction mixture and the highly reflective surface is observed. Within the first minute (micrographs A-B) the acetone is both consumed and evaporated, with an indication of the yellow products starting to form. Further heating deepens the colour of localised spots (micrograph C) suspected to be higher benzaldehyde containing regions on the larger alumina particles (from incomplete grinding), and the entire bed appears to have taken on a yellow colour. The micrograph (D) shows the white colour of the bed returning as the intermediate and product are removed, it is suspected that if heating was continued the remaining contents would be the white bed of alumina.

The Σ RGB profile shown in Figure 3.47 shows the initial dehydration between 0 and 5 minutes (approx. 60 a.u.) followed by the gain in yellow colour of the reaction between 5 and 40 minutes (35 to 70 °C). Although the overall reaction colour is changing the colour trace remains relatively stable between 70 and 120 °C, this is likely to be caused by averaging the darkening spots and the whitening of the remaining bed.

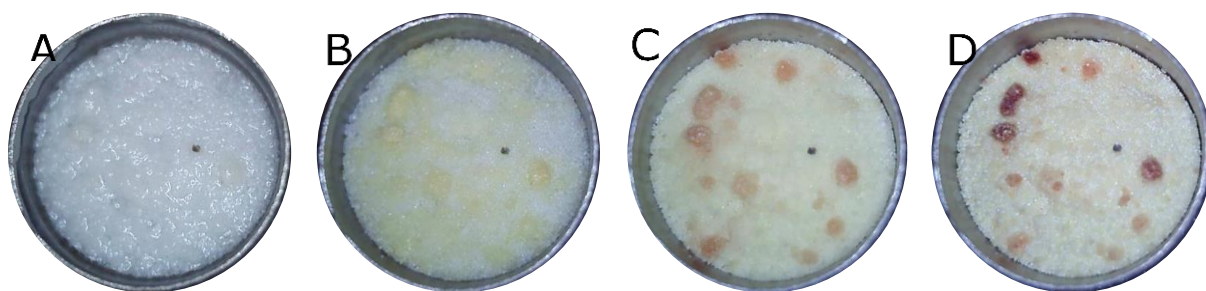


Figure 3.46 Micrographs of the dibenzylideneacetone, A) $t = 0$ min, B) $t = 1$ min, C) $t = 25$ min, and D) $t = \text{end}$.

Although the reaction appeared to work the current design and analysis method for reactions was not suited for a highly volatile reaction, due to increasing temperature and the high evaporation rate caused by the significant flow rate of helium from the DART.

Future work to repeat this experiment it is suggested that a DSC pan is used that has a transparent lid with the addition of a pin hole. This will prevent the volatile reactants from evaporating as quickly, whilst still allowing the sample to be imaged. The vapour that is evolved will be done so as a function of temperature as opposed to monitoring an almost evaporative process.

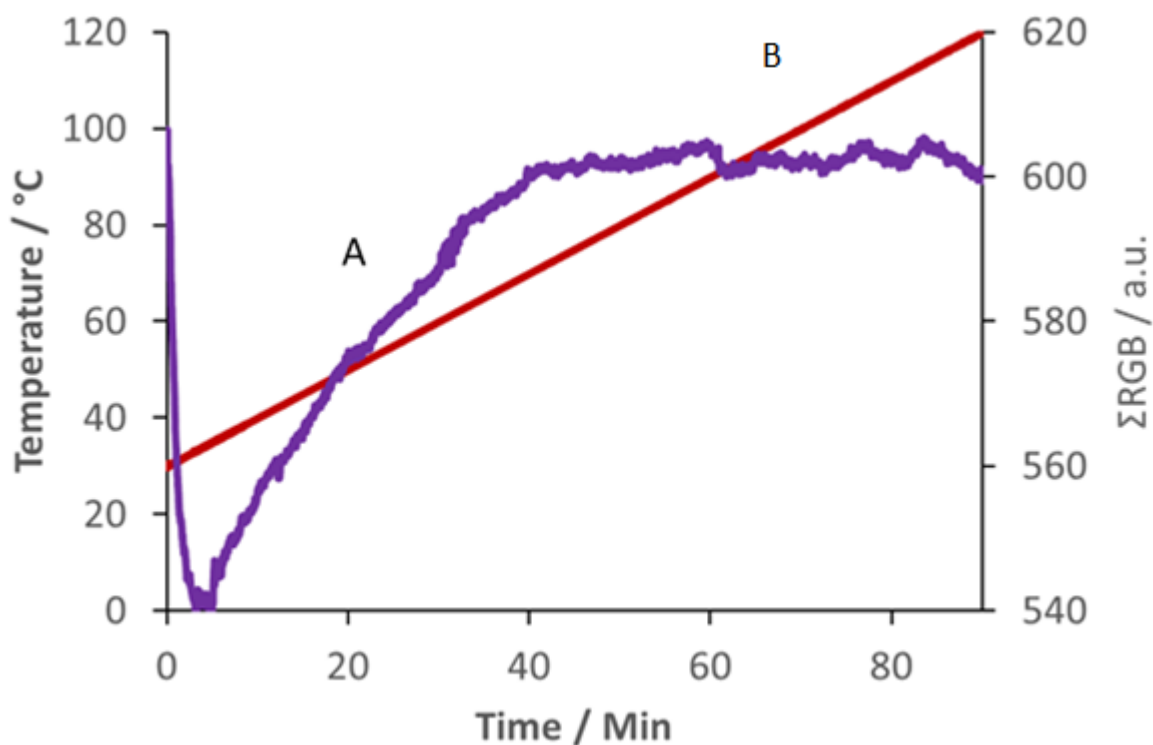
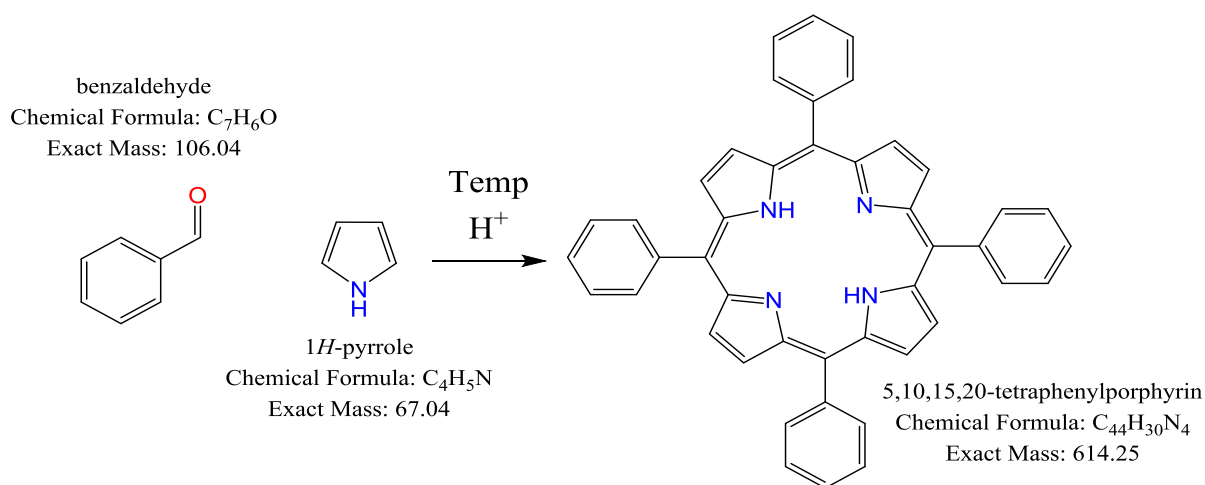


Figure 3.47 HDM colour profile for the dibenzylideneacetone reaction. A) Total colour of the reaction and B) Temperature.

3.10.2 Tetraphenylporphyrin

After a brief literature review for highly coloured reactions to trial on the HDM, many reactions based on porphyrins were found to yield high pigmentation. The following reaction between pyrrole and benzaldehyde (to form tetraphenylporphyrin) was decided to be investigated (Schematic 3.21).



Schematic 3.21 Overall reaction progression from benzaldehyde and pyrrole forming tetraphenylporphyrin.

Typical tetraphenylporphyrin synthesis usually relies on boiling pyrrole and benzaldehyde in an acidic medium (normally propionic acid) for several hours. As the project direction had led towards greener routes it was decided to investigate the synthesis over a solid acid catalyst, montmorillonite. The clay catalyst was activated as per the manufacturer's recommendations by heating at 350 °C for several hours, thus dehydrating the clay. The synthesis was inspired by literature that reported using silica as a support for the reactants to be heated under microwave radiation.⁸⁰

The reaction was trialled by mixing equimolar amounts of benzaldehyde and pyrrole and pipetting them onto a bed of activated montmorillonite. Figure 3.48 show normalised extracted ion chromatograms to represent the reaction process. As soon as the light brown solution was added to the off white catalyst a deep purple/black colour formed. Micrographs in Figure 3.49 shows a collection of images throughout the reaction, a purple solution is formed above the catalytic bed in the initial stages and further heating drives away residual reactants leaving a blue-purple solid.

The reaction colour suggests that some reaction has occurred. The dark blue-purple colour is indicative of the tetraphenylporphyrin product. Although colour suggests that the reaction has formed the desired product no evidence of the porphyrin exists within the mass spectrum signal over this temperature range. Again this reaction appears to have progressed very quickly possibly due to the intimate nature of the reactants with the catalyst itself. A range of transient intermediates appears to be observed with higher masses evolving with higher temperature (Figure 3.48); although more signals were noted a selection have been shown to give an overview of the process.

Since the liquid reactants boil away quickly and no liquid is observed it can be expected that the solid intermediates have become 'trapped' in this state by coming into no further contact with more feedstock material. So a thermal desorption process is likely to be occurring gradually removing the intermediates that are bound to the montmorillonite.

The final porphyrin signal is expected to be seen should the temperature be driven higher as within the upper temperature range of the reaction 400-450 °C the porphyrin product is expected to melt. MS optimisation will aid with monitoring the high molecular weight signals that will be produced relating to the final porphyrin compound as it was set within the few hundred Da region. The reaction was abandoned in pursuit of other more highly yielding reactions. Although if the project was revisited an interesting comparison would be to achieve higher temperatures (to fully desorb the compounds from the matrix).

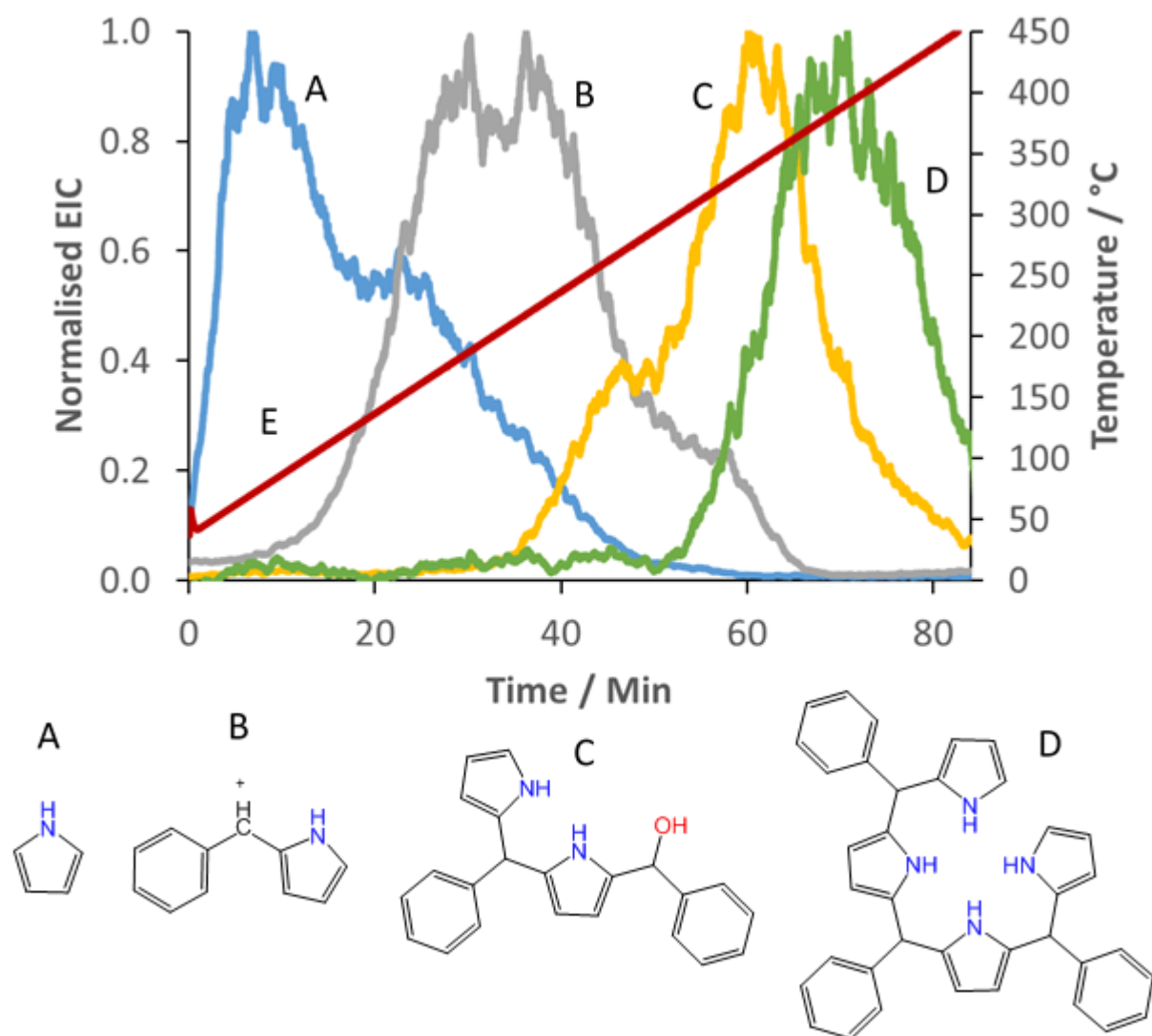


Figure 3.48 HDM reaction monitoring of tetraphenylporphyrin synthesis and related structures. A) Pyrrole 85 Da $[M+NH_4]^+$, B) Bnz-Pyrr carbocation Intermediate 156 Da $[M]^+$, C) (Pyrr-Bnz)₂ Intermediate 329 Da $[M+H]^+$, D) (Pyrr-Bnz)₃-Pyrr intermediate 550 Da $[M+NH_4]^+$ and E) Temperature.

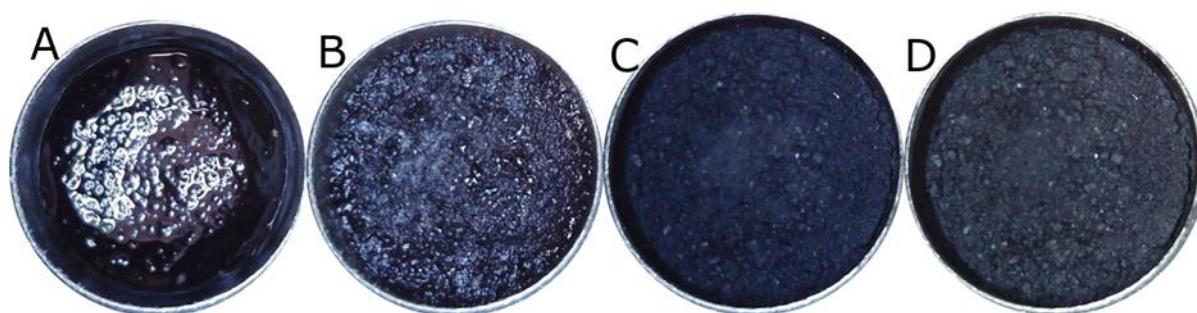
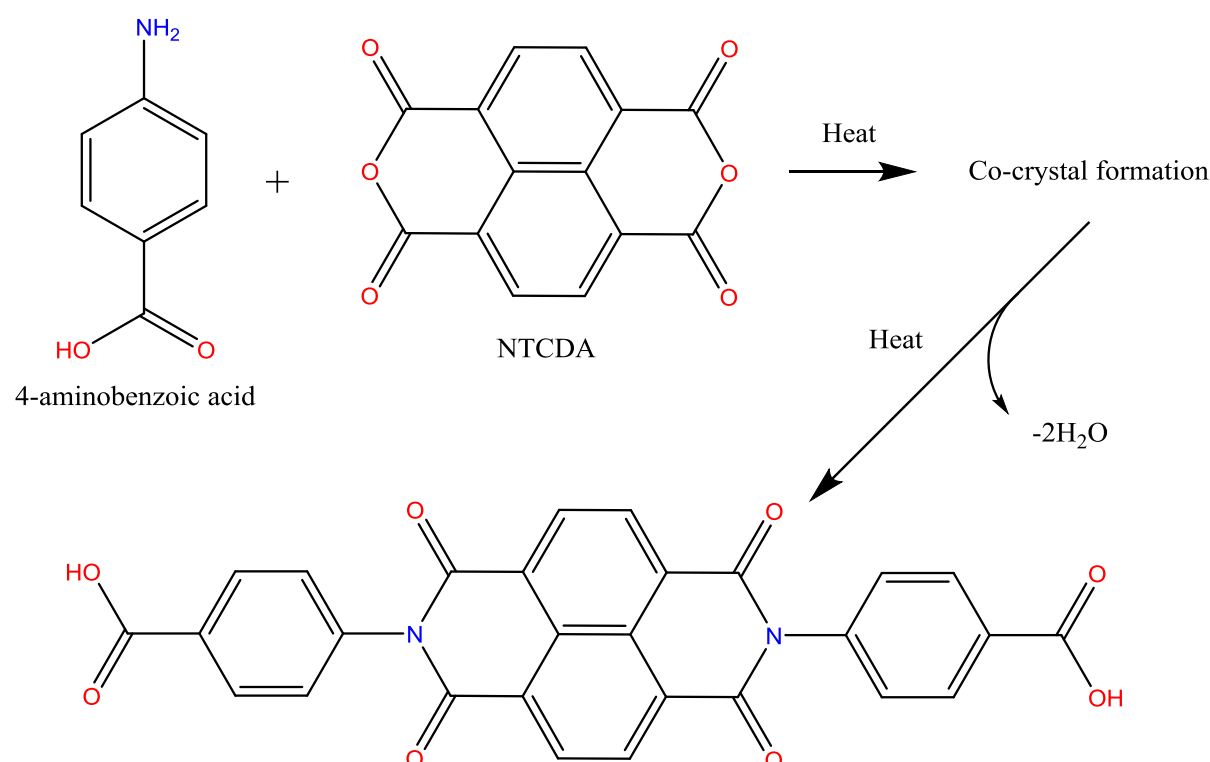


Figure 3.49 Micrographs of the tetraphenylporphyrin synthesis, A) 30 °C, B) 65 °C C) 250 °C and D) 450 °C

3.10.3 Diimide substituted NTCDA

In the initial literature search for reactions with dramatic colour changes a paper by Zaworotko *et al.* showed that through mechanical synthesis by grinding substituted arylamines and NTCDA (naphthalenetetracarboxylic dianhydride) together followed by heating the diimide product could be formed, importantly going through a number of obvious colour changes.⁸¹ To trial this reaction an arbitrary substituted arylamine (p-aminobenzoic acid, PABA) was selected and reacted with NTCDA as shown in Schematic 3.22.



Schematic 3.22 Overall reaction progression from arylamine and NTCDA forming the diimide upon heating.

PABA was added to NTCDA (2:1) and ground prior to addition to the analysis pan. The reaction was heated at 5 °C min⁻¹ over a broad temperature range to 400 °C to see if any notable colour changes could be observed. The reaction was initially trialled recording mass spectra in positive mode but it was soon found that only the protonated molecular ion of the PABA could be observed with no significant signals of products or intermediates present.

Polarity was moved to negative mode and the reaction was repeated. As before the final diimide product was not observed but the ring opened monosubstituted intermediate was shown as the deprotonated molecular ion 404 Da [M-H]⁻ and the ring closed imide itself as the molecular ion 387 Da [M]⁻ (Figure 3.51).

The starting material is shown to be released from the onset of heating but quickly begins to decline in intensity as the PABA is consumed (100 °C onwards), the trace appears to recover at 157 °C with the associated colour loss. When reviewing the micrographs (Figure 3.50) it can be seen that during the colour loss a red colour is formed and crystals (assumed to be PABA) grow from the reaction and are removed giving rise to another peak in signal.

The colour begins to return from 210 °C with the signal from the ring opened intermediate (B), as a red to pale yellow transition is shown. The assumed more thermally stable monosubstituted imide isn't noted until the temperature reaches 300 °C when it is quickly lost during the final stages of heating. The diimide is assumed to have not completely formed due to the expulsion of the PABA (around 150 °C) and the red colour shown is the cocystal not the diimide as noted by the previous authors.⁸¹ A very small indication of monosubstituted imide is shown around 150 °C indicating that the reaction had begun to progress.

In future work should this work be repeated an isothermal experiment within this region would be worthwhile investigating. Isothermally holding the experiment, or a gradual heating rate in this region may result in the formation of the diimide before the PABA is thermally removed.

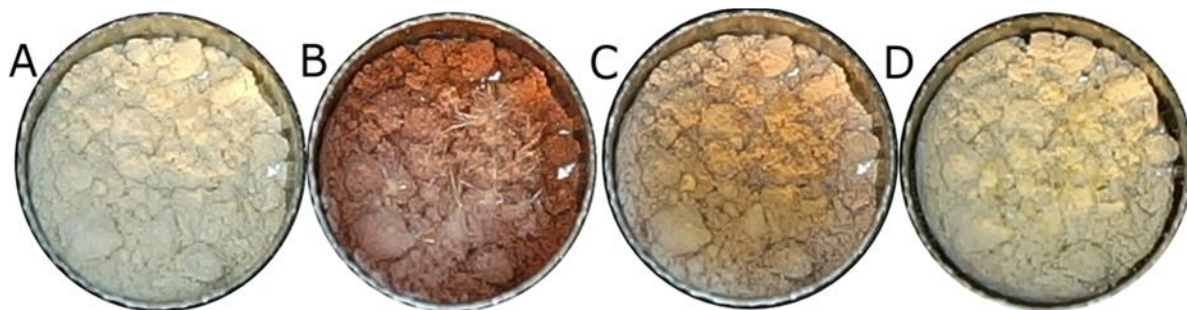


Figure 3.50 Micrographs of the diimide substituted NTCDA, A) 50 °C, B) 190 °C C) 260 °C and D) 380 °C.

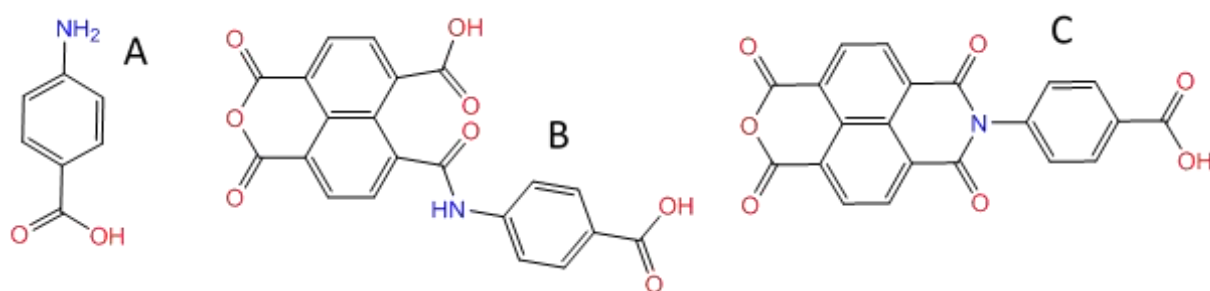
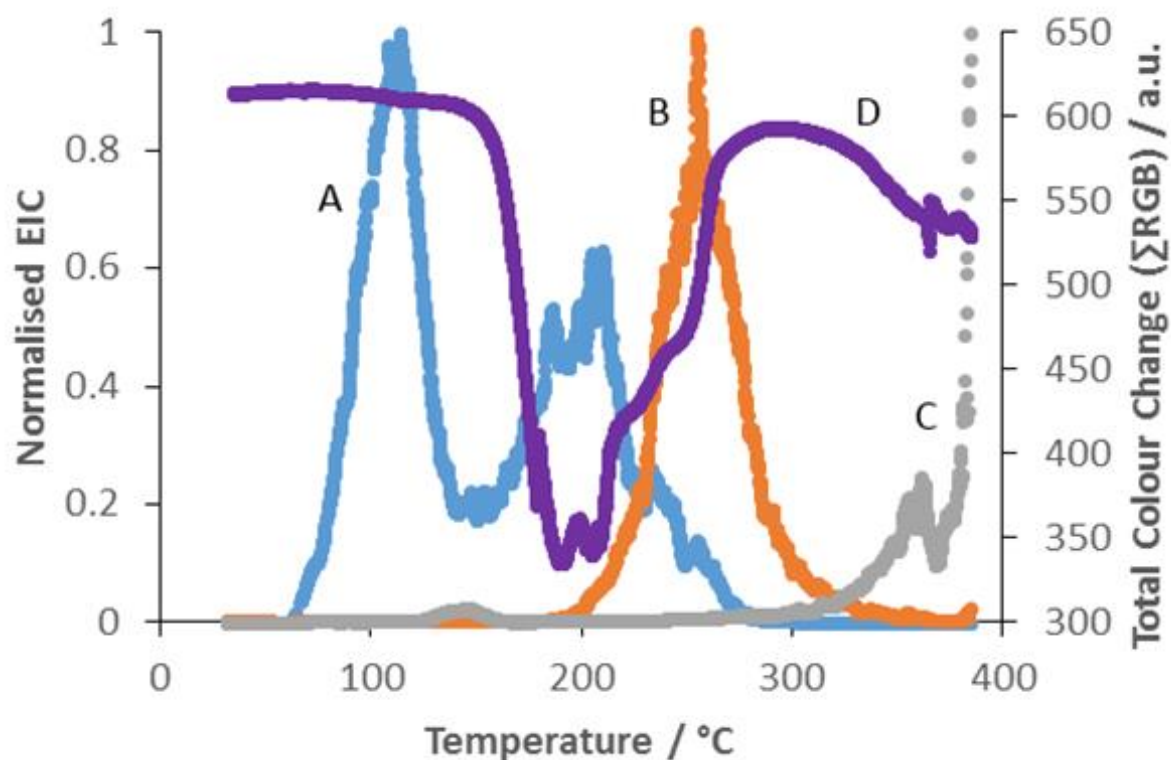
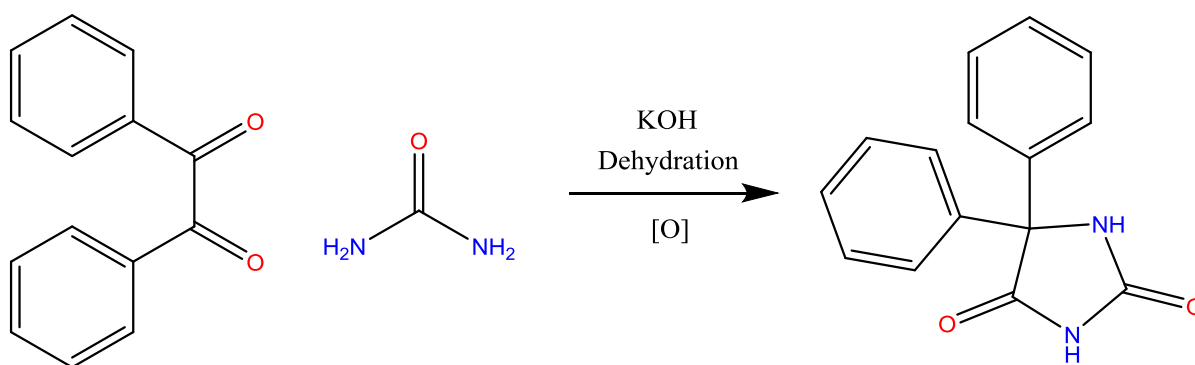


Figure 3.51 HDM reaction monitoring of imide substituted NTCDA synthesis and related structures. A) *p*-aminobenzoic acid 136 Da [$M-H$]⁻, B) ring opened monosubstituted intermediate 404 Da [$M-H$]⁻, C) monosubstituted imide 387 Da [M]⁻, and D) Total reaction colour.

3.10.4 Dilatin

The following reaction looks at a multicomponent synthesis attempted within the solid state, this reaction is commonly performed within a solution so it was possibly optimistic to trial the reaction in this manner. The raw reagents were scaled down and any auxiliary solvents were excluded to try the synthesis in a solventless system.

The reaction was monitored over a modest temperature range to 350 °C. As in previous examples benzil was shown as both its protonated and ammoniated form (211 Da and 228 Da respectively).



Schematic 3.23 Overall reaction forming dilatin from benzil, urea and potassium hydroxide

Benzil in the presence of base may undergo a benzilic acid rearrangement which also has the same nominal mass of 228 Da; EIC profiles show that the two signals are removed in parallel and are not thermally resolved suggesting that 228 Da is the ammoniated form. The major issue with this reaction was the entire reaction began to swell (micrographs Figure 3.52) and this appears to have inhibited the reaction or ionisation. Unfortunately no signals could be extracted from the mass spectra relating to the formation of dilatin reaction products.

Two major signals were noted after the decline of benzil, the first was 182 Da and the second was 298 Da. No clear assignments could be applied to these signals in relation to the reaction or possible side reactions. Added complexities of secondary reactions were likely to be the cause of the problems within this solventless reaction system. The reaction between urea and potassium hydroxide has been shown to form potassium cyanate, ammonia and water.⁸² The foaming has been attributed to the potassium salt forming and expansion caused by the release of the gaseous water and ammonia. Further reactions can occur thermally with the dimerisation and trimerisation of urea to form biuret and triuret respectively.⁸³ This combination of multiple components with chemically driven reactions and thermally driven side reactions gives an insight into the issues that the HDM can face when trying to resolve complex reactions. If trialled again the hydroxide concentration would be reduced in the hope of forming a melt reaction when benzil melts, after several attempts of the same reaction the reaction was abandoned to focus on other systems.

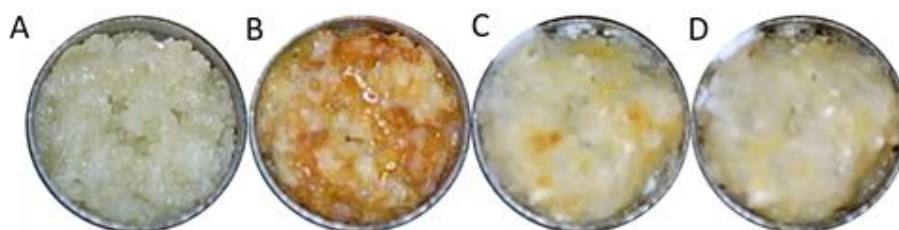


Figure 3.52 Micrographs of the dilatin synthesis, A) 30°C, B) 150°C C) 300°C and D) 350 °C

3.11 Conclusions

This chapter demonstrates how HDM may be applied to the study and profiling of organic reactions in a variety of physical states covering both heterogeneous and homogeneous synthesis.

HDM can profile organic reactions in relation to both time and temperature as demonstrated by selected linear heating and isothermal experiments.

The inclusion of the optical data of HDM emphasises the strength of the technique as a whole, complex mass spectral profiles can be better explained by visualising key stages during reactions through the use of micrographs and also colour profiles.

In turn, the mass spectrometer provides the necessary chemical information to explain what processes may be occurring during the reactions themselves.

A range of reactions were trialled typically based on forming Schiff-bases through dehydration reactions. Both aryl and alkyl synthetic reactions were achieved, with a number of heterocyclic ring structures being successfully synthesised including imidazole, quinoxaline, pyrazine and diazepine.

HDM was applied to the practice of 'green' chemistry trialling reactions on the lower milligram scale without the need for solvents, typically relying on the reactants themselves acting as their own solvents.

Some synthetic reactions that were deemed successful were then scaled up to a preparative scale to evaluate reaction feasibility with obtained products being purified and further characterised using NMR and DSC.

However, a range of reactions were found to be unsuccessfully monitored missing a key component such as an ion profile, colour, or general lack of reaction in a solventless system. These included reactions involving highly volatile materials or those involved with extreme pH's without solvent. The analysis of these systems would require further development to be successful with HDM which has been briefly discussed.

3.12 Reactions Profiling References

- ¹ B. Hemmateenejad, M. Akhond, Z. Mohammadpour and N. Mobaraki, *Anal. Methods*, (2012), **4**, 933-939
- ² L.R. Knopke, N.Nemati, A. Kockritz, A. Bruckner, *ChemCatChem*, (2010), **2**, 273-280
- ³ E.J. Rogers and S.F. Kudzin, *Microchemical Journal*, (1979), **24**, 426-430
- ⁴ D.A. Foley, A.L. Dunn and M.T. Zell, *Magn. Reson. Chem.*, (2016), **54**, 451-456
- ⁵ I. Peinado, M. Mason, F. Biasioli and M. Scampicchio, *Rapid Commun Mass Spectrom.* 2017, **32**, 57-62.
- ⁶ C. Petucci, J. Diffendal, D. Kaufman, B. Mekonnen, G. Terefenko and B. Musselman, *Anal. Chem.*, (2007), **79**(13), 5064-5070
- ⁷ G. Morlock and Y. Ueda, *J. Chromatogr A*, 2007, **1143**, 243-251
- ⁸ X. Yan, E. Sokol, X. Li, G. Li, S. Xu, and R. G. Cooks, *Angew. Chem. Int. Ed.* 2014, **53**, 5931 - 5935
- ⁹ T. Chen, J. Lin, J. Chen and Y. Chen, *JAmSoc Mass Spectrom*, 2010, **21**, 1547-1553.
- ¹⁰ A. Ray, T. Bristow, C. Whitmore and J. Mosely, *Mass Spec Rev.*, 2017, **9999**, 1-15.
- ¹¹ L.M. Sanchez, M.E. Curtis, B.E. Bracamonte, K.L. Kurita, G.Navarro, O.D. Sparkman and R.G. L'n'ngton, *Org. Lett.*, 2011, **13** (15), 3770-3773
- ¹² S. Zhou, M.W. Forbes and J.P.D. Abbatt, *Anal. Chem.*, 2015, **87**, 4733-4740
- ¹³ D.S. Cho, S.C. Gibson, D. Bhandari M.E. McNally, R.M. Hoffman, K.D. Cook and L. Song, *Rapid Commun. Mass Spectrom.* 2011, **25**, 3575-3580
- ¹⁴ P.T., Anastas, and J.C. Warner, *Green Chemistry: Theory and Practice*, Oxford University Press, New York, 1998.
- ¹⁵ G.P. Ashton, L.P. Harding and G.M.B. Parkes, *Analytical Chemistry*, 2017, **89**(24), 13466-13471
- ¹⁶ J. Frances, ROYAL SOCIETY. *The Athenaeum*. 1845(**920**), 590.
- ¹⁷ Y. Kwon, M.G. Kim, Y. Kim, Y. Lee and J. Cho, *Electrochemical and Solid-State Letters*. 2006, (**9**), 34-38.
- ¹⁸ O.F. Williams, J.C. Bailar, *J. Am. Chem. Soc.* 1959, **81**, 4464
- ¹⁹ T.I. Crowell and R.K. McLeod, *J. Am. Chem. Soc.*, 1956, **78**, 4030-4033
- ²⁰ A.L. Vogel, B.S. Furniss, *Vogel's textbook of practical organic chemistry, including qualitative organic analysis*. 3rd ed. London (etc.): Longman; 1974, 720
- ²¹ J.-M. Huang, J.-F. Zhang, Y. Dong and W. Gong, *The journal of Organic Chemistry*, 2011, **76**(9), 3511-3514
- ²² A.A.O. Sarhan and C. Bolm, *Chem. Soc. Rev.*, (2009), **38**, 2730-2744
- ²³ J.M. Brunel, *Chem. Rev.* 2005, **105**, 857-897
- ²⁴ B. Wang, P. Li, Y. Zhang and L. Wang, *Chin. J. Chem.*, 2011, **28** (12), 2463-2468
- ²⁵ S. Jana, S. Pande, A. K. Sinha, T. Pal, *Inorg. Chem.* 2008, **47**, 5558-5560.
- ²⁶ J. Doussot, A. Guy and C. Ferroud, *Tetrahedron Lett.* **2000**, 41, 2545.
- ²⁷ M. Shibasaki and S. Matsunaga, *Journal of Organometallic Chemistry*, 2006, **691**(10), 2089-2100
- ²⁸ L. Pu, *Acc. Chem. Res.* 2012, **45**(2), 150-163
- ²⁹ F. Toda, K. Tanaka and S. Iwata, *J. Org. Chem.*, (1989), **54**(13), 3007-3009
- ³⁰ B.E. Love and R.A. Bills, *Synthetic Communications*, 2002, **32**(13), 2067-2073
- ³¹ D. J. Pasto and C.R. Johnson, *Laboratory text for organic chemistry: a source book of chemical and physical techniques*, Englewood Cliffs, Prentice-Hall, 1979.
- ³² L. Meca, D. Reha, and Z. Havlas, *J. Org. Chem.*, **2003**, 68, 5677.
- ³³ K.K.W. Mak, *J. Chem. Educ.* 2004, **81**(11), 1636-1640
- ³⁴ Y. Yang, J.O. Escobedo, A. Wong, C.M. Schowalter, M.C. Touchy, L. Jiao, W.E. Crowe, F.R. Fronczek and R.M. Strongin, *J. Org. Chem.*, 2005, **70**(17), 6907-6912
- ³⁵ J.M. Jamison, K. Krabill and A. Hatwalkar, *Cell. Biol. Int. Rep.*, 1990, **14**, 1075-1084
- ³⁶ K. Hara, T. Horiguchi, T. Kinoshita, K. Sayama, H. Sugihara and H. Arakawa, *Solar Energy Materials and Solar Cells*, 2000, **64**, 115-134
- ³⁷ M. Dabiri, S.C. Azimi and A. Bazgir, *Chemical Papers*, 2008, **62**(5), 522-526
- ³⁸ B. Rajitha, B.S. Kumar, Y.T. Reddy, P.N. Reddy and N. Screenivasulu, *Tetrahedron letters*, 2005, **46**(50), 8691-8693.
- ³⁹ D. Liu, S. Zhou, J. Gao, L. Li and D. Xu, *J. Mex. Chem. Soc.*, 2013, **57**(4), 345-348
- ⁴⁰ A.A. Bartolomeu, M.L. Menezes and L.C. Silva-Filho, *Chemical Papers*, **68**(11), 1593-1600
- ⁴¹ S.I. Alaqeel, *J. Saudi Chem. Soc.* (2017), **21**, 229-237
- ⁴² Z. Kazimierzczuk, J.A. Upcroft, P. Upcroft, A. Gorska, B. Starosciak and A. Laudy, *Acta Biochim. Pol.* (2002), **49**, 185
- ⁴³ L.D.S. Yadav and D.R. Pal, *Ind. J. Chem.* (1996), **35**(B), 748

- ⁴⁴ M. Hranjec, K. Starcevic, S.K. Pavelic, P. Lucin, K. Pavelic and G.K. Zamola, *Eur. J. Med. Chem.*, (2011), **46**, 2274
- ⁴⁵ M. A. Phillips, *J. Chem. Soc.*, 1928, 2393
- ⁴⁶ L.Z. Fekri and R. Maleki. *Journal of Heterocyclic Chemistry*. 2017, **54**(2), 1167-71.
- ⁴⁷ H. Sharma, N. Kaur, N. Singh and D.O. Jang, *Green Chem.* 2015, **17**, 4263-4270
- ⁴⁸ F.K. Behbahani and P. Ziaei, *Chemistry of heterocyclic compounds*, 2012, **48**(7), 1011-1017
- ⁴⁹ A.M.S.E. Newahie, N.S.M. Ismail, D.A.A.E. Ella and K.A.M. Abouzid, *Arch. Pharm. Chem. Life. Sci.*, 2016, **349**, 309-326
- ⁵⁰ M.M. Hossain, M.M. Hossain, M.H. Muhib, M.R. Mia, S. Kumar and S.A. Wadud, *Bangladesh Med. Res. Counc. Bull.*, 2012, **38**, 47-50.
- ⁵¹ R. Sheng, Y. Xu, Q. Weng, Q. Xia, Q. He, B. Yang and Y. Hu, *Drug Discov. Ther.*, 2007, **1**(2), 119-123
- ⁵² Y.-M. Jing, F.-Z. Wang, Y.-X. Zheng and J.L. Zuo, *J. Mater. Chem. C.*, 2017, **5**, 3714-3724
- ⁵³ A.A. Kalinin, S.M. Sharipova, T.I. Burganov, A.I. Levitskaya, Y.B. Dudkina, A.R. Khamatgalimov, S.A. Katsyuba, Y.H. Budnikova and M.Y. Balakina, *Dyes and Pigments*, 2018, **156**, 175-184
- ⁵⁴ A.L. Vogel and B.S. Furniss, *Vogel's Textbook of Practical Organic Chemistry*, Harlow, Longman, 5th edn, 1989.
- ⁵⁵ K.N. Carter and K.N. Carter Jr., *J. Chem. Educ.* 1995, **72**(7), 647-648
- ⁵⁶ D. Kumar, K. Seth, D.N. Kommi, S. Bhagat and A.K. Chakraborti, *RSC Adv.*, 2013, **3**, 15157-15168
- ⁵⁷ F. Xie, M. Zhang, H. Jiang, M. Chen, W. Lv, A. Zheng and X. Jian, *Green Chem.*, 2015, **17**, 279-284
- ⁵⁸ M.S. Mohamed, R.A. El-Domany and R.H. Abd El-Hameed. *Acta Pharmaceutica*. 2009, **59**(2), 145-58.
- ⁵⁹ L. Shao, Q. Chen and C. Qi. *Kinetics and Catalysis*. 2017, **58**(6), 758-62.
- ⁶⁰ J.A. Maga and C.E. Sizer, *J. Agr. Food Chem.*, 1973, **21**(1), 22-30
- ⁶¹ K. Shimazaki, T. Inoue, H. Shikata and K. Sakakibara, *Journal of molecular structure*, 2005, **749**, 169-176.
- ⁶² A. Rajchl, H. Čížková, M. Voldřich, D. Lukešová and Z. Panovská, *Czech J. Food Sci.*, 2009, **27**(4), 259-266
- ⁶³ D. Davidson, M. Weiss and M. Jelleing, *J. Org. Chem.*, 1937, **02**(04), 319-327
- ⁶⁴ A. Schaarschmidt and H. Hofmeier, *J. Chem. Soc., Abstr.*, 1925, **128**, i-877-933;
- ⁶⁵ W.B. Leslie and G.W. Watt, *J. Org. Chem.*, 1942, **7**(1), 73-78
- ⁶⁶ M. Hagimori, N. Mizuyama, Y. Tominaga, T. Mukai and H.Saji, *Dyes and Pigments*, 2015, **113**, 205-209
- ⁶⁷ J.V. Alphen, *Recueil des Travaux Chimiques des Pays-Bas*, 1933, **52** (1), 47-54
- ⁶⁸ B. Willy, T. Dallos, F. Rominger, J. Schönhaber and T.J.J. Müller, *Eur. J. Org. Chem.*, 2008, **28**, 4796-4805
- ⁶⁹ M. Baumann, I.R. Baxendale, C.H. Hornung, S.V. Ley, M.V. Rojo and K.A. Roper, *Molecules*, 2014, **19**, 9736-9759
- ⁷⁰ Y.-M. Ren, C. Cai and R.-C. Yang, *RSC Advances*, 2013, **3**, 7182-7204
- ⁷¹ V. Starcevic, *Advances in Psychiatric Treatment*, 2012, **18**(4), 250-258
- ⁷² J.F. Pagel and B.L. Parnes, *Primary Care Companion J Clin Psychiatry*, 2001, **3**(3), 118-125
- ⁷³ T.K. Birkenhager, P. Moleman and W.A. Nolen, *International Clinical Psychopharmacology*, 19995, **10**, 181-195
- ⁷⁴ E. Vessally, R. Hosseinzadeh-Khanmiri, E. Ghorbani-Kalhor, M. Es'haghi and L. Ejlali. *Applied Organometallic Chemistry*. 2017, **31**(10), e3729
- ⁷⁵ C.I. Nieto, R.M. Claramunt, M.C. Torralba, M.R. Torres and J. Elguerod, *Acta Crystallogr E Crystallogr Communv.*, 2017, **73**(5), 647-650.
- ⁷⁶ L. Teng and Z. Wang. *Acta Crystallographica Section E*, 2008, **64**(8), 1562.
- ⁷⁷ L.M. Dudd, E. Venardou, E. Garcia-Verdugo, P. Licence, A.J. Blake, C. Wilson and M. Poliakoff, *Green Chem*, 2003, **5**, 187-192.
- ⁷⁸ F.-L. Bei, F. Jian, X. Yang, L. Lu, X. Wang, S. Shanmuga Sundara Raj and H.-K. Fun, *Acta Cryst.*, 2000, **C56**, 718-719
- ⁷⁹ T.H.E.-Sayed, A. Aboelnaga and M. Hagar, *molecules*, 2016, **21**(9), 1111-1119
- ⁸⁰ M.G. Warner, G.L. Succaw and J.E. Hutchison, *Green Chem*, 2001, **3**, 267-270
- ⁸¹ M.L. Cheney, G.J. McManus, J.A. Perman, Z. Wang and M.J. Zaworotko, *Crystal Growth & Design*, 2007, **7**(4), 616-617
- ⁸² G.L. Tucker and E.L. Blanton, US3935300A
- ⁸³ D. Gratzfield and M. Olzmann, *Chemical Physics Letters*, 2017, **679**, 219-224

4.0 Polymer studies

4.1 Introduction

Polymers are natural¹ and synthetic² macrostructures comprising several smaller regular repeating units known as monomers.³ In 2015 the UK's polymer sector had a turnover of £23.5 billion and was the second largest manufacturing industry employing over 170,000 people.⁴

Polymers find applications in many sectors including packaging,⁵ medicine⁶ and construction materials.⁷ The properties of these materials can be engineered by modification of the polymer itself. The strength can be increased through the addition of other materials such as glass fibres⁸ whilst the flexibility can be modified through the extent of crosslinking.⁹

A variety of different instrumental techniques are used for polymer analysis. Longevity studies of polymers may be performed using optical techniques such as optical microscopy (OM),¹⁰ atomic force microscopy (AFM)¹¹ and scanning electron microscopy (SEM).¹² These techniques monitor the extent of polymer degradation based on surface morphological changes.

The mechanical properties of polymers are evaluated using techniques such as dynamic mechanical analysis (DMA) which applies an oscillatory force to the sample. Typically, these experiments involve heating to evaluate how the polymers' mechanical properties vary with temperature.¹³

Other thermal analysis methods used to study polymers include scanning calorimetry (DSC) and thermogravimetric analysis (TGA). One key application of DSC to polymers is for the study of the glass transition temperature (T_g) where the mechanical properties of the polymer change from a brittle 'glassy' type state through to a mobile rubbery amorphous state via a process called relaxation.¹⁴ T_g is detected using DSC through a change in heat capacity which produces a step in the baseline. The glass transition is shown pictorially in Figure 4.1. Other physical changes that can occur during a glass transition include changes in the opacity (detected through a change in birefringence)¹⁵ and volume (measured through mechanical analysis)¹⁶ of the sample.

The detection of the T_g is essential for materials scientists, particularly for those developing new materials that may be exposed to a range of temperature environments. For example should a material be required as a dampener (a component to reduce mechanical strain) the desirable properties of the polymer would be to have it in a more flexible and rubbery state. If the material existed below its T_g then it would not have the desired dampening effect. By knowing the T_g and the application environment the material can be designed to ensure best performance without risk of material failure.

In addition to T_g , DSC can be used to detect enthalpic processes such as the melting point (T_m) and the crystallisation point (T_c). The combination of these values reveal how polymers will behave over a temperature range which can be of critical importance depending on the application the polymer is used for.

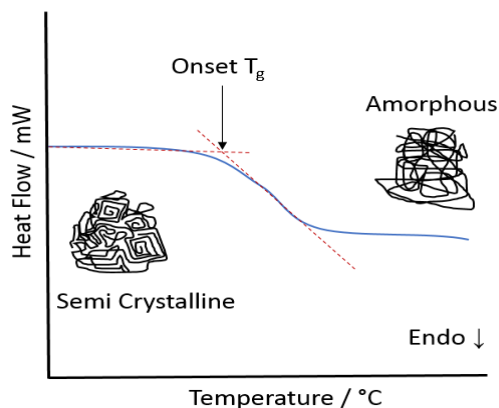


Figure 4.1 Representation of structural change in a polymer through the glass transition (T_g) as monitored through DSC analysis. Areas of crystallinity are removed as the sample becomes amorphous.

TGA is often used to evaluate the thermal stability of polymers with the onset of degradation being a critical value. In some cases, the degradation onset temperatures under both oxidative and inert atmospheres are compared with the latter typically being higher.¹⁷ In addition to determining degradation onset, TGA can be used to evaluate degradation kinetics to allow calculation of activation energies for oxidative or pyrolytic decompositions. This is of particular importance to the study of biopolymers as potential fuel feedstocks.¹⁸

Particular focus has been directed in recent years to the growing impact that synthetic polymers are having on the environment as a whole. Plastic pollution of the sea has attracted considerable interest with global incentives devoted to tackling this problem.¹⁹ Recent studies have also detected micro plastics in bottled drinking water²⁰ although the effects of these on human health is yet to be evaluated.²¹ There are also concerns about plasticisers-incorporated into many polymers, such as phthalates which have been detected leaching from plastic beverage bottles.²²⁻²³

4.1.1 Aims

The aims of this work were:

- To use HDM to evaluate common polymers physically and chemically.
- To investigate optical information gained during thermal processes of polymers including T_g , T_c and T_m .
- To compare HDM against existing DART-MS literature for silicone polymers

4.2 Polymer standards evaluation using HDM

The ability of HDM to monitor various changes in three common polymers (polystyrene (PS), polyethylene terephthalate (PET) and polyvinyl alcohol (PVOH)) as they are heated was evaluated.

4.2.1 Polystyrene (PS)

Polystyrene is made up from monomers of styrene (see Figure 4.2). It has been widely studied using thermal analysis with DSC being used to determine T_g and T_m . TGA reveals that polystyrene shows thermal stability past its melting point when under nitrogen, but rapidly decomposes in an oxidative atmosphere shortly after it starts to melt.²⁴

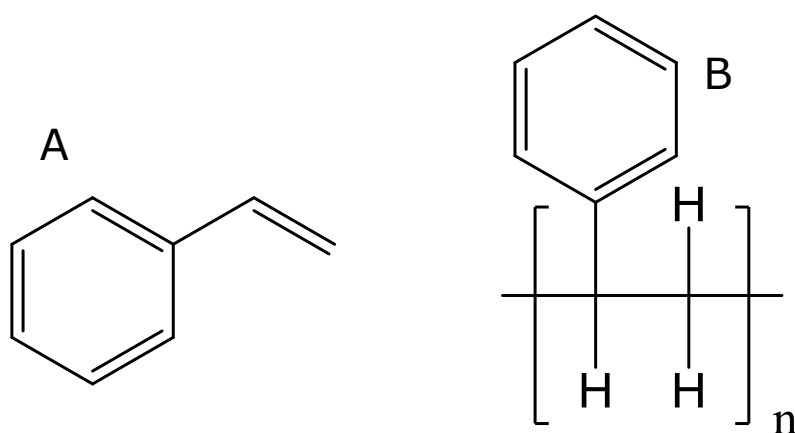


Figure 4.2 Structural representation of; A) styrene, B) polystyrene.

HDM analysis of polystyrene was performed using the following conditions;

A piece of polystyrene (4.36 mg, Average MW 250 kg mol⁻¹, Acros) was placed within a standard Inconel DSC pan and heated at 5 °C min⁻¹ between 30 and 285 °C. Images were taken throughout at 5 °C intervals whilst the mass spectrometer and DART were operated in positive mode.

Figure 4.3 shows the average mass spectral profiles of polystyrene over a range of temperatures. Repeating units can be shown for oligomers (both cyclic and linear) as their protonated molecular ions, with clusters of fragments accompanying each oligomer. It can be seen that higher molecular mass polymer fragments are observed with increasing temperature. In addition, at lower temperatures the mass peaks are sharper and better defined while with increased temperature peaks become broadened. This effect is attributed to an increase in the number of different fragments sharing similar nominal masses produced by thermal degradation and other reactions.

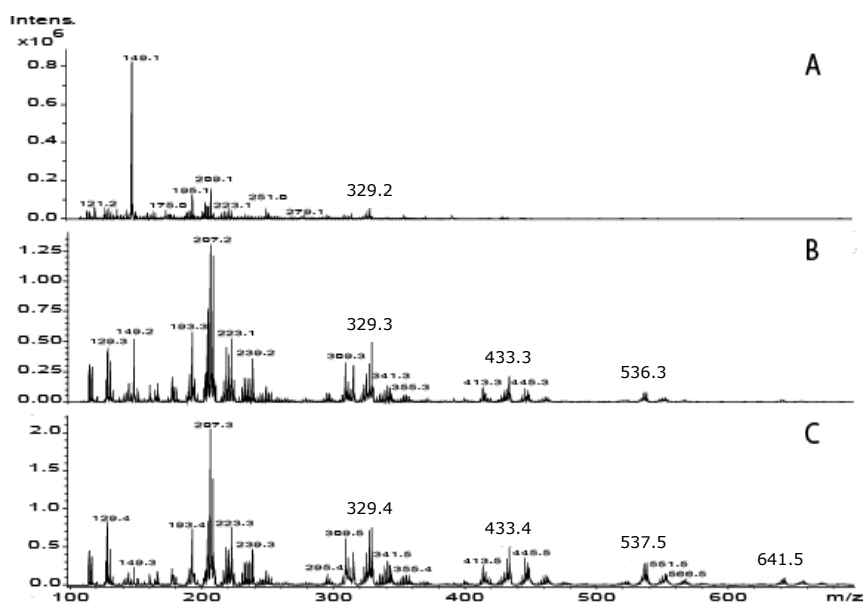


Figure 4.3 Average mass spectra of polystyrene over selected temperature ranges. A) 195 to 225 °C, B) 225 to 255 °C and C) 255 to 285 °C.

Figure 4.4 shows the total ion count (TIC) as a function of temperature. During the initial heating process very few ions are observed and the TIC gives a steady baseline. However, as the polystyrene starts to melt and decompose the number of fragments increases sharply. This experiment is in general agreement with the previous literature reported by Fernandes *et al.* who used TGA to monitor the degradation of polystyrene.²⁴

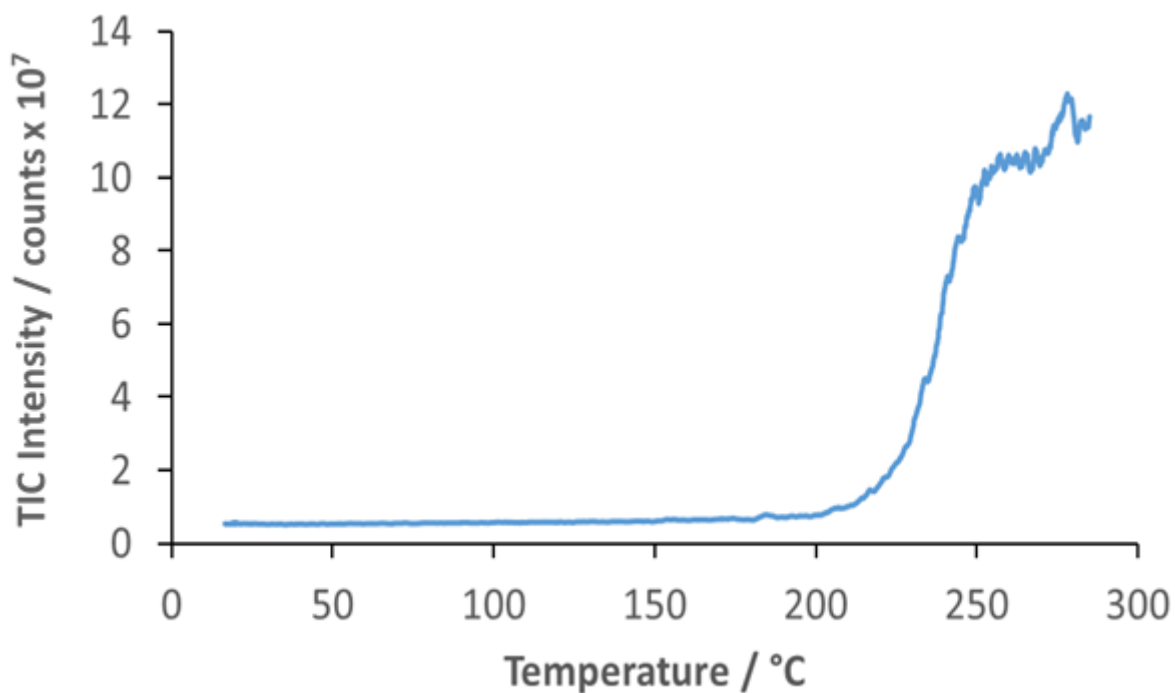


Figure 4.4 HDM analysis showing total ion count as a function of temperature for polystyrene.

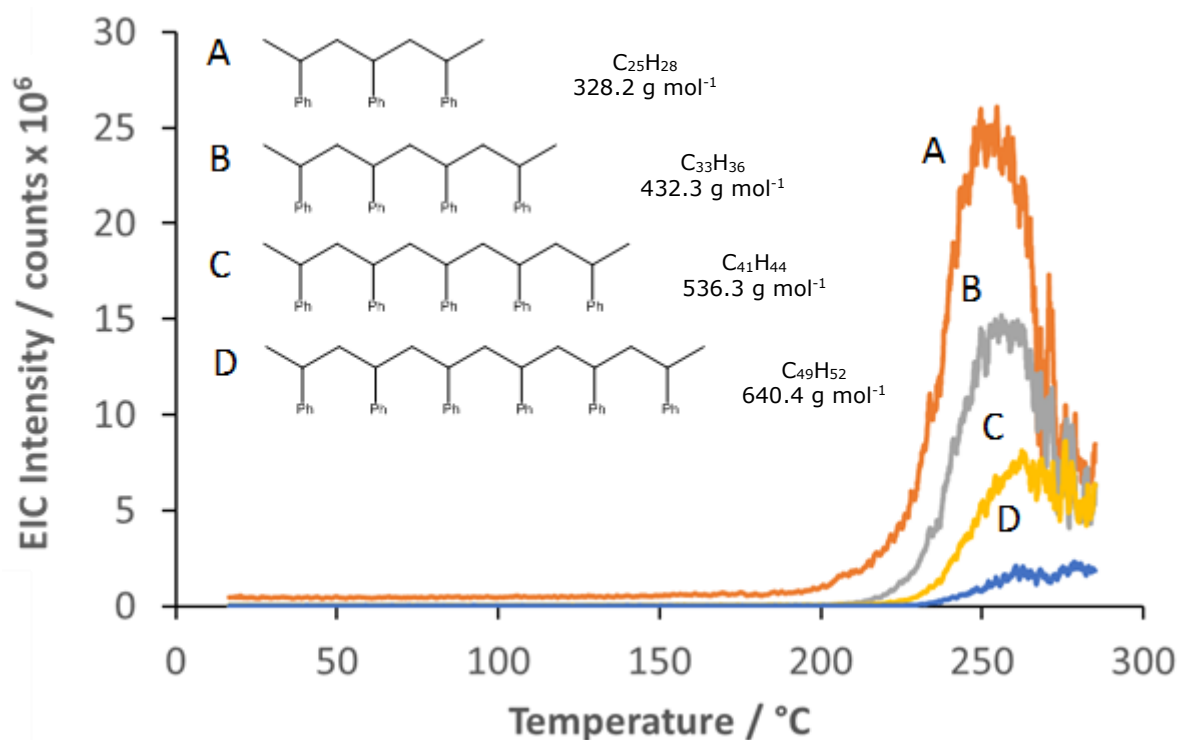


Figure 4.5 Selected EICs for polystyrene oligomers plotted as a function of temperature with associated structures. A) $C_{25}H_{28}$ $[M+H]^+$ 329 Da, B) $C_{33}H_{36}$ $[M+H]^+$ 433 Da, C) $C_{41}H_{44}$ $[M+H]^+$ 537 Da and D) $C_{49}H_{52}$ $[M+H]^+$ 641 Da.

Figure 4.5 is similar to figure 4.4 but showing the appearance of various oligomers as the polystyrene decomposes. Again, little is detected until the onset of melting at 200 °C.

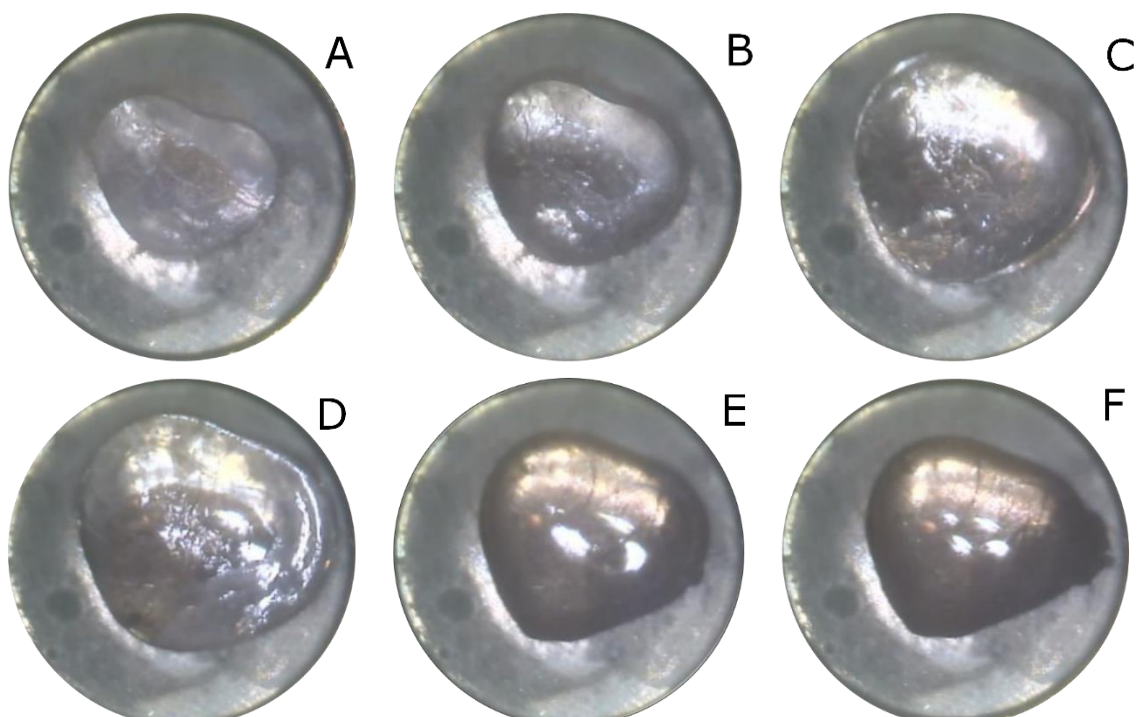


Figure 4.6 Micrographs of polystyrene during HDM analysis. A) 100 °C, B) 120 °C, C) 220 °C, D) 230 °C, E) 240 °C and F) 280 °C.

Figure 4.6 shows selected micrographs taken during the experiment. The glass transition at 110 °C is revealed in the small change in both opacity and volume of the sample in micrographs A and B.

Micrographs C to E show the melting which, since the sample was relatively large, appears to start at the bottom and move upwards. Maximum transparency is observed when the whole sample is in liquid form but a faint brown colour is apparent (micrograph F) as degradation products form (as detected by the mass spectrometer).

Figure 4.7 shows the ΔRGB colour profile for the experiment. It can be seen that it is highly complementary to the events observed in the micrographs with the T_g and T_m (extrapolated at the onset at 112 °C and 238 °C respectively) clearly apparent. T_g shows an apparent gain in colour but is likely due to the polymer expanding during the relaxation process. T_m however, shows the event as a further step change, the micrographs aided with the absolute melting point determination. A small event is noted around 190 °C, this has been correlated to a small shift in sample location within the analysis pan. T_g and T_m are in close agreement with the literature values of 113 and 240 °C respectively.²⁴

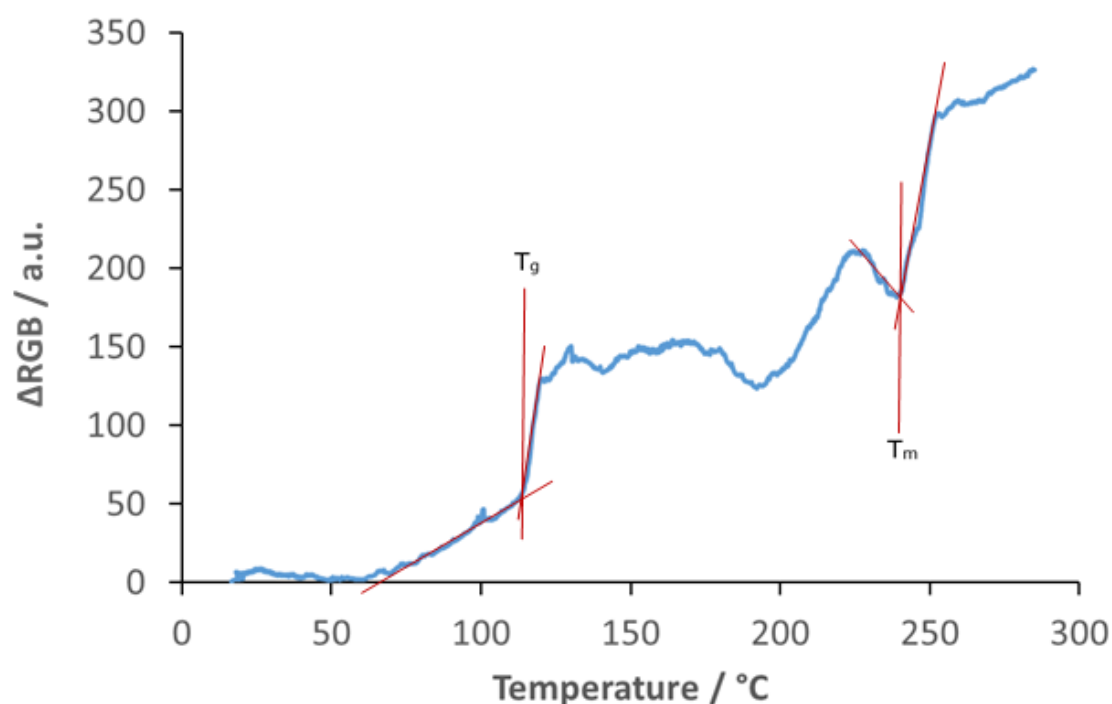


Figure 4.7 Total colour change ΔRGB as a function of temperature for polystyrene.

HDM was successfully applied to monitoring the key processes during the analysis of polystyrene. The HDM mass spectral profiles obtained for polystyrene are only apparent subsequent to the polymer melting around 200 °C. Optically, the micrographs and colour traces show the glass transition and melting point of the polymer. The micrographs also show an increase in the brown colour as the polymer begins to degrade.

4.2.2 Polyethylene terephthalate (PET)

Polyethylene terephthalate (PET) is one of the most commonly used thermoset plastics globally and is industrially synthesised from terephthalic acid and ethylene glycol.²⁵ PET is mainly used for food containers and drinks bottles. Figure 4.8 shows the structural representation of PET and its monomer bis(2-hydroxyethyl) terephthalate.

Yoshii *et al.* performed DSC analysis of PET and identified several key features; $T_g = 75$ °C, $T_c = 110$ °C and $T_m = 240$ °C (based on average MW 25 Kg mol⁻¹).²⁶ Bandyopadhyay *et al.* used TGA to show that PET exhibits thermal stability until *ca.* 400 °C under both inert and oxidative atmospheres (based on a 10% mass degradation step).²⁷

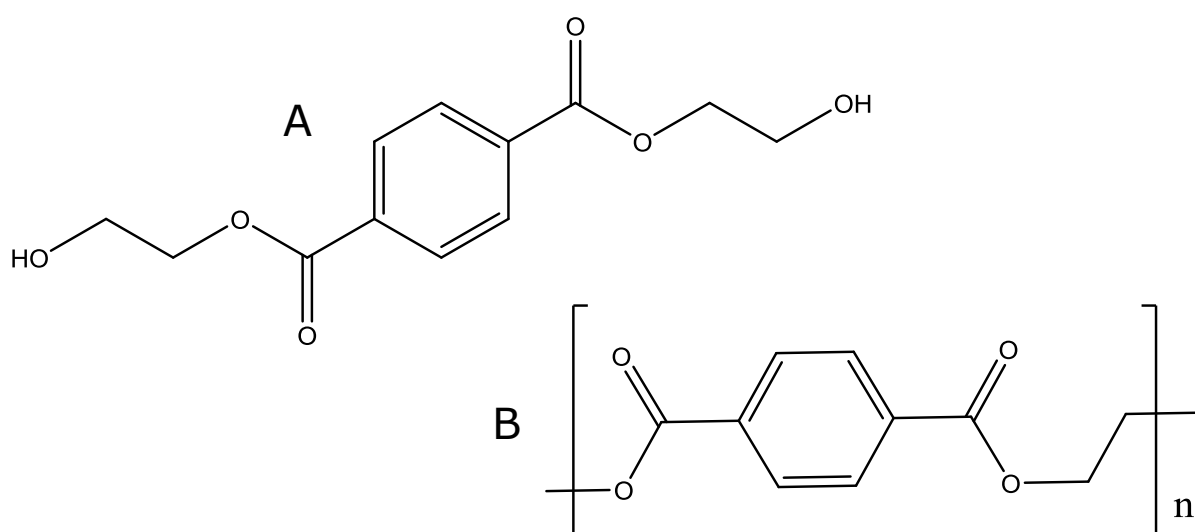


Figure 4.8 Structural representation of; A) bis(2-hydroxyethyl) terephthalate, B) polyethylene terephthalate.

HDM analysis of PET was performed using the following conditions:

A sample of PET (3.68 mg, Average MW 280 kg mol⁻¹, Aldrich) was placed within a standard Inconel DSC pan and heated at 5 °C min⁻¹ between 30 and 280 °C. Images were taken throughout at 5 °C intervals whilst the DART and MS were operated in positive mode.

Selected average mass spectra from the HDM analysis of PET are shown in Figure 4.9. During the initial stages of heating (A) minimal peaks are observed, the large peak at 149 Da is attributed to a common background phthalate ion that does not solely originate from the sample and is commonly observed throughout MS analysis. Further heating initiates the decomposition process with fragments corresponding to PET rising above background levels (B). The major peak at 594 Da has been attributed to the ammoniated molecular ion of the cyclic trimer of PET and has been noted to be the most dominant of the PET cyclic oligomers.²⁸ A key degradation product of PET has been shown as the protonated molecular ion 193 Da,²⁹ along with other key related degradation products discussed later. These main peaks increase in intensity as the temperature increases (C).

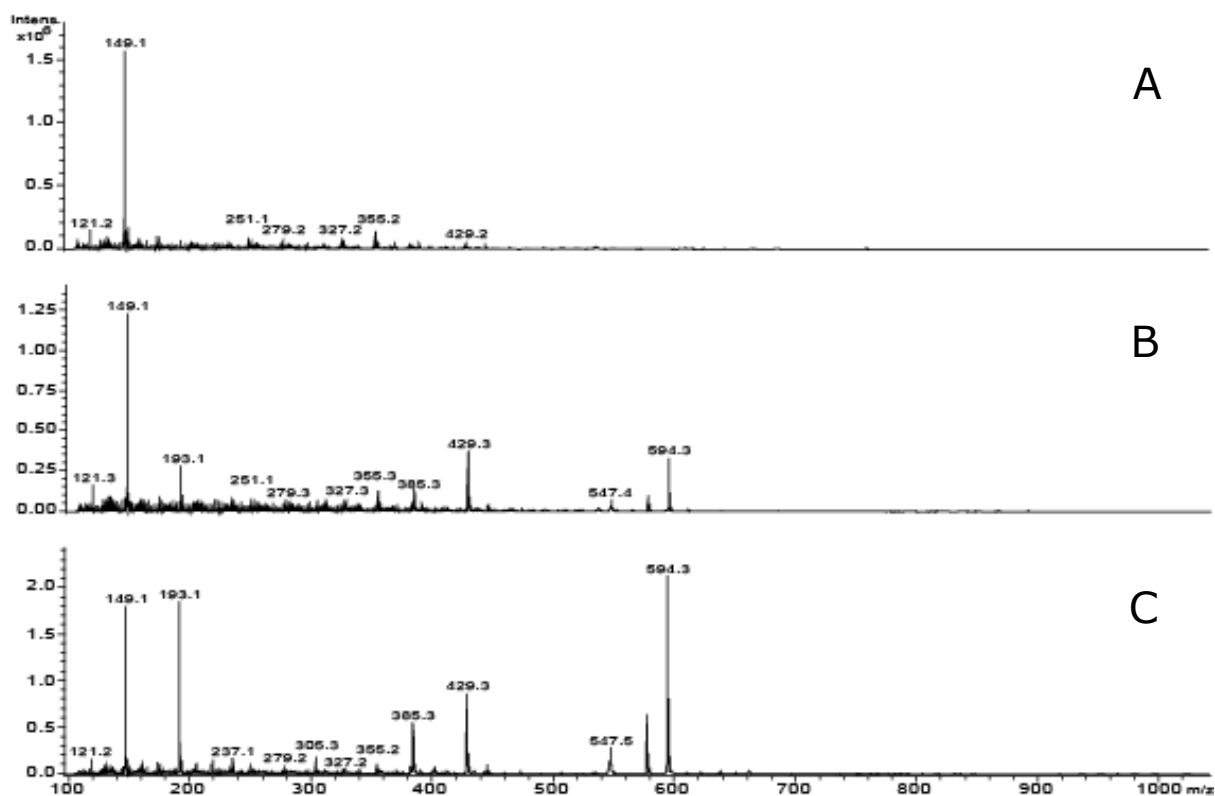


Figure 4.9 Average mass spectra of PET over selected temperature ranges. A) 220 to 240 °C, B) 240 to 260 °C and C) 260 to 280°C.

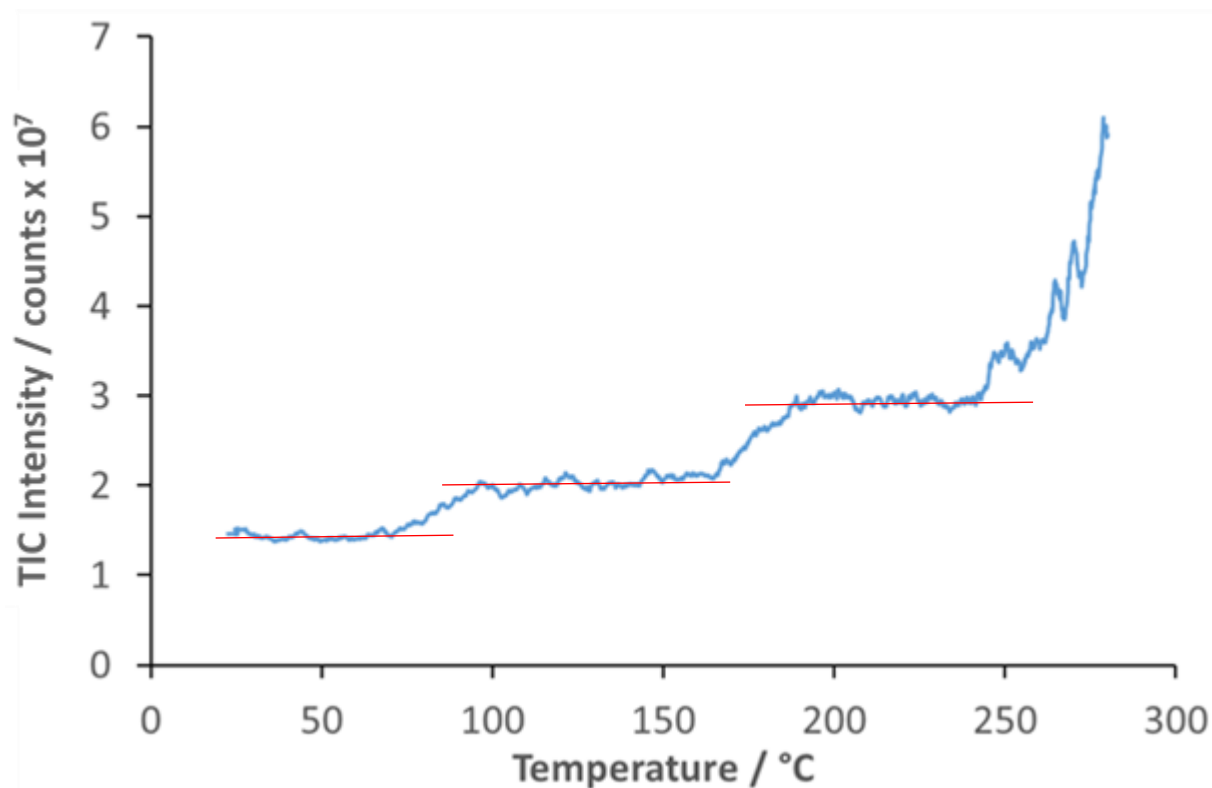


Figure 4.10 Total ion count as a function of temperature for PET. Red lines are included to show step changes observed around key thermal events.

Figure 4.10 shows the total ion count of PET as a function of temperature. A small rise in intensity is shown at 70 °C which has been attributed to a release of unassigned polymer products during the softening stage as the material goes through its glass transition. At 160 °C a step increase is shown as existing small chain oligomers are thermally desorbed from the bulk material. Further heating past the melting point (*ca.* 240 °C) produces a sharp increase in overall profile as the PET begins to decompose. These features have been tentatively assigned as further reproducibility studies are required.

Key fragments for PET were identified from the literature and their EIC's plotted as a function of temperature as shown in Figure 4.11. As with polystyrene, most species are only apparent once the PET has melted with relatively little noted before this event. Profiles A and B (ammoniated cyclic trimer and protonated vinyloxy species) show a steep rise in intensity as the PET melts, whilst C and D (protonated linear degradation product and protonated cyclic dimer) are produced follow a similar profile but at a lower overall intensity.

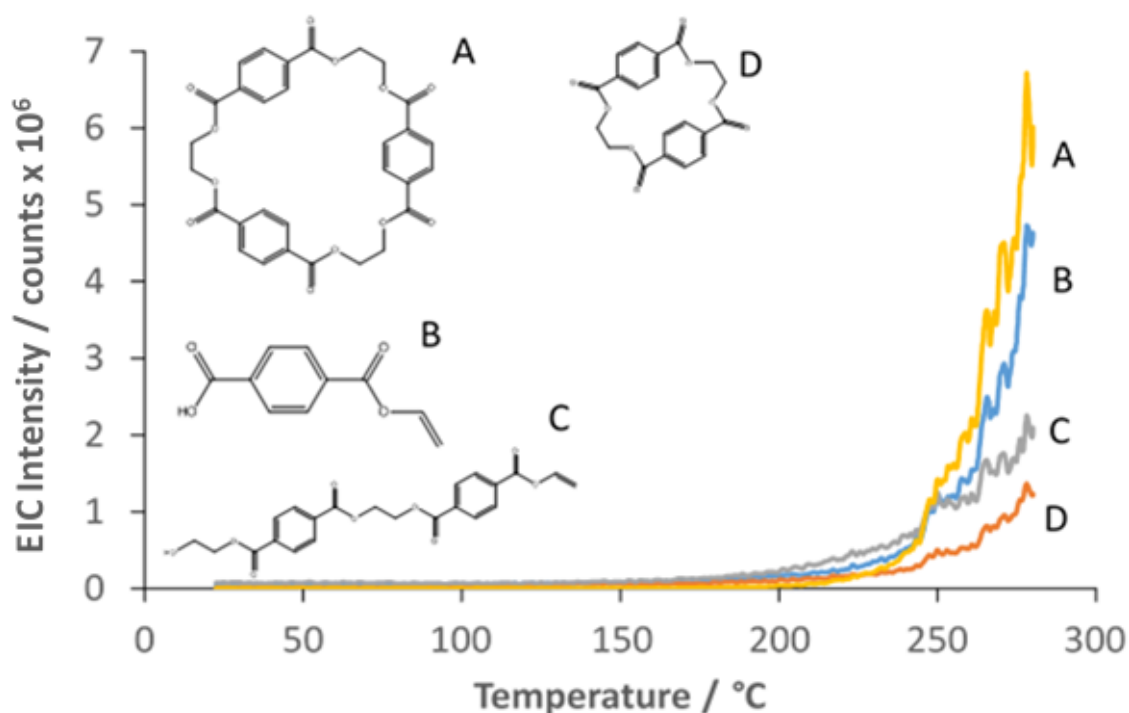


Figure 4.11 Selected EICs for PET analytes plotted as a function of temperature with associated structures. A) $C_{30}H_{24}O_{12} [M+NH_4]^+$ 594 Da, B) $C_{10}H_8O_4 [M+H]^+$ 193 Da, C) $C_{22}H_{20}O_9 [M+H]^+$ 429 Da and D) $C_{20}H_{16}O_8 [M+H]^+$ 385 Da.

The Δ RGB colour profile (Figure 4.12) shows some key physical events that can be linked to the micrographs (Figure 4.13). A softening of the PET material is shown at 59.6 °C which has been attributed to T_g , micrographs A-B show this subtle softening effect as the material slightly expands showing a 4.1% increase in total area covered using dimensional analysis. T_g is monitored through a step change in colour as in Figure 4.7. A cold

crystallisation (T_c , an event that occurs between T_g and T_m when the polymer has sufficient energy to change from its amorphous form to crystalline) is shown at 130.6 °C, (micrographs C-F) and the slightly transparent PET becomes opaque as the crystals form shown by the 'dip' in the ΔRGB profile. The final melt of PET is shown at 248 °C (micrographs G-H) as the opaque PET becomes transparent and melts, giving a very sharp signal in the ΔRGB profile. These values appear close to the literature value quoted by Yoshii *et al.* although it is worth noting the significant difference in molecular weight of the polymers compared 25 vs 280 kg mol⁻¹.

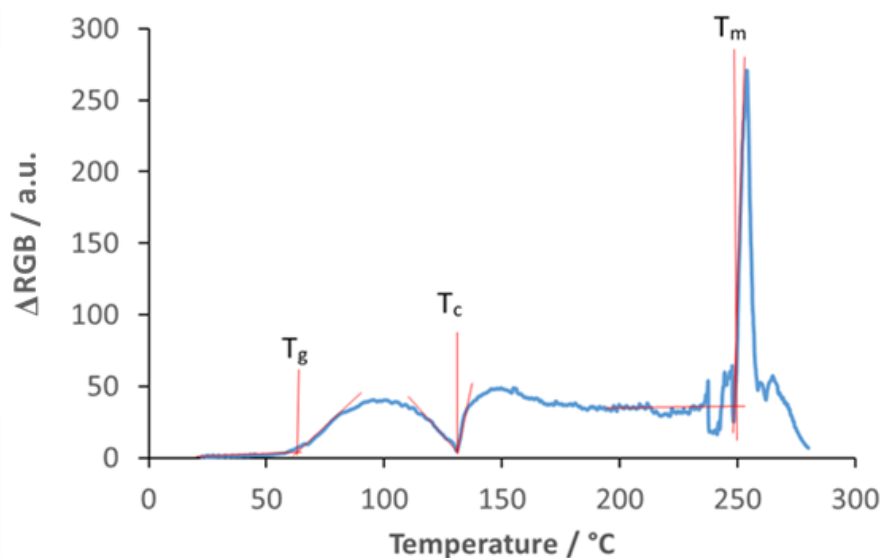


Figure 4.12 Total colour change ΔRGB of PET monitored as a function of temperature.

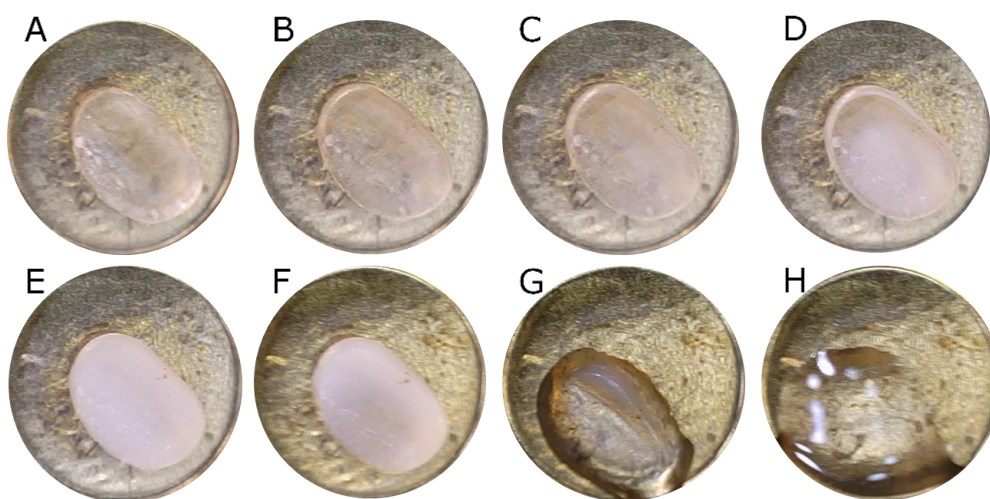


Figure 4.13 Micrographs of PET during HDM analysis. A) 50 °C, B) 90 °C, C) 100 °C, D) 120 °C, E) 130 °C, F) 140 °C, G) 240 °C and H) 250 °C.

HDM has successfully managed to monitor three key thermal events related to PET, T_g , T_c and T_m as observed through micrographs and colour profiles. The mass spectra generated are in agreement with commonly observed degradation products of PET shortly after T_m .

4.2.3 Polyvinyl Alcohol (PVOH)

Polyvinyl alcohol (PVOH or PVA) is a polymer and is extensively used in industry as a wood adhesive and is also exploited for its water soluble material properties. However, PVOH exhibits poor thermal properties when compared to many other polymers. Industrially PVOH is manufactured by the vinyl acetate monomer being converted to the polymer through free radical reaction forming polyvinyl acetate. This polymer is further reacted with sodium methoxide to yield the desired PVOH. Figure 4.14 shows the reaction mechanism and key species.

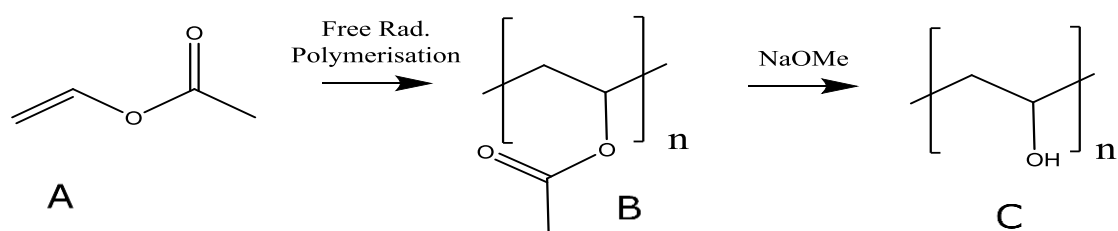


Figure 4.14 Structural representation of, A) Vinyl acetate monomer, B) Polyvinyl acetate precursor and C) Polyvinyl alcohol and their position in the overall polymerisation processes.

Holland and Hay performed thermogravimetric analysis of PVOH and showed that some mass is lost before the melt (*ca.* 5%, 200 °C) which they attributed to water losses through polymer dehydration with significant degradation occurring when the polymer melted around 230 °C.³⁰ The authors also studied PVOH with DSC and observed similar trends, an endothermic process was observed prior to the melt, and they also attributed a reaction forming a range of polyalkenes to the dehydration process.

A piece of PVOH (3.85 mg, Average MW 80 kg mol⁻¹, 99% hydrolysed, Aldrich) was placed in a standard Inconel DSC pan and heated at 5 °C min⁻¹ between 30 and 260 °C. Images were taken throughout at 5 °C intervals whilst the mass spectrometer and DART were operated in positive mode.

Figure 4.15 shows a series of average mass spectra from different stages of the analysis. The overall intensity rises attributed to a range of thermal decomposition products shown from A-C. Masses are mainly noted over the 100-500 Da range typically separated by 2 Da.

Many ions are observed therefore it is difficult to formally assign them (and more importantly be able to discriminate them without more advanced MS methods such as MSⁿ being used). For this reason the total ion count (TIC) alone is plotted (see Figure 4.16) without any extracted ion profiles as with the polystyrene and PET. An initial rise in profile is noted around 200 °C this is expected to be linked to the onset of thermal decomposition. A final sharp step is observed in the profile as the sample melts and the thermal decomposition products are released from the solid.

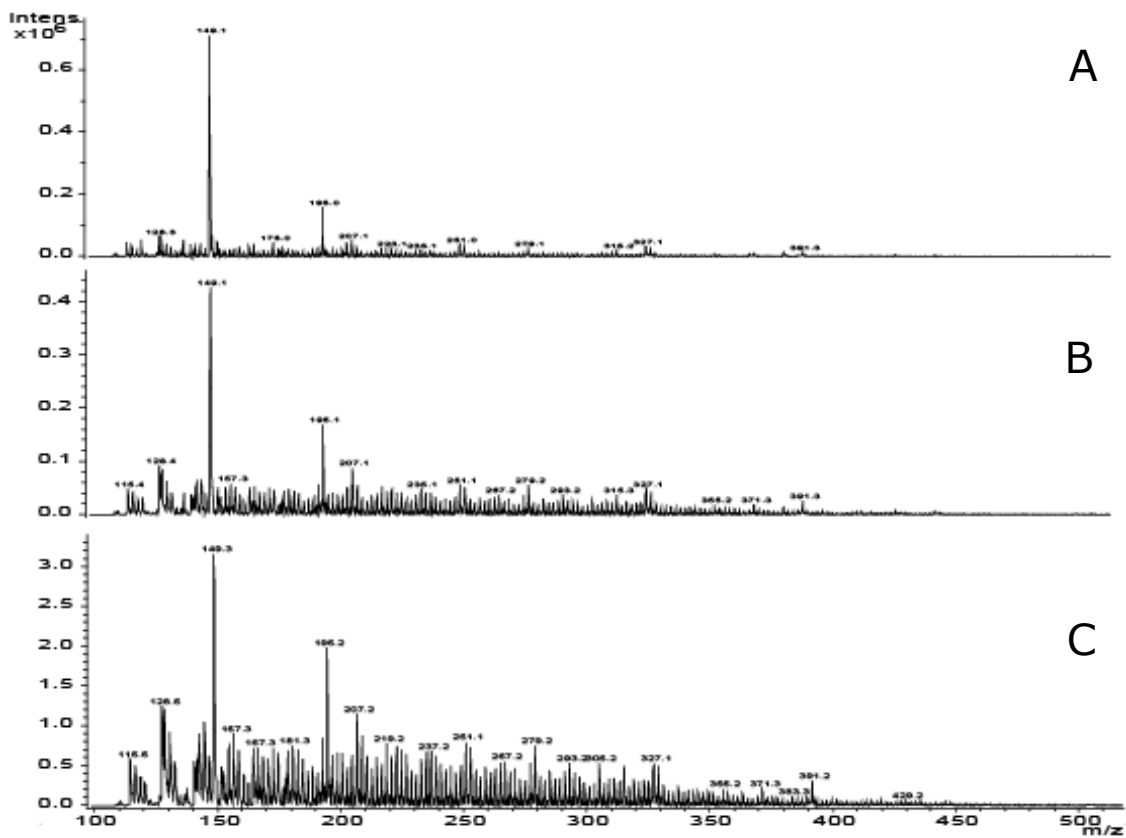


Figure 4.15 Average mass spectra of PVOH over selected temperature ranges. A) 180 to 200 °C, B) 200 to 220 °C and C) 220 to 260°C.

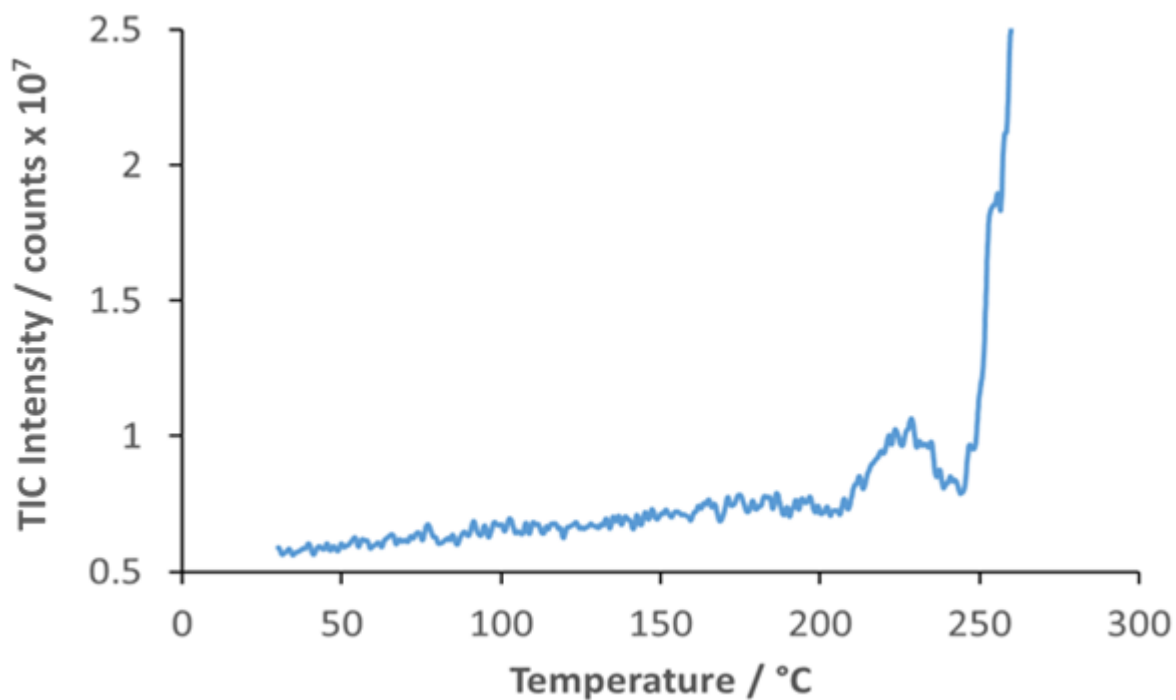
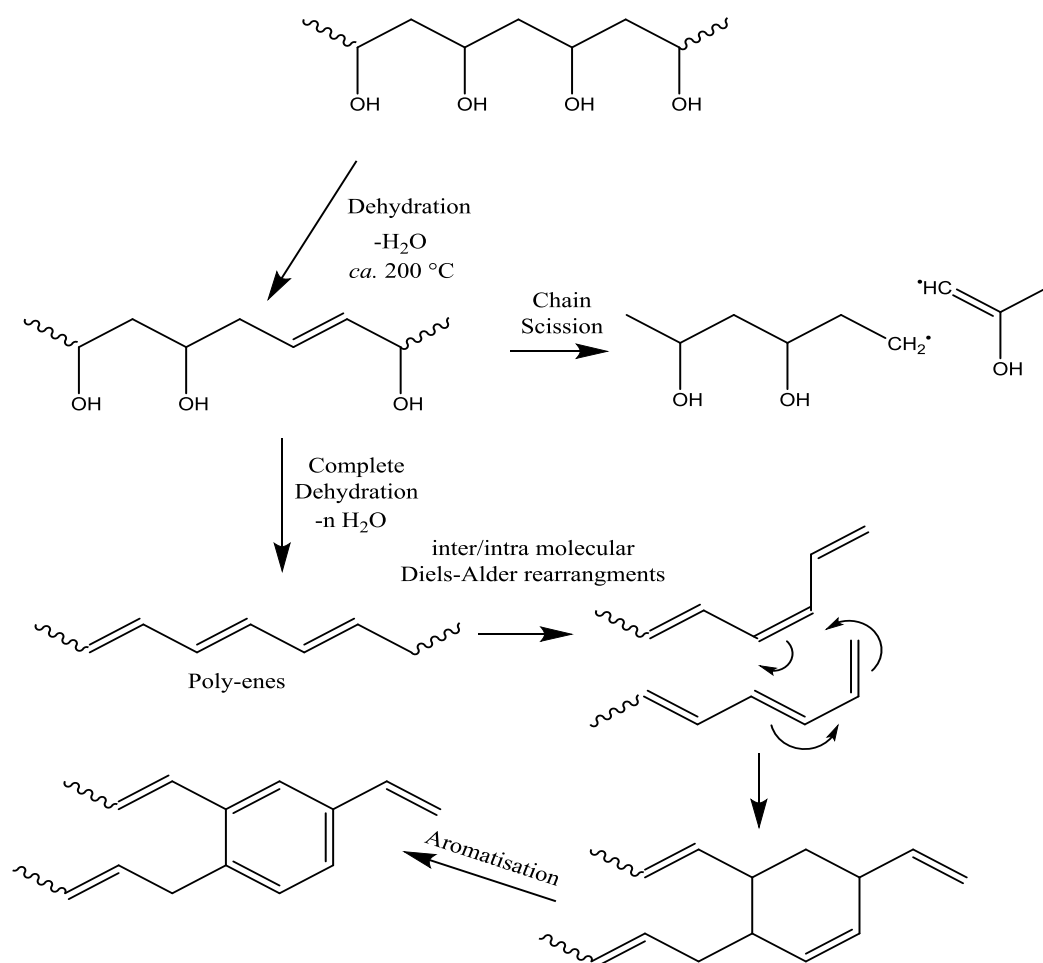


Figure 4.16 Total ion count as a function of temperature for PVOH.

Pandey *et al.* investigated some of the routes that the decomposition of PVOH may take.³¹ The findings are presented in Schematic 4.1 as a degradation schematic. It is clear that a large number of products may be formed many having overlapping nominal masses which explains the complexity of the mass spectra. Yang *et al.* noted that the extent of hydrolysis of the starting polymer directly relates to the extent of decomposition, that is, the more hydroxyl groups on the starting polymer the more likely the PVOH will be thermally driven to complete decomposition.³²



Schematic 4.1 Possible thermal PVOH decomposition routes. Adapted from³¹

Figure 4.17 shows the Δ RGB colour profile as a function of temperature and Figure 4.18 shows selected micrographs for the experiment. As the PVOH is heated it appears thermally stable between 30 and 180 °C (micrographs A-B). At around 200 °C the sample shows a slight yellow discoloration (micrograph C) and the Δ RGB profile begins to increase. This colour change continues up until the melting point of the PVOH, as the sample begins to turn brown (micrograph D). As the melting point is reached around 240 °C a further change is shown in the Δ RGB colour profile as the sample becomes much more reflective (see micrographs E-G).

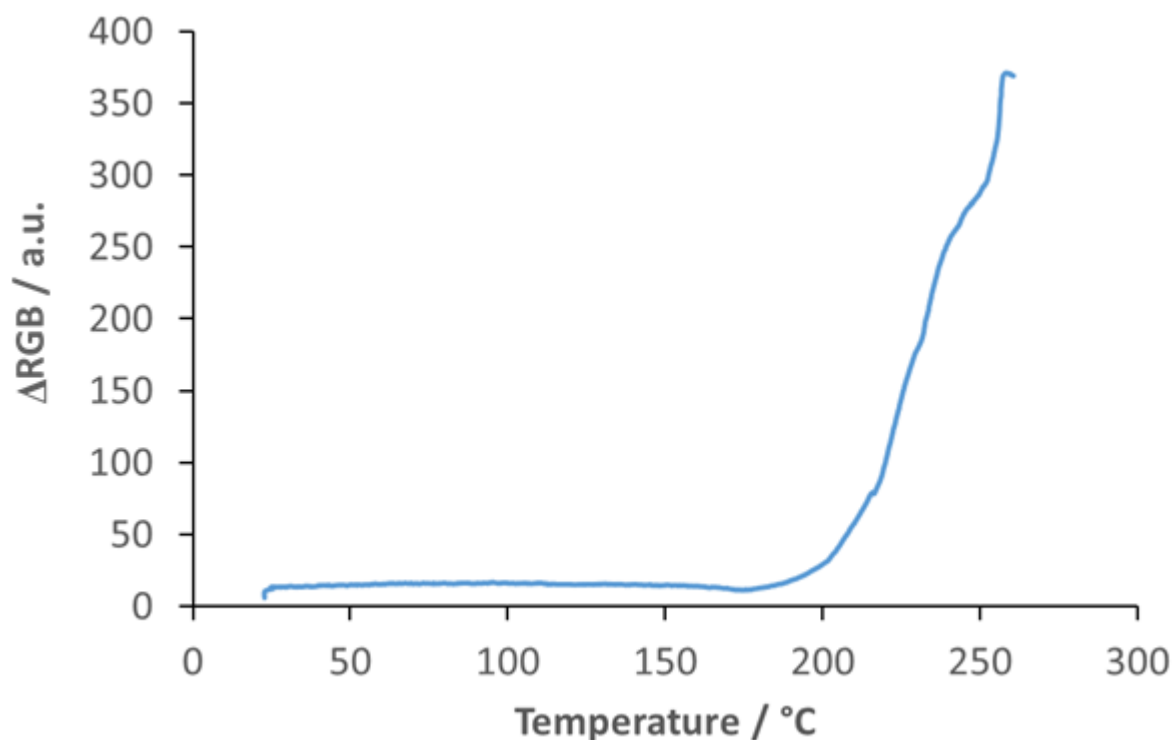


Figure 4.17 Total colour change (ΔRGB) as a function of temperature for PVOH

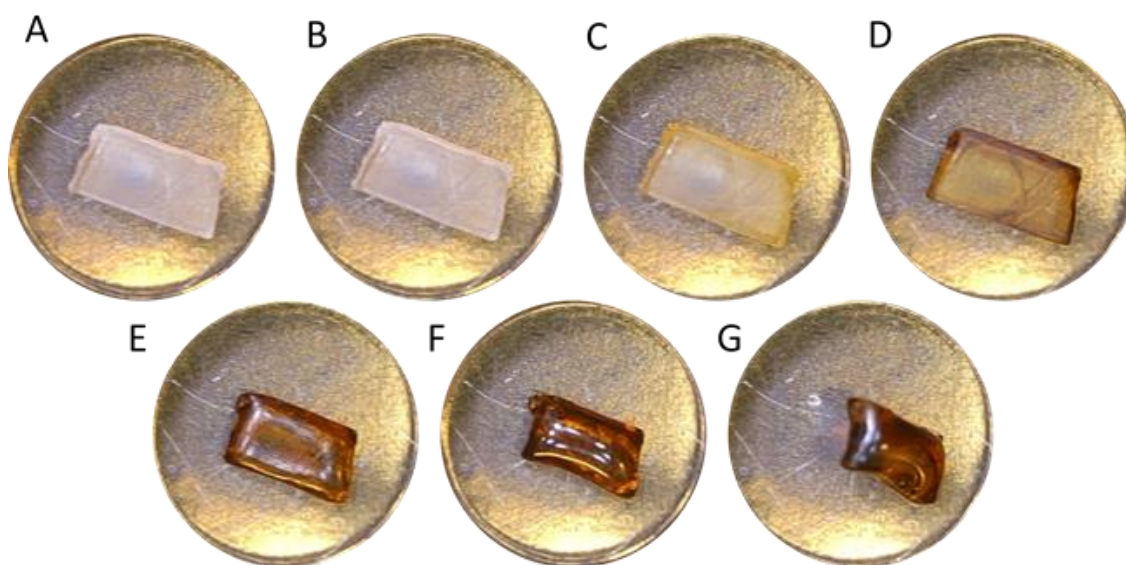


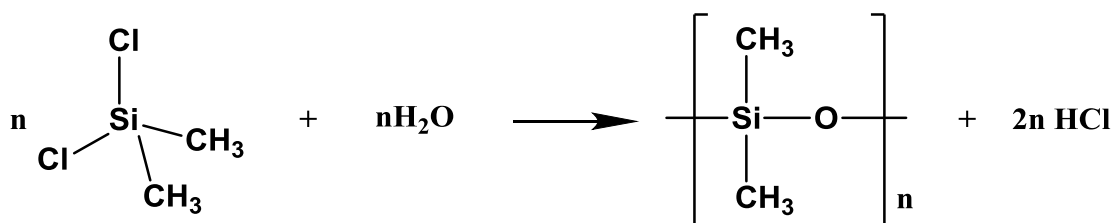
Figure 4.18 Micrographs of PVOH during HDM analysis. A) 30 °C, B) 150 °C, C) 200 °C, D) 230 °C, E) 240 °C, F) 250 °C and G) 260 °C.

HDM appeared to follow the complete decomposition of the PVOH, but the complex nature of the mass spectral profile made it difficult to propose structures of evolved products. However, the optical components of HDM performed well for the analysis of PVOH, monitoring the degradation of the sample before the melt.

4.3 HDM and silicone polymers

After the initial evaluation of HDM with polymers, a more detailed study of silicone polymers was undertaken. This work was partly inspired by the findings of Gross who, using DART-MS, reported that on heating a variety of domestic silicone polymers, oligomeric species were evolved.³³ Further investigations into silicone bakeware made of polydimethylsiloxanes (PDMS) revealed that these oligomers could migrate into food cooked using these products.³⁴ It is still unclear about the long term effects that these oligomers might have on the human health, although PDMS samples with molecular weights above 1 Kg mol⁻¹ have been shown to be non-bioavailable and are typically thought to be too large to pass through the lipid bilayer of cell membranes when investigated in the marine environment.³⁵

PDMS contains the standard -Si-O- backbone present in all silicone polymers and is synthesised by the hydrolysis of the monomer dimethyldichlorosilane (Schematic 4.2). Other silicone polymers vary by the numbers and types of aryl or alkyl chains attached to the silicon atom. Typically, silicones are used above their glass transition temperatures giving them the desired rubbery and flexible properties.



Schematic 4.2 Hydrolysis of dimethyldichlorosilane to form the PDMS polymer.

Following on from the work of Gross, it was decided that silicone polymers would be an excellent system for a comparative study between HDM and conventional DART-MS. Gross was restricted in both the temperature control and the sample positioning. It was hoped that the repeatable sample positioning and greater control of the heating provided by HDM would allow for improved temperature profiling of single pieces of silicone.

Most of the experiments in this section utilised a green silicone egg poacher (*Kitchen Corner, Birmingham, UK*) purchased from a local store. The sample was selected for its colour which provided a large contrast against the background of the pans used with HDM which, although not essential, was beneficial particularly with the experiments using optical methods to monitor changes in sample geometry (see Section 4.5). Analytical grade PDMS silicones may be purchased but due to their lack of colour were not purchased for this study, instead the commonly encountered bakeware silicones were used.

4.3.1 Initial experiment to replicate the work of Gross

The results of an initial experiment using the silicone and approximating the experimental conditions used by Gross with heating solely supplied by the DART-100 source are shown in Figure 4.19. *Samples of the silicone were held in front of the DART-100 at three temperatures (150, 250 and 350 °C) and the average MS profiles were obtained.*

It is worth noting that many experimental variations existed between these findings and those reported by Gross for example, different silicone polymers, different DART sources and different spectrometers. Nonetheless, the results obtained were similar to those of Gross with larger oligomeric species being released as at higher temperatures.

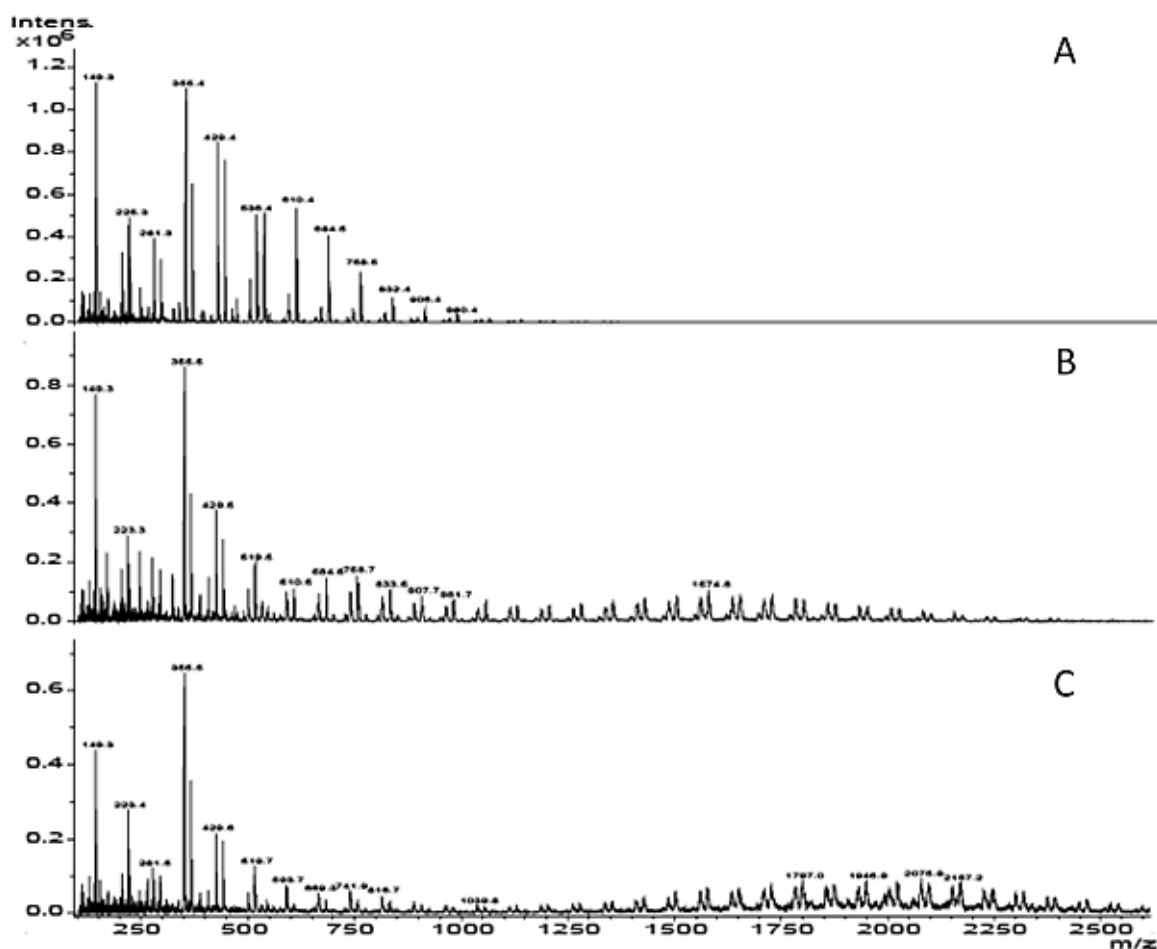


Figure 4.19 Average MS profiles from singular pieces of silicone bakeware at varying temperatures; A) 150 °C, B) 250 °C and C) 350 °C.

This is also consistent with the work of Fianingam who noted that higher molecular mass oligomers had lower vapour pressures which is a commonly observed feature for polymers.³⁶

Manufacturer's guidelines for these products suggest that they are washed and baked a few times before use in cooking presumably as a precaution that any residual semi-volatile products from the manufacturing process are removed, which may be observed here.

4.3.2 Isothermal step experiments using the HDM

The next experiments investigated stepping isothermally the temperature of the hot-stage and comparing the evolved species detected by the mass spectrometer over each isothermal period.

A sample of the silicone egg poacher (5 x 5 x 0.5 mm) was placed within a DSC pan (Inconel). A temperature programme comprising a series of 30 minute isothermal steps in 20 °C increments between 140 and 200 °C was used. Average mass spectra were obtained over each isothermal period. The DART-MS was operated in positive mode, as the ions were shown to exist in their protonated and ammoniated forms.

Figure 4.20 shows the average mass spectra of each isothermal period (A = 140 °C, B = 160 °C, C = 180 °C & D = 200 °C). As noted previously, increasing temperature produces higher molecular mass oligomers in the mass spectra. The mass spectra were relatively constant over the duration of each isothermal period although the overall intensity of the lower mass oligomers declined with continued thermal exposure.

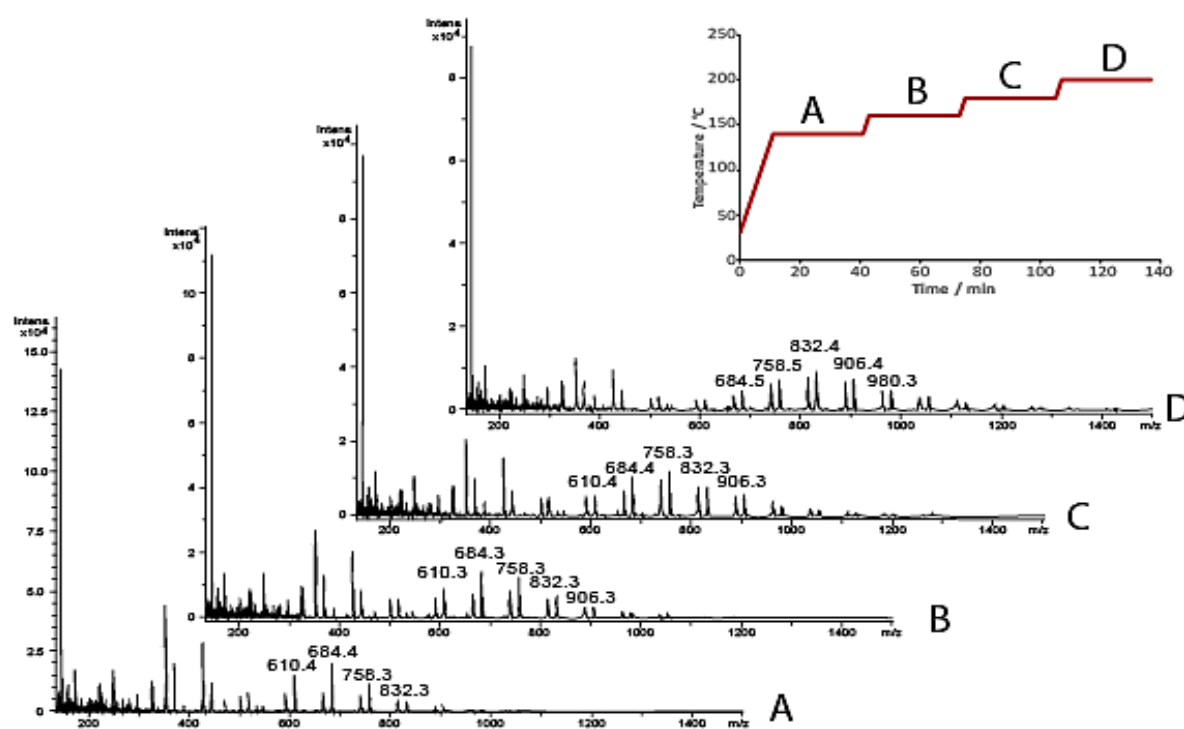


Figure 4.20 HDM isothermal profiling of silicone egg poacher. Insert Shows temperature profile. A) 140 °C isotherm with average MS, B) 160 °C isotherm with average MS, C) 180 °C isotherm with average MS & D) 200 °C isotherm with average MS.

4.3.3 Linear heating and cooling experiments

An experiment using a slower heating and cooling was performed, partly to demonstrate the temperature control of the HDM but primarily to determine if material continued to be removed from the polymers over longer exposure times to higher temperatures or if thermal treatment permanently removed the observed oligomers. An upper temperature of 200 °C was chosen to approximate what would be achieved during conventional cooking.

A sample of the silicone egg poacher (5 x 5 x 0.5 mm) was placed within a DSC pan (Inconel). The sample was subjected to a linear heating of 0.8 °C min⁻¹ between 30 and 200 °C followed by a linear cooling of 0.8 °C min⁻¹ from 200 °C to 50 °C. The DART & MS were operated in positive mode.

Figure 4.21 shows a plot of 4 extracted ions over the course of the experiment. For clarity, the figure is displayed as a function of time with the heating and cooling profile superimposed. The ammoniated molecular ions for each of the cyclic species [(SiC₂H₆O)_n + NH₄]⁺ where n= (A=9, B=10, C=11 and D=12) have been averaged so that each point represents approximately 300 data points.

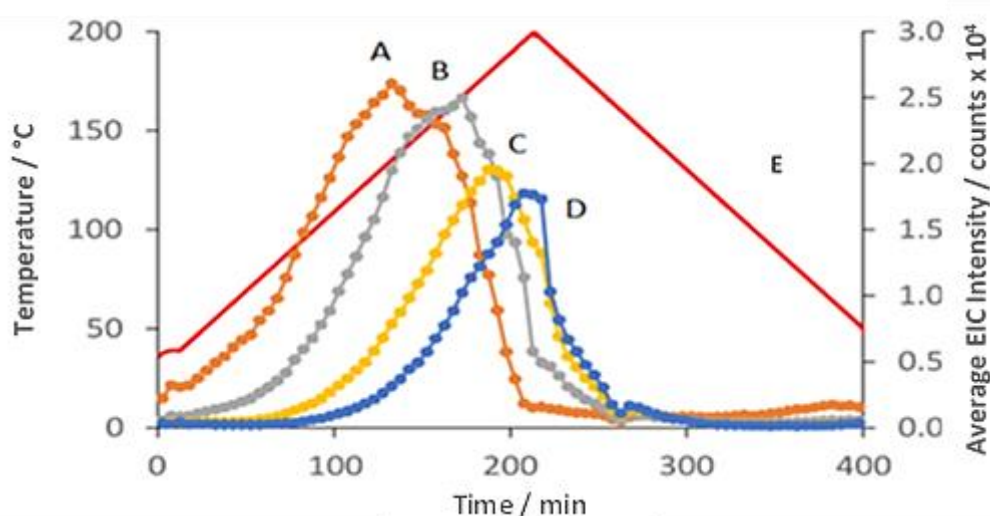


Figure 4.21 Thermal profiling of silicone polymers showing extracted ions monitored during heating and cooling. EICs; A) 684 Da [(SiC₂H₆O)₉ + NH₄]⁺, B) 758 Da [(SiC₂H₆O)₁₀ + NH₄]⁺, C) 832 Da [(SiC₂H₆O)₁₁ + NH₄]⁺, D) 906 Da [(SiC₂H₆O)₁₂ + NH₄]⁺ and E) Temperature.³⁷

The lowest selected molecular weight oligomer (A) was shown to be released and removed before the temperature had reached the maximum of 200 °C. This suggests that the oligomers can be 'thermally removed' and also that they are not the result of thermal decomposition within this temperature range. The same effect is noted for oligomers B and C both of which reach their maximum levels and begin to decline before the maximum temperature is reached. Oligomer D appears to have just reached its maximum level shortly before the cooling stage commences.

4.3.4 Cyclic isothermal step experiments

To further investigate the thermal removal of the oligomeric material from the silicone a similar experiment to the original isothermal stepping experiment (Section 4.3.2) was set up but incorporating repeated heating cycles.

A sample of silicone egg poacher (5 x 5 x 0.5 mm) was cut and placed in a DSC pan (Inconel). A complex temperature programme comprising a series of 30 minute isothermal steps in 20 °C increments from 140 to 200 °C and then 200 to 140 °C was used. This temperature programme was cycled a total of three times. The DART and MS were operated in positive mode

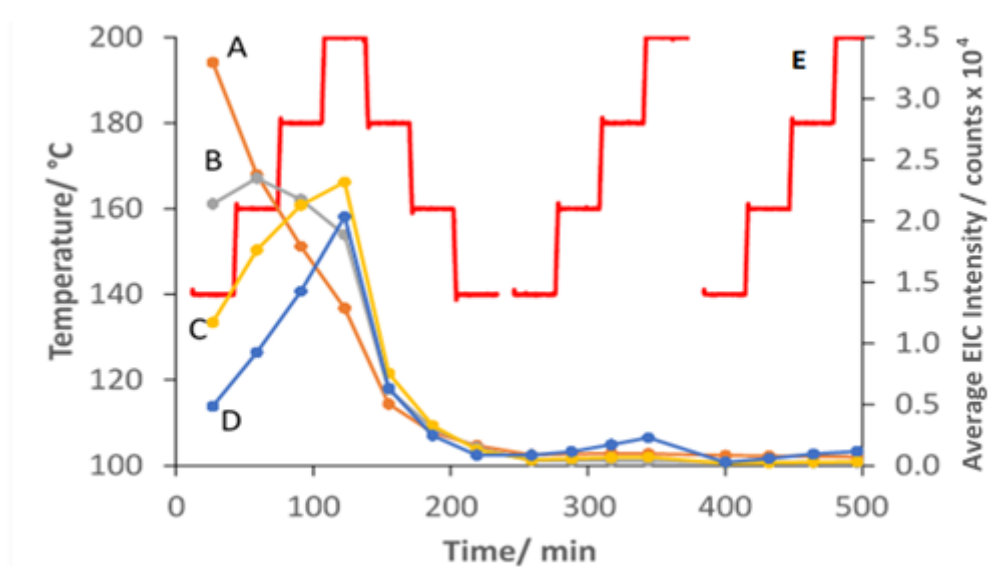


Figure 4.22 Cycled isothermal stepping of silicone polymer, EICs; A) 684 Da $[(\text{SiC}_2\text{H}_6\text{O})_9 + \text{NH}_4]^+$, B) 758 Da $[(\text{SiC}_2\text{H}_6\text{O})_{10} + \text{NH}_4]^+$, C) 832 Da $[(\text{SiC}_2\text{H}_6\text{O})_{11} + \text{NH}_4]^+$, D) 906 Da $[(\text{SiC}_2\text{H}_6\text{O})_{12} + \text{NH}_4]^+$ and E) Temperature.

Figure 4.22 shows the results for the experiment with temperature profile and EICs plotted as a function of time. Each point represents the average intensity for that specific ion during the isothermal period. From the onset of heating, it can be seen that the intensity of oligomer A reduces. Subsequent heating steps do not show this oligomer and it is assumed to have been completely desorbed/removed during the first temperature cycle.

Similar profiles are obtained for oligomers B and C, during the initial heating the oligomers are shown to increase in intensity but this declines on cooling. No apparent increase is observed during subsequent heating cycles, again, suggesting the oligomers have been desorbed/removed. In contrast, oligomer D shows continued release as the temperature is increased, and reduction as the polymer is cooled. During the second and third heating cycles the oligomer shows a slight increase in profile intensity as heat is applied, but this becomes successively less with each cycle. This effect is attributed to an increase in the thermal lability of this higher mass oligomer as opposed to an increase in concentration resulting from thermal degradation.

4.3.5 Cyclic linear heating and cooling experiments

The previous experiment indicated that it was possible to permanently thermally desorb/remove material from the silicone by heating to 200 °C and that significant thermal degradation did not occur up to this temperature. To investigate whether an overall indication of the extent of oligomer removal could be determined using the TIC a cyclic linear heating and cooling experiment was performed.

A sample of silicone egg poacher (4.0 mm d, 0.5 mm) was cut and placed in a DSC pan (Inconel). A temperature programme comprising heating from 30 °C to 200 °C and cooling from 200 °C to 30 °C, both at 5 °C min⁻¹, was used. This temperature programme was cycled a total of three times. The DART and MS were operated in positive mode with a TIC range of 600 to 2800 Da extracted. This range was chosen to include the masses of all materials likely to be produced by the polymer but exclude common background masses which typically fall below 600 Da with DART-MS. Integration was performed post analysis using Microsoft Excel. Integration was made between thermal cycles above the background 600 – 2800 Da level.

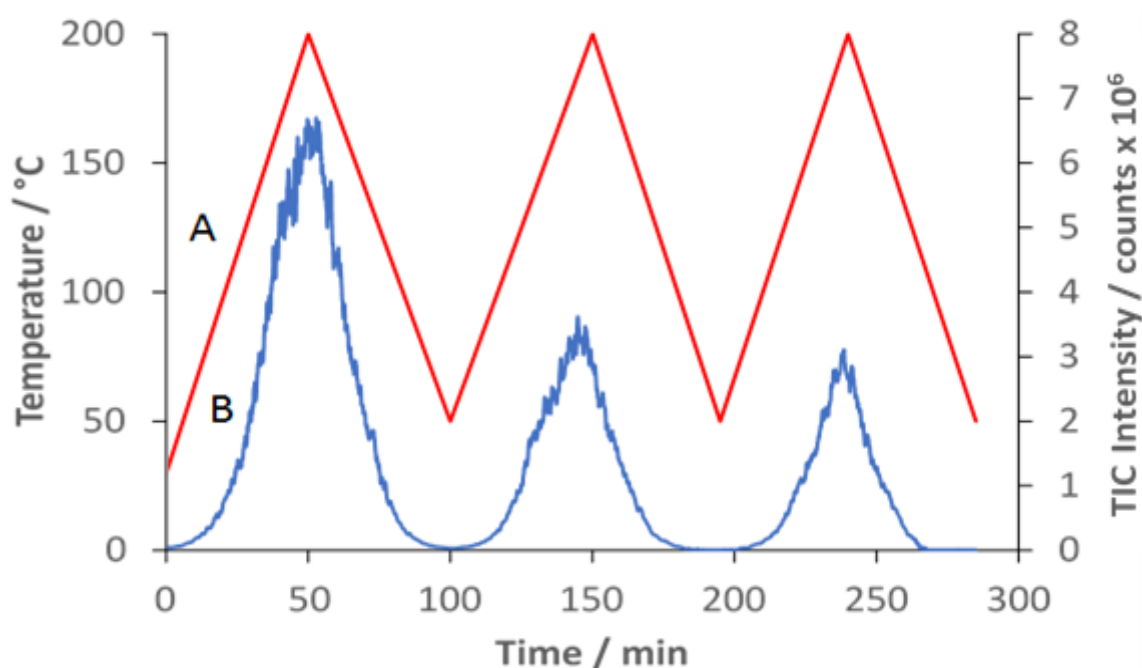


Figure 4.23 Thermal cycling of silicone polymer using HDM. A) Temperature and B) TIC range 600 – 2800 Da.

Figure 4.23 shows the TIC and temperature profiles as a function of time for the experiment. It can be seen that there is a reduction in overall intensity between heating cycles as shown in the previous examples. Integration of each peak area yields 215 x10⁶ count.mins, 99 x10⁶ count.mins and 70 x10⁶ count.mins respectively. This equates to a reduction between the first and second cycle of 54 % and overall a reduction of 67 % across the three cycles.

4.3.6 Cyclic linear heating and cooling experiments with pre-treated and untreated samples

This experiment was designed to eliminate the possibility that the HDM conditions (e.g. heating under a flowing ionised helium gas stream) had an effect on the results observed on the previous experiments. To achieve this, a comparison was made using a fresh sample that was thermally pre-treated in a furnace at 200 °C for 28 hours prior to analysis.

All experimental parameters were as for Section 4.3.5.

Figure 4.24 shows a comparison of the TIC of the untreated polymer from the previous experiment (B) and the isothermally treated sample (C). It is clear from these profiles that an overall reduction in the amount of material desorbed/removed results from the thermal pre-treatment of the sample.

Integration of the TIC peak during the first heating cycle shows that this reduction is about 90 %. However, it is interesting to note that even after a significant amount of time exposed to increased temperatures, oligomeric species are produced. Apart from the magnitude of the TIC, there were two other differences. Firstly, the onset of oligomer release for the treated sample was approximately 160 °C as opposed to 50 °C for the untreated sample.

Secondly, comparison of the ions seen within the TIC profile indicates a greater proportion of higher molecular mass oligomers for the treated sample, implying that the more volatile lower mass species have been removed by the pre-heating.

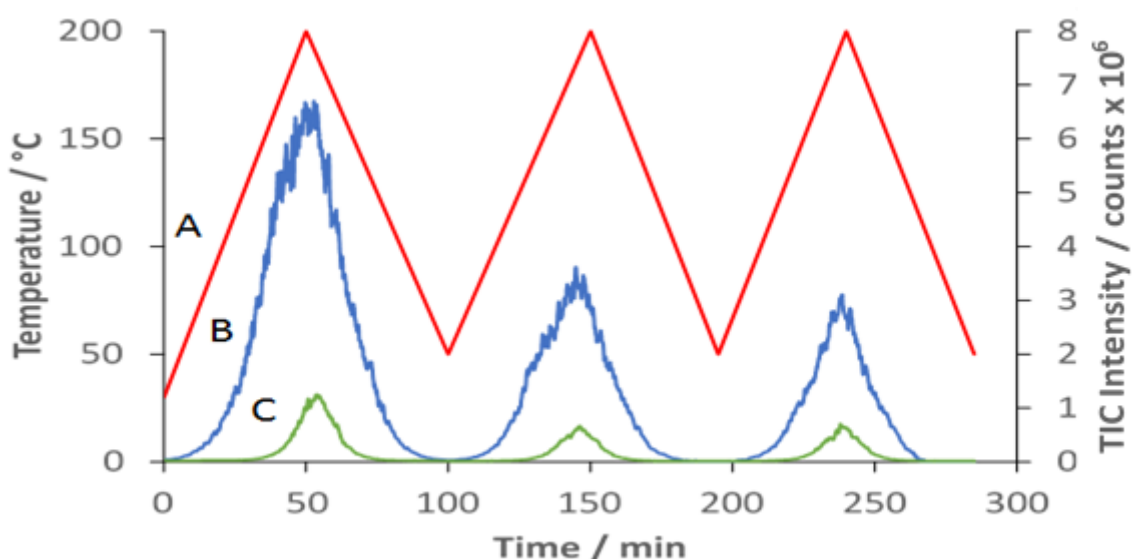


Figure 4.24 Comparison of raw and pre-treated silicone samples under thermal cycling. A) Temperature, B) Raw sample TIC range 600 – 2800 Da and C) Pre-treated sample TIC range 600 – 2800 Da.

The result of this experiment seemed to suggest that the polymer may be undergoing a slight degradation at lower temperatures than was previously noted in the literature.³⁸

4.3.7 Cyclic linear heating and cooling experiments to a higher maximum temperature

The final experiment used a maximum temperature of 300 °C, (higher than manufacturer's recommended limit of 260 °C), to determine if a clear onset to thermal degradation could be detected.

Experimental conditions were as for Section 4.3.5 with the exception that the maximum temperature was 300 °C rather than 200 °C.

Figure 4.25a shows the result of the experiment using cyclic heating to 300 °C with TIC profile and temperature plotted as a function of time. The TIC peaks have been integrated with the regions falling below 200 °C being shaded in blue and the regions falling between 200 °C and 300 °C being shaded yellow. Figure 4.25b shows average mass spectra for regions above and below 200 °C for the first heating cycle.

In the first cycle the TIC can be resolved into two events. The first blue shaded area shows the thermal desorption of the oligomers seen in previous experiments (figure 4.25b, i). This first region shows a marked shoulder, shortly above 200 °C in the yellow shaded area, the TIC increases and new species (figure 4.25 b, ii) begin to appear which are assumed to be thermal degradation products based on the findings of Camino *et al.* who determined the onset of degradation to be around 260 °C.³⁹ The average mass spectrum of this area shows regular repeating units are separated by 86 Da which are consistent with methylvinylsiloxane oligomers used as silicone crosslinkers.⁴⁰ However, the peaks are poorly resolved and appear very broad and it is probable that there is a combination of vinyl based oligomers and broad spectrum decomposition products. On cooling below 200 °C (second blue shaded area), no further decomposition products are noted and there are only very small traces of the cyclic oligomers barely above the background (figure 4.25b, iii).

During the second heating the TIC peak shows that there is very little material removed below 200 °C. The yellow shaded area is smaller than for the first peak and almost completely comprises polymer degradation products. The cyclic oligomers noted in significant quantities during the first cycle are not apparent. Literature suggests crosslinking reactions taking place within this higher temperature region may be the cause of the liberation of these new products.³⁹

Finally, the third TIC peak is only significant above 200 °C and shows a further reduction in area with mass spectra only showing degradation products. This trend is assumed to continue until pure silica remains through complete degradation of the organic components of the PDMS.

Table 4.1 shows the peak areas for the shaded areas of the three TIC peaks. The majority of the cyclic oligomeric species are removed during the first cycle, observing a 98% reduction between cycle one and two.

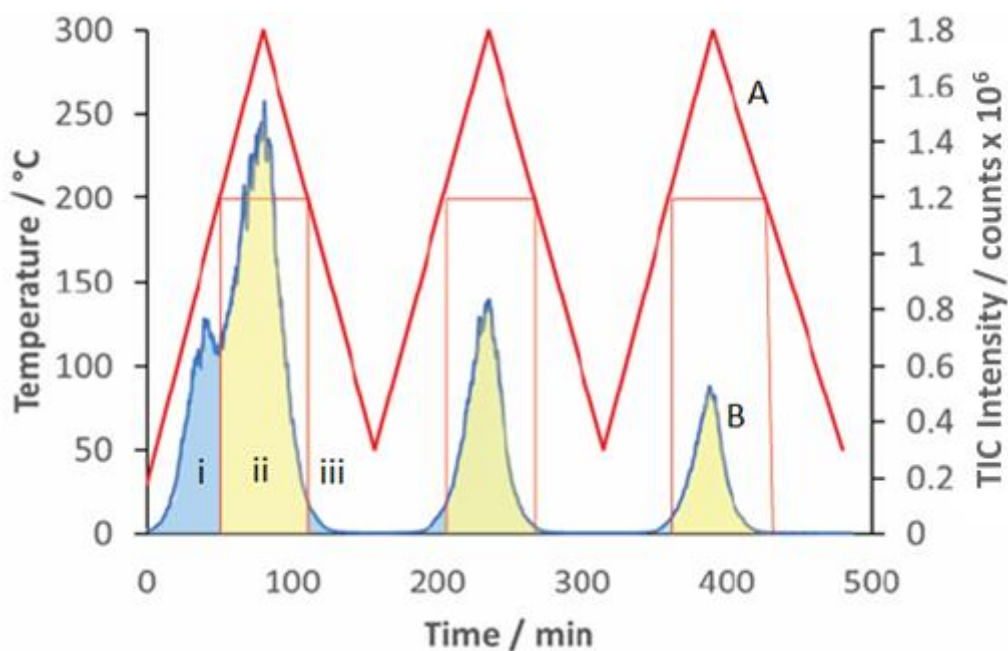


Figure 4.25a Thermal cycling of silicone polymer using HDM profiling cumulative ions between 600 and 2800 Da. A) Temperature and B) TIC range 600 – 2800 Da.

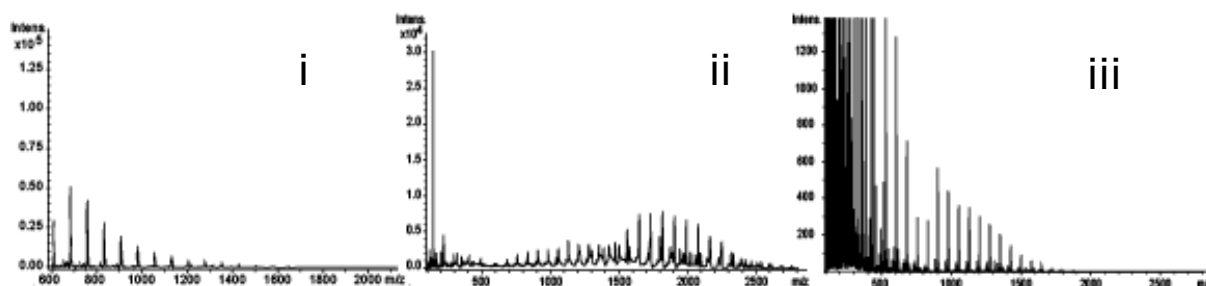


Figure 4.25b Average MS profiles for the first heating cycle (Figure 4.25a) i) first blue shaded area, ii) yellow shaded area and iii) second blue shaded area.

Table 4.1 Integration values for the TIC peaks from Figure 4.25a.

	Blue shaded areas / count.mins x10 ⁷	Yellow shaded area / count.mins x10 ⁷
1 st Heating Cycle	1233	3428
2 nd Heating Cycle	22	1419
3 rd Heating Cycle	14	722

4.4 Monitoring the thermal expansion of silicone polymers using HDM

An examination of the micrographs from the previous experiments on the thermal degradation of silicone indicated that significant thermal expansion occurred during heating. It was decided to investigate this phenomenon further, partly as a means of evaluating the effectiveness of the 'in range pixel counting' (IPC) feature of the HDM software (see Chapter 2, Section 2.3.3). The thermal expansion of silicone has been previously studied by Yamauchi *et al.* who found that for a particular silicone rubber the extent of expansion could be controlled through the addition of silica particulates during the manufacturing process, generally the more filler that was added the greater the reduction in expansion that was noticed.⁴⁰

The coefficient of thermal expansion (CTE) of a material is given the symbol α and subscript dimension either linear, area or volume (L,A,V respectively). Instrumentally this property is measured using thermomechanical analysis introduced in Chapter 1, Section 1.6.3. The CTE can be calculated from measuring the extent of expansion as a function of temperature using Equation 4.1.⁴²

$$CTE \alpha_A = \frac{1}{A_0} \times \frac{\Delta A}{\Delta T}$$

Equation 4.1) The coefficient of thermal expansion (Area)

4.4.1 Initial thermal expansion experiment

A sample of the silicone egg poacher (5 x 5 x 1 mm) was placed within a DSC pan (Inconel) and subjected to a linear heating of 0.8 °C min⁻¹ to 700 °C.

Figure 4.26 shows selected micrographs from 30 °C to 700 °C. The expansion of the silicone between A and E (note the sample corners touching the pan walls) is apparent. Above 500 °C the green dye fades, presumably as the dye (currently unknown) decomposes. The sample then starts to shrink up to 700 °C as the PDMS decomposes to an off-white solid (presumably silica). The material cracks during the contraction stage as the polymer becomes very brittle and gaseous decomposition products are expected to be released.

The micrographs were individually loaded into PowerPoint (Microsoft) and the length and width of the sample measured using the ruler feature. From this an area could be calculated and expressed as a percentage of the starting size.

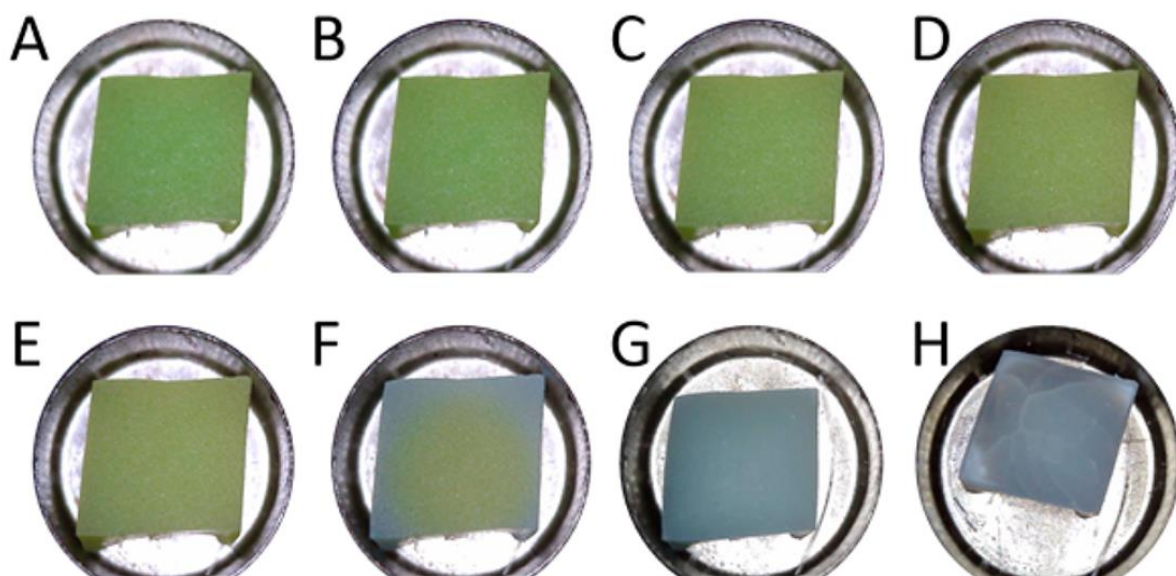


Figure 4.26 Micrographs of silicone egg poacher at various temperatures; A) 30 °C, B) 100 °C, C) 200 °C, D) 300 °C, E) 400 °C, F) 500 °C, G) 600 °C and H) 700 °C.³⁷

Figure 4.27 shows the manually calculated area (A) and the Δ RGB colour profile (B) plotted as a function of temperature.

The area is shown to increase in a linear fashion up until the PDMS begins to decompose around 500 °C when the area begins to decrease. The colour profile shows a corresponding trend and the point where the sample starts to contract clearly matches the change from expansion to contraction.

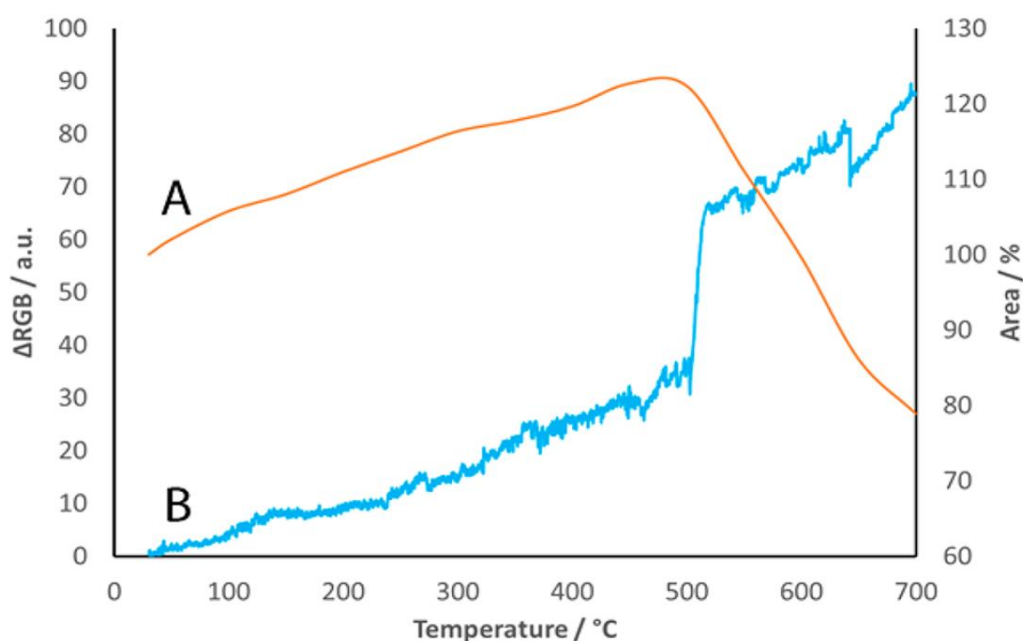


Figure 4.27 Area expansion and colour monitoring as a function of temperature for silicone egg poacher. A) Area change of silicone polymer and B) colour change monitored by Δ RGB.³⁷

4.4.2 Development of a method to monitor thermal expansion using real-time processing of pixel values

The correlation between the colour profile and area seen in the previous experiment led to a development of the HDM software to support a form of real-time sample size analysis.⁴³ This used IPC (in range pixel counting, discussed in Chapter 2, Section 2.3.3).

To recap, IPC monitors the colours of all the pixels in a selected region of the image recording their values 0 - 255 for each primary colours (red, green and blue), or 0-765 for a summated colour value. Normally, the colour profile changes as the sample changes colour. However, it will also be affected if the sample expands or contracts to cover or expose any of the sample pan in the image. IPC adds the additional aspect of counting the number of pixels whose colour values fall within a user-selectable range.

For example, if a green sample was used on a black background the IPC method could be set to count pixels with a high green value as black pixels have a very low green value. Therefore, any increase in size of the green sample would result in an overall gain in green pixels being counted (assuming the background colour remains constant). This can then be expressed as a percentage change from the number of green pixels counted at the start of the experiment. Similarly, a fall in the green pixel count would occur if the sample contracted.

The method does have limitations and care has to be taken to consider a few factors when using the IPC method size analysis:

- *Is the sample likely to change colour during analysis?*
If the sample degrades and changes colour then skewed values for the size will be given as pixels may be counted that are associated with degradation and not a morphological change.
- *Will the sample become transparent or less opaque?*
As the size monitoring is based solely on colour should the sample become transparent an apparent rise in the background will be shown, potentially indicating that the sample has reduced in size to zero.
- *Is the contrast high enough?*
A large difference in colour between the background (typically the sample pan) and the sample reduces the error as fewer pixels will be erroneously counted (or omitted). Looking at a white sample on a highly reflective pan would be difficult as both materials have similar RGB values.

The silicone polymers used in this study were particularly amenable to the IPC approach. The polymers had excellent solid colours, did not change in opacity and were relatively thermally inert over a broad temperature range. Use of a graphite sample pan provided

both a chemically and thermally resistant background with the added benefit of providing a highly contrasting colour with most materials.

For all the experiments described below a sample of green silicone polymer was used with 5 mm circular pieces being cut using a metal punch to ensure standardisation of size and shape.

To allow comparison with the IPC method of size determination, the manual method for size determination based on PowerPoint described earlier was used. It should be noted that, for speed and simplicity, this involved selecting micrographs at 25 °C intervals from those collected after an experiment. In contrast, the IPC method calculates size once per second.

4.4.3 Measuring expansion and contraction during thermal cycling to 200 °C

This experiment aims to evaluate if the sample retains its ability to reversibly expand and contract whilst keeping below the degradation temperature.

This experiment involved three repeat heating and cooling cycles from 50 °C to 200 °C at 5 °C min⁻¹ for the same piece of silicone.

Figure 4.28 shows two micrographs of the green silicone at 50 °C and 200 °C. A red circle was overlaid on the image so as to match the perimeter of the silicone sample at 50 °C (A). The same circle is overlaid on the image taken at 200 °C (B) demonstrating how the silicone has expanded.

Figure 4.29 shows the IPC area (A, green trace) and the manually calculated area (B, blue trace) as a function of time together with the temperature (C, red trace). It can be seen that the IPC area method matches the manually calculated area very closely. The manual area profile appears much smoother in comparison to the IPC method but this is primarily due to a frequency of sampling effect, with one data point being sampled every 25 °C (300 seconds) compared to once per second.

In terms of the sample, it can be seen that the silicone polymer exhibits reversible expansion and contraction over these three cycles, but with an apparent overall decline in the extent of expansion with each cycle (comparing peak maximum to the peak minimum between cycles).

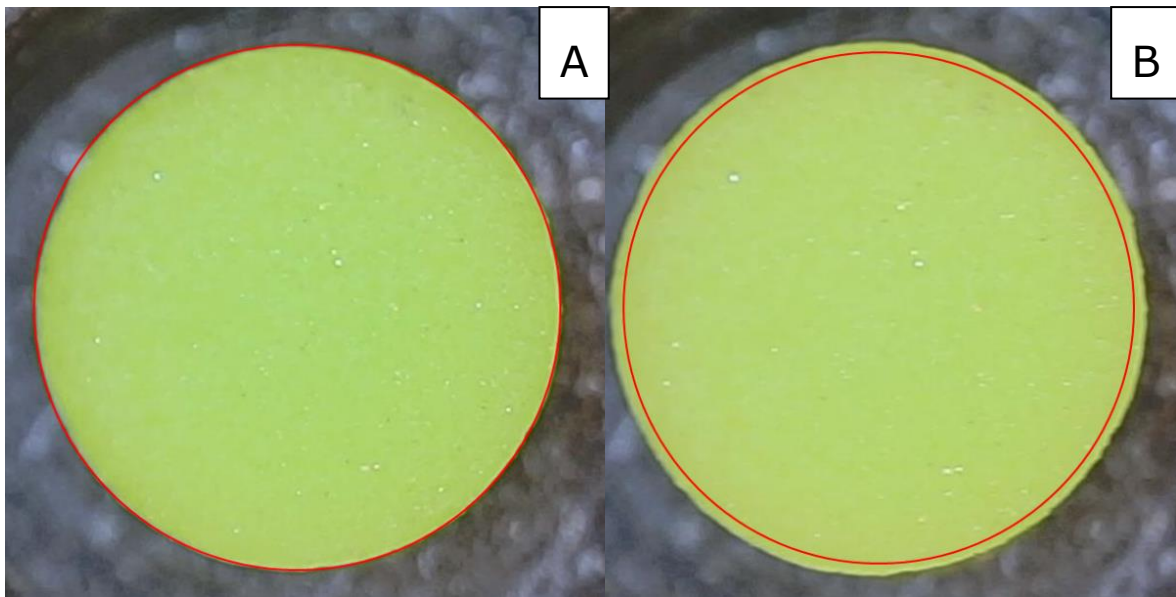


Figure 4.28 Micrographs of the silicone sample at 50 °C (A) and 200 °C (B). The overlaid red circle is the same size in both cases indicating the expansion

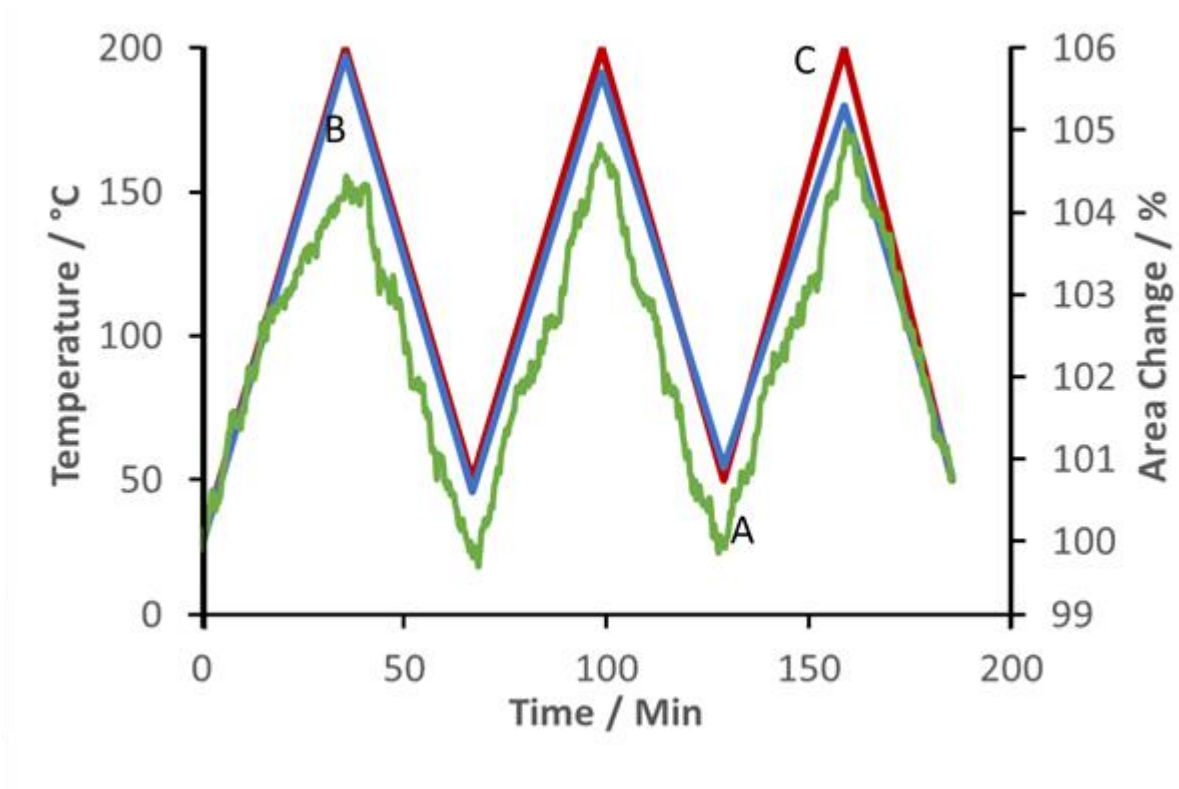


Figure 4.29 IPC & manual area measurement during thermal cycling up to 200 °C; A) IPC Area (green), B) Manual Area (blue), C) Temperature (red).

4.4.4 Measuring expansion and contraction during thermal cycling to 300 °C

To investigate whether the decrease in expansion and contraction observed in the previous experiment was linked to initial traces of thermal degradation, a repeat experiment was performed but using a maximum temperature of 300 °C.

Figure 4.30 shows the IPC area (A, green trace) and the manually calculated area (B, blue trace) as a function of time together with the temperature (C, red trace). Again, there is reasonable agreement between the IPC and manually calculated area profiles

The extent of expansion appears linear into the higher temperature range showing that the polymer retains some of its elastic properties even though it is expected to have begun decomposition.

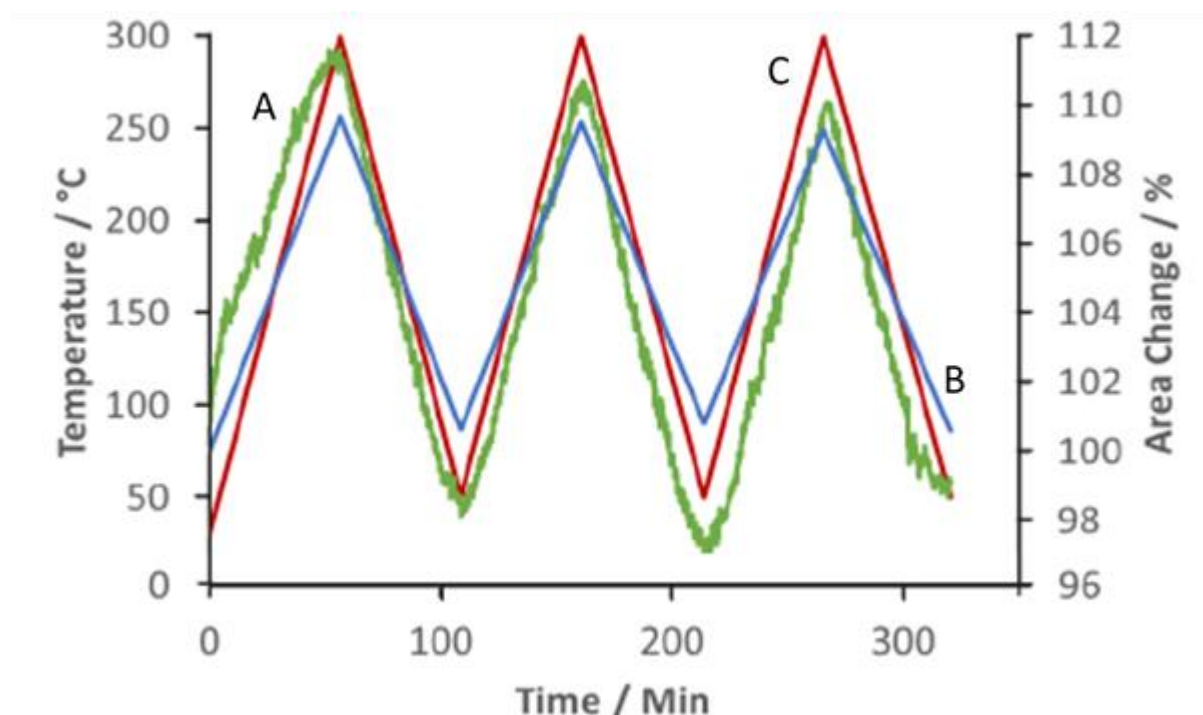


Figure 4.30 IPC & manual area measurement during thermal cycling up to 300 °C; A) IPC Area, B) Manual Area, C) Temperature.

Comparing the maximum and minimum values between each cycle for the manual measurements (B blue trace) it is apparent that the expansion reduces between the first and third cycle. The expansion extent, 9.66% (cycle 1) and 8.47% (cycle 3) shows an overall reduction of 1.20%. In this example the IPC method (A, green trace) is consistent with a linear change but the values are much harder to compare directly to the manual measurements. The difference in values is almost certainly due to the colour beginning to fade which, as mentioned earlier can affect the operation of IPC. The results suggest that there may be some irreversible changes in the physical properties of the silicone even when subjected to a maximum temperature of 200 °C.

4.4.5 Monitoring of change in size during a 9 hour isotherm at 200 °C

The final experiment involved holding the sample isothermally at 200 °C for 9 hours. The aim was to evaluate IPC size measurement monitoring capabilities over a longer period of time but at a temperature below which the green colour would fade. In addition, it was hoped to be able to more reliably determine whether there were irreversible physical changes in the sample at 200 °C.

Figure 4.31 shows the result of the 9 hour isothermal experiment with the area profile and temperature plotted as a function of time. The start and end sizes are highlighted as the two blue points. During the isothermal period each orange point represents an average area taken over 25 minutes.

It can be seen that the area increases, as expected, during the initial heating stage. During the isothermal period there is slow overall decline in area which correlates well with that noted in the previous cycled experiments comparing their expansion reductions. The contraction appears to be relatively linear with an R^2 of 0.92 although the trace shows some oscillations around the best fit line, which may be due to changes in lighting (strong day light changes in the laboratory) over the period affecting the IPC.

After the isothermal period the area contracts more rapidly as the sample is cooled. The overall contraction in area was 1.32% equating to 0.006 % for each minute held isothermally at 200 °C.

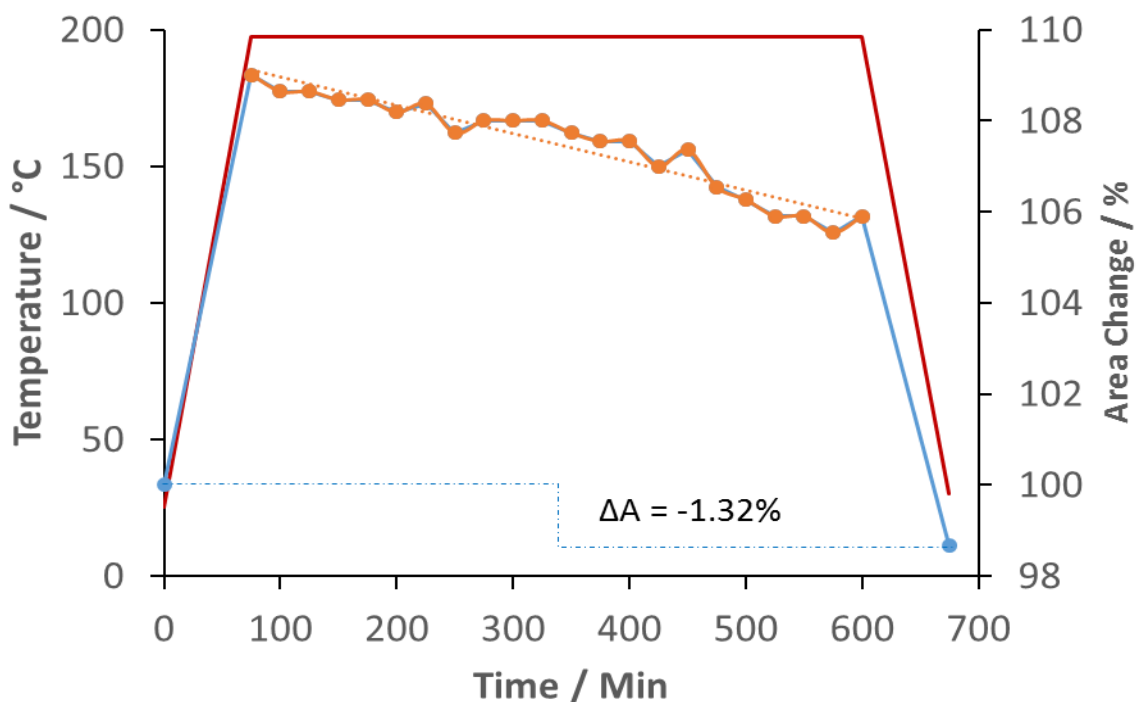


Figure 4.31 200 °C isothermal hold of a silicone sample monitoring the area change. Red) Temperature, Orange) Area change and the blue points indicate the starting and finishing areas.

4.4.6 Using optical data to calculate the coefficient of thermal expansion

As well as providing information on visual and colour changes, the data obtained using HDM's IPC method can be used to calculate the CTE (coefficient of thermal expansion) of a material directly. The data shown below in Table 4.2 was obtained for a sample of silicone heated from 25 °C to 200 °C at a rate of 5 °C min⁻¹. The values shown are the absolute IPC values for the two temperatures 25 and 200 °C.

Table 4.2 HDM IPC size analysis the silicone polymer.

Temperature	Size / %
25 °C (T ₀)	100 (A ₀)
200 °C	109.11

Using the CTE equation introduced earlier (Equation 4.1):

$$CTE \alpha_A = \frac{1}{A_0} \times \frac{\Delta A}{\Delta T} \quad \alpha_A = \frac{1}{100} \times \frac{109.11-100}{200-25} \quad \alpha_A = 5.21 \times 10^{-4} \text{ } ^\circ\text{C}^{-1}$$

Typically the values for CTE are quoted as the volumetric expansion α_v , as silicone polymers behave isotopically, the property that allows a material to expand equally in all directions, a conversion factor ($\times 0.66$)⁴⁴ can be applied to the α_A value to yield the commonly quoted volumetric expansion;

$$\alpha_v = \alpha_A \times 0.66 \quad \alpha_v = 5.21 \times 10^{-4} \times 0.66 \quad \alpha_v = 3.44 \times 10^{-4} \text{ } ^\circ\text{C}^{-1}$$

The value is in agreement with that reported by Sim *et al.*⁴⁵ for general PDMS silicone rubbers of *ca.* $3.0 \times 10^{-4} \text{ } ^\circ\text{C}^{-1}$. However, no absolute value was found for the particular sample of silicone used in these experiments as it was not obtained from the manufacturer.

Further testing is required to evaluate how various physical properties of the material such as diameter and thickness effect the CTE value, and the absolute size and shape may need to be standardised should this method be used for comparative studies.

Since the optical method of obtaining volumetric expansions is limited to isotopic materials, those that behave non-isotopically (expand unequally in all directions) are unable to have their α_v values calculated using HDM. Although, the HDM's IPC method is capable of measuring the area as viewed in a single plane for all materials.

4.5 Conclusions and further work

The application of HDM to the thermal analysis of common polymers was successfully demonstrated. Results showed that the optical component of HDM could monitor thermal events, commonly observed in DSC analysis, such as glass transitions (T_g), cold crystallisations (T_c) and melting points (T_m). The mass spectrometer component of HDM provided complementary chemical information. For PS and PET the fragmentation patterns consistent with the polymer were observed, particularly after the sample melted, while for PVOH thermal degradation products were detected.

Silicone polymers, used in kitchen bakeware, were investigated initially following on from previous DART-MS work of Gross and co-workers. Using HDM, these polymers were found to leach oligomeric material during heating but at much lower temperature than previously reported and comfortably within common cooking temperatures ($< 200\text{ }^\circ\text{C}$). At higher temperatures, silicones were shown to degrade. HDM was used to evaluate various properties of the silicone including size analysis, colour changes and observation of polymer decomposition products.

To enhance the ability of HDM to monitor changes in sample geometry in real time, an optical method based on counting the number of pixels in the image within a given colour range was developed. This was successfully applied to the measurement of the thermal expansion of silicones. The IPC method is much less laborious than taking manual measurements of the polymers post experiment and initial findings on the silicone polymers suggest the method looks promising.

There are innate limitations in that consistent sample colour and good contrast with the background (sample pan) is required. However, improvements in terms of software (increased sampling frequency (with smoothing) and better real-time image processing to reduce pixel noise) and hardware (particularly improved lighting) are planned using newer COB LED halo type lighting to ensure external lighting effects (shadows, daylight etc.) are minimised.

A longer term aim would be to add a geometry component to the software allowing the recognition of a predefined shape. The combination of shape monitoring and the current IPC method will create a significantly more robust size monitoring system allowing for the automated monitoring of geometry during colour change process such as degradation.

In addition to general improvements of the technique, planned future work with IPC will involve:

a) Calibration

Many metals have a well-characterised thermal expansion property, do not degrade and have a consistent colour making them suitable to calibrate the technique. Although, the thermal expansion of many pure metals is often small by comparison to the silicone polymers studied earlier (Aluminium $\alpha_L = 2.3 \times 10^{-6} \text{ }^\circ\text{C}^{-1}$).⁴⁶

b) Applications to crystals

Some inorganic (such as barium titanate)⁴⁷ and polymeric (including HDPE)⁴⁸ materials have been shown to have directional expansion properties that may be amenable to this technique

The controlled heating provided by HDM would also allow more detailed studies linking extent of degradation of other polymers to their thermal expansion.

Finally, no quantitation experiments were performed during this study. The intention would be to continue this work and perform an evaluative study between TGA-(MS) and HDM to evaluate the extent of polymer degradation during heating.

4.6 Polymers Studies References

- ¹ O. Olatunji, *Natural Polymers: Industry Techniques and Applications*, 1st edn., Springer International Publishing, Cham., 2016.
- ² I. Campbell, *Introduction to synthetic polymers*, 2nd ed., Oxford University Press, Oxford, 2000.
- ³ D.J. Walton & J.P. Lorimer, *Polymers*, Oxford University Press, Oxford, 2000.
- ⁴ British Plastics Federation, <http://www.bpf.co.uk/Industry/Default.aspx> (accessed June 2018)
- ⁵ S. Ebnasajjad, *Plastic films in food packaging: materials, technology, and applications*, William Andrew, Oxford, 2013.
- ⁶ M.M.Pradas, *Polymers in regenerative medicine: biomedical applications from nano- to macro-structures*, John Wiley & Sons, Hoboken, New Jersey. 2015
- ⁷ S. Senise, V. Carrera, F.J. Navarro, & P. Partal, *Construction and Building Materials*, 2017, **157**, 873-884.
- ⁸ D.-U. Choi, S.-C. Chun & S.-S. Ha, *Engineering Structures*, 2012, **34**, 303-313
- ⁹ S. Lin & L. Gu, *Materials*, 2015, **8**, 551-560
- ¹⁰ J. Nicholas, M. Mohamed, G.S. Dhaliwal, S. Anandan & K. Chandrashekhara, *Composites Part B*, 2016, **94**, 370-378.
- ¹¹ R. Hiesgen, I. Wehl, S. Helmly, A. Haug, M. Schulze, A. Bauder, H. Wang, X. Yuan & K. Andreas Friedrich, *Journal of Electroanalytical Chemistry*, 2011, **662**(1), 240-250.
- ¹² J. Yong, J. Huo, Q. Yang, F. Chen, Y. Fang, X. Wu, L. Liu, X. Lu, J. Zhang, and Xun Hou, *Adv. Mater. Interfaces*, 2018, **5**, 1701479
- ¹³ K.P. Menard *Dynamic mechanical analysis: a practical introduction*, 2nd edn, CRC, London, 2008
- ¹⁴ J.E.K. Schawe, *Thermochimica Acta.*, 2002, **391**(1-2), 279-295
- ¹⁵ L.A. Bicalho, J.M.J. da Silva, J.A. Covas & S.V. Canevarolo, *Journal of Thermal Analysis and Calorimetry*, 2017, **130**(3), 2093-2103.
- ¹⁶ M.H. Yazdi & P. Lee-Sullivan, *Journal of Thermal Analysis and Calorimetry*, 2009, **96**(1), 7-14.
- ¹⁷ M.A. Corres, M. Zubitur, M. Cortazar & A. Mugica, *Polymer Degradation and Stability*, 2013, **98**, 818-828.
- ¹⁸ J. Luo, Q. Li, A. Meng, Y. Long and Y. Zhang, *Journal of Thermal Analysis and Calorimetry*, 2018, **132**, 553-562
- ¹⁹ R.C.P. Monterio, J.A. Ivar do Sul & M.F. Costa, *Environmental Pollution*, 2018, **238**, 103-110
- ²⁰ D. Schymanski, C. Goldbeck, H.-U. Humpf & P. Furst, *Water Research*, 2018, **129**, 154-162
- ²¹ S. Ribnitzky, *Effects of micro plastic marine pollution on humans remain unclear*, dpa Deutsche Presse-Agentur GmbH, Hamburg. 2015
- ²² J. Annamalai & V. Namasivayam, *Journal of Food Measurement and Characterization*, 2017, **11**, 2222-2232.
- ²³ I. Katsikantami, S. Sifakis, M.N. Tzatzarakis, E. Vakonaki, O.I. Kalantzi, A.M. Tsatsakis & A.K. Rizos, *Environmental International*, 2016, **97**, 212-326.
- ²⁴ L. Fernandes, H. Gaspar and G. Bernardo, *Polymer Testing*, 2014, **40**, 63-69; J.R. Wunsch, *Polystyrene: Synthesis, Production and Applications*, iSmithers Rapra Publishing, 2000
- ²⁵ P.M. Subramanian, *Conservation and Recycling*, 2000, **28**, 253-263.
- ²⁶ T. Yoshii, H. Yoshida and T. Kawai, *Thermochimica Acta*. 2005, **431**(1-2), 177-181
- ²⁷ J. Bandyopadhyay, S.S. Ray and M. Bousmina, *J. Ind. Eng. Chem.*, 2007, **13**(4), 614-623
- ²⁸ A.L.M. Nasser, L.M.X. Lopes, M.N. Eberlin & M. Monteiro, *Journal of Chromatography A*, 2005, **1097**(1-2), 130-137.
- ²⁹ S.V. Levchik & E.D. Weil, *Polymers for advanced technologies*, 2004, **15**, 691-700
- ³⁰ B.J. Holland and J.N. Hay, *Polymer*, 2001, **42**, 6775-6783
- ³¹ S. Pandey, S.K. Pandey, V. Parashar, G.K. Mehrota and A.C. Panday, *J. Mater. Chem.*, 2011, **21**, 17154-17159
- ³² H. Yang, S. Xu, L. Jiand and Y. Dan, *Journal of macromolecular science, part B Physics*, 2012, **51**, 464-480.
- ³³ J.H. Gross, *Journal of the American Society for Mass Spectrometry*, 2015, **26**(3), 511-521
- ³⁴ J.H. Gross, *European Mass Spectrometry*, 2011, **21**(3), 313-319
- ³⁵ C. Stevens, D.E. Powell, P. Makela & C. Karman, *Marine Pollution Bulletin*, 2001, **42**(7), 536-543
- ³⁶ O.L. Fianingam, *Journal of Chemical and Engineering Data*, 1986, **31**(3), 266-272
- ³⁷ G.P. Ashton, L.P. Harding & G.M.B. Parkes, *Analytical Chemistry*, 2017, **89**(24), 13466-13471
- ³⁸ T.S. Radhakrishnan, *Journal of Applied Polymer Science*, 2006, **99**, 2679-2686.
- ³⁹ G. Camino, S. Lomakin and M. Lazzari, *Polymer*, 2001, **42**, 2395-2402.
- ⁴⁰ Wacker, https://www.wacker.com/cms/media/publications/downloads/6709_EN.pdf, accessed June 2018.

- ⁴¹ N. Suzuki, S. Kiba, Y. Kamachi, N. Miyamoto & Y. Yamauchi, *J. Mater. Chem.*, 2011, **21**, 5338-5344
- ⁴² H. Li, S. Zhou, S. Zhang & X. Cao, *Physica C*, 2006, **449**(1), 41-46
- ⁴³ S.E. Pownall, *An investigation into the thermal behavior of polymer cookware using conventional and novel thermal analysis techniques*, submitted as final year MChem project dissertation, University of Huddersfield, 2018.
- ⁴⁴ P. Hidenert & W. Souder, *National Bureau of Standards circular*, 1950, 486.
- ⁴⁵ L.C. Sim, S.R. Ramanan, H. Ismail, K.N. Seetharamu & T.J. Goh, *Thermochimica Acta*, 2005, **430**(1-2), 155-165
- ⁴⁶ P. Hidnert & H.S. Krider, *Journal of Research of the National Bureau of Standards*, 1952, **48**(3), 209-220
- ⁴⁷ Y. Hi, *Thermochimica Acta.*, 2004, **419**, 135-141
- ⁴⁸ C.L. Choy, F.C.Chen & E.L.Ong, *Polymer*, 1979, **20**(10),1191-1198

5.0 Desorption Studies

5.1 Introduction

Desorption is defined as the release of a substance or substances from a surface, this may either be through the surface or from the surface.¹ Before desorption, sorption of a compound must occur. Sorption is defined by two pathways; adsorption and absorption focusing on different fundamentals of the sorption process. Both sorption mechanisms are comprised of a further two components; physisorption and chemisorption.²

Adsorption is the process in which a surface effect is noted, when gases or liquids bind to the surfaces of liquids or solids.

Absorption on the other hand is focused on bulk properties of the material, more than a surface effect the substance of interest may move beyond the surface layer of the material and into the bulk volume.

Physisorption is concerned with weak attractive forces between the sorbent and the substance of interest. These forces are typically experienced as surface level electrostatic interactions such as van der Waals, that is, the attraction of dipoles either permanent or transient. Concerning a bulk material, physisorption may occur when an inert substance dissolves or migrates into the sorbent without chemically altering the surface.

Chemisorption processes are far more energetic than physisorption processes due to new chemical bonds being formed, usually in the form of new covalent bonds between the sorbent and sorbate.

These effects are exploited in chromatography and are a key driving force for the separation technique.³ Analytes are introduced onto a column and are moved through it using a mobile phase, commonly an organic solvent in LC (liquid chromatography) or a gas in GC (gas chromatography). As the analytes pass through the column they can be adsorbed to the surface of the stationary phase or if the stationary phase is porous the analytes may be absorbed. The interaction between sorption and desorption processes is what creates separation in chromatography driven by a number of interactions including dipole interactions, complexation and acid-base interactions. Analytes that have more affinity to the mobile phase will be eluted first, whereas those that have more affinity to the stationary phase will be eluted later.

Desorption is often an important factor in mass spectrometry. Many techniques require sample introduction through a desorption process, particularly those of ambient ionisation. A few techniques that utilise desorption as part of the sample preparation and introduction method are outlined below.

DESI (desorption electrospray ionisation) is an ambient ionisation technique and as the name suggests is based on desorption.⁴ The DESI desorption process works through

pneumatic action, aiming a high velocity and charged solvent spray towards a solid sample. The sample partially solvates within the spray solvent forming a thin surface coating, which is then desorbed by further incoming solvent physically 'knocking off' the solvated ions and through electrostatic repulsion generated through the accumulation of a localised charge, and driven towards the MS (introduced earlier in Chapter 1).

Thermal desorption (TD) is also a key sample introduction method for techniques such as TD-GC-MS (thermal desorption gas chromatography mass spectrometry),⁵ DART-MS⁶ and DAPPI (desorption atmospheric pressure photoionisation).⁷ These techniques utilise heat energy to remove materials from surfaces through thermal desorption. As the heated material gets hotter the surface molecules gain sufficient energy to overcome surface forces binding the material.

The term 'surface residency' is used to describe how long on average a molecule will remain at the surface of a specific material at fixed conditions of pressure and temperature. The surface residency of a molecule is exponentially dependant on temperature, meaning that as temperature is increased the surface residency time is exponentially reduced until all surface bound molecules are removed and the surface becomes clean.⁸

Many of the ambient plasma techniques utilise a two stage thermal desorption ionisation process. DART itself thermally desorbs compounds from the introduced material via the heated gas stream and not through contact with a heated plasma. The ionisation is provided from the flow of metastable and energetic molecules exiting the source (see Chapter 1)

HDM (hot-stage microscopy direct analysis in real-time mass spectrometry) separates these two processes that occur in DART, in this way HDM behaves analogously to TG-GC-MS. The hot-stage of HDM thermally desorbs introduced materials, separation is provided thermally depending on the properties of the material/mixture, whilst the detection is initiated by DART's ionisation and final mass spectrometer detection.

Since HDM relies on thermal desorption to introduce samples into the gas phase and in turn ionisation from the DART, experiments were designed to investigate how samples desorb from materials used to introduce analytes to HDM.

5.1.2 Aims

- To investigate the removal of compounds from powdered matrices using HDM.
- To investigate HDM's use for the analysis and identification of energetic materials.
- To evaluate swabbing materials that may be used in the HDM and the desorption stage, comparing material degradation and its effects on background levels.
- To investigate the use of dopants and adding dopants to HDM during analysis.

5.2 Dyes

A series of desorption studies was designed to evaluate how compounds could be removed from surfaces, these initially focused on the removal of dye compounds from stable inorganic oxides primarily alumina. The use of alumina had two clear benefits, it has excellent thermal stability (>2000 °C) and the lack of colour gave a high contrast making it significantly easier to visualise the desorption process.

Dyes have been shown to interact with alumina through both physisorption and chemisorption. Many factors determine the absolute sorption process onto alumina such as pH, temperature and ancillary ions present in solution.⁹ This study was less focused on the mechanisms of the uptake of the dyes by the alumina, rather, the intention was to form homogenous dry powders as a platform for thermal desorption analysis using HDM.

A range of coloured pens was purchased and the ink components were extracted by soaking the cartridges in methanol (10 ml, HPLC grade) until highly pigmented solutions of unknown concentrations were obtained. To each of these solutions was added alumina (1 g, Aldrich 99.9%) that had been previously thermally treated (600 °C, 4 hrs) ensuring the alumina was activated through removal of surface water and other potential surface bound contaminants. The alumina was allowed to soak in the concentrated solutions for 15 mins under sonication, before extraction through gravity filtration. The samples were then dried on a hot-plate at 50 °C for 30 minutes expected to remove all the residual solvent. Samples were subjected to individual heating programs and monitored using mass spectrometry in positive ion mode.

5.2.1 Selected ink example

Figure 5.1 shows the removal of two major components in the orange pen ink from alumina. profile A has been assigned to the protonated molecular ion of a common azo dye found in writing inks (Orange III, 212 g mol⁻¹, 213 Da [M+H]⁺), profile B has been attributed to the dechlorinated molecular ion of a xanthene pigment (rhodamine B, 478 g mol⁻¹, 443 Da [M-Cl]⁺). Other ions expected to be related to the ink binding agents were noted but primary focus was paid to the pigment desorption processes for correlation with the micrographs and colour profiles obtained. The sample was heated at a rate of 3.5 °C min⁻¹ between 50 and 350 °C as a general profiling temperature and ramp rate.

Orange III is shown to be removed quite sharply from 100 °C until the eventual decline after 170 °C, this decline is accompanied by the gradual removal of rhodamine B. Possible signal suppression of rhodamine B appears to be taking place by the Orange III, once the majority of the Orange III has been removed the rhodamine B profile rapidly increases in intensity around 250 °C. The rhodamine B declines in intensity from 310 °C as the pigment is desorbed from the alumina.

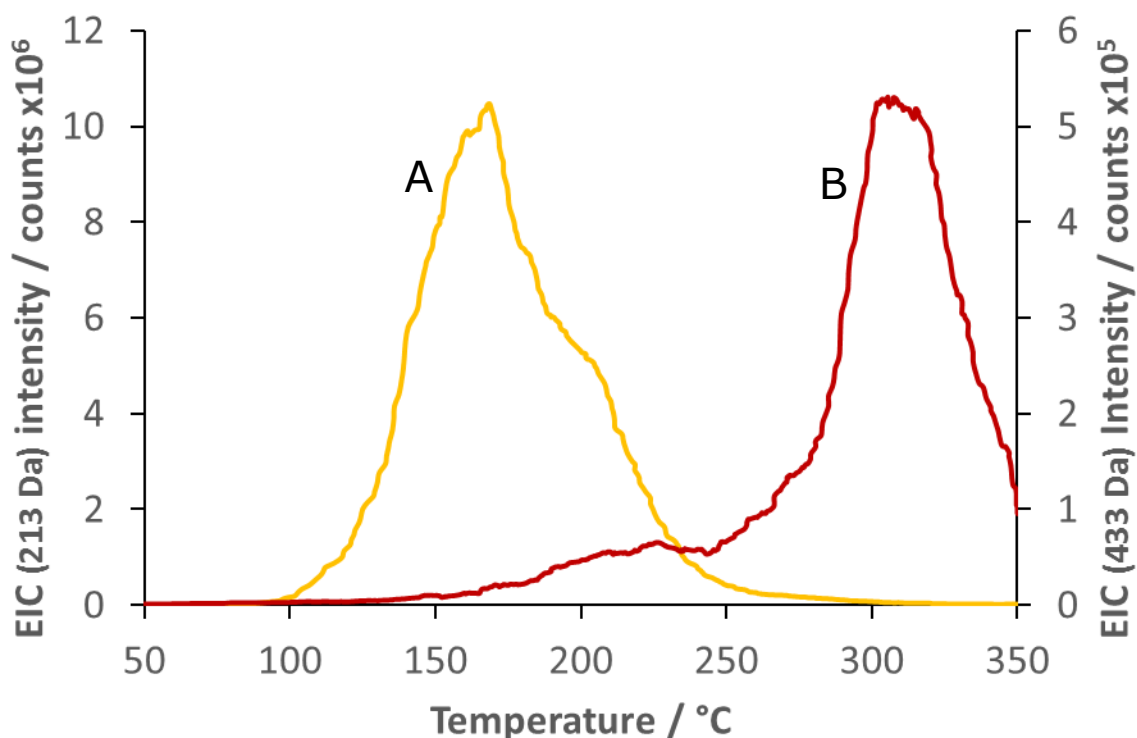


Figure 5.1 Ion intensity profiles plotted as a function of temperature for the thermal desorption of orange ink from alumina. A) Orange III, 213 Da $[M+H]^+$ and B) rhodamine B, 443 Da $[M-CI]^+$.

The micrographs (Figure 5.2) show the thermal desorption through the changes in colour and are complimentary to the ion profiles discussed previously. Initially the alumina appears a light orange in colour, as the orange III is removed the colour changes from orange to a faint pink (micrographs A-D) this is in keeping with the ion profiles as the remaining rhodamine B is red-pink in colour. Further heating between 200 and 300 °C shows the removal of the rhodamine B as the alumina goes from pink to an off white, micrographs D-H. The off white colour is expected to be remnants of organic degradation products from pigments and binders.

Finally, the colour profile in Figure 5.3 shows the colour removal from the supporting alumina matrix. A relatively stable level in the change in colour (ΔRGB) is shown until 100 °C as a shallow trough in the profile appears, correlating with the onset of removal of the orange III both through the EIC trace and micrographs. An approximate constant rate of colour change is observed between 150 and 250 °C as the orange colour is removed leaving behind a pink colour. A slight rate change is noted at 250 °C as the rhodamine B is rapidly evolved, confirmed by its ion profile (B). The colour becomes stable again above 290 °C as the majority of the rhodamine B has been desorbed and the remaining components on the alumina begin to thermally degrade, leaving behind the off white powder.

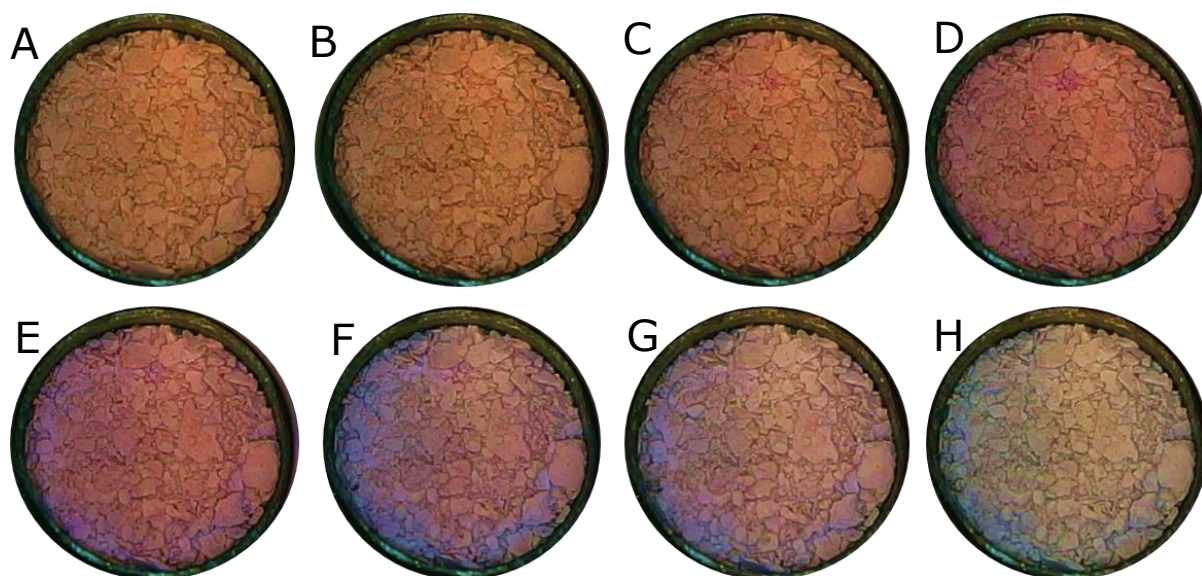


Figure 5.2 Micrographs of orange ink desorption from alumina. A) 100 °C, B) 150 °C, C) 200 °C, D) 225 °C, E) 250 °C, F) 300 °C, G) 325 °C and H) 350 °C.

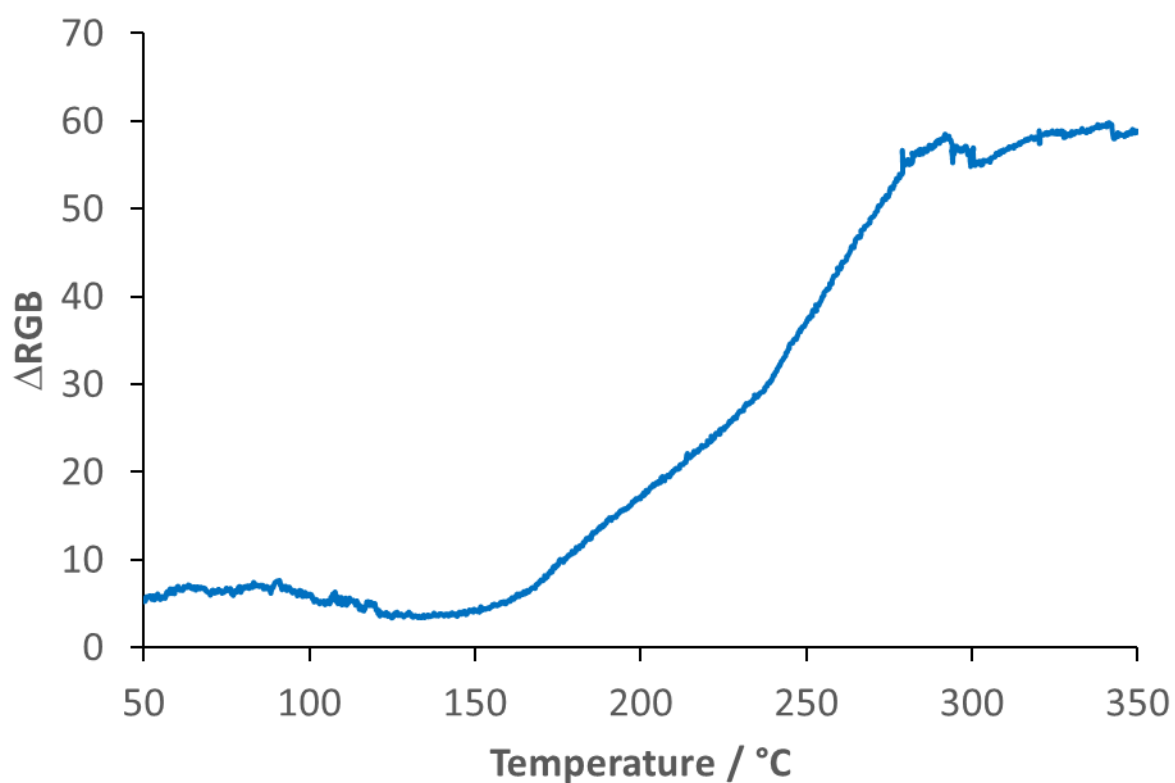


Figure 5.3 Change in colour profile for the thermal desorption of orange ink from alumina, plotted as a function of temperature.

5.2.2 Overview of inks

Many of the inks analysed display similar trends to the orange ink (Section 5.2.1); although the ink compounds gave significant mass spectral profiles absolute assignment of ions was difficult when dealing with large mixtures of unknown compounds. Other mass spectral techniques could have been used to further discriminate and assign the ink components such as tandem mass spectrometry but this was outside the scope of this investigation.

A collection of profiles from a range of coloured inks is shown below. All typically show the same trends; heating desorbs the most volatile compounds first, the colour of the alumina is lost, at high temperatures the alumina remains discoloured due to thermal degradation of remaining organic compounds.

Figure 5.4 shows the HDM thermal profiling of blue ink dried on alumina. Two compounds (B & C) were identified from the ink matrix, although the compounds with masses 314 Da (C) and 422 Da (B) remain unassigned. The colour profile (A) was also plotted as a function of temperature, around 150 °C a dip is shown, the small change is negligible and doesn't appear related any of the pigmented components. Instead, the change is attributed to the matrix drying. The colour profile remains quite constant even though overall there are clear signs of degradation from the micrographs (blue to grey in colour).

Figure 5.5 shows the HDM thermal profiling of green ink dried on alumina. Again, two unassigned compounds were attributed to pigment components 314 Da (B) and 240 Da (C). The colour profile (A) remains constant until above 270 °C when the colour gradually starts to darken, also documented by the micrographs.

Figure 5.6 show the HDM thermal profiling of purple ink dried on alumina. This time only one evident pigment compound existed, the ion at 443 Da was attributed the dechlorinated rhodamine B ion as in the previous orange ink example and is removed from 150 °C until around 250 °C. In this example the colour profile (A) monitors the desorption much more closely. The 'dip' of the colour profile correlates with the maximum of the 443 ion's release. The micrographs show the removal of the intense purple down to a pale mauve colour.

Finally, Figure 5.7 shows the thermal profiling of pink ink dried onto alumina. The colour, mass spectrum and micrographs suggest that the major ink component is rhodamine B. Again, the desorption profile (B) starts from 150 °C and reaches a maximum by 240 °C when it begins to reduce.

This section was designed to evaluate how materials desorbed from a powdered alumina using HDM and shows how powdered matrices maybe applied to HDM unlike conventional DART. Some peaks were tentatively attributed to certain compounds due to similarities with literature findings, commonness of compounds and general mass spectral profiles.

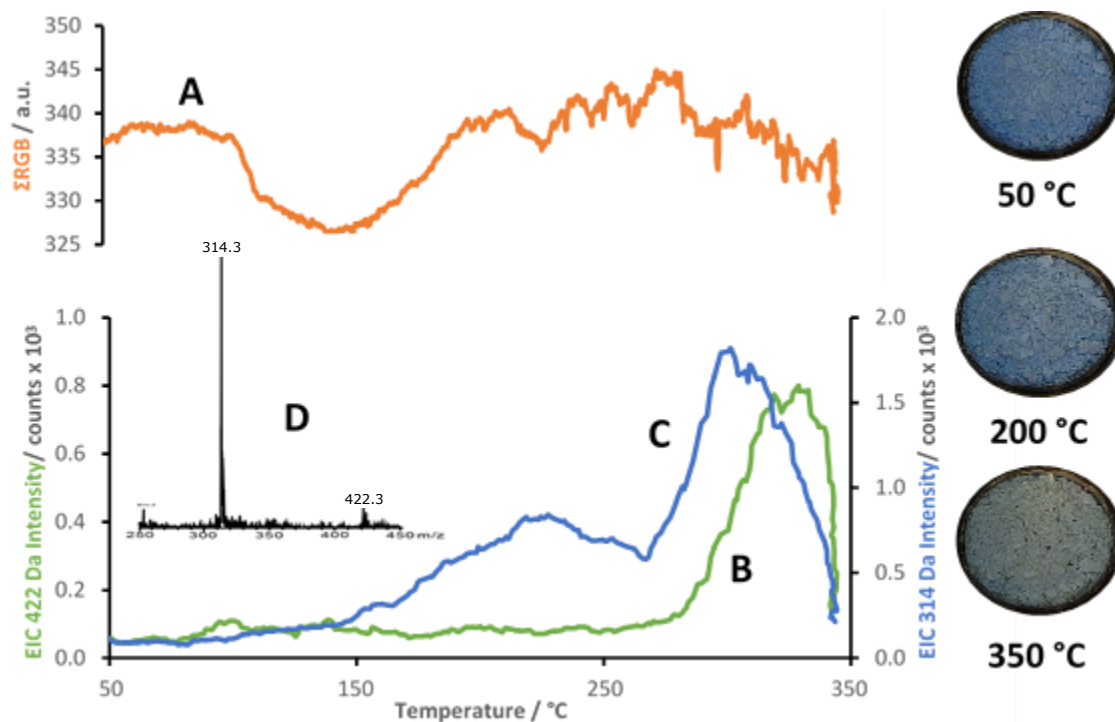


Figure 5.4 HDM analysis of blue ink desorbed from alumina. (A) Shows Σ RGB change as a function of temperature, (B & C) show EIC profiles of 422 Da and 314 Da (respectively) as a function of temperature, (D) shows a region of interest from an averaged mass spectrum over the entire experiment. Micrographs of the desorption process at three temperatures are displayed to the right hand side.

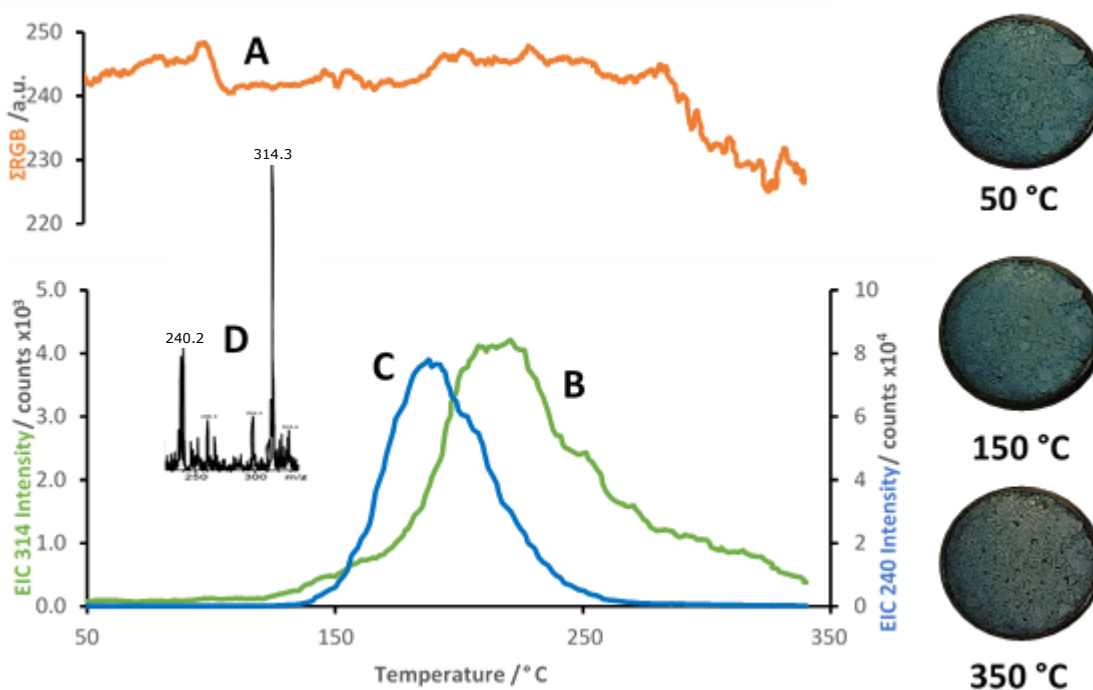


Figure 5.5 HDM analysis of green ink desorbed from alumina. (A) Shows Σ RGB change as a function of temperature, (B & C) show EIC profiles of 314 Da and 240 Da (respectively) as a function of temperature, (D) shows a region of interest from an averaged mass spectrum over the entire experiment. Micrographs of the desorption process at three temperatures are displayed to the right hand side.

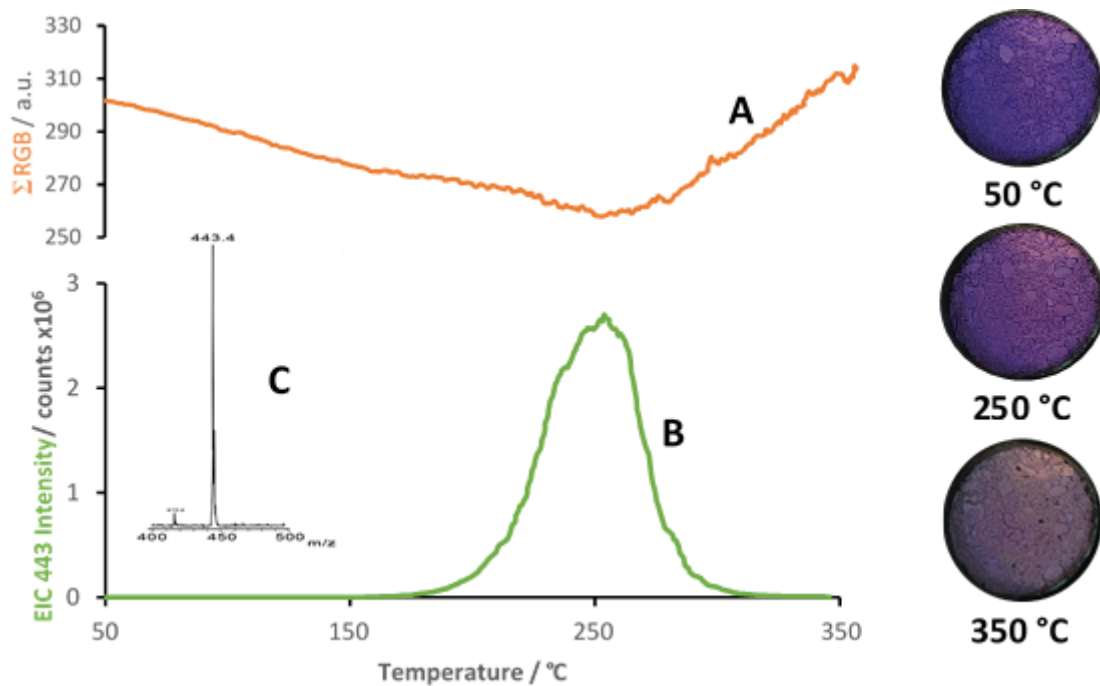


Figure 5.6 HDM analysis of purple ink desorbed from alumina. (A) Shows Σ RGB change as a function of temperature, (B) shows the EIC profile of the 443 Da ion as a function of temperature, (C) shows a region of interest from an averaged mass spectrum over the entire experiment. Micrographs of the desorption process at three temperatures are displayed to the right hand side.

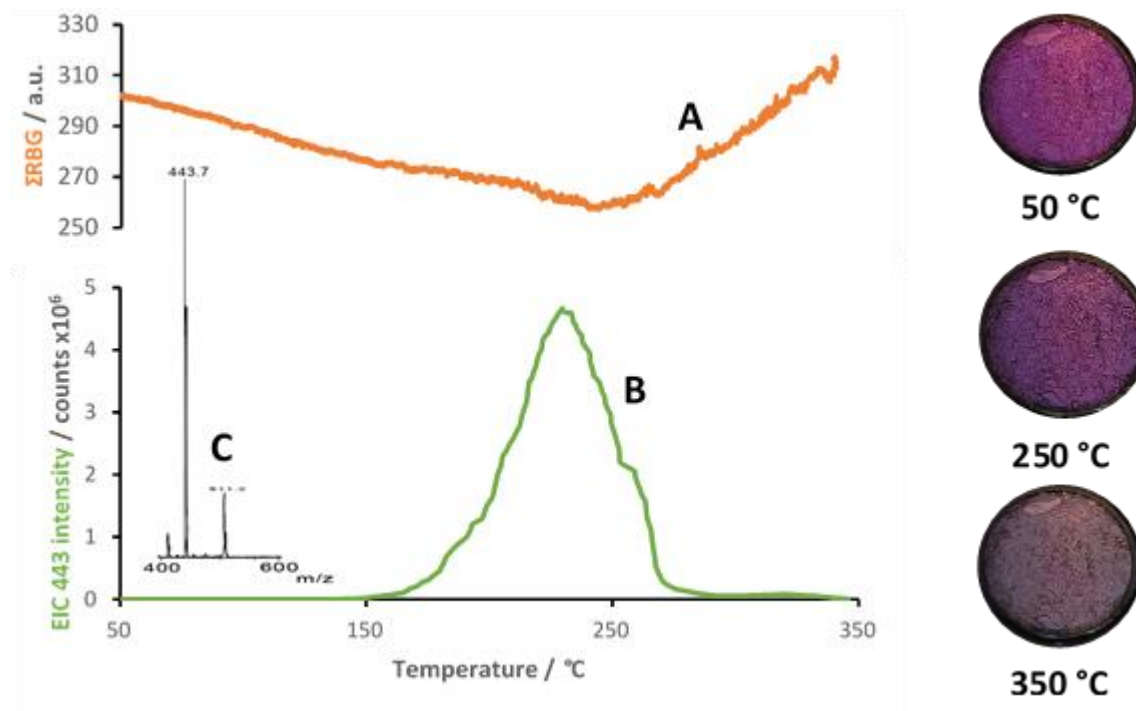


Figure 5.7 HDM analysis of pink ink desorbed from alumina. (A) Shows Σ RGB change as a function of temperature, (B) shows the EIC profile of the 443 Da ion as a function of temperature, (C) shows a region of interest from an averaged mass spectrum over the entire experiment. Micrographs of the desorption process at three temperatures are displayed to the right hand side.

5.2.3 Quantitation

As the compound rhodamine B was highly pigmented, readily ionised and commonly encountered (Section 5.2.2) it was decided to investigate the removal of the pure dye from an alumina surface. The experiment was used to evaluate the desorption process from an alumina matrix without the interference of other compounds found within the ink cartridges.

As both profiles for the pink and purple inks appeared to show a characteristic shape during the removal of the rhodamine B from the alumina, experiments were designed to evaluate if the colour curves could be used in a quantitative or semi-quantitative manner. Solutions were prepared as follows:

Rhodamine B was added to methanol (25 mg or 100 mg of rhodamine B in 10 ml of methanol, HPLC grade). An aliquot of stock solution (100 μ L) was deposited onto alumina (100 mg, activated at 600 $^{\circ}$ C for 4 hrs), the mixture was then sonicated for 15 minutes. The solutions were allowed to evaporate overnight and 10 mg of each of the dried mixtures were analysed individually, resulting in 25 and 100 μ g amounts of rhodamine B used during HDM analysis. A heating rate of 5 $^{\circ}$ C min^{-1} was used between 50 and 350 $^{\circ}$ C.

Figure 5.8 documents the thermal desorption of two amounts of rhodamine B from alumina both in terms of colour and extracted ion profiles (443 Da, [M-Cl]⁺). Both profiles show the desorption process occurring from *ca.* 170 $^{\circ}$ C through to approximately 270 $^{\circ}$ C. Integration of the extracted ion (between 150 and 350 $^{\circ}$ C) profiles yields 1.38×10^7 and 5.39×10^7 counts \cdot° C for 25 and 100 μ g respectively, giving a ratio of 1:3.9. A similar result is obtained for the integration of the colour profiles (Σ RGB shaded areas in Figure 5.8, between 150 and 350 $^{\circ}$ C) integration values of 2.94×10^4 and 1.11×10^5 a.u.. $^{\circ}$ C (units of colour change over a temperature range) for 25 and 100 μ g respectively giving a ratio of 1:3.8. Both ratios indicate that the technique may at least be used semi-quantitatively in a relative sense. Further development is required across a wider range of sample concentrations with concentration (and hence mass calculation) validation against existing techniques such as UV-Vis spectroscopy.

The micrographs shown in Figure 5.9 and Figure 5.10 monitor the removal of rhodamine B from alumina at 100 and 25 μ g respectively. Both amounts show how a light pink colour (A) moves to an off white colour (E) as the rhodamine is desorbed. Any remaining that isn't desorbed is decomposed, leaving behind the off white colour.

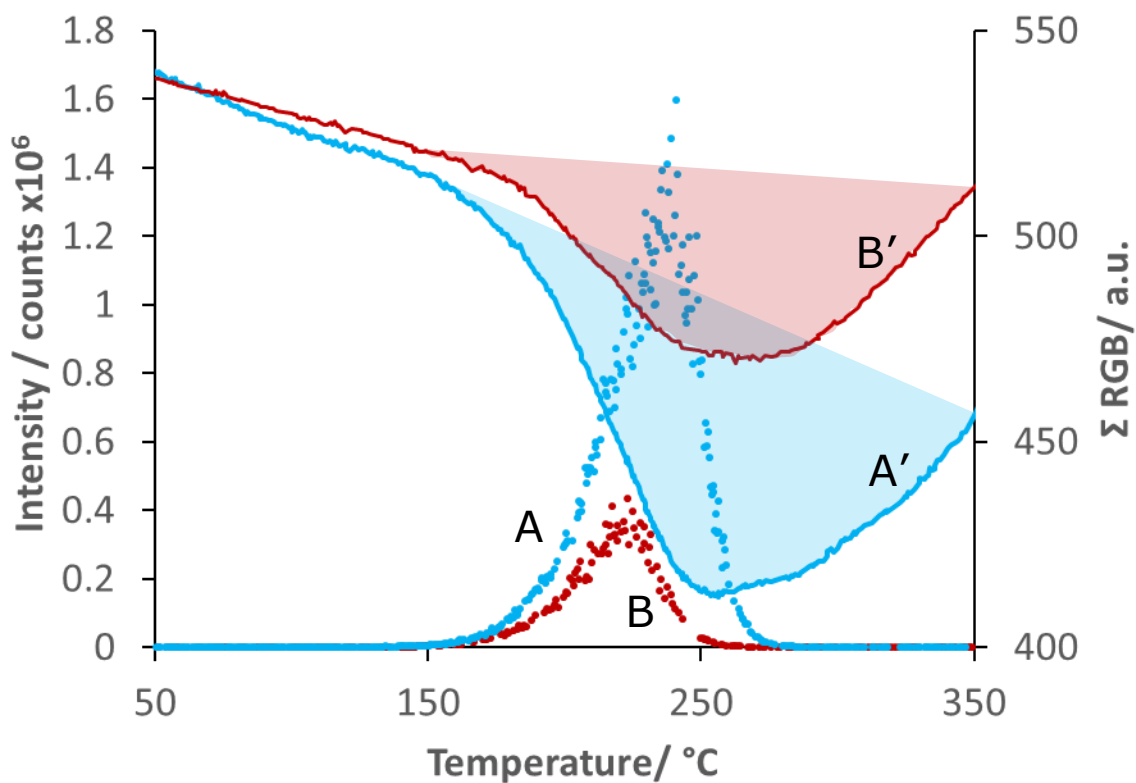


Figure 5.8 Thermal desorption of rhodamine B from alumina. A) 100 μg of rhodamine B EIC 443 Da $[\text{M}-\text{Cl}]^+$, B) 25 μg of rhodamine B EIC 443 Da $[\text{M}-\text{Cl}]^+$, A') 100 μg colour desorption profile and B') 25 μg colour desorption profile. Shaded area represent integrated areas taken from 150 $^{\circ}\text{C}$ until 350 $^{\circ}\text{C}$.

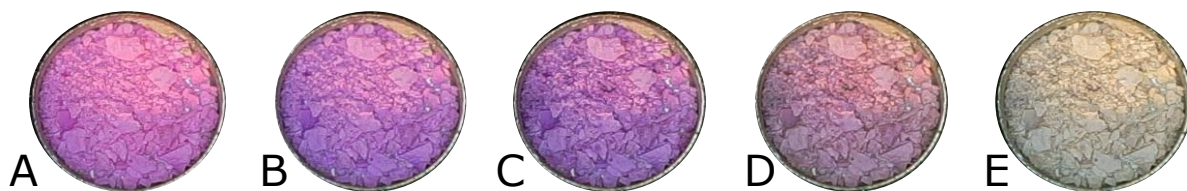


Figure 5.9 Micrographs of rhodamine B (100 μg) desorption from alumina during heating. A) 50 $^{\circ}\text{C}$, B) 150 $^{\circ}\text{C}$, C) 210 $^{\circ}\text{C}$, D) 250 $^{\circ}\text{C}$, E) 350 $^{\circ}\text{C}$.

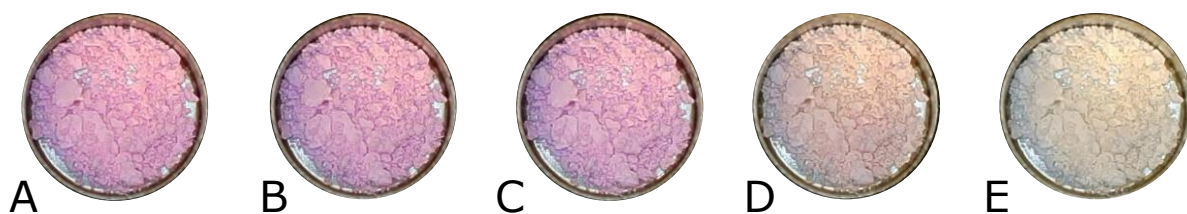


Figure 5.10 Micrographs of rhodamine B (25 μg) desorption from alumina during heating. A) 50 $^{\circ}\text{C}$, B) 150 $^{\circ}\text{C}$, C) 210 $^{\circ}\text{C}$, D) 250 $^{\circ}\text{C}$, E) 350 $^{\circ}\text{C}$.

5.3 Energetic Materials

Energetic materials (such as explosives, fuels and propellants) are defined as materials that store a large amount of chemical energy within their molecular structure. These materials typically require a small amount of externally applied energy such as heat, friction or current to initiate their decomposition and release of their potential energy moving from the solid or liquid state to primarily gas phase products.

Ambient ionisation methods have been extensively applied to the study of energetic materials and DART-MS has shown promise in the detection and quantitation of explosives. The detection of IEDs (improvised explosive devices) and general munitions is paramount for modern day security efforts and often these materials containing other materials such as binders, accelerants and oxidants.

As a forensic screening tool DART-MS is required to analyse trace and ultra-trace quantities of materials from surfaces either directly from a section of the material of interest or through a transfer method such as a swab or wipe. Nilles *et al.* investigated the removal of a range of commonly encountered nitro-aromatic compounds from various surfaces such as glass, steel and wood.¹⁰ The group used a modified transfer method to analyse solids transferred onto the surface of interest as opposed to solution deposition from a pipette, known amounts of samples were first deposited onto aluminium foil and when dried they were abrasively removed from the aluminium foil onto the surface of interest, thus simulating deposition of solid material after an explosion. The group successfully managed to detect a range of transferred nitro-aromatic compounds by adding dichloromethane as a dopant near the DART source itself primarily and detecting the compounds as the chloride adducts.

Another increasingly used method for the detection of energetic materials (and other controlled substances) is ion mobility spectrometry (IMS) where its relative simplicity lends itself for use in places like airports. IMS works by separating analytes based on their drift velocities as opposed to their m/z ratios like MS. Analytes are typically thermally desorbed into a drift region and are accelerated between the gate (the starting point) and the detector (the end point) using a series of charged plates. The separation occurs as the accelerated ions drift against a counter flow of gas, the result is the largest ions are the slowest and the smallest are the fastest.

There is a growing trend to couple DART-MS with other complimentary techniques and linking with IMS would provide the necessary separation technique before MS detection. This instrumental combination was used by Krechmer *et al.* to study lipid profiling from natural oils, fish, olive and human sebum oils.¹¹ The DART-IMS-MS technique would provide incredibly useful for energetic materials evaluation. The DART-IMS technique

appears to be in its infancy and after a review of the literature no applications towards energetic materials could be found.

Another technique that has been used in conjunction with DART-MS is DAPNe (Direct analyte-probed nanoextraction). DAPNe relies on the nanoextraction of materials from a surface by precisely positioning a micro syringe and a capillary tip for analyte removal before the latter are introduced directly into the DART sampling region. Verbeck *et al.* found that using DAPNe-DART-MS trace quantities of energetic materials to be removed from latent fingerprints without damaging them.¹² The solvation and removal methods of DAPNe provide a technique that removes analytes from the overall matrix and reduces background levels typically observed during standard DART-MS analysis of surfaces.

With so much emphasis placed on the use of DART-MS as an analysis tool for energetic materials, it was decided to evaluate HDM with these types of system.

5.3.1 Conventional HDM analysis

As an initial investigation a range of samples was investigated using HDM in the standard mode of analysis, using the Inconel pan in the hot-stage.

A summary of the samples analysed is shown in Table 5.1. All samples were nitro-functionalised aryl or alkyl compounds and were purchased as fixed concentration solutions (typically 1 mg per ml, AccuStandards) which were diluted so that known amounts (10 µg) of sample could be deposited on the individual pans. Solvent was removed by drying in the air for at least 30 minutes prior to analysis in the negative ion mode.

All compounds tested had well defined peaks significantly above the background levels of the DART-MS spectrum. Figure 5.11 shows selected examples that had been thermally desorbed from the analysis pan during HDM analysis.

All samples were exposed to a linear heating rate of 5 °C min⁻¹ between 30 and 300 °C.

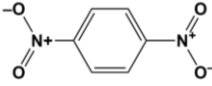
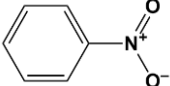
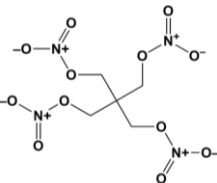
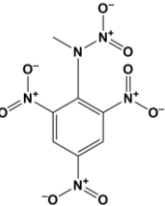
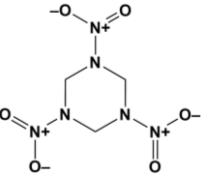
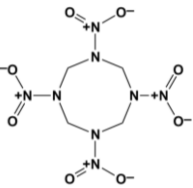
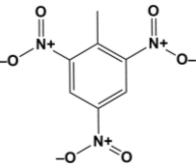
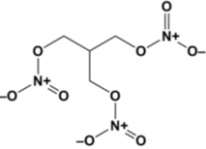
It is worth noting that the digital microscope typically used in HDM lacked the magnifying power to be informative when looking at trace levels of analytes. However, should a microscope with increased magnification be used it is possible that HDM could monitor the individual crystals of these energetic materials. Particular care was taken to minimise contamination of the instrument and negligible 'carry over' was noted between runs.

Profile A shows the removal of the deprotonated molecular ion of nitrobenzene (NB) 122 Da [M-H]⁻; although a volatile liquid at room temperature very little NB is noted until it reaches its boiling point of 210 °C. After the boiling point is reached the NB rapidly evolves until around 300 °C when the heating ramp finishes, although the profile appears to be plateauing around this temperature.

Profile B monitors the removal of PETN as its hydroxylated molecular ion 333 Da [M+OH]⁻ over the 300 °C temperature range. Again the profile begins to increase in significant intensity after the boiling point has been reached (ca. 180 °C) and decomposes above 215 °C.¹³ The profile rises above the boiling point until a maximum evolution at 240 °C and then declines, probably due to a combination of material exhaustion and decomposition, until a stable signal is noted around 280 °C.

Profile C shows the removal of the denitrated molecular ion of tetryl 241 Da [M-NO₂]⁻. Tetryl melts around 130 °C and reaches its explosive limit at its flash point of 180 °C in air. The tetryl appears to become volatile around this temperature showing the onset of release around 185 °C and is continued to be evolved until 260 °C as the material becomes exhausted and the profile declines until the end of the experiment at 300 °C. Materials may exist beyond their flash point without a source of ignition, this is slightly different to the auto-ignition temperature where a material may spontaneously ignite and decompose.

Table 5.1 A table of nitro-based compounds investigated using HDM

Material	Structure	Molecular formula and weight (g mol ⁻¹)	Ions observed
1,4-Dinitrobenzene (1,4-DNB)		C ₆ H ₄ N ₂ O ₄ = 168.1	167 Da [M-H] ⁻
Nitrobenzene (NB)		C ₆ H ₅ NO ₂ = 123.1	122 Da [M-H] ⁻ 185 Da [M+NO ₃] ⁻
2,2-Bis[(nitrooxy)methyl]propane-1,3-diy dinitrate (PETN)		C ₅ H ₈ N ₄ O ₁₂ = 316.1	315 Da [M-H] ⁻ 333 Da [M+OH] ⁻ 378 Da [M+NO ₃] ⁻
2,4,6-Trinitrophenylmethylnitramine (Tetryl)		C ₇ H ₅ N ₅ O ₈ = 287.2	241 Da [M-NO ₂] ⁻ 349 Da [M+NO ₃] ⁻
1,3,5-Trinitro-1,3,5-triazinane (RDX)		C ₃ H ₆ N ₆ O ₆ = 222.1	268 Da [M+NO ₂] ⁻ 284 Da [M+NO ₃] ⁻
1,3,5,7-Tetranitro-1,3,5,7-tetrazocane (HMX)		C ₄ H ₈ N ₈ O ₈ = 296.2	342 Da [M+NO ₂] ⁻ 358 Da [M+NO ₃] ⁻
2,4,6-trinitrotoluene (TNT)		C ₇ H ₅ N ₃ O ₆ = 227.1	226 Da [M-H] ⁻
Propane-1,2,3-triyl trinitrate (Nitroglycerin, NG)		C ₃ H ₅ N ₃ O ₉ = 227.1	289 Da [M+NO ₃] ⁻

Profile D shows the removal of the deprotonated molecular ion of TNT 226 Da $[M-H]^-$. Little is observed until around 80 °C when the TNT melts.¹⁴ Above this temperature, the profile rises exponentially until around 260 °C (TNT's boiling point)¹⁵ when it falls sharply as material is exhausted.

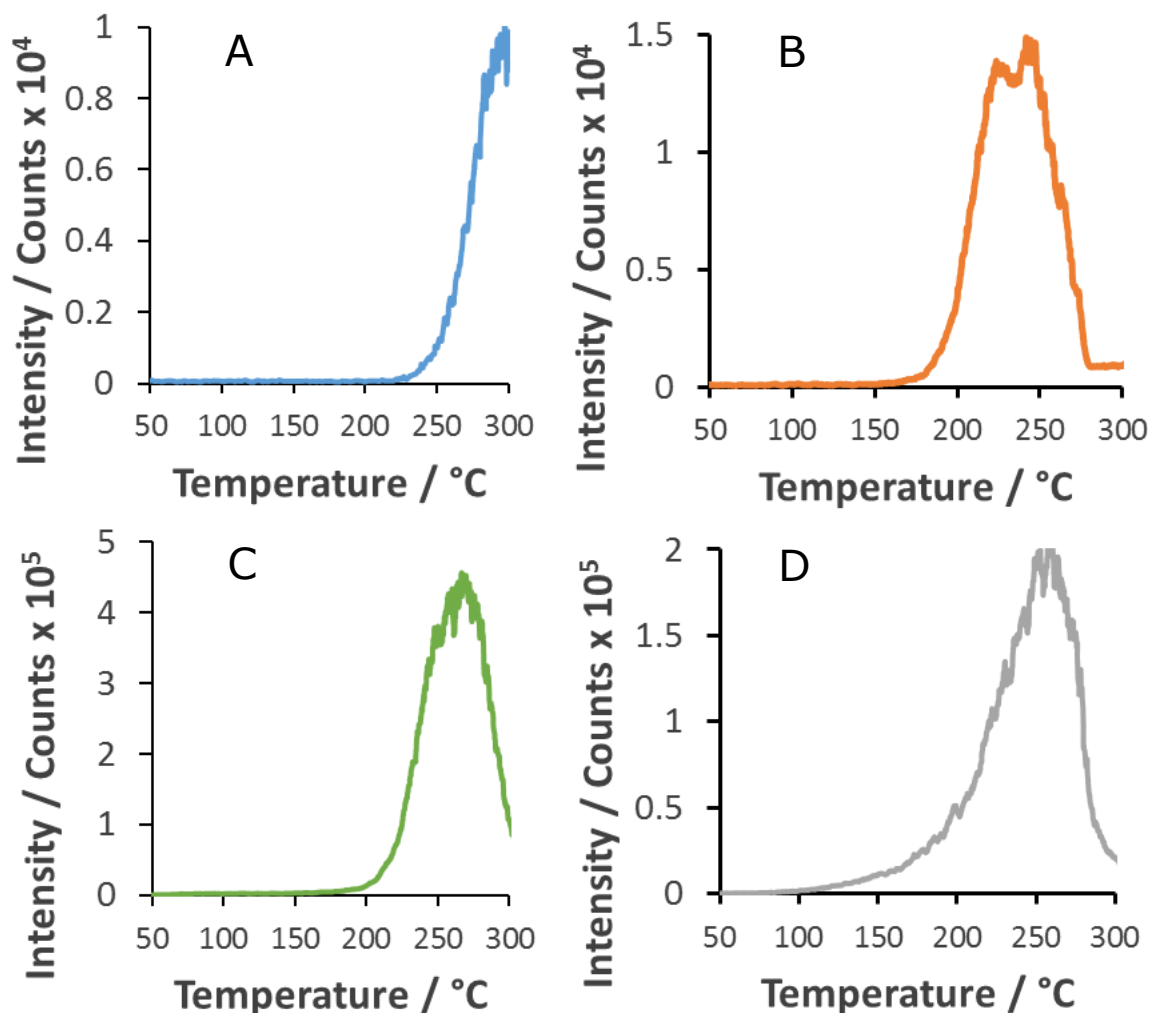


Figure 5.11 Selected examples of thermal desorption of nitro compounds from Inconel analysis pans plotted as the respective EIC vs Temperature. A) NB 122 Da $[M-H]^-$, B) PETN 333 Da $[M+OH]^-$, C) Tetryl 241 Da $[M-NO_2]^-$ & D) TNT 226 Da $[M-H]^-$.

5.3.2 Limits of detection using conventional HDM analysis

The identification of the major ions allowed experiments to determine the limits of detection (LOD) with HDM for a selection of compounds.

The LOD is defined as the lowest level of analyte that can be reliably and repeatedly measured or distinguished from the background or a 'blank' sample.¹⁶ The LOD is compound specific for each MS technique and hence needs to be evaluated per compound system. A range of factors determine the LOD for ambient ionisation MS analysis: the inherent background noise from an open source mass spectrometer, the respective ion affinities for different adducts and hence the ease of ionisation, the substrate or matrix of the analyte leading to matrix effects and/or possible ion suppression.

A standard model for the instrumental limit of detection is that the magnitude of the analyte signal must be at least 3 standard deviations plus the average of the background level for the ion of interest, whereas the instrumental limit of quantitation (LOQ) is defined as being at 10 standard deviations of the background level plus the average.

Since the HDM relies on temperature profiling another vector is added, the moving temperature vs ion relationship. It has been noted throughout many experiments that the background level of the HDM varies with increasing temperature, as even atmospheric background ions will fragment at a given temperature. To collect background profiles representative of the instrument, the experimental conditions were fixed to match the conditions of sample analysis.

Full range mass spectral scans were performed using an empty pan over the entire temperature range that the sample would be subjected to. The background scans were repeated three times between each analyte series to gain a triplicate average for the background levels and from this the ion of interest could be averaged and extracted. This process has been depicted in Figure 5.12 for an arbitrary mass of 200 Da, selected for its naturally low background levels and does not correspond to any analyte of interest.

Profile A shows three averaged total ion thermograms for the mass range 50 to 2800 Da and, even with an empty pan, an underlying shape is noted across the temperature range. The general profile shape has been tentatively attributed to the increase in the amount of nitrate 62 Da $[\text{NO}_3]^-$ and the protonated nitrate dimer 125 Da $[2(\text{NO}_3)+\text{H}]^-$ over the 50 to 250 °C temperature range. This may be due to the presence of NO_x species which have been noted to form through the operation of atmospheric plasma sources.¹⁷

Profile B is a plot of three extracted ion thermograms (grey) for an arbitrary mass of 200 Da representative of a background level of interest. The three profiles are then averaged together to make the background EIC of 200 Da (blue).

The average intensity across the temperature range of interest is calculated for the 200 Da mass (122 counts) and three standard deviations (calculated from the three background experiments) are added to this for the LOD (red dashes) and ten standard deviations are added for the LOQ (orange dashes) shown in profile C.

This method was used throughout to determine if selected compounds could be monitored above their respective LOD. Many compounds have not been pushed to the absolute LOD using HDM, instead they were evaluated in the 1-100 nanogram range representative of trace levels. Again, the use of the LOQ was considered of less importance as the longer-term aim would be to use HDM as a qualitative technique for rapid and confident analysis of whether a compound of interest poses a potential threat.

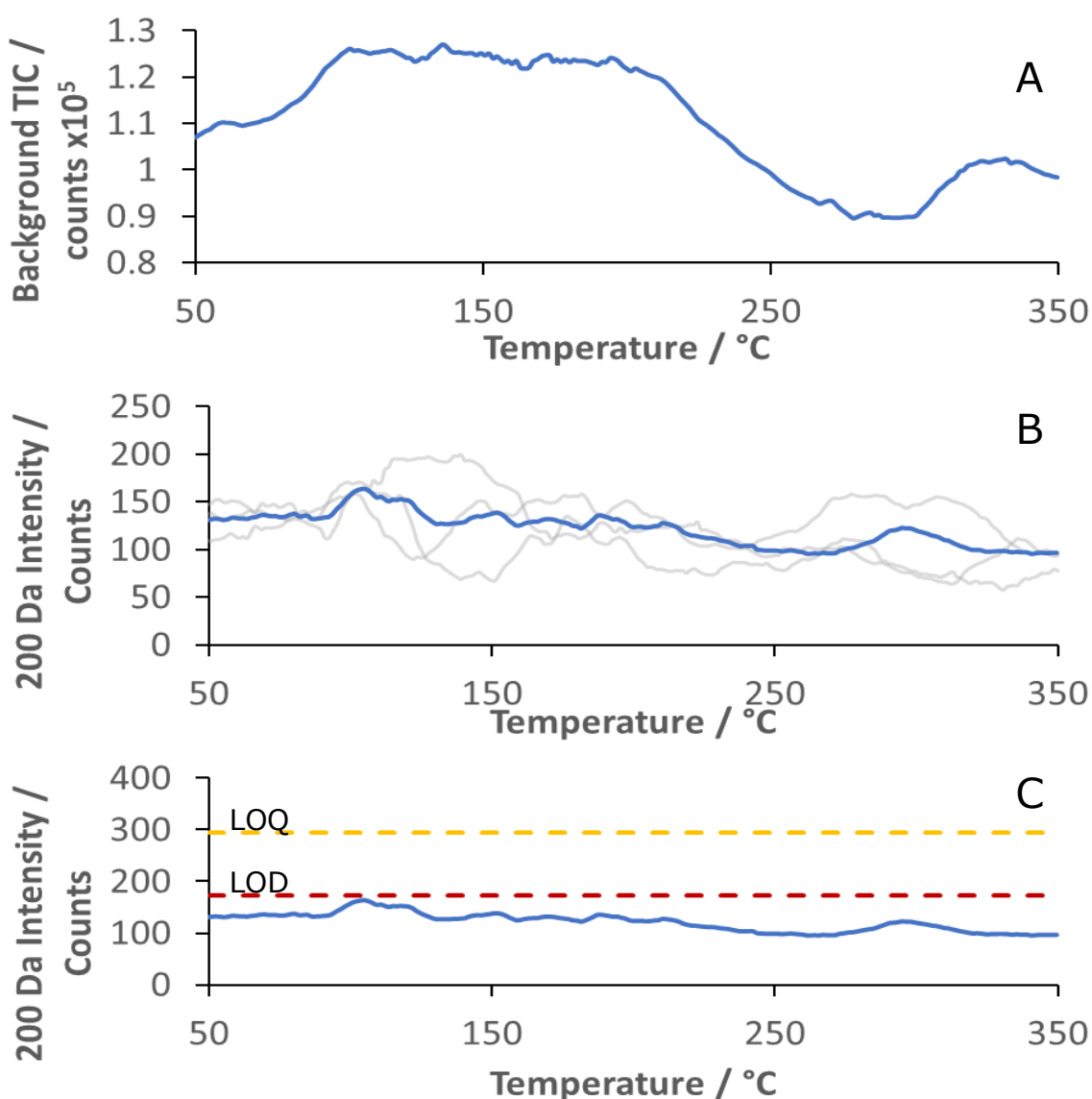


Figure 5.12 Collection and processing of background ion levels. A) Triplicate average of background total ion thermograms plotted against temperature, B) EIC of 200 Da triplicate average, showing the average (blue) and three repeats (grey), C) Application of LOD (red dash) and LOQ (orange dash) to the 200 Da profile.

The absolute LOD of a selection of compounds was investigated. The following example shows the evaluation of tetryl using HDM in its 'raw' form, that is, without the assistance of dopants commonly used within conventional DART-MS analysis. The factor of most importance for increasing the sensitivity of the system was the heating rate (as is true for other TA systems). Most systems investigated with HDM used standard heating rates between 5 and 10 °C min⁻¹, but here the upper heating rates of the HDM instrument were evaluated to achieve maximum sensitivity.

A linear heating rate of 5 °C min⁻¹ was applied to each of the samples until the ion intensity began to decline and fall close to the LOD, several samples commonly had shown multiple peaks relating to the compound of interest. Tetryl mainly gave the denitrated molecular fragment ion 241 Da [M-NO₂]⁻ and the nitrated molecular adduct ion 349 Da [M+NO₃]⁻. Figure 5.13 shows how tetryl forms two ions depending on the desorption temperature, the adduct (349 Da) forms in preference at lower temperatures, whilst the fragment ion (241 Da) shows preferential formation at the higher temperatures attributed to a thermal degradation process, note how the onset of the degradation product appears at the same temperature of the decline of the adduct profile.

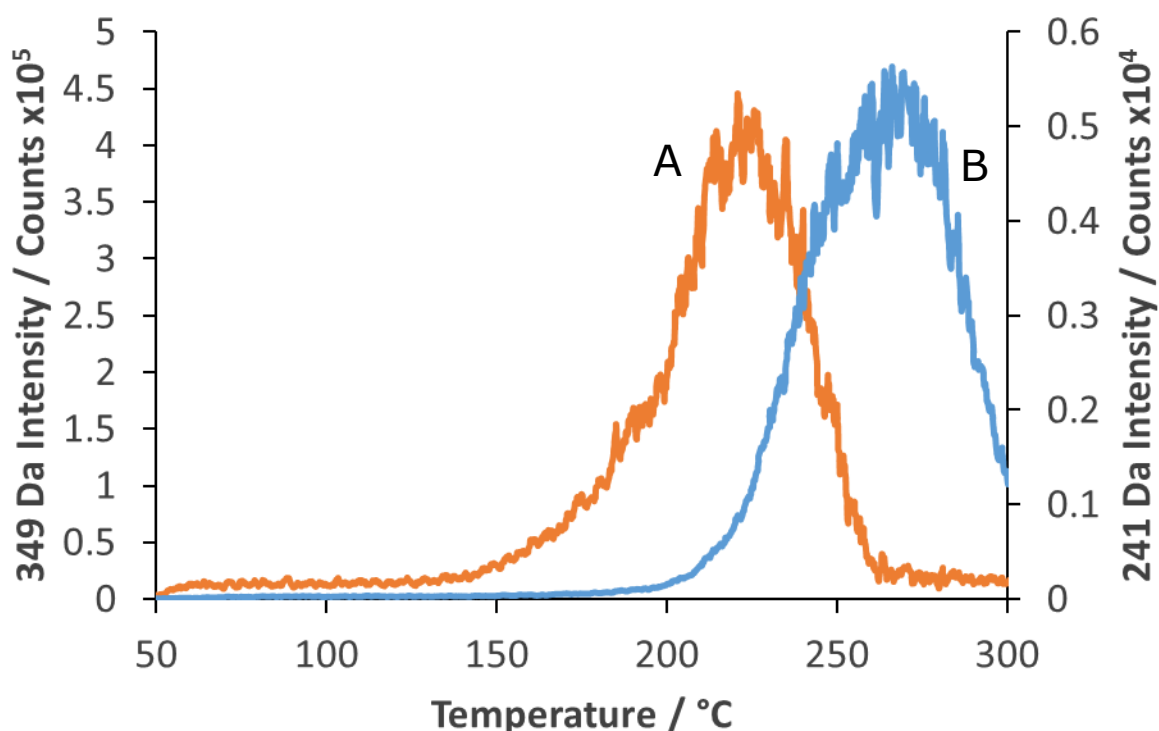


Figure 5.13 Thermal desorption of 10 µg of tetryl from the HDM stage. Ion profiles A) molecular adduct 349 Da [M+NO₃]⁻ and B) fragment ion 241 Da [M-NO₂]⁻.

As many of the samples could be monitored in the microgram range the solutions were made significantly more dilute to evaluate more conventional 'trace' levels within the nanogram range. Solutions of tetryl were prepared via serial dilution methods to obtain fixed concentrations, solutions were aliquoted into each pan to contain a known mass of tetryl. Once dried the samples underwent HDM analysis at various heating rates.

Figure 5.14 shows the removal of 1 ng of tetryl 349 Da $[M+NO_3]^-$ at $5\text{ }^\circ\text{C min}^{-1}$ (profile A) compared against the same sample amount but heated at $50\text{ }^\circ\text{C min}^{-1}$ (profile B), the respective LODs have been added for comparison. Although the slower heating rate yielded a significant response above the LOD, it is evident that a sharper and more pronounced profile is obtained at higher heating rates. Encouragingly, the background profiles do not appear to fluctuate significantly with heating rate. The increased heating rate is also advantageous due to the volatile nature of the materials, leading to increased turnaround of samples. So far the experimental times could be viewed as an apparent weakness of the HDM system when compared to the core DART-MS technique, although slower heating rates yield increased resolution between thermal events.

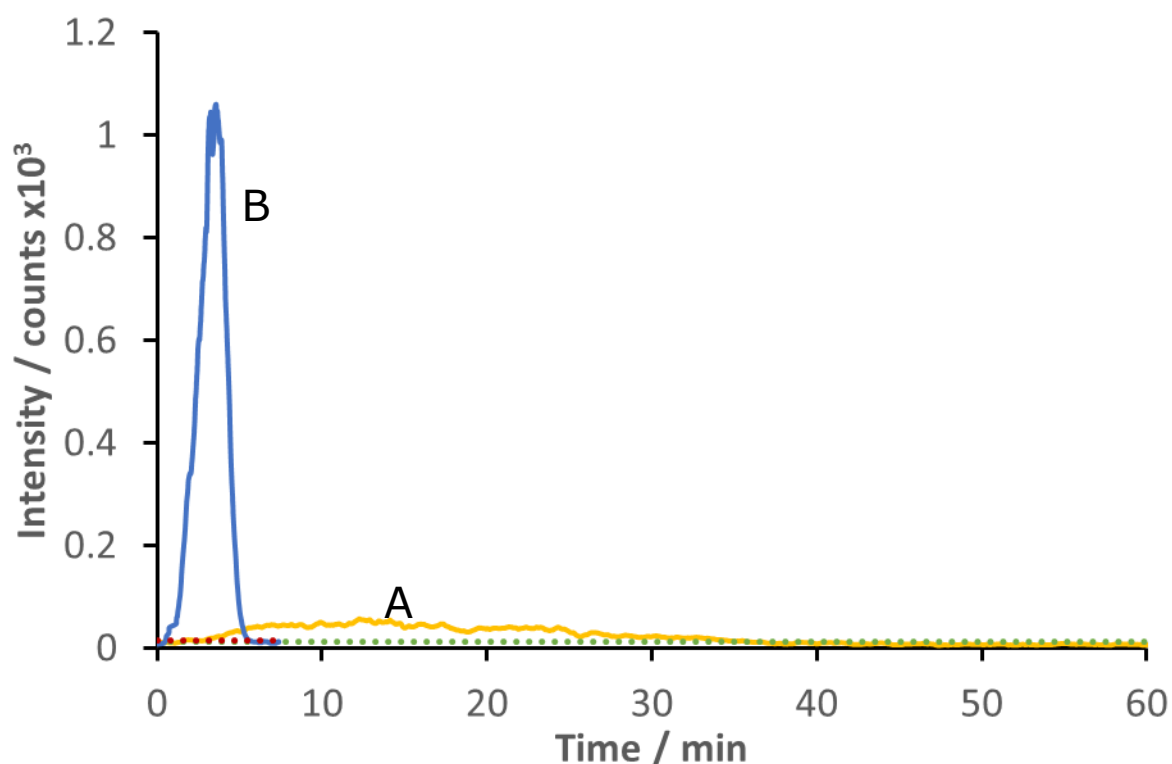


Figure 5.14 Heating rate comparison of the thermal desorption of 1 ng of tetryl 349 Da $[M+NO_3]^-$ from a HDM analysis pan. A) Heating rate of $5\text{ }^\circ\text{C min}^{-1}$ removal of 1 ng of tetryl, B) Heating rate of $50\text{ }^\circ\text{C min}^{-1}$ removal of 1 ng of tetryl. LOD; dashed green trace $5\text{ }^\circ\text{C min}^{-1}$ heating rate and dashed red trace $50\text{ }^\circ\text{C min}^{-1}$ heating rate.

The heating rate was capped at 50 °C min⁻¹ as a safety feature to prevent damage to the hot-stage itself through potential thermal shock. However, it is worth noting that higher heating rates can be achieved with the system but were not investigated as part of this study.

The lowest detectable limit observed so far using the HDM system was 100 pg of tetryl using the 50 °C min⁻¹ heating rate. Figure 5.15 shows the desorption profile of 100 pg of tetryl. The LOD (red dashed line) was included for comparison against the tetryl profile, again the trace remains comfortably above the LOD.

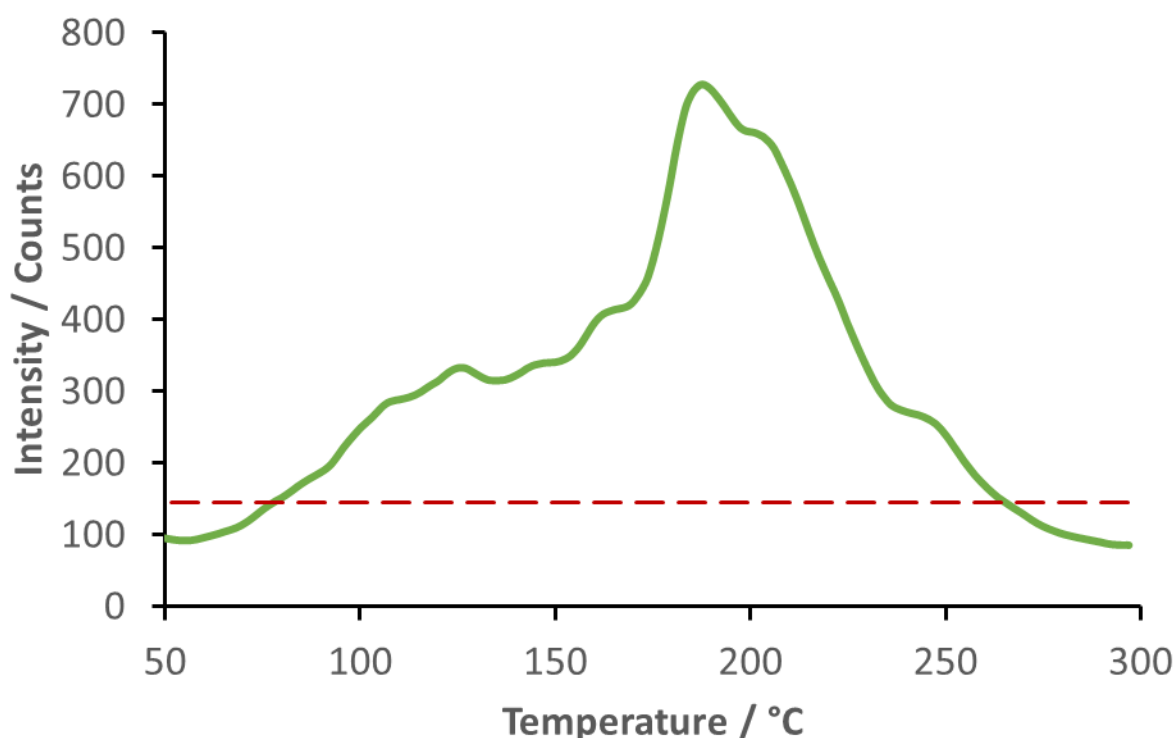


Figure 5.15 Thermal desorption of 100 pg of tetryl 349 Da $[M+NO_3]^{-1}$ from the HDM stage, linear heating at 50 °C min⁻¹. Red dashed line shows the LOD for tetryl.

Tetryl, TNT, RDX, HMX and PETN were evaluated at a 100 ng level, showing significant detection above their respective LODs. Since the preliminary studies had been based on direct deposition of sample into an analysis pan, a process which is very far from an actual field collection technique, an evaluation of different swabbing materials was undertaken to more closely replicate a real-life application.

5.3.3 Evaluation of swabbing materials

A clear benefit that DART-MS has over HDM is the ability to analyse a variety of sample morphologies and that it isn't confined to analysis from a sample pan. The premise for the HDM approach is ensuring even heating across the sample, leading to complete desorption of the sample from the surface of interest.

After reviewing the literature an array of swabbing materials and techniques were identified including both destructive and non-invasive techniques; swabs,¹⁸ wipes¹⁹ and complete destruction of surfaces of interest²⁰ are currently used for investigations into suspected energetic contact materials (items that have been in contact or stored near energetic materials). The field of collection materials appears to be growing particularly for materials scientists working on the design of better collection materials.²¹

A range of surface collection materials (shown in Figure 5.16) was evaluated first by analysing the background generated by the material and then comparison with the same material but spiked with a known amount of energetic material. This method then allowed for background spectra to be representative of the potential decomposition products of the collection material itself.

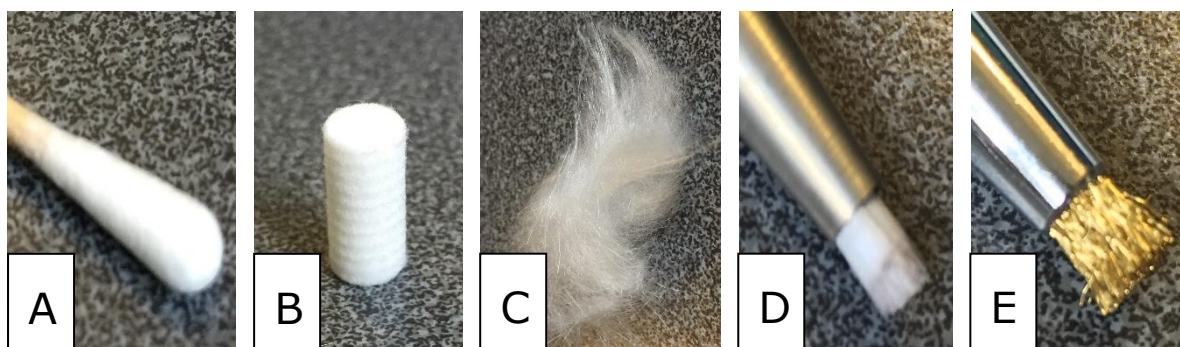


Figure 5.16 Images of the collection materials. A) Cotton Swab, B) Cellulose acetate filter, C) Quartz wool, D) Fibre glass and E) Brass fibres.

The collection materials were chosen based on their ability to fit into a HDM pan and also with the future aim to analyse them using the planned desorption stage discussed in Chapter 2, Section 2.7.

Each collection material was thermally profiled in its untreated state to account for any background ions generated. In the profiles from experiments where the swabbing materials were spiked with analyte, 100% of the material is assumed to be desorbed. From these profiles the efficiency of surface sampling can be evaluated by depositing a solution of analyte with the same concentration onto a fixed surface and swabbing the

surface with the collection material. Integration of the peaks found above the LOD band were then taken, the spiked collection material representing 100% collection and the swab representing a percentage collection.

As many factors as possible were kept constant to evaluate the collection process for direct comparisons between materials.

A volume of tetryl solution (containing 100 ng) was deposited directly onto a collection material, the solution was then allowed to evaporate for 1 hour at room temperature. The materials were then placed within an Inconel pan, added to the hot-stage and subjected to a heating rate of 10 °C min⁻¹ between 30 and 300 °C. The DART and MS were operated in negative mode, and all masses were collected between 50 and 500 Da. EIC profiles were obtained for a constant fingerprint ion of tetryl 241 Da [M-NO₂]⁻. The LOD for the 241 Da ion was found for each collection material by analysing the raw material itself under the same analysis conditions. Once the spiked and raw material profiles were obtained a 'swabbing' procedure was developed to evaluate the collection efficiency of the collection materials. Samples were spiked onto a clean surface (an Eppendorf vial lid) and allowed to dry for 1 hour under the same conditions as the spiked examples. The analysis of the swabbing material was identical to the spiked and raw examples discussed previously in Section 5.3.2.

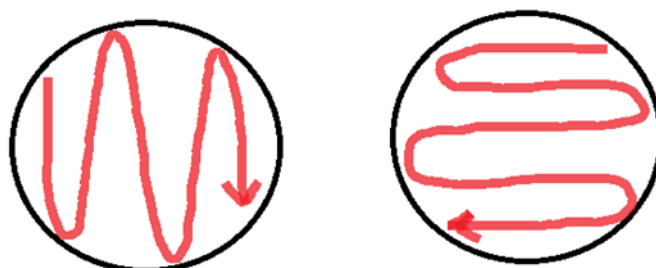


Figure 5.17 Pictorial representation of the swabbing procedure, the circle represents an Eppendorf vial lid and the red arrow shows the swabbing direction, vertical and then horizontal.

Figure 5.17 shows a pictorial representation of the procedure used to remove the samples from the chosen surface (the lid of an Eppendorf vial). The procedure followed a vertical sinusoidal pattern on the first pass, and then on the same lid the corresponding horizontal pass. The lids provided a reproducible sampling area and were economical since they are disposable. Profiles were taken by swabbing the lids directly without any sample deposition, the swabs from the lids were not found to have any effect on the overall level of the 241 Da ion and thus were disregarded for the following series. The technique, although crude, aimed to reduce some of the uncertainty of duration in swabbing by standardising the process. This is not representative of a real scenario and was solely aimed at being a comparative evaluation for material collection.

5.3.3.1 Cotton medical swab

The first material evaluated was a cotton medical swab (Figure 5.16, A). The exact material composition was not identified on the packaging only that the main body was 100% cotton. The cotton itself appeared to have been adhered to the wooden stem either by an adhesive or mechanical adhesion through high speed spinning. It was of importance to ensure all components were included for collecting a background profile, as the whole collection swab material is hoped to be deposited directly into the planned desorption stage.

Background profiles were obtained respective to each ion of interest. Figure 5.18 shows a comparison of the 100 ng tetryl spiked and collected using the cotton swab against the calculated LOD from the cotton swab itself based using the fragment ion 241 Da $[M-NO_2]^-$. The shaded profiles for the spiked and swab samples are used for integration. This area is taken above the LOD for the medical swab material. The spiked sample gave an integration value of 5.06×10^5 counts. $^{\circ}C$ representative of 100% collection, whilst the surface recovered sample gave 3.43×10^5 counts. $^{\circ}C$ overall totalling a 67.8% recovery using the cotton swab.

Since the cotton is a thermal insulator the peak shape is broadened over a wider temperature range. This is innately a drawback to using these types of materials, as the resolution between peaks (when analysing mixtures) will be diminished. Similar effects were noted by the research group in an earlier project showing how the introduction material may vary the resultant mass spectral profile due to the thermal properties of the material.²²

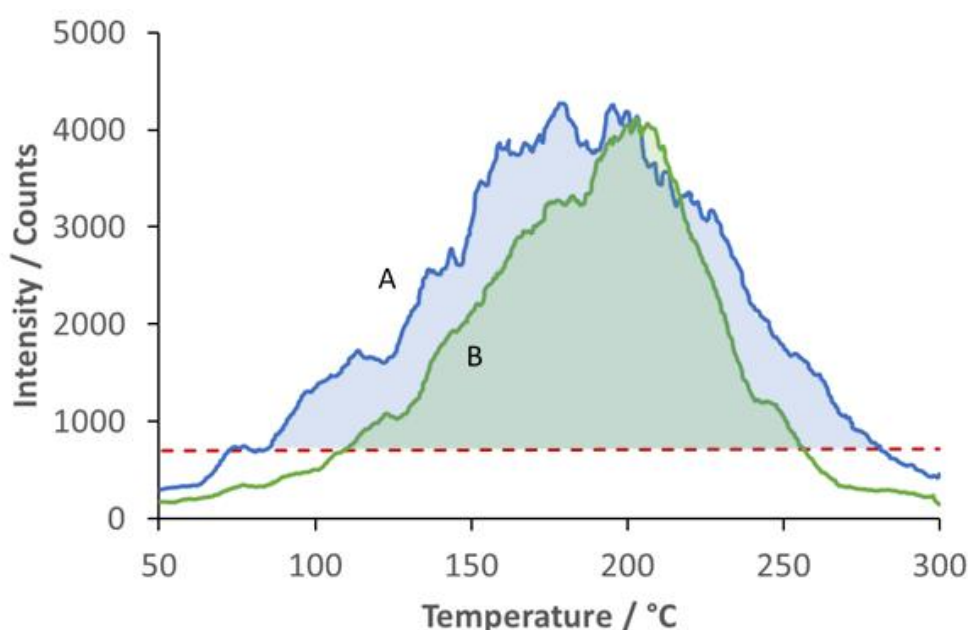


Figure 5.18 Medical cotton swab removal of tetryl observed as 241 Da $[M-NO_2]^-$ profiled as a function of temperature. A) Spiked Swab, B) Surface recovered sample and Red dashed line LOD.

5.3.3.2 Cellulose acetate filter

The second collection material investigated was a cigarette filter (Figure 5.16, B), purchased from a local high street store. The filter provided a smooth collection surface, was the correct size/geometry for HDM and also is a very economical collection material. The filter material is primarily composed of cellulose acetate, which gave a significant background fingerprint particularly in positive mode. The energetic materials evaluated so far gave the largest responses in negative mode, thus reducing the concern of high backgrounds from the cellulose acetate itself. The filter did eventually decompose under heating between 250 and 300 °C, shown as a series of micrographs insert Figure 5.19.

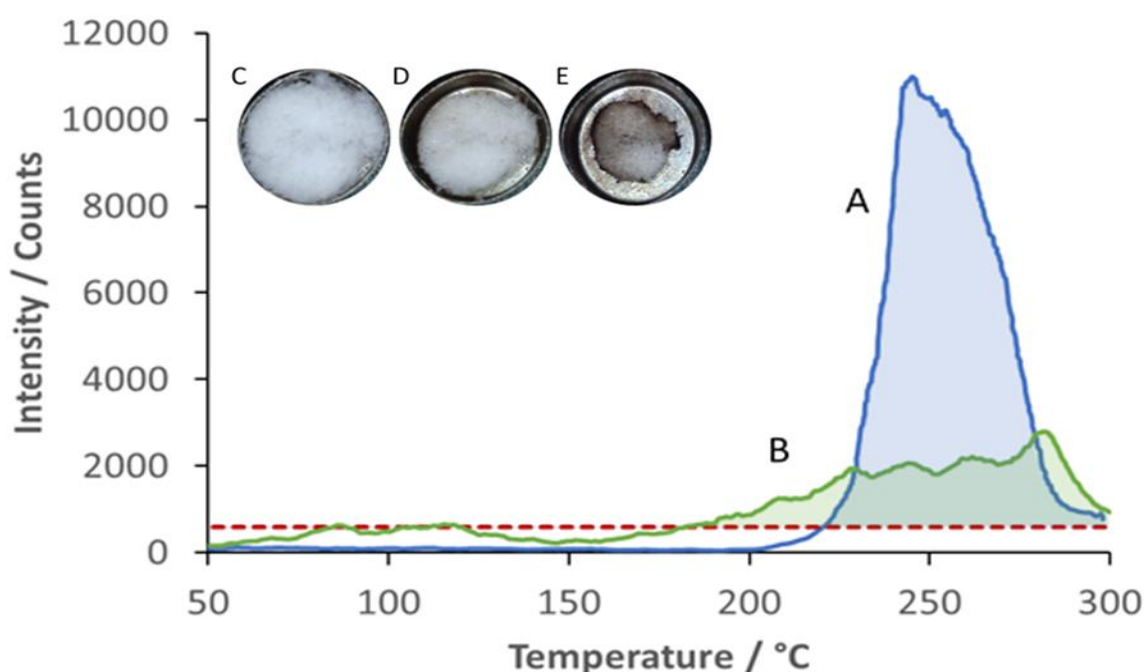


Figure 5.19 Cellulose acetate filter removal of tetryl observed as 241 Da [M-NO₂]- profiled as a function of temperature. A) Spiked filter, B) Surface recovered sample and Red dashed line LOD. Micrographs of a cigarette filter under linear heating using HDM. C) 200 °C, D) 250 °C and E) 300 °C.

Although the cellulose acetate is likely to behave as a thermal insulating material the profile for tetryl stays relatively sharp (Figure 5.19) when compared to the previous cotton example. This is likely due to the extent of packing of the cellulose material, having an apparent higher density than the loosely wrapped cotton which had significant air gaps between the fibres. The LOD for this ion (241 Da) using the cigarette filter is also marginally lower than the cotton example. This is not likely to be the case for many ion values though as overlapping decomposition products are likely to be a significant issue. Integration of the peaks above the LOD are 2.95×10^5 and 6.12×10^4 counts.°C for the spiked and recovered samples respectively. The surface recovery was 20.8 %.

5.3.3.3 Quartz wool

The third collection material was quartz glass wool (Figure 5.16, C). The benefit of this material is a low background was observed across a wide mass range as it has a crystalline structure which will not undergo decomposition until extreme temperatures and it will not be easily ionised due to the soft ionisation provided by the DART source.

The use of quartz wool is expected to be a very 'soft' collection technique, relying on physically up taking materials within the loose fibres by gentle abrasion as opposed to true sorption processes that may occur for the organic based collection materials.

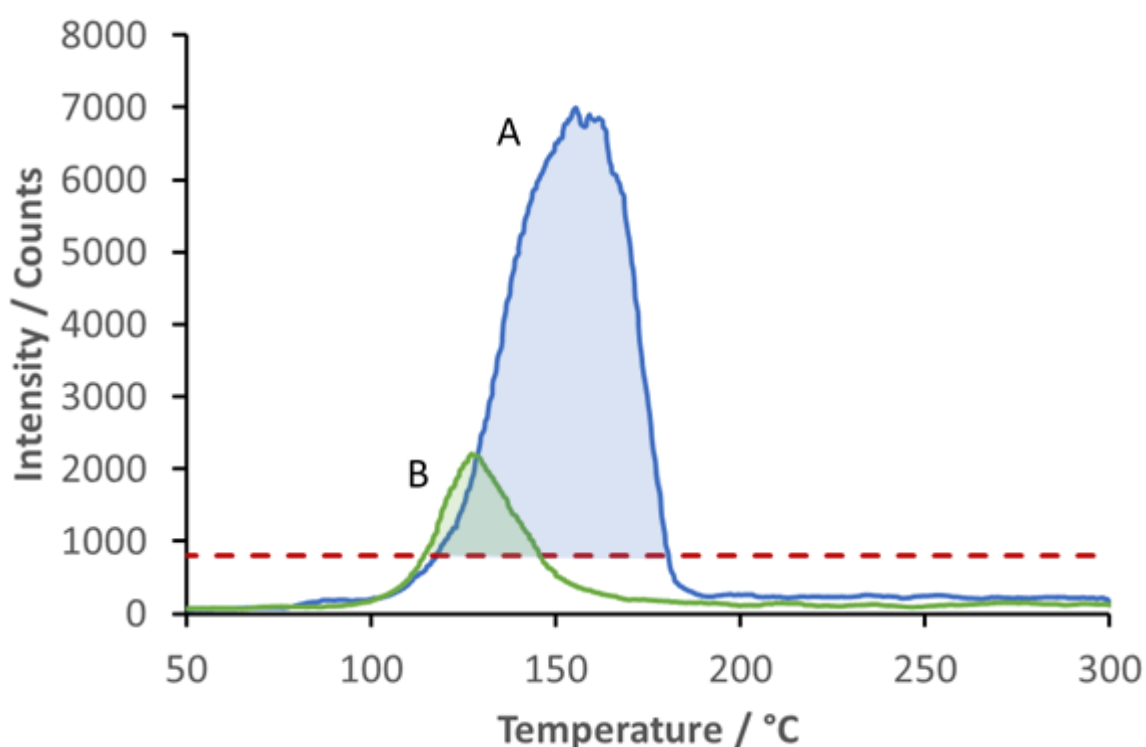


Figure 5.20 Quartz wool removal of tetryl observed as 241 Da $[M-NO_2]^+$ profiled as a function of temperature. A) Spiked wool, B) Surface recovered sample and Red dashed line LOD.

The profiles in Figure 5.20 show excellent peak shapes with significant response above the LOD band for the spiked quartz wool (A). In this example the profile has shifted to a significantly lower temperature range with the onset of removal shortly after 100 °C, this effect has been attributed to the more intimate contact that the glass fibres can make with the pan when deposited as they lay flat to the pan's surface. Interestingly, the fragment ion is shown at much lower temperatures than was noted when tetryl was analysed directly from the sample pan (Figure 5.13). The surface recovered material (B) also gives a very clean profile but is evidently weak at recovery. Peak integration yields 2.74×10^5 and 4.88×10^4 counts.°C for the spiked and swabbed quartz wool. The overall percentage recovery was 17.8 % for the quartz wool as a recovery material.

5.3.3.4 Fibre glass

The previous quartz wool example gave overall low background across the full mass scan range, so a similar product was investigated, a fibre glass cleaning pen (Figure 5.16, D). The pen is designed for removing debris from surfaces by gentle abrasion, again this type of collection material is assumed to be highly suited for surface sampling, being inorganic in composition (non-ionisable using DART) and having significantly more strength than the quartz wool to ensure thorough surface contact.

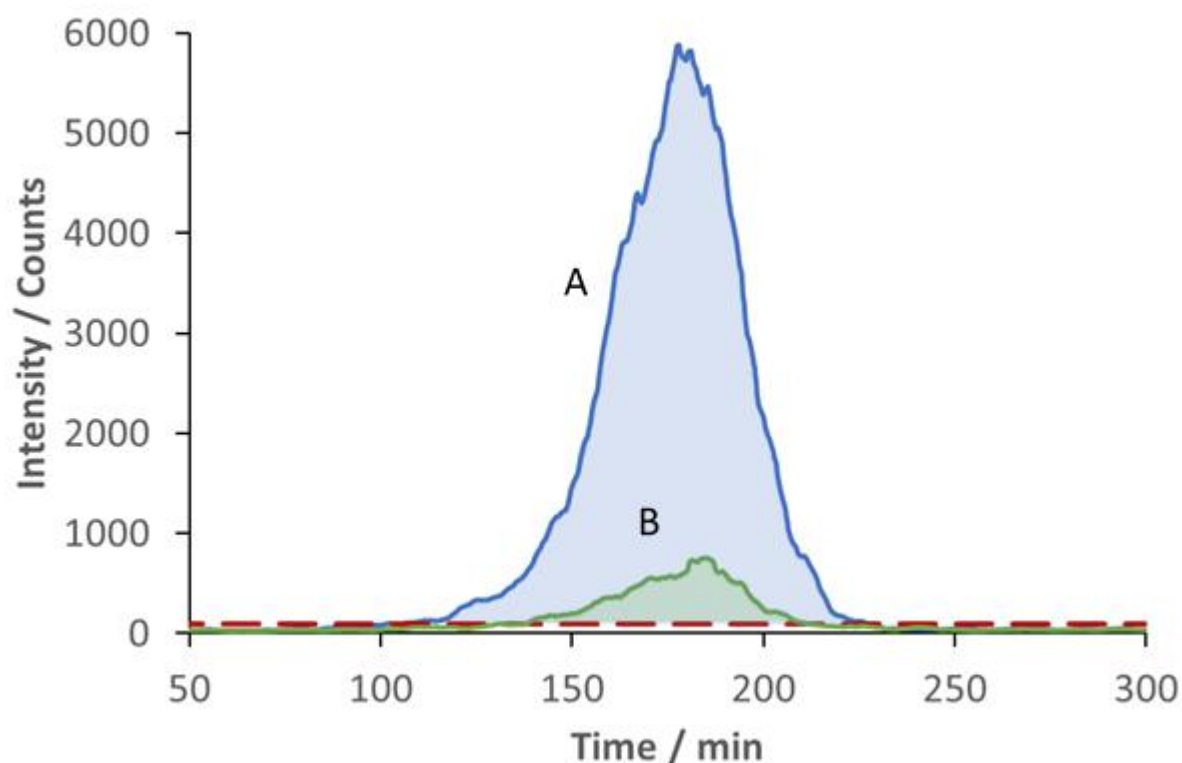


Figure 5.21 Fibre glass removal of tetryl observed as $241\text{ Da } [M-\text{NO}_2]^-$ profiled as a function of temperature. A) Spiked fibre glass, B) Surface recovered sample and Red dashed line LOD.

Figure 5.21 shows the comparison using the fibre glass pen. The removal of tetryl using the fibre glass pen and quartz wool appeared comparable for the spiked samples, although the collection efficiency of the fibre glass actually appeared marginally worse, peak integration of the spiked fibre glass (A) and surface recovered (B) tetryl was 2.43×10^5 and 2.83×10^4 counts. $^\circ\text{C}$ respectively resulting in an 11.6% recovery. The LOD for the fibre glass is significantly lower than the quartz wool but the reason for this is unclear as both sources are composed of silica. However, this effect appears reproducible across a range of different selected ions. Although the recovery is poor the significantly lower LOD band across the entire sampled mass range is an encouraging feature of the material.

5.3.3.5 Brass fibres

The final collection material evaluated was another abrasive pen but using brass fibres (Figure 5.13, E). This were assumed to be similar in collection mechanism to the glass fibres evaluated previously. Brass has a significantly higher thermal conductivity when compared to silica glass and organic materials investigated so far, assisting with the uniformity of heating across the collection material.

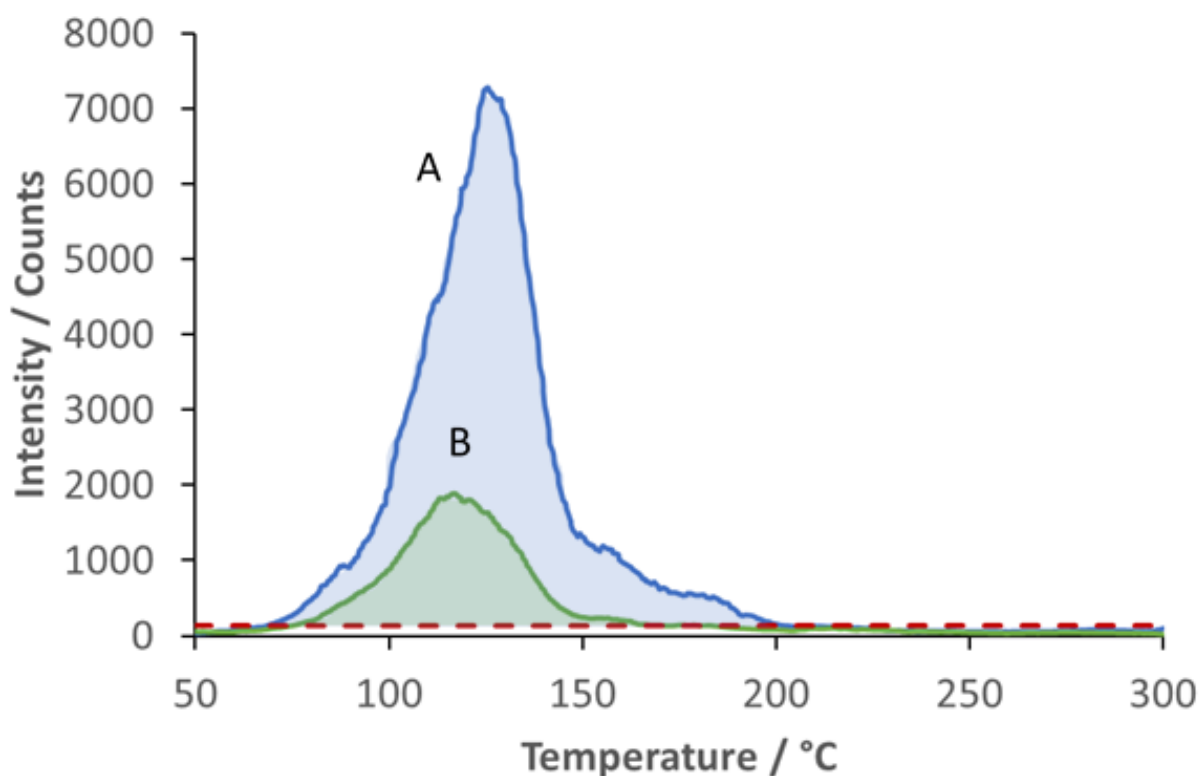


Figure 5.22 Brass fibres removal of tetryl observed as $241 \text{ Da } [M-\text{NO}_2]^-$ profiled as a function of temperature. A) Spiked brass, B) Surface recovered sample and Red dashed line LOD.

Figure 5.22 shows the comparison of using the brass fibres. The brass collection material provided excellent levels of low background across the entire mass range, giving a very low LOD for the ion at 241 Da. The profiles for the spiked and swabbed tetryl ion appear at a lower temperature when compared to the sample removed directly from the analysis pan.

Each analyte is likely to have a temperature-material dependency, that is, a characteristic temperature region at which ions are noted for a specified material. This idea will be explored further in the upcoming section (Section 5.4). The brass collection material had a 27.7 % recovery after peak integration of 2.79×10^5 and 7.71×10^4 counts. °C for the spiked and surface recovered samples respectively.

The materials evaluation was only conducted for one compound but was explored to give an insight into how surface collection material is likely to be an important factor when using DART-MS and HDM. The collection efficiencies for tetryl are summarised in Table 5.2.

Table 5.2 Comparison for recovery of 100 ng of tetryl from a plastic surface using a variety of swabbing materials.

Material	Spiked peak area integration / counts.°C	Swabbed peak area integration / counts.°C	Recovery / %
Cotton Medical swab	5.06 x10 ⁵	3.43 x10 ⁵	67.8
Cellulose acetate filter	2.95 x10 ⁵	6.12 x10 ⁴	20.8
Quartz wool	2.74 x10 ⁵	4.88 x10 ⁴	17.8
Fibre glass	2.43 x10 ⁵	2.83 x10 ⁴	11.6
Brass fibres	2.79 x10 ⁵	7.71 x10 ⁴	27.7

The organic medical swab based on cotton gave the best recovery of 67.8%, although observed significantly higher background levels and respective LOD. The analysis temperature must be reduced as thermal decomposition of the organic materials takes place, resulting in an upward shift in the background noise level.

Contrastingly, the brass fibres provided lower collection efficiency at 27.7 % recovery, but the material was highly inert with negligible background over the whole analysis temperature range giving significantly reduced detection limits when compared to organic materials.

5.3.4 Thermal separation

Often energetic materials are found as compositional mixtures, particularly in improvised explosive devices (IED).²³ If analysis of a substance relies on looking for fingerprint ions within the mass spectra, interpretation can become difficult when analysing multicomponent mixtures from the extra ions generated. Thermally profiling mixtures may provide some separation to create simplified spectra at certain temperatures, with the added benefit of obtaining potentially temperature dependent ion profiles. The temperature dependency could be of particular importance when ions share the same nominal mass, this may assist with material discrimination without the need for more advanced practices such as tandem mass spectrometry, increasing the throughput of samples.

Following on from the surface recovery work evaluated in the previous section (Section 5.3.3), the brass fibres were used for the continued thermal separation evaluation study. Although the brass fibres were representatively poor at efficiency of recovery they offered low background levels, apparently identical to analysing an empty pan across the full mass scan range. Several examples have been included to show the thermal separation capabilities of HDM analysing multiple component mixtures.

A linear heating rate of 50 °C min⁻¹ was used between 50 and 300 °C for all thermal separation studies.

Figure 5.23 shows the results of a 'proof of concept' experiment using 100 ng of TNT and 100 ng of tetryl deposited in an Inconel pan. The TNT 226 Da [M-H]⁻ (profile A) appears to evaporate from the start of the experiment, with a rapid decline in intensity until around 100 °C. Further heating shows the removal of tetryl 349 Da [M+NO₃]⁻ (profile B) primarily over the range 100 to 150 °C, with both compounds completely desorbed from the pan by 200 °C.

Figure 5.24 shows the thermal separation of TNT 226 Da [M-H]⁻ (profile A) and RDX 268 Da [M+NO₂]⁻ (profile B). The energetic materials can be separated and characterised after recovery using the brass fibres, the surface was spiked with 1µg of each substance.

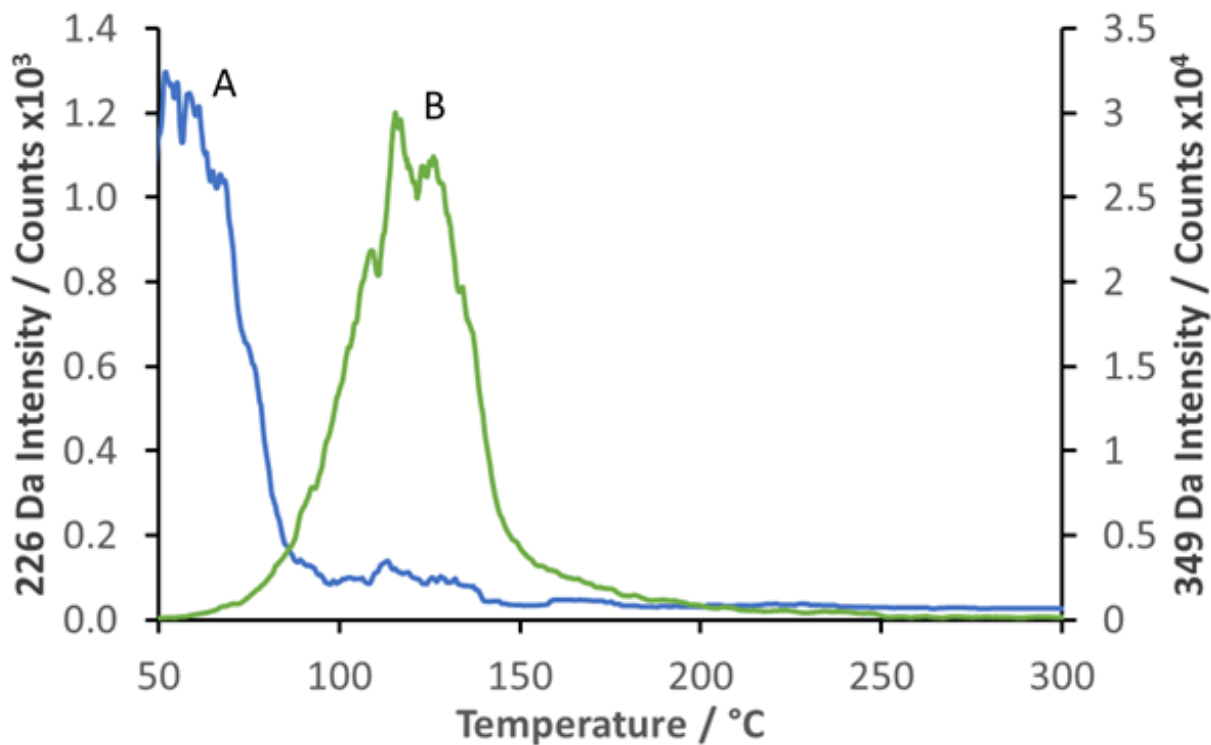


Figure 5.23 Thermal separation of pan deposited energetic materials at 100 ng amount. A) TNT 226 Da $[M-H]^-$ and B) tetryl 349 Da $[M+NO_3]^-$.

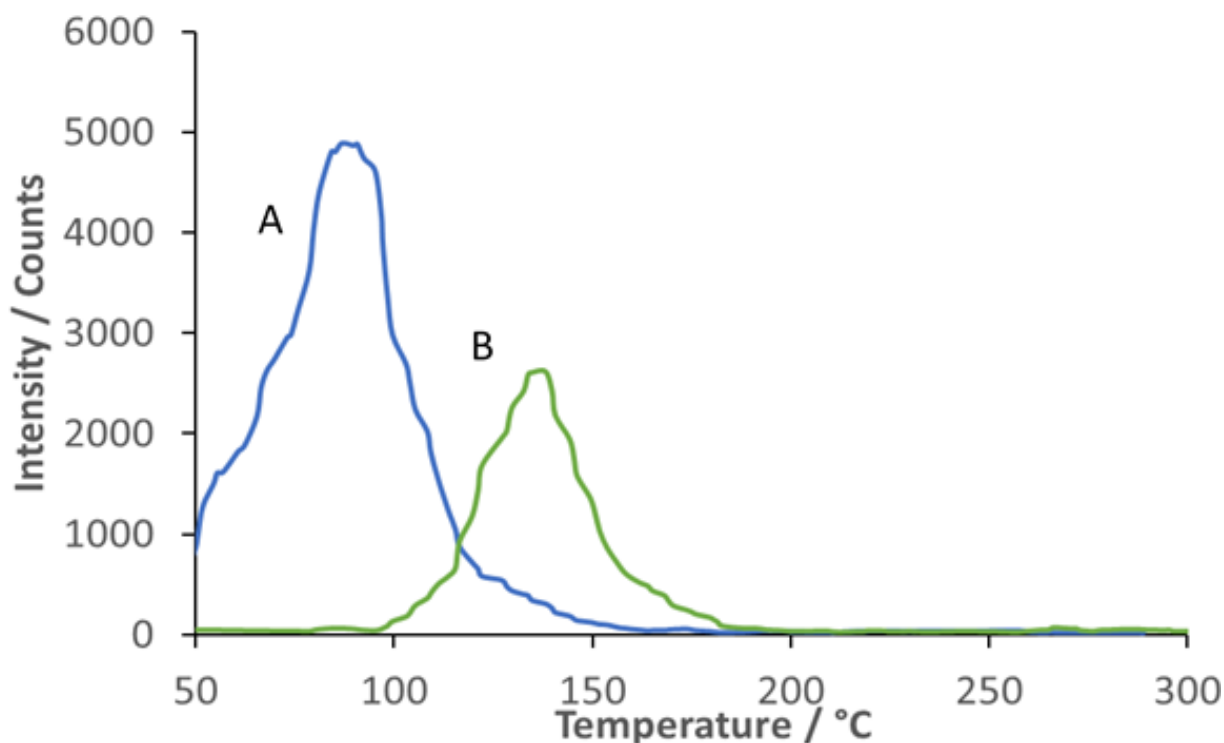


Figure 5.24 Thermal separation of surface recovered energetic materials at 1 μg amount. A) TNT 226 Da $[M-H]^-$ and B) RDX 268 Da $[M+NO_2]^-$.

The μ -DART (see Chapter 2, Section 2.6) was used in an experiment of a three component mixture of 100 ng of each of TNT, PETN and RDX collected using brass fibres.

Figure 5.25 shows that the HDM system successfully managed to thermally resolve this three component mixture. Profile A is TNT as the deprotonated molecular ion 226 Da $[M-H]^-$ which has a maximum between 50 and 150 °C. Profile B is the nitrated molecular ion of PETN 378 Da $[M+NO_2]^-$ which has a maximum between 75 and 160 °C. Profile C is the nitrated molecular ion of RDX 268 Da $[M+NO_2]^-$ which has a maximum between 100 °C and 200 °C. The three profiles were normalised for clarity after the separation of each component of the mixture.

Although, in this case, the mass spectrometer can readily distinguish between these ions (having significantly large mass differences) it does indicate how multiple component mixtures can be thermally separated for improved identification. The HDM system allows for more complex temperature programmes giving enhanced separation.

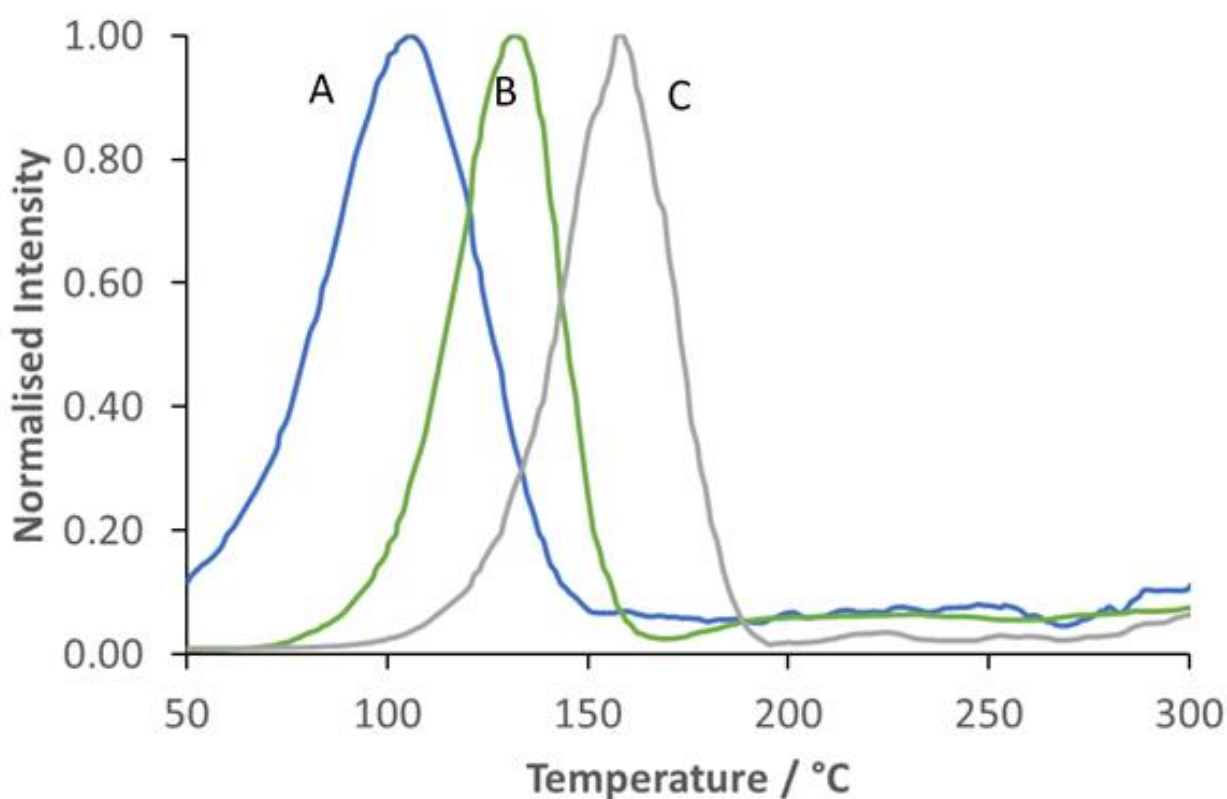


Figure 5.25 Thermal separation of brass recovered materials (100 ng each) analysed using the μ -DART. A) TNT 226 Da $[M-H]^-$, B) PETN 378 Da $[M+NO_2]^-$ and C) RDX 268 Da $[M+NO_2]^-$.

5.3.5 Dopants

Many authors have shown the benefit that using dopant gases can give on DART mass spectra.²⁴⁻²⁵ Typically, a dopant is added to the localised zone around the DART source and assists with the formation of charged ions (as in the APCI mechanism described in Chapter 1, Section 1.2.3) that are detected by the spectrometer. One of the commonly added dopants to DART-MS experiments is ammonium (NH_4^+) usually supplied in the form of ammonium hydroxide. The use of ammoniating agents was shown to increase the sensitivity of TAGs (triacylglycerols) within food oils 10-fold when compared to the non-doped samples.²⁶

This practice is commonly applied to energetic materials, particularly those of nitro-aromatic origin. DCM (dichloromethane) vapours placed in the vicinity of the DART source have been shown to significantly increase the formation of chloride adducts which was found to increase the detection limits for this class of explosives.²⁷

Figure 5.26 shows the result of an experiment that demonstrates this effect using 100 ng of RDX 268 Da $[\text{M}+\text{NO}_2]^-$ and 284 Da $[\text{M}+\text{NO}_3]^-$ thermally desorbed from an Inconel pan at a rate of $50\text{ }^\circ\text{C min}^{-1}$. Mass spectrum A is without any dopants added while mass spectrum B is with addition of a DCM soaked cotton swab as a chloride source near the hot-stage (both are taken as average mass spectra). It can be seen that there is a significant increase in chloride adducts 257 Da $[\text{M}+^{35}\text{Cl}]^-$ and 259 Da $[\text{M}+^{37}\text{Cl}]^-$ in mass spectrum B which are in the expected isotope ratio of 3:1. The mass spectra show how the addition of a dopant can increase the sensitivity with a relative gain in the total number of observed RDX ions, assisting with the overall certainty of assignment and discriminatory power of HDM.

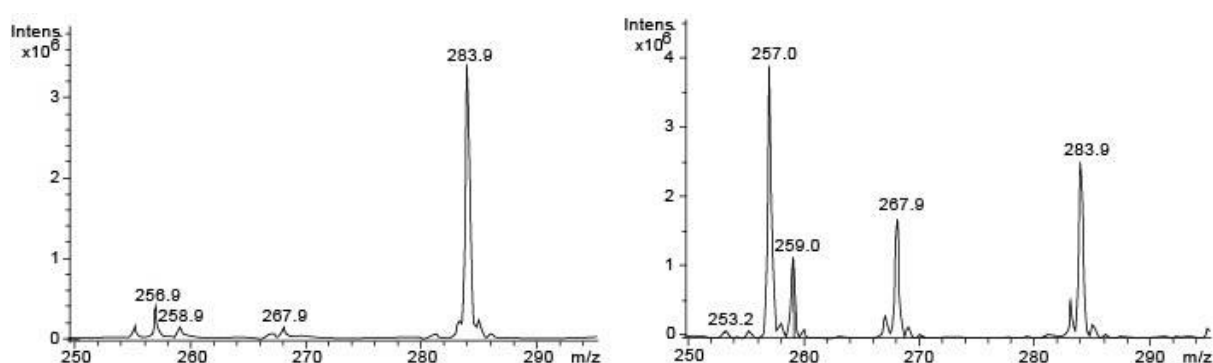


Figure 5.26 HDM analysis of 100 ng of RDX without (A) and with (B) a chloride dopant.

Figure 5.27 shows the result of an experiment using DCM as dopant with another energetic material, PETN. As in the previous example 100 ng of material (PETN) was deposited as a solution and allowed to dry before applying a $50\text{ }^\circ\text{C min}^{-1}$ temperature ramp to the stage.

The average mass spectrum (A) is without the addition of dopant and is dominated by the nitrated molecular adduct 378 Da $[M+NO_3]^-$. The run was repeated but with a piece of cotton soaked DCM nearby (mass spectrum B), this time the chloride adducts are noted in preference as 351 Da $[M+^{35}Cl]^-$ and 353 Da $[M+^{37}Cl]^-$ in the correct 3:1 isotope ratio. A 3.5×10^5 increase in relative sensitivity gain has been observed when comparing the intensity of the original nitrated adduct (of 0.5×10^6) and the chlorine doped ion (0.85×10^6).

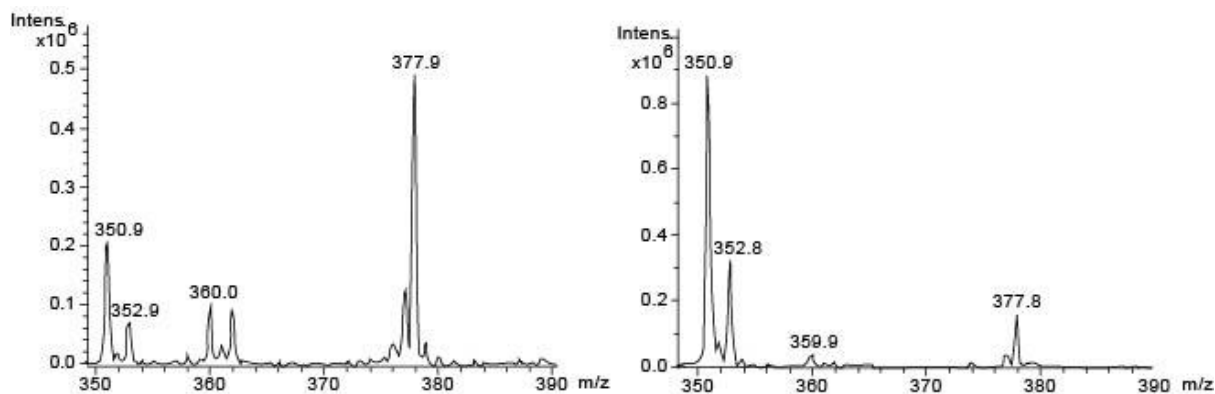


Figure 5.27 HDM analysis of 100 ng of PETN without (A) and with (B) a chloride dopant.

The current, rather crude, method of adding dopants is innately going to be quite poor in terms of vapour introduction reproducibility for use with quantitation, as the amount of dopant will vary both throughout and between experiments. Many factors affect the resultant mass spectrum when introducing a dopant and these are discussed in the following section.

5.4 Further work

Significant work is needed to evaluate the HDM system for use with actual 'field collected' samples. Part of that evaluation would require swabs to be taken from a variety of surfaces with a range of textures.

Better trace transfer methods need to be evaluated similar to the contact practices used by Nilles *et al.*¹⁰ In their method, samples are deposited on aluminium as a solution containing a known concentration and transferred via gentle abrasion onto the contact surface to be sampled.

The reliable detection and identification of energetic materials is often of greater importance than the quantification of an absolute amount of material since even trace amounts of these materials may give indication of possible threats. As the energetic materials studied have all been shown to have a thermal component, that is, a specific temperature (although reproducibility studies are needed to confirm this) at which the energetic material is thermally desorbed from a particular surface, this feature is another variable that can be used as an aid to identification and profiling.

Under strict conditions and with significant number of repeats a library of energetic materials could be developed. With the addition of chemometric analysis (mathematic and statistical analysis used to correlate data sets) in combination with the library, a software routine could be developed to indicate the presence of a particular material above a selected threshold.

The benefits of replacing the expensive, and increasingly rare, helium with a gas such as nitrogen as the ionisation gas discussed in Section 1.5. For a HDM system to be deployable 'in the field' using air would be further beneficial in terms of reducing instrumental complexity. However, interpretation of the resultant mass spectra would be made more difficult as the generation of oxygen radicals would inevitably affect many samples.

There are clear benefits to using dopants for the analysis of many compounds. The addition of DCM vapours nearby the DART source was shown to induce preferential formation of chloride adducts, confirmed by the chlorine isotopic ratio, which raised the apparent sensitivity of the technique.

However, to be effective the dopant concentration needs to be controlled in a quantitative manner: too low and the maximum sensitivity is not achieved, too high and suppression effects may occur.

Chapter 2 (Section 2.7) describes a planned desorption stage that incorporates a dopant inlet. Figure 5.28 (A) shows a schematic of how a humidity controller operates. The controller adjusts the amount of vapour generated (usually by heating a reservoir) that is introduced into a sample chamber and operates under a feedback loop.

Figure 5.28 (B & C) show two possible simple designs for how a controlled introduction of dopants may be achieved. Both would simply pass a stream of gas (matching the ionisation gas of the DART source) through a vial and remove the head space vapours generated which would then be vented to the desorption stage. B represents the removal of the head space vapours for high volatility solvents whilst C is expected to be better for solvents that are less volatile.

In both methods the flow rate of the dopant stream will be controlled and is expected to be proportional to the concentration of dopant delivered.

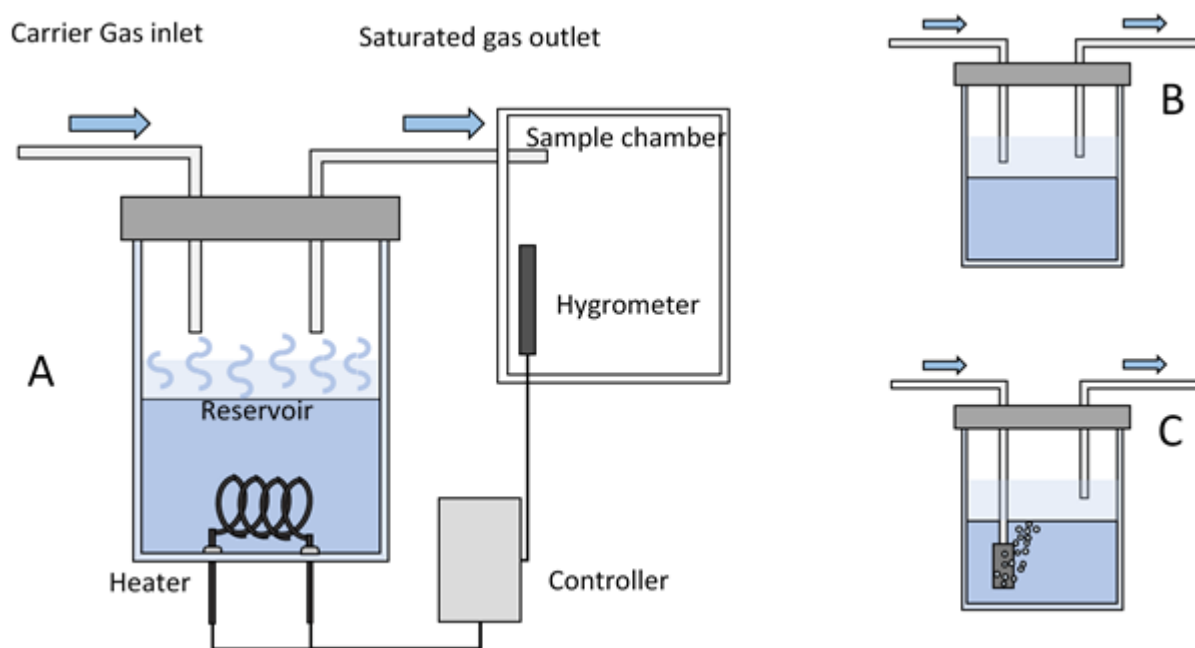


Figure 5.28 A) Schematic representation of how relative humidity is commonly controlled, B) reservoir for high volatility dopants, C) reservoir for low volatility dopants.

5.5 Conclusion

The major aim of the desorption experiments was to evaluate the capability of HDM to thermally desorb samples from a range of surfaces including TA pans, powdered matrices (alumina) and a range of surface collection materials (cottons, fibres and metals).

A range of dried pen inks were thermally desorbed from a relatively complex matrix, powdered alumina. Powdered samples would typically be very difficult to analyse directly using standard DART-MS techniques due to the high flow rates hitting the powdered sample, possibly losing the sample before significant thermal desorption has occurred. The benefit of HDM using a pan has allowed the prepared powdered samples to be analysed *in situ* as compounds are thermally desorbed and ionised upon reaching the helium stream above the sample.

Compounds were tentatively assigned during the dye desorption from alumina, although a few remained unassigned. A common pigment, rhodamine B, was found in several of the ink compositions adding a pink-red hue to the final colour. A trial experiment was performed to use the HDM system quantitatively comparing two different loadings of the pigment 25 and 100 µg. Both the colour and EIC profiles yield a ratio around 1:3.8, indicating the HDM technique may be used semi-quantitatively, a core development required for the use within DART-MS technology.

A range of energetic materials have been detected using HDM, samples have been thermally desorbed using a variety of heating rates. Beneficially for sample throughput higher heating rates were shown to give stronger more uniform profiles for desorbed compounds. The primary benefit that a rapid heating rate gave was the ability to lower the limits of detection for energetic materials. So far the lowest observed quantity of material was 100 pg of tetryl using a heating rate of 50 °Cmin⁻¹. This gave a significant signal above the limits of detection without the addition of dopant materials in the HDMs 'raw' form.

The addition of dopants to the HDM system was found to increase the relative sensitivity for selected energetic materials, but further testing of the addition of dopants in a controlled manner is required to evaluate whether this will lead to improvements in reproducibility. Energetic materials have been shown to generate multiple ions that appear to be both surface and temperature dependant, although this introduces sample variability when analysing unknown materials it can also introduce specificity to aid with the material identification useful for materials discrimination for those that share similar nominal masses.

5.6 Desorption Studies References

- ¹ E.M. McCash, *Surface chemistry*, 2001, Oxford University Press, Oxford, NY.
- ² J. Rouquerol, F. Rouquerol, P. Llewellyn, G. Maurin & K.S.W. Sang, *Adsorption by powders and porous solids : Principles, Methodology and Applications*, 2013, 2nd Ed., Elsevier Science & Technology, Oxford, UK.
- ³ E. Lundanes, L. Reubsæet & T. Greibrokk, *Chromatography : Basic Principles, Sample Preparations and Related Methods*, 2013, 1st Ed., John Wiley and Sons, Inc. NJ.
- ⁴ Z. Takáts, J.M. Wiseman, B. Gologan & R.G. Cooks, *Science*, 2004, **306**, 471-473
- ⁵ W. PiJttmann, C.B. Eckardt & R.G. Schaefer, *Chromatographia*, 1988, **25**(4), 279-287
- ⁶ R.B. Cody, J.A. Laramée & H.D. Durst, *Analytical Chemistry*, 2005, **77**, 2297-2302
- ⁷ M. Haapala, J. Pól, V. Saarela, V. Arvola, T. Kotiaho, R.A. Ketola, S. Franssila, T.J. Kauppila & R. Kostianen, *Analytical Chemistry*, 2007, **79**(20), 7867-7872
- ⁸ G.A. Somorjai, Y. Li, *Introduction to Surface Chemistry and Catalysis*, 2010, 2nd ed., John Wiley & Sons, NJ, 375
- ⁹ S. Banerjee, S. Dubeya, R. Kumar, G.M.C. Chattopadhyayab & Y.C.Sharmaa, *Arabian Journal of Chemistry*, 2017, <http://dx.doi.org/10.1016/j.arabjc.2016.12.016>
- ¹⁰ J.M. Nilles, T.R. Connell, S.T. Stokes & H.D. Durst, *Propellants Explos. Pyrotech.* 2010, **35**, 446-451
- ¹¹ J. Krechmer, K.J. Neeson, G. Isaac, J. Tice, M.V. Gorenstein, A. Millar, M.P. Balogh, J. Langridge, G. Astarita, Application Report, Retrieved from Waters, July 2018, <http://www.waters.com/webassets/cms/library/docs/720004611en.pdf>
- ¹² K. Clemons, J. Dake, E. Sisco, G.F.Verbeck, *Forensic Science International*, 2013, **231**(1-3), 98-101.
- ¹³ R.J. Lewis, *Sax's Dangerous Properties of Industrial Materials*, 2004, 11th Ed, Wiley-Interscience, Wiley & Sons Inc, Hoboken NJ, **V3**
- ¹⁴ M.J. O'Neil, *The Merck Index - An Encyclopedia of Chemicals, Drugs, and Biologicals*, 2001, 13th Ed., Whitehouse Station, Merck and Co. Inc., NJ, 1733
- ¹⁵ R.J. Lewis, *Sax's Dangerous Properties of Industrial Materials*, 2004, 11th Ed, Wiley-Interscience, Wiley & Sons Inc, Hoboken NJ, **V3**, 3606.
- ¹⁶ D.A. Arinbruster, M.D. Tillman & L.M. Hubbs, *Clin. Chem.*, 1994, **40**(7), 1233-1238.
- ¹⁷ M.J. Pavlovich, T. Ono, C. Galleher, B. Curtis, D.S. Clark, Z. Machala and D.B. Graves, *J. Phys. D: Appl. Phys.*, 2014, **47**, 505202
- ¹⁸ D. Fisher, R. Zach, Y. Matana, P. Elia, S. Shustack, Y. Sharon, Y. Zeiri, *Talanta*, 2017, **174**, 92-99
- ¹⁹ J.R. Verkouteren, J.A. Lawrence, M.E. Staymates, E. Sisco, *J. Vis. Exp.*, 2017, **122**, 55484
- ²⁰ M.E. Sigman and C.-Y. Ma, *Anal. Chem.*, 1999, **71**, 4119-4124
- ²¹ G.L. McEnef, B. Murphy, T. Webb, D. Wood, R. Irlam, J. Mills, D. Green & L.P. Barron, *Scientific Reports*, 2018, **8**, 5815
- ²² L. P. Harding, G. M. B. Parkes, J. D. Townend, *Analyst*, 2014, **139**, 4176.
- ²³ J.P. Hutchinson, C.J. Evenhuis, C. Johns, A.A. Kazarian, M.C. Breadmore, M. Macka, E.F. Hilder, R.M. Guijt, G.W. Dicoski, & P.R. Haddad, *Anal. Chem.*, 2007, **79** (18), 7005-7013
- ²⁴ R.B. Cody & A.J. Dane, *Rapid Commun. Mass Spectrom.* 2016, **30**, 1181-1189
- ²⁵ E. Sisco & J. Dake, *Anal. Methods*, 2016, **8**, 2971-2978
- ²⁶ L. Vaclavik, T. Cajka, V.Hrbek & J. Hajslova, *Analytica Chimica Acta.*, 2009, **645**(1-2), 56-63
- ²⁷ E.S. Chernetsova, G.E Morlock & I.A. Revelsky, *Russian Chemical Reviews*, 2001, **80**, 235-255

6.0 Overall Conclusions

The DART-100 source was found to have significant variations between the set gas temperature (used to thermally desorb analytes from matrices) and the temperature achieved within the sampling region of the source. Typically, this was found to be ca. 80 °C in difference. In addition, investigations into whether suppression effects could be correlated to the physical appearance of a sample revealed the additional benefit information a camera system could give to mass spectra when studying selectively layered materials.

To implement these initial findings a miniaturised hot-stage microscope was constructed to fit between the DART source and mass spectrometer. The hot-stage itself was constructed as commercial hot-stages were too large to fit within the confined geometry between the DART outlet and the mass spectrometer. Readily available USB microscopes were found to provide sufficient quality images and magnification for the project.

The hyphenated technique was abbreviated to HDM. Software was written to control the hot-stage and microscope, whilst manufacturer's software was used to control the DART and MS. Samples are introduced to the hot-stage within standard thermal analysis (TA) crucibles at milligram or microliter amounts. The developed software allows a temperature programme to control the hot-stage for use as a standard piece of TA instrumentation. The current version of HDM is capable of heating rates between 0.1 and 50 °C, with a temperature range from 30 to 750 °C. During operation the software records time, temperature, colour properties and micrographs.

The data sets between the HSM and DART-MS can be correlated through a shared time function to allow mass spectra to be visualised as a function of temperature and be correlated directly to the optical properties of the sample. This allows the HDM system to link physical and chemical phenomena together within one single experiment.

A miniaturised DART source was constructed termed the μ -DART. The source was characterised and evaluated against the existing DART-100 to produce comparable mass spectra. The reduced size has offered more flexibility, allowing for pseudo-simultaneous dual polarity analysis which has been utilised during the project.

The HDM system was evaluated in many different fields and has been summarised into three main bodies of work, synthetic reaction monitoring, polymer analysis and thermal desorption profiling.

DART-MS is commonly used to indicate synthetic reaction progression through introduction of reaction solution on glass capillaries. With HDM online reaction profiling has been

achieved for both homogeneous and heterogeneous systems. Emphasis is placed on the ability to monitor solution state reactions within a reaction pan, which conventional DART-MS cannot achieve. Reactants, products and transient intermediates have been profiled as a function of temperature to indicate reaction progression. The general size of the reaction is suitably applied towards 'green chemistry', monitoring reactions at reduced levels. The green aspect has been demonstrated further by trialling solvent free synthesis and has been achieved during solid-liquid interactions during the melting of the reactants. Weaknesses of the HDM reaction profiling method have been highlighted and includes a discussion how these issues may be resolved.

A range of common polymeric materials was analysed using HDM. The technique offered a qualitative optical measure of thermal events including melting, cold crystallisations and glass transitions, whilst mass spectra highlighted polymer degradation. Comparisons between HDM and current DART-MS research into the leaching of silicone oligomers from bakeware gave similar profiles. However, the oligomers were found to leach at lower temperatures than previously reported, within cooking temperature range (*ca.* 200 °C). The silicone polymers were shown to expand under heating, so a software routine was developed to evaluate morphological changes based on comparisons between pixels. This method has enabled the calculation of the coefficient of thermal expansion through optical means, a property normally analysed using thermomechanical analysis.

HDM was also applied to the study of desorption. Pen inks were thermally desorbed from powdered alumina matrices, conventional DART-MS would be incapable of this due to the introduction of a powdered sample directly into a high gas flow. Comparisons were made between colour and ion profiles and were found to give semi-quantitative results based on different concentration loadings of pigment. Energetic materials were also analysed using HDM, through deposition as solutions and from a range of collection materials used to remove energetic materials from surfaces. By using higher heating rates (50 °C min⁻¹), many compounds were analysed significantly above their limits of detection with the current lowest observable detection of 100 pg for tetryl. HDM also provided capabilities to thermally resolve mixtures, increasing discrimination of ions that may share the same nominal mass. Further studies are required to evaluate the quantitative and reproducibility aspects of HDM used for desorption studies work.

Developments have been proposed and some are currently under construction for the HDM system. Instrumental developments such as differential temperature measurement or sample controlled thermal analysis techniques have been discussed to further enhance thermal resolution. Many new application and confirmatory studies have been suggested including evaluation of HDM against other hyphenated techniques such as thermogravimetry-mass spectrometry.